EFFECTS OF HEAVY AGRICULTURAL VEHICLE LOADING ON PAVEMENT PERFORMANCE

A THESIS
SUBMITTED TO THE FACULTY OF THE GRADUATE SCHOOL
OF THE UNIVERSITY OF MINNESOTA
BY

JASON LIM

IN PARTIAL FULFILLMENT OF THE REQUIREMENTS
FOR THE DEGREE OF
MASTER OF SCIENCE

ADVISOR: LEV KHAZANOVICH
CO-ADVISOR: JOSEPH F. LABUZ

JANUARY 2011

Acknowledgements

My deepest gratitude goes to my advisor, Professor Lev Khazanovich, for his guidance and willingness to convey unending knowledge and wisdom, both within and outside of my academic pursuit. I wish to express my warm and sincere thanks to my co-advisor, Professor Joseph Labuz, for his invaluable support and for providing me with the opportunity to pursue my master's degree here at the University of Minnesota. I am grateful to Professor Douglas Hawkins, for his time and effort in reviewing my thesis and for agreeing to serve on my exam committee.

To my many friends and colleagues who were and were not "assigned volunteers" throughout the field testing of this research, I am indebted to you all. I am especially grateful to Kyle Hoegh, Mary Vancura, Peter Bly, Priyam Saxena, Luke Johanneck, Kairat Tuleubekov, Derek Tompkins, Madhavan Vasudevan, Simon Wang, and Andrea Azary. I am particularly grateful to my undergraduate research assistant, Jacob Hanke, for the large amount of time and effort spent on this research.

I would like to acknowledge the project sponsors: the Local Road Research Board, the Professional Nutrient Applicators Association of Wisconsin, Iowa Department of Transportation, Illinois Department of Transportation, Wisconsin Department of Transportation, and Minnesota Department of Transportation. It has been an honor to work with Dr. Shongtao Dai from the Minnesota Department of Transportation and I would like to extend my appreciation for his expertise and advice.

Lastly, and most importantly, I wish to express my loving thanks to my family: to my parents, Jerry Lim and Ann Kok for all their love and immeasurable support, and to both my sisters, Sylvia Lim and Agnes Lim, for their continuous moral encouragement. To them, I dedicate this thesis.

Abstract

Agricultural equipment manufacturers have been producing equipment with larger capacity to meet the demands of today's agricultural industry. This rapid shift in equipment size has raised concerns within the pavement industry, as these heavy vehicles have potential to cause significant pavement damage. At present, all implements of husbandry are exempted from axle weight and gross vehicle weight restrictions in Minnesota. However, they must comply with the 500 lb per inch of tire width restriction which may lead to very large loads as long as the tires are sufficiently wide.

A full scale accelerated pavement test was conducted at the MnROAD test facility. Both flexible and rigid pavements were tested in this study. This thesis presented analysis performed on the flexible pavement sections. The flexible pavement sections consisted of a "thin section" which represented a typical 7-ton road and a "thick section" which represented a 10-ton road. Both sections were instrumented with strain gages, earth pressure cells, and LVDTs to measure pavement responses generated by these heavy agricultural vehicles. These response measurements were compared to responses generated by a typical 5-axle semi truck. Additionally, tire contact area and contact stresses of these vehicles were measured.

Through this research, it was determined that traffic wander, seasonal changes, time of testing, pavement structure, and gross vehicle weight have profound effects on pavement response measurements. The effect of vehicle speed and benefits of flotation tires over radial ply tires were not significant in this study. Additionally, all agricultural vehicles loaded above 80% of full capacity generated higher subgrade stresses compared to the 80-kip 5-axle semi truck.

Layered elastic programs, BISAR and MnLayer were used in the modeling analysis. The contact areas of these vehicles were approximated through multi-circular area estimation. This detailed modeling of the contact area yielded a more realistic representation of the

actual vehicle footprint. DAKOTA-MnLayer optimization framework was introduced to perform backcalculation analysis to determine Young's moduli of the pavement layers. The backcalculated Young's moduli resulted in a close match between predicted responses and field measurements.

Table of Contents

List of Figures

List of Tables

Chapter 1 Introduction

Agriculture is one of the largest industries in the United States, and its economic impact is especially important in the Midwest region. According to the Minnesota Department of Agriculture, as of 2008, seven of the top ten agricultural producers in the nation are located in the Midwest [1]. However over the past decade, there has been a declining trend of number of farms nationwide (Census of Agriculture 2007). Even so, U.S farms experienced an increase in sales in agricultural products between 2002 and 2007 [2]. This increase in production numbers developed a demand for higher efficiency within the industry. The agricultural equipment manufacturers responded by improving farming techniques, as well as producing equipment with greater capacity. Modern agricultural equipment is fitted with innovations such as improved tire designs, flotation tires, and steerable axles. However, increasing the capacity leads to larger and heavier equipments.

This rapid shift in equipment size has raised concerns within the pavement industry, as these large and heavy vehicles are being operated on public highways and local roads. Pavement design methodologies and state statutes are not quick enough to respond to this change in the agricultural industry, and there is potential for these vehicles to cause significant pavement damage. The weights of agricultural vehicles are defined as "implements of husbandry" in the Minnesota statutes. At present, the law states that all implements of husbandry are exempted from axle weight and gross vehicle weight restrictions in Minnesota. However, implements of husbandry must comply with the 500 lb per inch of tire width restriction. Therefore, these vehicles are capable of legally operating on public roads with very large loads as long as the tires are sufficiently wide. Although some restrictions exist, they are typically difficult to enforce and most vary from state to state [3, 4]. There are still a number of states in the Midwest that completely exempt agricultural vehicle from any load restrictions. On the other hand, some studies have been conducted to address pavement damage generated by heavy agricultural vehicle loading.

1.1 Background

A field study conducted in 1999 by the Iowa Department of Transportation evaluated the effects of several heavy agricultural vehicles on both flexible and rigid pavements. The study concluded that in the spring season, agricultural vehicles with 20% increase in axle weight over the reference 20,000 lb single axle, dual tire configuration semi truck would produce the same effect on flexible pavements and a 40% increase in the fall season. Based on the results, the state of Iowa passed legislation that placed restrictions on the allowable loads of agricultural vehicles [5, 6]. The South Dakota Department of Transportation conducted a similar study in 2001, combining field testing and theoretical modeling. Results from the study recommended that regulations regarding certain types of agricultural vehicles should be changed. For instance, the Terragator models 8103 and 8144 should only be allowed to operate empty on unpaved roads and flexible pavements. Single axle grain carts should only be allowed to operate at the legal load limit on unpaved roads and flexible pavements [7].

The Minnesota Department of Transportation performed a scoping study in 2001 that investigated the impact of agricultural vehicles on Minnesota's low volume roads, and whether these vehicles were responsible for pavement damage across the state. Reviews of several county roads revealed that pavement damage was indeed caused by heavy vehicle loading. However, it was indefinite as to whether the damage was caused solely by agricultural vehicle loading, since other types of heavy equipment also traveled on the reviewed county sections. The study suggested that the Minnesota statutes should be simplified and revised based on the findings of previous studies. Additionally, the study also recommended that a thorough field study should be conducted at the MnROAD test facility [3].

1.2 Objectives and Methodology

The main objectives of this research are to determine pavement responses generated by selected types of agricultural vehicles and to compare them to responses generated by a typical 5-axle semi truck. To accomplish this, a full scale accelerated pavement test was conducted at the MnROAD test facility with resources acquired from the Transportation Pooled Fund Program. Two flexible pavement sections at the MnROAD farm loop were constructed and instrumented. One of the sections represents a typical 10-ton road with a 5.5 in. asphalt layer and a 9.0 in. gravel base. The other section represents a 7-ton road with a 3.5 in. asphalt layer with an 8.0 in. gravel base. In addition to that, two existing rigid pavement sections were tested at the low volume loop. One of the rigid pavement sections is doweled and consists of a 7.5 in. concrete layer with 12 in. class-6 base. The other section is undoweled and consists of a 5.0 in. thick concrete layer with 1.0 in. class-1f base on top of a 6.0 in. class-1c subbase.

The flexible pavement sections were instrumented with strain gages, earth pressure cells, and linear variable differential transformers (LVDT) to measure essential pavement responses under heavy agricultural vehicles, while the rigid pavement sections were instrumented with strain gages and LVDTs. Testing was scheduled to be conducted in the spring and fall seasons to capture responses when the pavement is deemed to be at its weakest state. In addition to that, various agricultural vehicles operate at a higher frequency in the spring and fall seasons. A crucial item that was absent in previous studies is the measurement of vehicle traffic wander which was measured in this study by video recording the vehicle passes as they travel on top of length scales installed onto the pavement surface. Also included in this study was the actual tire footprint measurement of the tested vehicles. This measurement was successfully obtained using the Tekscan device.

Design of the test program was to accommodate various control variables identified prior to the field test. These control variables include, but are not limited to, vehicle load levels, target wheel path, target speed, and tire pressure. The test developments and overview, as well as testing procedures, are explained in the subsequent chapter. Data reduction process and preliminary data analysis of the effects of the aforementioned control variables, pavement structure, and environmental factors on pavement responses under heavy agricultural vehicle loadings are presented herein. This document only presents findings and analysis on the flexible pavement sections.

1.3 Organization

The thesis contains five major chapters. Chapter 2 describes details of the pavement test sections and testing procedures carried out at the MnROAD test facility. Chapter 3 contains information regarding data processing. Chapter 4 describes the results of this study which is based on data analysis and observations. Chapter 5 includes semi-analytical modeling using layered elastic theory and Chapter 6 summarizes the findings of this study.

Chapter 2 Testing

2.1 Test Sections

A total of four instrumented pavement sections were tested throughout this field study, including two newly constructed flexible pavement sections and two rigid pavement sections. The flexible pavement sections were constructed at the stockpile area of the MnROAD test facility known as the farm loop and the rigid pavement sections were located at the MnROAD low volume test loop. The flexible pavement consisted of two sections, Cell 83 and Cell 84 which represented the "thin" and "thick" sections, respectively. The two rigid pavement sections, Cell 32 and Cell 54 also represented "thin" and "thick" sections, respectively.

Figure 2.1 and Figure 2.2 show the aerial view and cross-sectional details, while Table 2.1 summarizes the pavement structure of the flexible pavement section. Figure 2.3 shows the rigid pavement sections at the low volume loop and the pavement structures are given in Table 2.2.

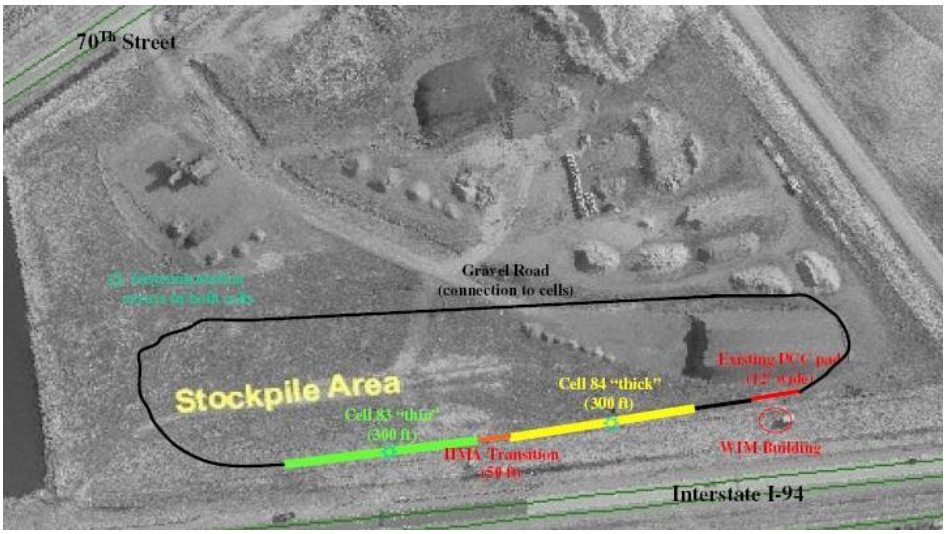

Figure 2.1. Aerial view of flexible pavement test sections Cell 83 and 84 at the farm loop

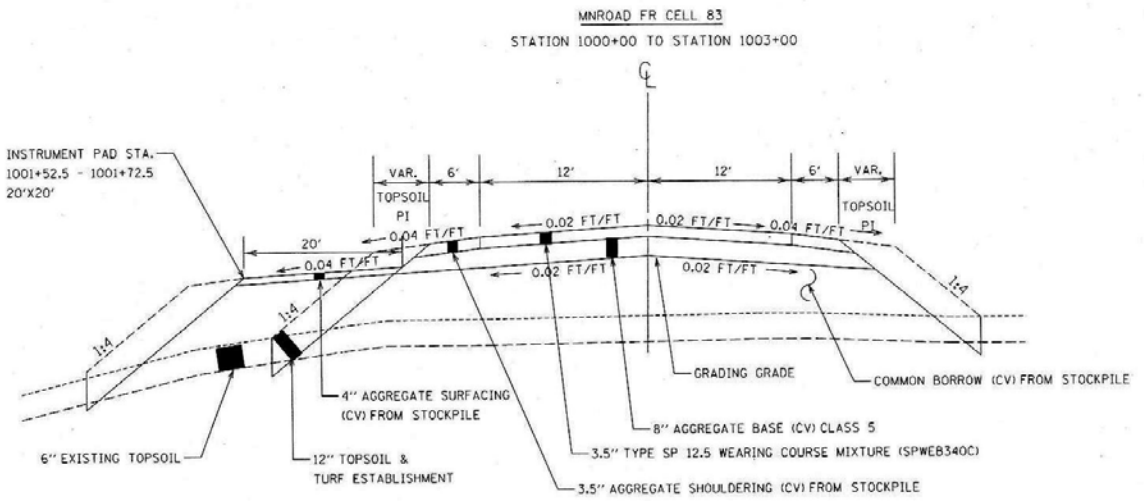

(a)

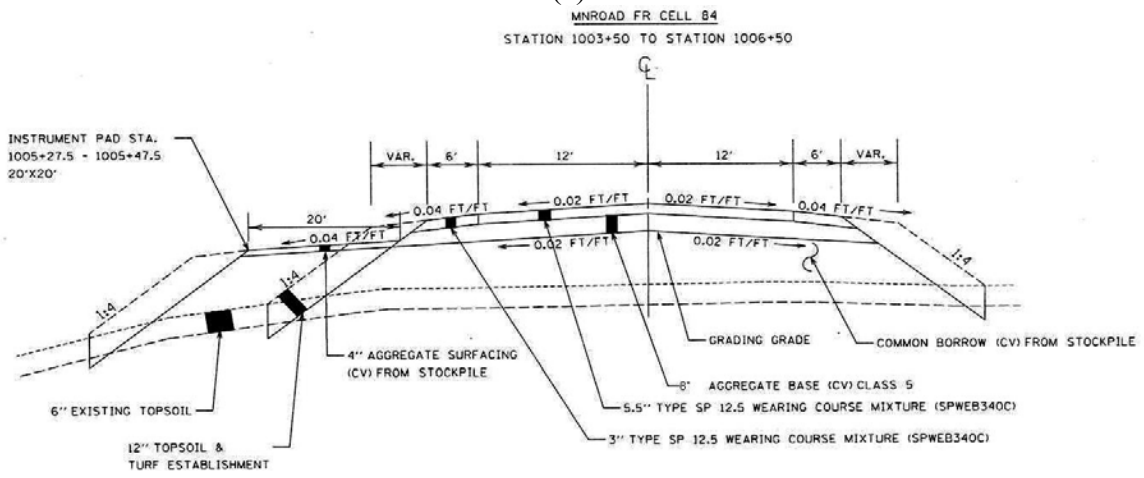

(b)

Figure 2.2. Cross-sectional view of (a) "thin" flexible pavement section, Cell 83 (b) "thick" flexible pavement section, Cell 84

Table 2.1. Pavement geometric structure of flexible pavement sections

Section	Cell 84 (Thick section)	Cell 83 (Thin section)
Surface	5.5 in. thick HMA with PG58-34	3.5 in. thick HMA with PG58-34
Base	9 in. gravel aggregate	8 in. gravel aggregate
Subgrade	A-4 subgrade soil (existing subgrade soil)	A-4 subgrade soil (existing subgrade soil)
Shoulder	6 ft paved shoulder	6 ft aggregate shoulder

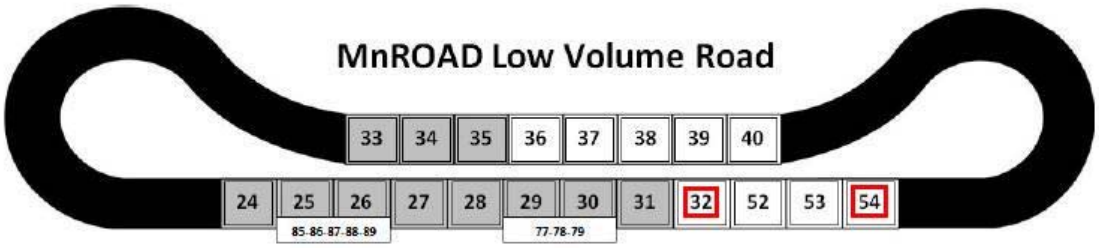

Figure 2.3. Rigid pavement test sections Cell 32 and Cell 54 at the low volume loop

Table 2.2. Pavement geometric structure of rigid pavement sections

Section	Cell 54 (Thick section)	Cell 32 (Thin section)
Surface	7.5 in. thick PCC 15 ft × 12 ft with 1 in. dowel	5 in. thick PCC 10 ft × 12 ft undoweled
Base	12 in. Class-6	1 in. Class-1f 6 in. Class-1c
Subgrade	A-4 subgrade soil (existing subgrade soil)	A-4 subgrade soil (existing subgrade soil)

2.2 Instrumentation

In order to obtain in situ pavement responses generated by various types of heavy agricultural equipment, the pavement test sections were heavily instrumented with sensors that were able to measure major responses within the pavement structure. Both flexible and rigid pavement sections employed a slightly different instrumentation scheme.

2.2.1 Flexible Pavement Sections

Instrumentation of both Cells 83 and 84 of the flexible pavement sections were similar. Horizontal asphalt strain gages were placed at the bottom of the asphalt layer to measure dynamic strain response under moving traffic loads. The flexible pavement was instrumented with the H-shape asphalt embedment strain gage ASG-152 by Construction Technologies Laboratories (CTL), shown in Figure 2.4(a). These gages were typically

pre-calibrated by the manufacturer to determine the relative change in electrical resistance to the actual strain. The relationship between the change in resistance and strain is known as the strain gage factor. The strain gages installed at the flexible test sections were set at the manufacturer's recommended calibration gage factor of two, (GF2). Earth pressure cells were placed on top of the subgrade layer to measure dynamic vertical stress response under moving traffic loads. The earth pressure cells installed at the flexible pavement sections were Geokon 3500 with Ashkroft K1 transducers shown in Figure 2.4(b). Additionally, linear variable differential transformers (LVDT) were installed at mid-depth of the base layer to measure vertical and horizontal displacements in the base layer. It was also important to determine environmental effects within the pavement structure during testing periods. Therefore, the flexible pavement sections were equipped with thermocouple trees and time domain reflectometry (TDR) to measure variations in temperature and in situ moisture contents, respectively. All the sensors were connected to the MnROAD data acquisition systems: the Megadec-TCS for strain gages and earth pressure cells and the NI system for the LVDTs as shown in Figure 2.5.

(a) (b)

Figure 2.4. Flexible pavement instrumentation (a) H-shape asphalt strain gage (b) Earth pressure cell

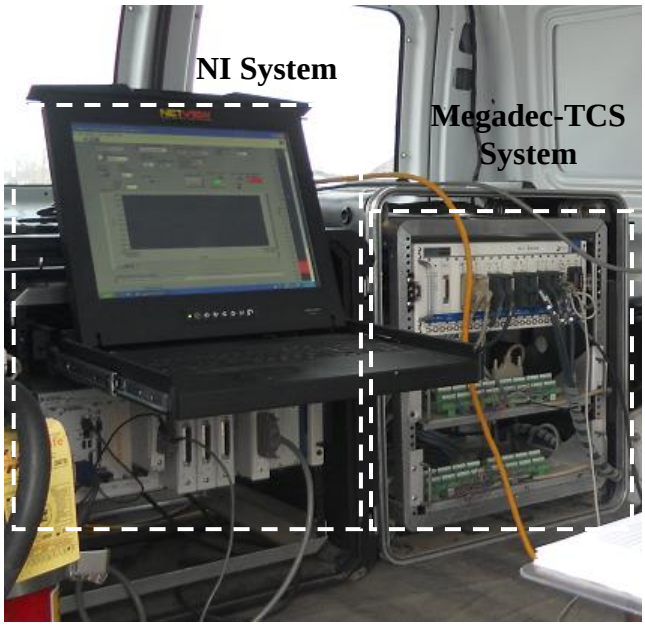

Figure 2.5. Megadec-TCS and NI data acquisition systems

Both traffic lanes (eastbound and westbound) of the flexible pavement sections were instrumented. On the westbound lane, both Cells 83 and 84 consist of nine asphalt strain gages, three earth pressure cells, three LVDTs, one thermocouple tree, and one TDR each. Figure 2.6 shows the cross-sectional detail of the instrumentation and Figure 2.7 shows the sensor layout for Cells 83 and 84, respectively for the westbound lane. Similar layout was replicated for the eastbound lane with the exception of LVDTs.

The strain gage array was separated into three sets to capture critical pavement responses under the various types of axle configurations found on agricultural vehicles. This sensor arrangement allowed for redundancy in the measurements. Emphasis was made on the outer wheel path of the vehicles; hence the first set of strain gages was installed one foot from the pavement edge. The next two sets were spaced two feet apart, transverse to the direction of traffic. For each strain gage set, a corresponding earth pressure cell was installed along the same transverse offset. Each strain gage set consisted of three orientations, which were placed longitudinally, angled at 45º, and transversely to the direction of traffic. These three strain gages were installed two feet apart longitudinally. LVDTs were installed with two feet spacing longitudinally and three feet from the

pavement edge. Both the thermocouple and TDR were installed at center lane with four feet apart longitudinally.

Because of the wide variety of sensor orientations and positions, an appropriate sensor labeling system was adopted. Longitudinal, angled, and transverse strain gages were denoted as LE, AE, and TE, respectively. All earth pressure cells were denoted as PG. Each sensor set corresponds to the transverse offset from the pavement edge; therefore numeric labels were used to denote these sensor sets. The westbound lane sensor sets were numbered 4, 5, and 6 with set 4 being closest to the pavement edge and set 6 being closest to center lane. On the eastbound lane, sensor sets were numbered 1, 2, and 3 with 1 being closest to the pavement edge and 3 being closest to center lane. Final designation for those sensors had the following form: [Cell #]-[Sensor Type]-[Set #]. For example, the angled strain gage closest to the pavement edge of Cell 83 was designated as 83AE4. Instrumentation of LVDTs on the westbound lanes of the flexible sections were placed three feet from the pavement edge. The purpose of the LVDTs was to measure displacements in the base layer in three directions; two horizontally in the longitudinal and transverse directions and one vertically. These sensors were denoted as AL1, AH2, and AV3, respectively. Because LVDTs were installed at one transverse offset, the numeric notations from the above sensors do not apply. For example, the vertically oriented LVDT of Cell 84 was denoted as 84AV3. Figure 2.8 shows the sensor designations on the sensor layout for westbound lanes of the flexible pavement sections Cells 83 and 84.

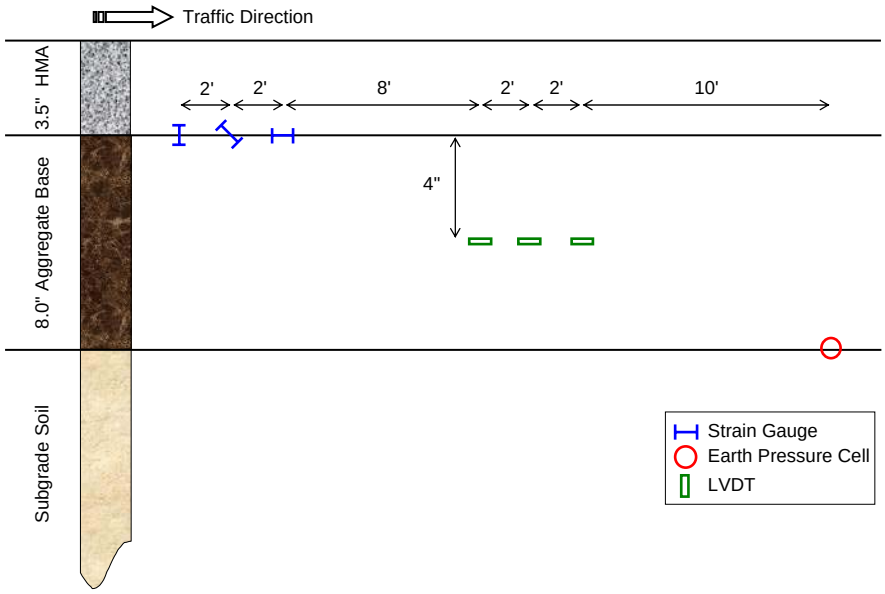

(a)

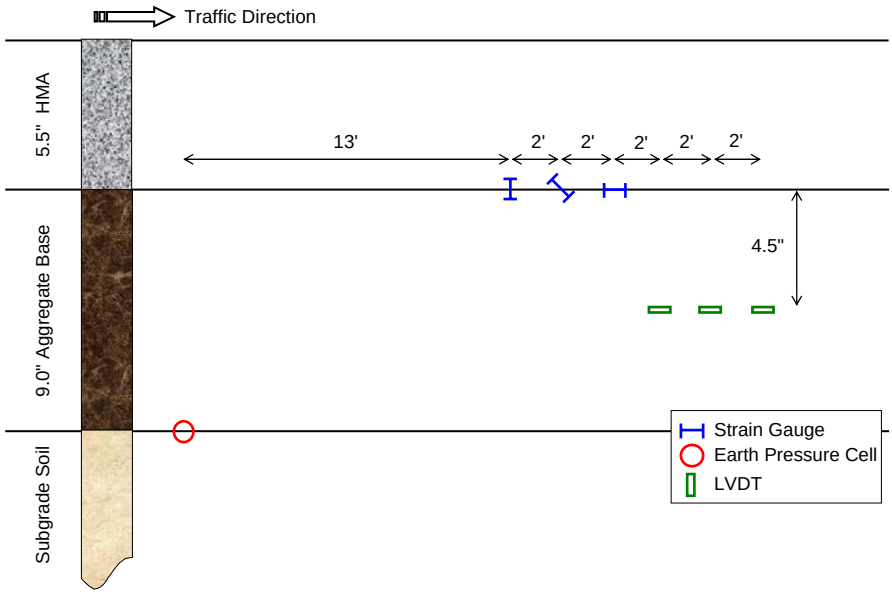

(b)

Figure 2.6. Cross-sectional instrumentation detail of (a) Cell 83 (b) Cell 84

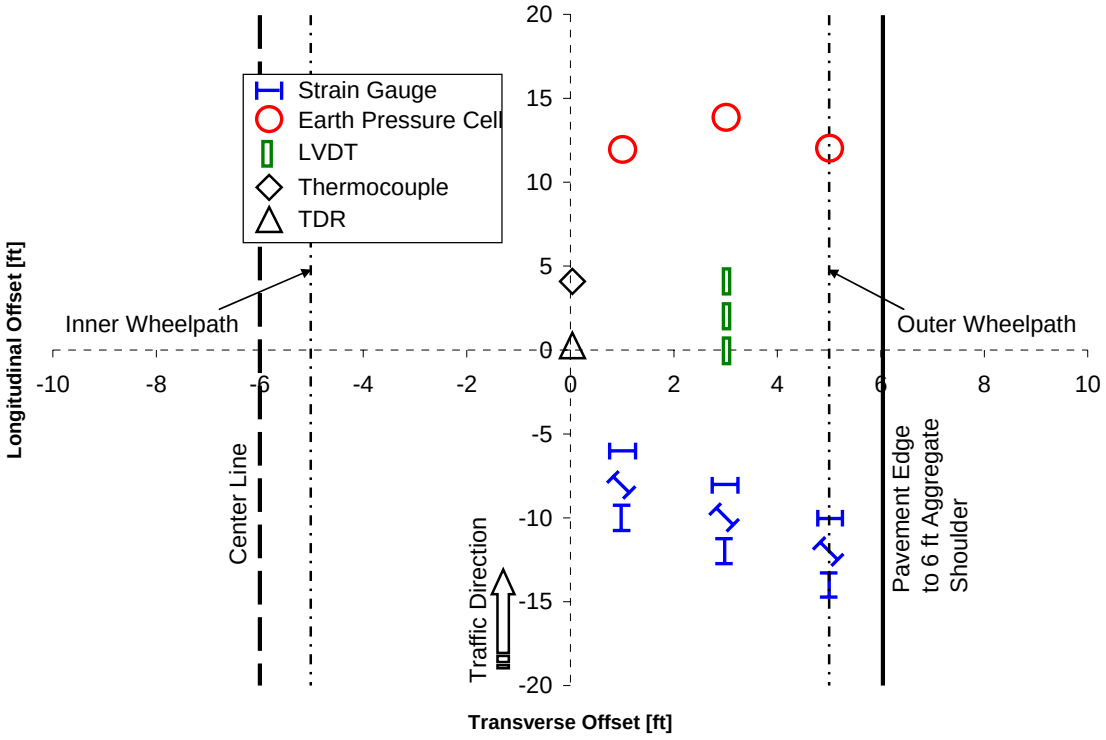

(a)

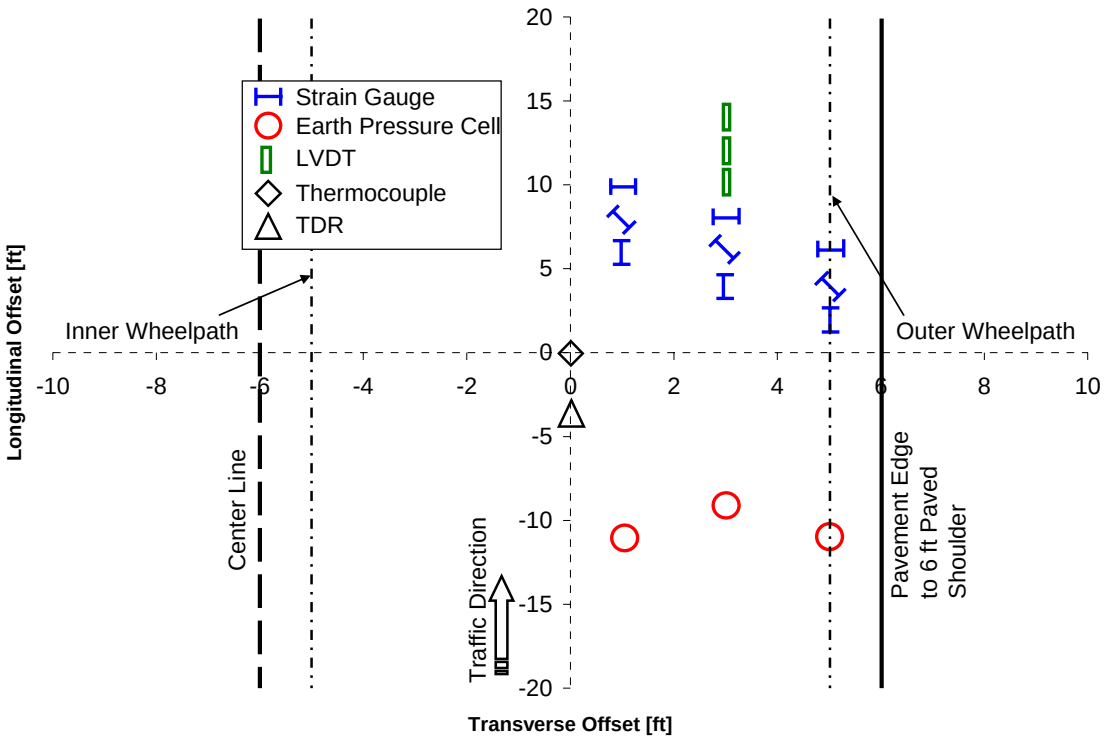

(b)

Figure 2.7. Sensor layout for flexible pavement sections (a) Cell 83 (b) Cell 84

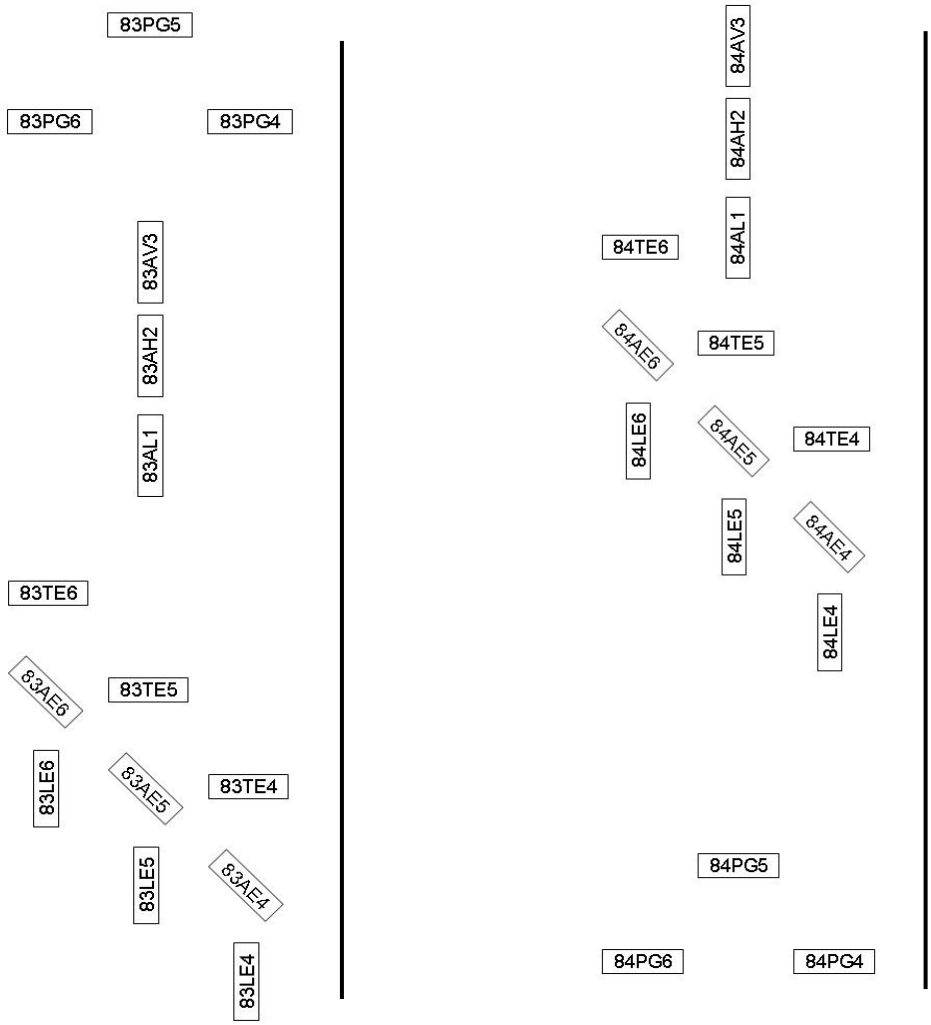

(a) (b)

Figure 2.8. Flexible pavement sections sensor designations for westbound lanes of (a) Cell 83 (b) Cell 84

As mentioned previously, the data acquisition systems employed in this study to collect pavement response data were the Megadec-TCS system for strain gages and earth pressure cells and the NI system for the LVDTs as shown in Figure 2.5. These systems collect response measurements at a rate of 1,200 data points per second (1,200 Hz) and each vehicle pass typically have a collection time of fifteen to eighteen seconds. In total there are approximately 18,000 to 22,000 data points per sensor. These data points provide a response waveform of the asphalt strains, subgrade stresses, and base

deflections of a vehicle pass. Figure 2.9 shows an example of the strain response waveform obtained from a particular strain gage.

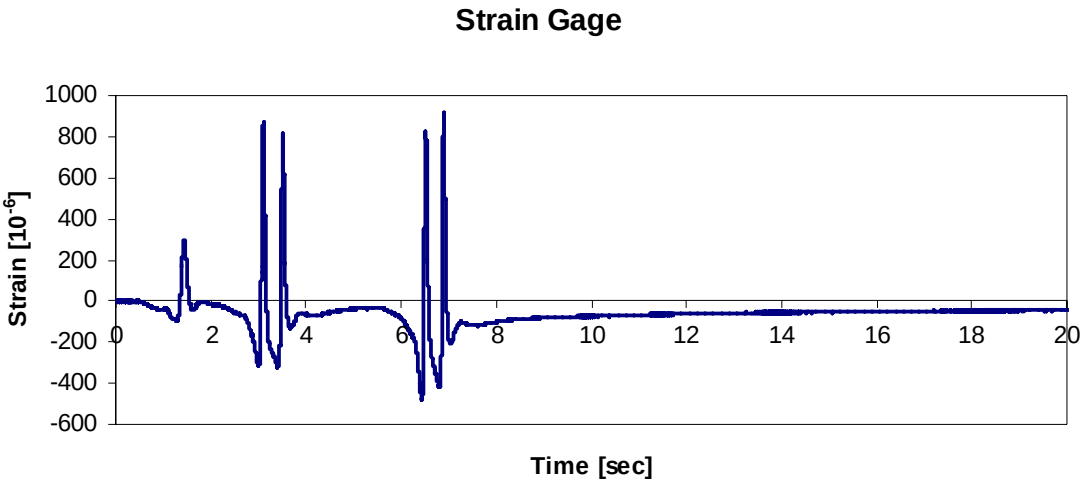

Figure 2.9. Example of strain response waveform

2.2.2 Rigid Pavement Sections

The rigid pavement sections used for testing were Cells 32 and 54 of the low volume loop at the MnROAD test facility. These sections were instrumented during the initial construction; however, additional sensors were installed at strategic locations of the rigid pavement sections in this study. Vertical deflections at the edge of the concrete slabs were measured using LVDTs, which were the Lucas Schaevitz HCD-500 DT, as shown in Figure 2.10(a). Concrete strain gages were embedded at the top and bottom of the concrete layer to measure dynamic strain responses in the horizontal direction under moving traffic loads. These bar shaped concrete strain gages were Tokyo Sokki PML-60, as shown in Figure 2.10(b). Additionally, horizontal movements between the concrete slabs particularly at the joints were monitored using horizontal clip gages. The Tokyo Sokki PI-5 horizontal clip gages (Figure 2.10(c)) were installed at saw cut joints of the rigid pavement concrete slab. The rigid pavement test sections were also equipped with

thermocouple trees to measure pavement temperature at various depths of the concrete and base layers. The same data acquisition systems that were used at the flexible pavement section were also used at the rigid pavement section. The NI system and the Megadec-TCS system collected LVDT measurements and strain measurements, respectively.

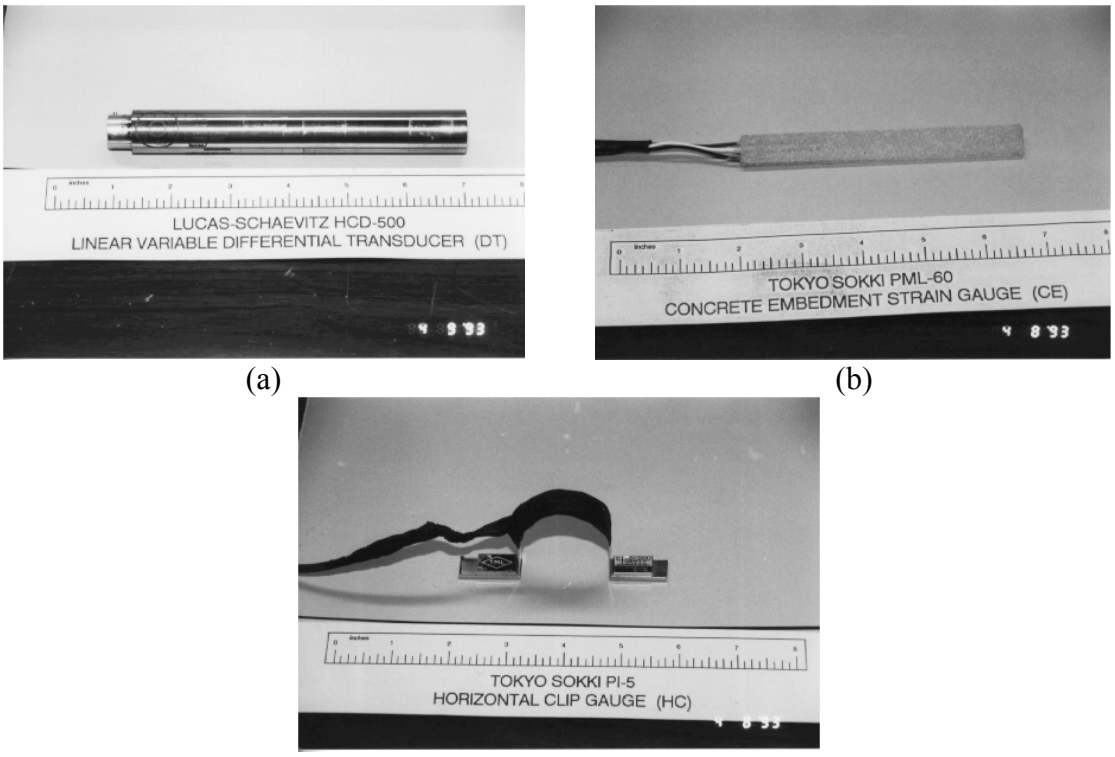

(a) (b)

(c)

Figure 2.10. Rigid pavement instrumentation (a) Linear variable differential transformer (LVDT) (b) Bar shape strain gage (c) Horizontal clip gage

The tests performed at the rigid pavement sections were conducted in the eastbound lanes. It should be noted that instrumentation of the rigid pavement sections (Cells 32 and 54) are different from one another. At Cell 32, only the embedded bar shape strain gages were installed in addition to thermocouples. A total of ten strain gages were installed at Cell 32: five of which measure strain transverse to the direction of traffic, two in the longitudinal direction, and three strain gages were angled at 45º. These strain gages were installed at the near surface to measure strains at the top of the concrete layer.

Cell 54 consisted of a wider array of sensors compared to Cell 32. Cell 54 was instrumented with four vertical LVDTs at the slab edge, six horizontal LVDTs and six horizontal clip gages in between joints, three strain gages embedded at the edge of the concrete slab, and six more strain gages at the edge of the concrete slab. Thermocouples were also installed in Cell 54 at varying depths. Figure 2.11 shows the cross-sectional detail of the instrumentation and Figure 2.12 shows the sensor layout for Cells 32 and 54 for the eastbound lane.

Similar to the flexible pavement sections, each of the installed sensors was given a unique sensor label. Sensors were labeled according to their cell location, sensor type, and number as such: [Cell #]-[Sensor Type]-[Sensor #]. Strain gages were denoted as CE and SS whereas LVDTs and clip gages were denoted as DT and HC, respectively. For Cell 54, several sensors were overlapped as seen in the layout view (Figure 2.12(b)). It should be noted that the horizontal LVDTs are 0.5 in. above the horizontal clip gages (i.e. LVDTs 54DT1 to 54DT6 are placed above clip gages 54HC1 to 54HC6, respectively). Strain gages 54SS1 and 54SS3 are located 6 in. above strain gages 54SS2 and 54SS4, respectively. Sensor 54SS5 is located 5.5 in. above 54SS6. Unfortunately, these designations do not provide information regarding the sensor orientations. Figure 2.13 shows the sensor designations for both Cells 32 and 54.

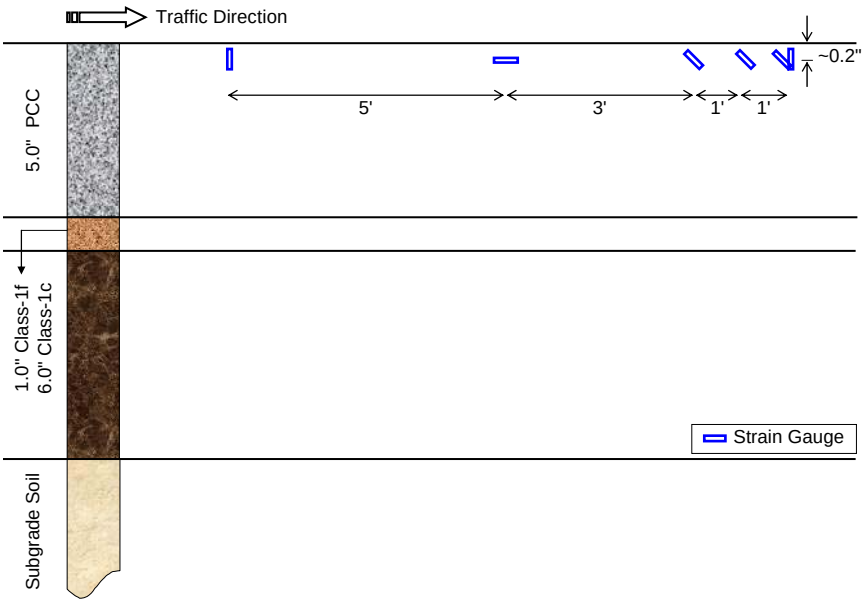

(a)

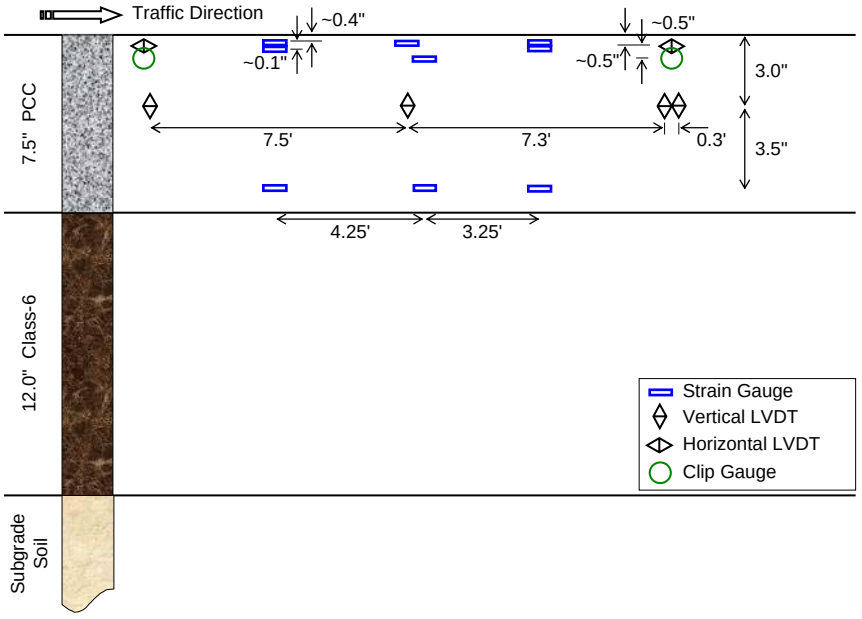

(b)

Figure 2.11. Cross-sectional instrumentation detail of (a) Cell 32 (b) Cell 54

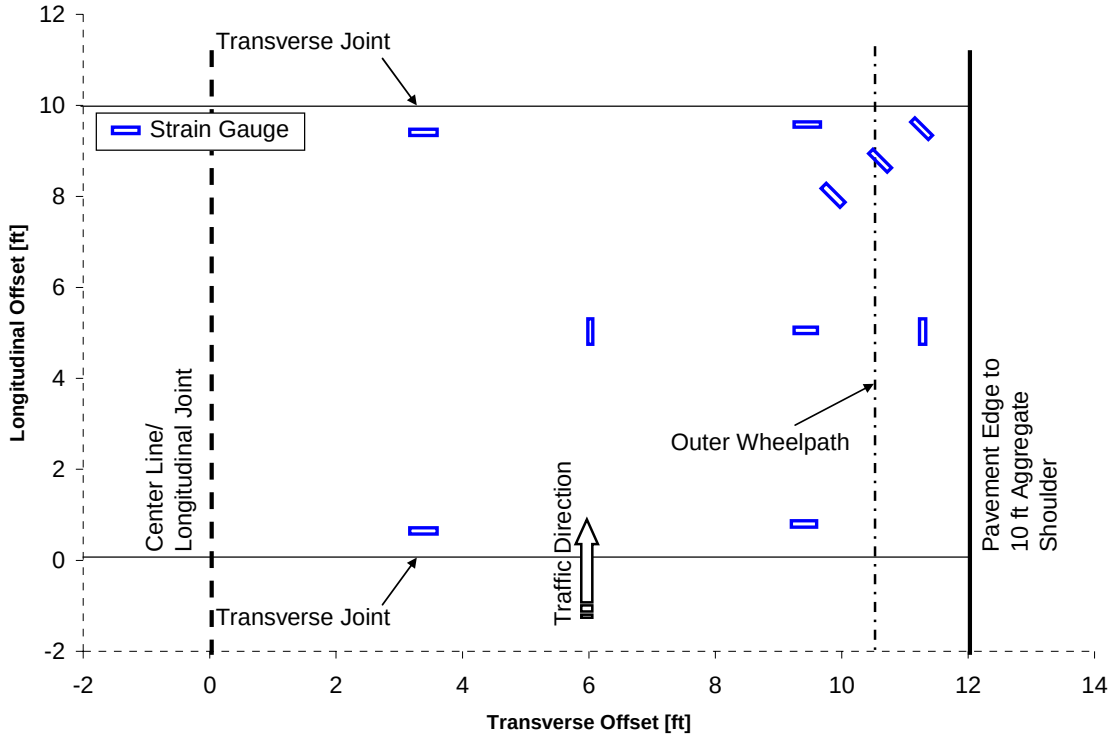

(a)

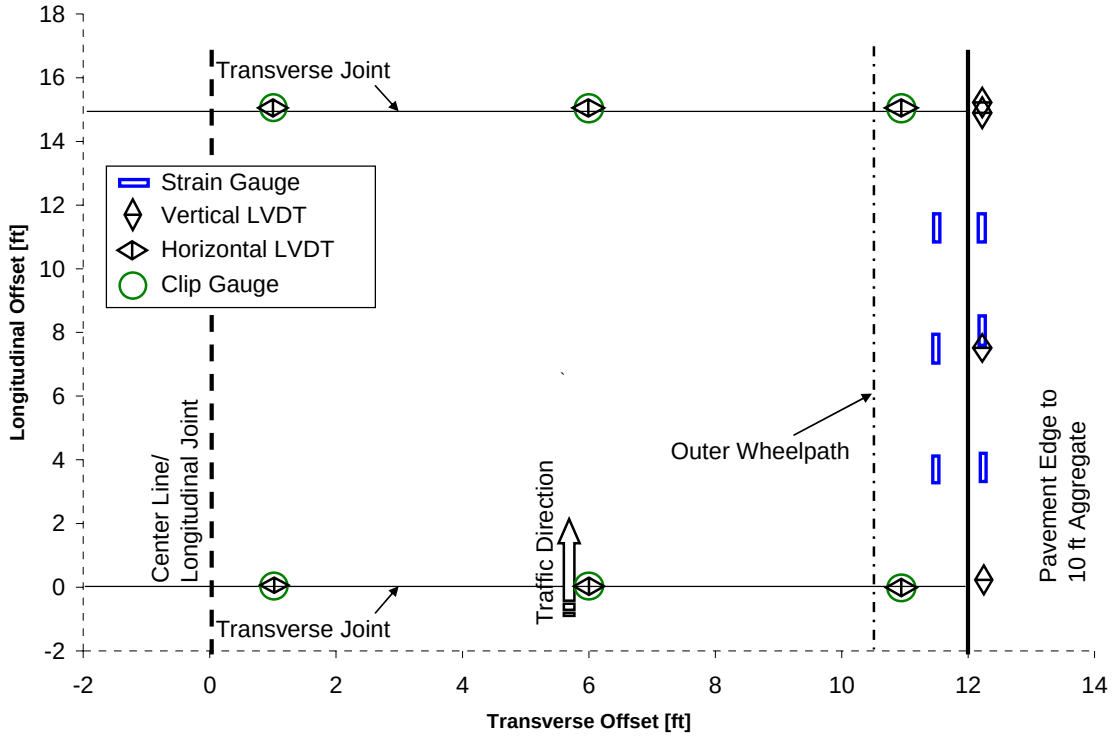

(b)

Figure 2.12. Sensor layout for rigid pavement sections (a) Cell 32 (b) Cell 54

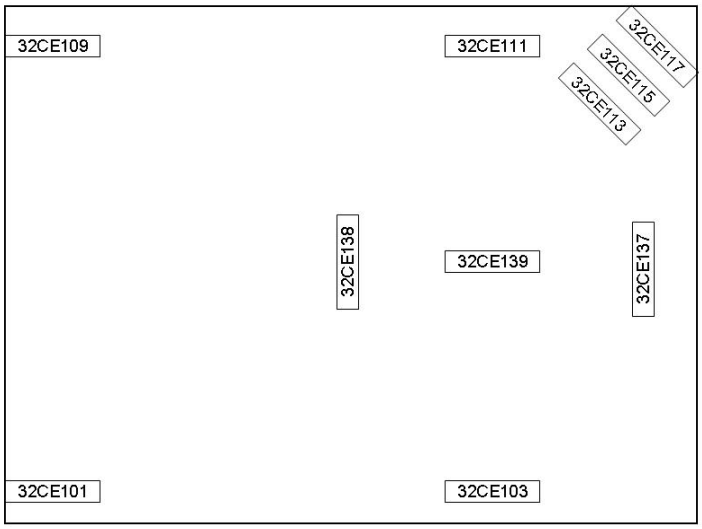

(a)

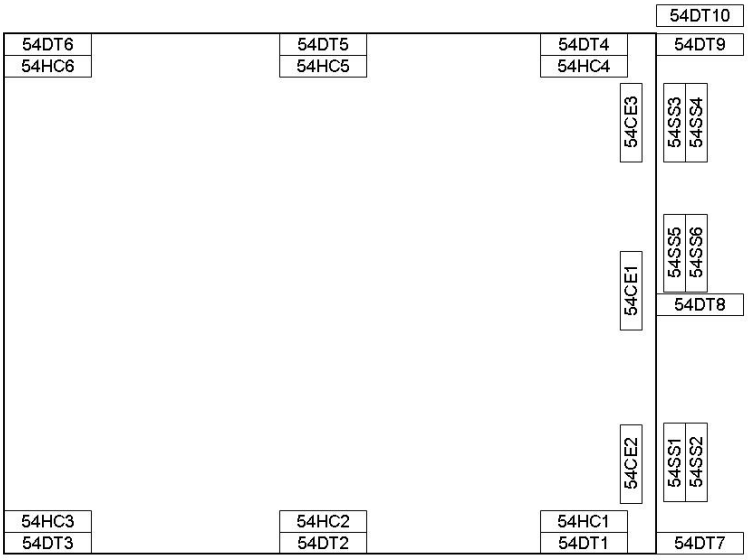

(b)

Figure 2.13. Rigid pavement sections sensor designations for eastbound lanes of (a) Cell 32 (b) Cell 54

2.3 Field Testing

A significant portion of heavy agricultural traffic occurs in spring and fall seasons. Pavement behavior and corresponding damage accumulation during these seasons can be quite different. Temperature and moisture variations induce changes in the material properties of the pavement structure. To account for these effects, field testing was conducted twice a year, in March and August.

Tests conducted in March aimed to evaluate pavement behavior under spring conditions. During the spring season, the frozen layers within the pavement structure begin to thaw, saturating the layers with trapped water. This saturation creates a pore pressure and cohesionless condition mainly in the base and subgrade layers, resulting in a generally weakened state of the pavement structure.

In the fall season, a relatively high volume of heavily loaded agricultural vehicles can be expected. The asphalt layer is also less stiff than in spring, and more prevalent damage to the asphalt layer can be expected under similar loading conditions. While September is the month most representative of typical fall conditions, testing was conducted in August due to unavailability of agricultural vehicles and operators supplied by the industry. In this document, tests conducted in August were referred to as fall season tests. Since August is one of the hottest months of the year in Minnesota, the results obtained for August may be somewhat conservative for fall conditions.

Large amounts of information were obtained during testing, most importantly strain, stress, and deflection data of the pavement through the heavily instrumented pavement sections. Pavement response data were collected using two data acquisition systems set up by MnROAD personnel. The Megadec-TCS system controlled and collected data from the strain gages and earth pressure cells whereas the NI system was dedicated only to the LVDTs. Every successful vehicle pass corresponded to one Megadec-TCS file and one NI file. Each of these files had unique filenames and was recorded in the test

program data logs. In addition, information regarding the tested vehicles was also obtained such as vehicle axle configurations, wheel dimensions, and wheel weights at different load levels. It was also determined that traffic wander is a crucial piece of information in this study that was measured for every vehicle pass. Since agricultural vehicles have complex tire patterns, the footprint of each vehicle was recorded at various load levels. This was made possible with the use of the Tekscan device which is capable of measuring tire contact area and contact stress.

Field testing was conducted in 2008, 2009, and 2010. For each round of testing, a test program was developed specifically for the availability of vehicles and manpower. A total of twelve agricultural vehicles were tested throughout the duration of this study. An additional two typical five-axle semi tractor-trailer were included in the test to be used as reference vehicles. These semis have a gross vehicle weight of 80 kip and 102 kip labeled as Mn80 and Mn102, respectively. Due to the large number of vehicles, each vehicle was given a unique vehicle ID to simplify the identification process. A list of vehicles that were tested in this study is summarized in Table 2.3. Images of all tested vehicles are shown in Figure 2.14.

Table 2.3. List of vehicles tested

Vehicle ID	Type	Vehicle Make	Size	# of Axles	Spring 08	Fall 08	Spring 09	Fall 09	Spring 10	Fall 10
S4	Truck	Homemade	4,400 gal	3	●		●			
S5	Truck	Homemade	4,400 gal	3	●		●			
S3	Terragator	AGCO Terragator 8204	1,800 gal	2	●					
R4	Terragator	AGCO Terragator 9203	2,400 gal	2		●	●			
R5	Terragator	AGCO Terragator 8144	2,300 gal	2			●	●		
R6	Terragator	AGCO Terragator 3104	4,200 gal	2					●	
T1	Tanker	John Deere 8430 w/ Houle tank	6,000 gal	4	●					
T2	Tanker	M. Ferguson 8470 w/ Husky tank	4,000 gal	4	●					
T6	Tanker	John Deere 8430 w/ Husky tank	6,000 gal	4	●	●				
	Tanker	John Deere 8230 w/ Husky tank	6,000 gal	4			●	●	●	
	Tanker	New Holland TG245 w/ Husky tank	6,000 gal	4						●
T7	Tanker	Case IH 245 w/ Houle tank	7,300 gal	5		●				
	Tanker	Case IH 335 w/ Houle tank	7,300 gal	5			●			
	Tanker	Case IH 275 w/ Houle tank	7,300 gal	5				●		
T8	Tanker	Case IH 485 w/ Houle tank	9,500 gal	6		●				
	Tanker	Case IH 335 w/ Houle tank	9,500 gal	6			●	●		
G1	Grain Cart	Case IH 9330 w/ Parker 938 cart	1,000 bushels	3						●
Mn80	Semi Truck	Navistar	NA	5	●	●	●	●	●	●
Mn102	Semi Truck	Mack	NA	5			●	●	●	●

S4 (Homemade 4,400 gal – radial tires)

S5 (Homemade 4,400 gal – flotation tires)

S3 (AGCO Terragator 8204)

R4 (AGCO Terragator 9203)

R5 (AGCO Terragator 8144)

R6 (AGCO Terragator 3104)

T1 (John Deere 8430, 6,000 gal)

T2 (M. Ferguson 8470, 4,000 gal)

T6 (John Deere 8230, 6,000 gal)

T7 (Case IH 335, 7,300 gal)

T8 (Case IH 335, 9,500 gal)

G1 (Case IH 9330, 1,000 bushels)

Mn80 (Navistar 80-kip)

Mn102 (Mack 102-kip)

Figure 2.14. Images of tested vehicles

2.3.1 Workplan Details

The test program was developed to include a range of vehicle load levels (weight), target wheel path (offset), target speed, and tire pressure. The test program was also developed to increase the redundancy of vehicle passes in order to obtain a more complete and repeatable data set. However, number of vehicle passes was governed by the time and manpower constraints.

Field testing was normally carried out in five days, four on the flexible pavement sections and one on the rigid pavement sections. Each day on the flexible pavement corresponds to a different load level. Since only one day of testing was dedicated to rigid pavement sections, only two load levels could be tested.

An estimated eight hours per day were available for testing. Approximately two hours were used for measuring vehicle weights, loading and unloading of the tanks, and lunch break. Actual testing was performed in the remaining six hours. A minimum target interval of 1.5 minutes between passes was selected to provide enough time for the pavement to recover before the subsequent vehicle pass. Thus a total of 240 passes per day was estimated. This estimation was used as a guideline that was adopted after the fall 2008 test. Fewer passes were made if onsite problems were encountered and conversely, additional passes were made when weighing, loading or unloading was completed quicker. Flexible pavement sections consisted of westbound lanes of Cells 83 and 84 (traffic was switched to Cell 83 eastbound when the westbound lane failed). Rigid pavement sections consisted of eastbound lanes of Cells 32 and 54.

Vehicles were tested at five load levels: 0%, 25%, 50%, 80%, and 100%. This was achieved by filling the manure tanks with water and the grain cart with actual grains. At every load level, the weights of each wheel on every axle of the tested vehicles were measured using portable weighing scales provided by MnROAD. Vehicles were also tested at various target speeds: creep, 5 mph, 10 mph, and high speed (approximately 15

to 25 mph). Testing at operating speeds was not possible due to insufficient distance at the end of the test sections for the vehicles to slow down.

One of the objectives of the test program was to evaluate the effect of vehicle traffic wander on pavement responses. The pavement edges were marked as the fog line and vehicles were directed to travel with the target offsets of 0 in., 12 in., or 24 in. from the fog line. To determine the actual wheel paths, length scales were painted onto the pavement surfaces in fall 2008 which were later replaced by permanent steel scales. Videos of the vehicle passes were recorded using a video camera.

As the tests were conducted, the data acquisition operator recorded the actual time of each vehicle pass and the corresponding data files which were saved by two of the data acquisition systems. This step was necessary to remove any false triggering of the acquisition system and to make sure that the acquired data files corresponded correctly to the pass information. An example of the test program is shown in Appendix A.

2.3.2 Vehicle Measurements

The test program required vehicles to be tested at varying load levels. For each load level, measurements of the all vehicle weights were obtained using portable scales. Portable scales were placed in front of each of the vehicles' wheels and the vehicle was carefully driven to place each wheel on top of the scales. It was ensured that the entire vehicle was leveled and no weight bias occurred between axles and between wheels. Figure 2.15 shows an example obtaining weight measurements using the portable scales. Additionally, vehicle axle configurations, wheel spacing, and wheel widths were measured for all tested vehicles. Appendix B contains the vehicle axle weights and dimensions.

Figure 2.15. Weighing vehicles using portable scales

2.3.3 Traffic Wander Measurements

As already discussed, the test program required the vehicles to travel at various distances (offsets) from the pavement edges. These offsets were targeted at 0, 12, and 24 in. from the pavement edges and were based on the center of the most rear axle for every vehicle to maintain consistency. Although vehicle operators were often precise with their steering control to achieve the target offsets, it was still important to determine the vehicles' actual position. To achieve this objective, length scales were installed and vehicle positions were recorded during each pass.

Initially, scales were painted onto the pavement surface using scaled pavement stencils, but the paint quickly faded with increasing number of traffic. Therefore, steel scales with 1 in. teeth spaced 1 in. apart were fabricated and installed onto the pavement surface at each of the test sections (i.e. Cells 83, 84, 32, and 54) as a more permanent solution. Figure 2.16 shows the initial painted scale and the more permanent steel scale installed at Cell 84 of the flexible pavement section. The scales were installed as close as possible to the sensor locations, but not too close as it may affect pavement response measurements. Video cameras were placed at each cell of the test sections and configured to produce the

optimal view of the scale. A Sony and a Panasonic video camera were used in this measurement. Figure 2.17 shows the video camera used for this measurement and an example of a vehicle pass as it drives over the painted scale.

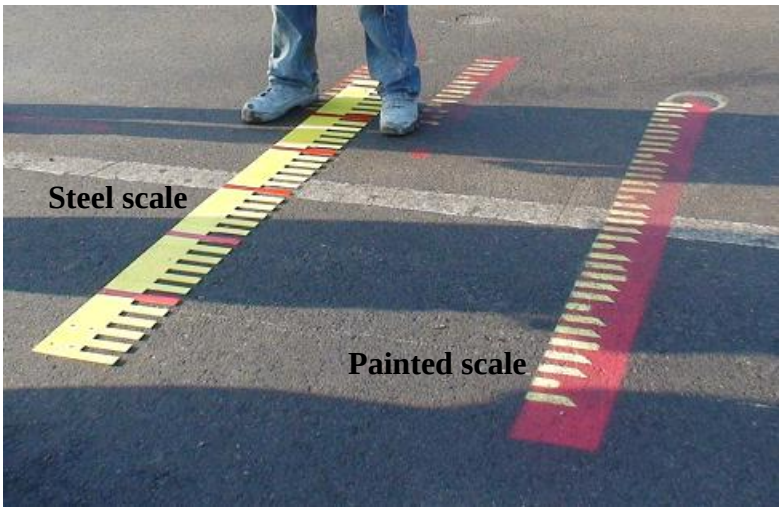

Figure 2.16. Permanent steel scale and painted scale at Cell 84

(a)

(b)

Figure 2.17. Traffic wander measurements (a) using the Panasonic video camera (b) for a vehicle pass

Video recordings of each vehicle pass were taken as the vehicle travels across the scales. Camera operators began recording the videos as the vehicle approaches the scale and called out the test number and vehicle ID in the video recording. This ensured that the videos can be properly matched with the corresponding data files and pass information. The videos were later viewed and evaluated individually to determine the actual vehicle offsets.

2.4 Tekscan

As mentioned previously, heavy agricultural vehicles are equipped with tires that have complex load distributions in terms of tire-soil interaction. Characteristics of these tires depend on the construction whether they are radial ply or bias ply. In addition, there are also flotation tires that are now increasingly common in the agricultural industry. Flotation tires are designed to have a much wider footprint and lower inflation pressure compared to conventional tires. These tires have tread patterns (tire lugs) that allow the vehicle to maneuver safely and efficiently as well as provide the vehicle with adequate support over soft materials. In the agricultural industry, a larger footprint and lower inflation pressure is sought because it helps to reduce rutting and compaction of the soil in the field.

In this study, measurements of tire footprint and vertical contact stress were obtained using a device called Tekscan. This device consists of four sensorial mats (model 5400N) and four data handles (Evolution Handles) with attached USB cables, as shown in Figure 2.18. Each of the sensorial mats is approximately 24 in. by 36 in. with a sensing area of 22.76 in. by 34.80 in. The mats were placed according to the 5400NQ sensor map as per Tekscan Inc. recommendation, shown in Figure 2.19. This setup requires four 5400N sensorial mats to be positioned in a two by two arrangement. Using the 5400NQ setup, the sensing area is 45.51 in. by 69.61 in. Each sensorial mat was connected to one Evolution Handle as shown in Figure 2.19 and connected to the USB ports of the computer. Data was collected using the I-Scan version 5.90 software.

(a)

(b)

Figure 2.18. Tekscan hardware components (a) 5400N sensor mats (b) Evolution Handle

The Tekscan setup and testing involved the following steps [8]:

1. The 5400N sensorial mats and Evolution Handles were placed as shown in Figure 2.19. Sensorial mats were placed on top of a flat steel sheet to protect it from the underlying rough pavement surface. These mats were also protected with plastic sheets to prevent damage from the vehicle pass.
2. Handles A and B were positioned from left to right along the top of the array while handles C and D were positioned from left to right along the bottom of the array.
3. Sensorial mats A and D were placed with the words “This Side Up” facing right side up while sensorial mats B and C were positioned with the words “This Side Up” facing down.
4. All sensorial mats were clamped to the corresponding handles according to their positions.
5. The handles were connected to a computer and checks were performed to ensure that all connections were secured and complete.
6. The Sensor OK LED must be lit green to indicate that sensorial mats were correctly inserted to the handles. The Power LED must be lit green to indicate handles are receiving power and has been initialized by the computer.

7. The I-Scan version 5.90 software was launched and the 5400NQ sensor map was selected together with all four available handles.
8. Sensitivity of sensorial mats and recording parameters were configured prior to conducting the test. Note that equilibration of the sensors was not performed during actual testing due to lack of resources (uniform pressure loading apparatus).
9. Test vehicles were driven over the sensorial mats of the 5400NQ setup while the I-Scan software records information from the pass. Note that the 5400NQ setup was only wide enough to accommodate one side of the vehicle's axle.
10. As the vehicle proceeds over the sensorial mats, the vehicle operator was not allowed to execute any steering adjustments, accelerate, or decelerate while the tires are on or approaching the mats.

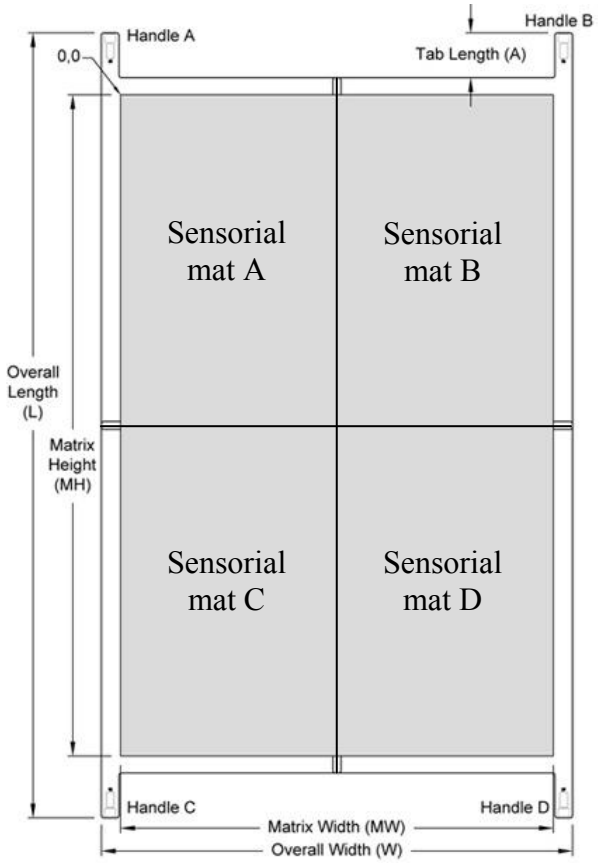

Figure 2.19. 5400NQ sensor map layout (adopted from Tekscan User Manual [8])

Testing was limited to the availability of the vehicles but Tekscan measurements were obtained for almost all the vehicles tested in the farm loop, as shown in Table 2.4.

Table 2.4. Tekscan tested vehicle list

Test Date	Vehicles	Load Levels [%]
March 17 2008	S4, S5, T1	0, 50, 80
March 26 2008	S3, T2, T6, Mn80	0, 50, 80
August 28 2008	R4, T7	0, 25, 80
August 29 2008	T8	0, 25, 80

2.5 Test Overview

The following experiments were conducted during each round of testing:

- Spring 2008 (March 17 to 19 and 24 to 26)
  - Tested seven vehicles; S3, S4, S5, T1, T2, T6, and Mn80.
  - Load levels: 0%, 25%, 50%, and 80%.
  - Vehicle speeds: creep, 5 mph, and 10 mph.
  - Vehicle offsets: 0 and 12 in.
  - Tire pressure for vehicle T1: 33 and 42 psi.
  - No measurements of traffic wander.

- Fall 2008 (August 26 to 29)
  - Tested five vehicles; R4, T6, T7, T8, and Mn80.
  - Load levels: 0%, 25%, 50%, and 80%.
  - Vehicle speeds: creep, 5 mph, and 10 mph.
  - Vehicle offsets: 0 and 12 in.
  - Excluded need to change tire pressure. All vehicles have tire pressures which they normally operate by.
  - Scales were painted onto the pavement surface and videos of vehicle wheel path were recorded to estimate traffic wander.

- Spring 2009 (March 16 to 20)
    - Tested nine vehicles; S4, S5, R4, R5, T6, T7, T8, Mn80, and Mn102.
    - Load levels: 0%, 25%, 50%, and 80%.
    - Vehicle speeds: 5 mph, 10 mph, and high speed (15 to 25 mph). Excluded creep speed.
    - Vehicle offsets: 0 and 12 in.
    - Permanent steel scales were installed onto the pavement to assist in traffic wander estimation.
    - Failure occurred at Cell 83 westbound during test at 50% load level. Failure was propagated at 80% load level.
    - Failed section was patched for upcoming tests.

- Fall 2009 (August 24 to 28)
    - Tested six vehicles; R5, T6, T7, T8, Mn80, and Mn102.
    - Load levels: 0%, 50%, and 100%. Excluded 25% load level.
    - Vehicle speeds: 5 mph, 10 mph, and high speed.
    - Vehicle offsets: 0, 12, and 24 in. 24 in offsets were included due to recommendations from the technical committee.
    - Failure at patched section of Cell 83 westbound during test at 0% load level on the first day. Testing was switched to Cell 83 eastbound.
    - Failure at Cell 83 eastbound during test at 50% load level on the second day. Testing was switched back to Cell 83 westbound with steel sheets placed over failure section.
    - Failure propagated at Cell 83 westbound during test at 100% load level.
    - Failure sections on both east and westbound lanes of Cell 83 were not repaired for consecutive tests. Instead, steel sheets which were placed will remain for future tests. Additional steel sheets were placed at propagated failure sections.

- Spring 2010 (March 15 to 18)
    - Tested four vehicles; R6, T6, Mn80, and Mn102.
    - Load levels: 0%, 50%, and 100%.
    - Vehicle speeds: 10 mph and high speed. 5 mph vehicle speeds were excluded.
    - Vehicle offsets: 0, 12, and 24 in.
    - Existing failure on Cell 83 westbound continued to propagate.
    - Both westbound and eastbound lanes of Cell 83 were dismissed from future tests.

- Fall 2010 (August 18 to 19)
    - Tested four vehicles; T6, G1, Mn80, and Mn102.
    - Load levels: 0% and 100%. Other load levels were excluded due to availability of vehicle G1.
    - Vehicle speeds: 10mph only. Other vehicles speeds were excluded from the test.
    - Vehicles offsets: 0, 12, and 24 in.

Table 2.5 summarizes the number of vehicle passes made on the flexible (AC sections) and rigid (PCC sections) pavement sections for each round of testing.

Table 2.5. Overview of previous test

Test Season	**Test Dates**	**Vehicle Passes**	
		AC	**PCC**
Spring 2008	March 17 – 19 & 24 – 26	400	48
Fall 2008	August 26 – 29	282	72
Spring 2009	March 16 – 20	960	170
Fall 2009	August 24 – 28	782	360
Spring 2010	March 15 – 18	776	344
Fall 2010	August 18 – 19	426	204
	Total	3,626	1,198

2.6 Pavement Distress Monitoring

After each round of testing, distress surveys were conducted. Initial signs of pavement distress were observed on third day of testing during spring 2009 (18 March 2009). At Cell 83 westbound lane, a longitudinal crack developed approximately 12 in. away from the pavement edge toward the center line. The condition of the pavement surrounding the longitudinal crack further deteriorated with increasing number of vehicle passes. At the end of the following day of testing (19 March 2009), the pavement section had completely failed in extreme rutting. The total length of the rut was approximately 31.5 ft. at just 14.5 ft. away from the closest sensor location. Figure 2.20 and Figure 2.21 show the initial longitudinal crack and the subsequent rutting failure of Cell 83 westbound lane in spring 2009.

Figure 2.20. Failure at Cell 83 westbound lane on 18 March 2009

Figure 2.21. Failure at Cell 83 westbound lane on 19 March 2009

The failed section of Cell 83 westbound lane was repaired and patched in preparation for fall 2009 test. On 24 August 2009 which was the first day of testing in fall 2009, the patched area experienced slippage cracks shown in Figure 2.22. This failure was due to insufficient bonding between the wearing and binder courses of the asphalt layer. Testing was shifted to Cell 83 eastbound lane where it unexpectedly failed on the 25 August 2009. Before testing was shifted back to Cell 83 westbound lane, the previous slippage cracks were overlaid with ¾ in. steel plates in an attempt to slow down the pavement deterioration as number of vehicle passes and load levels increase. However, deterioration of that section was imminent and rutting at the pavement edge continued to propagate until the last day of fall 2009 test (27 August 2009). A forensic study was conducted on the failure site and a report prepared by the Minnesota Department of Transportation suggested that the clay borrow layer was the cause for the pavement failure [9].

Figure 2.22. Slippage cracks at Cell 83 westbound lane on 24 August 2009

Chapter 3 Data Processing and Archiving

Since a large amount of information was collected in this study, it was necessary to develop procedures for efficient processing and archiving of the collected data. Raw data acquired directly from the field tests needed to be summarized in a usable format for analysis. The raw data includes video files containing vehicle traffic wander, pavement response data containing time history of asphalt strains, subgrade stresses, and base deflections generated by the vehicles, and Tekscan measurements containing contact area and contact stress information of the tested vehicles. This chapter contains information pertaining to initial processing of this information and organization into summary tables. This is followed by a description of the data organization and archiving that was developed to provide convenient accessibility to the data for subsequent analysis.

3.1 Determining Vehicle Traffic Wander

Test vehicles were directed to travel at lateral distances of 0, 12, and 24 in. away from the pavement edge. The actual traffic wander could be significantly different from the target offsets. To provide the necessary precision for interpreting the data the actual vehicle offsets were measured. Scales were installed on the pavement surface at both cells of both test sections and video cameras were used to record the vehicle pass as it travels across the scales. As the vehicle approaches the scales, the camera operator mentioned the test number and vehicle ID as per the test program so that the videos could be matched with the corresponding data file and pass information.

The video files were stored in an external hard disk. Depending on the video camera manufacturer, the video files were saved in different file extensions. Videos recorded using a Panasonic camera have extensions ".mod" while files ending with extension ".moi" were ignored. Videos from the Sony camera have file extensions ".mts". After transferring the video files, they were then played in a preferred media player. During

this step, identification of the video file corresponding to the test number and vehicle ID was performed. Once the video file was matched to its corresponding pass information, it was renamed according to the following format: [Load Level]-[Pass #]-[Target Speed]-[Vehicle ID]-[Cell #]. For example, a raw video file named MOV006.mod of Cell 83, Day 1 (08-24-09) was found to correspond to test number two for vehicle R5. Hence the file was renamed to 0%-1-5-R5-C83. The next step involved determining the actual offset of the vehicles' wheel path as described below:

1. For each vehicle pass, video files were played in a preferred media player. The video was paused when the last axle of the vehicle was directly on top of the steel scale (see Figure 3.1).
2. The red strip on the steel scale placed on the outer edge of the fog line (pavement edge) was designated as the origin. Wheel paths toward the centerline of the pavement were considered to be positive while toward the shoulder were considered to be negative.
3. The wheel edge offset was obtained by counting the number of teeth and gaps (each 1 in. wide) from the origin to the last visible tooth or gap at the edge of the wheel of the vehicle's last axle (see Figure 3.2).
4. Wheel center offset was obtained by simply adding the wheel edge offset to half the tire width of the last axle.

Figure 3.3 shows an example of obtaining the wheel edge and center offsets for a generic 11 in. wide tire.

Figure 3.1. Snapshot of wheel edge offset for vehicle R5 measured as 14 in at Cell 83

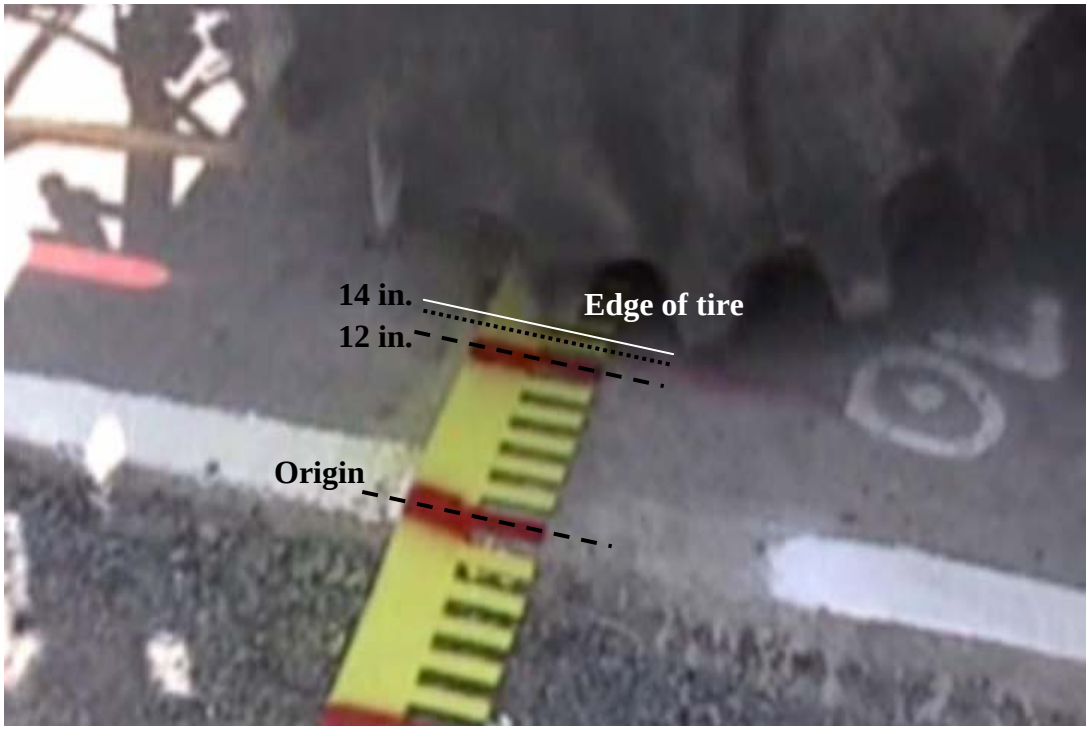

Figure 3.2. Zoomed in area of the snapshot

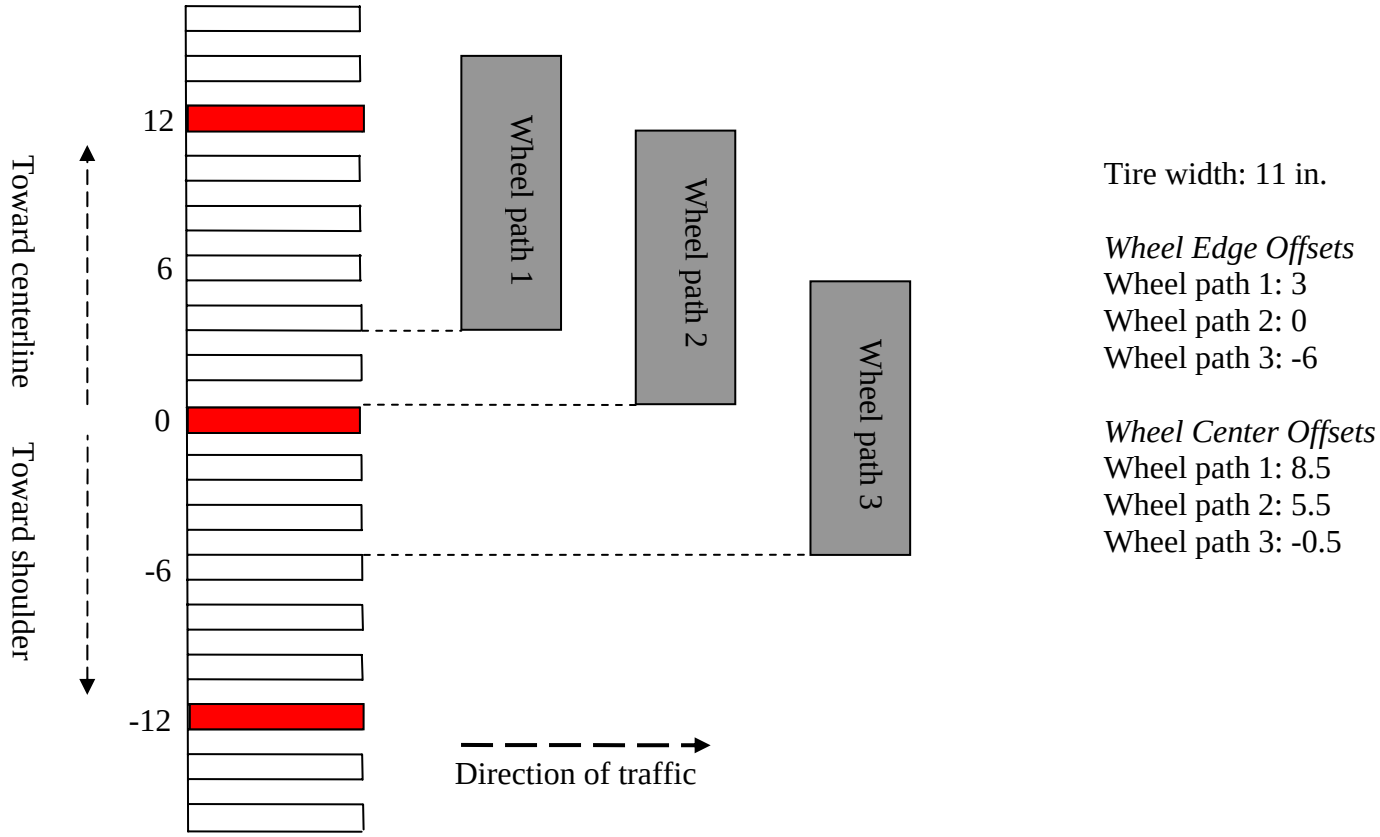

Figure 3.3. Wheel edge and wheel center offsets for a generic 11 in. tire width

3.2 Pavement Response Data

Several steps were required in analyzing the pavement response data. This includes the strain and stress data files acquired through the Megadec-TCS acquisition system and the LVDT data files acquired through the NI acquisition system. The process began with determination of which sensors were properly functioning. Next, the Peak-Pick analysis was performed on the data files to extract pertinent axle responses. The Peak-Pick output files were then filtered and arranged in a format which was convenient to perform further analysis.

3.2.1 Determining Sensor Status

Before any data analysis was performed, it was imperative to determine which of the installed sensors were giving adequate responses. This check was done randomly for each day of testing for at least five percent of the collected data. Example of responses from a properly functioning strain gage, earth pressure cell, and LVDT are shown in Figure 3.4 through Figure 3.6. Examples of responses from improperly functioning sensors are shown in Figure 3.7 and Figure 3.8. Improperly functioning sensors were determined when no trace of the response was found or the response was too noisy. A list of the sensor status for each test season is included in Appendix C.

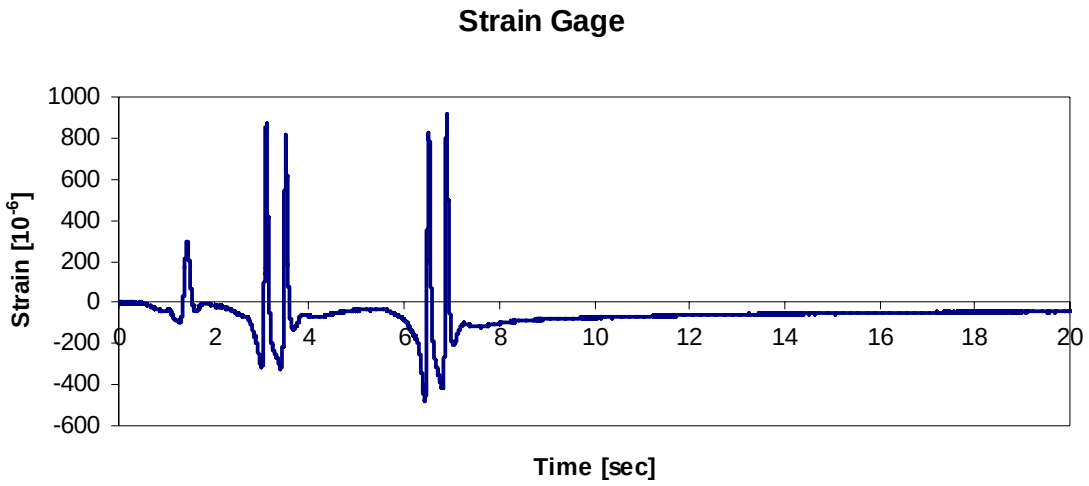

Figure 3.4. Response from a working strain gage

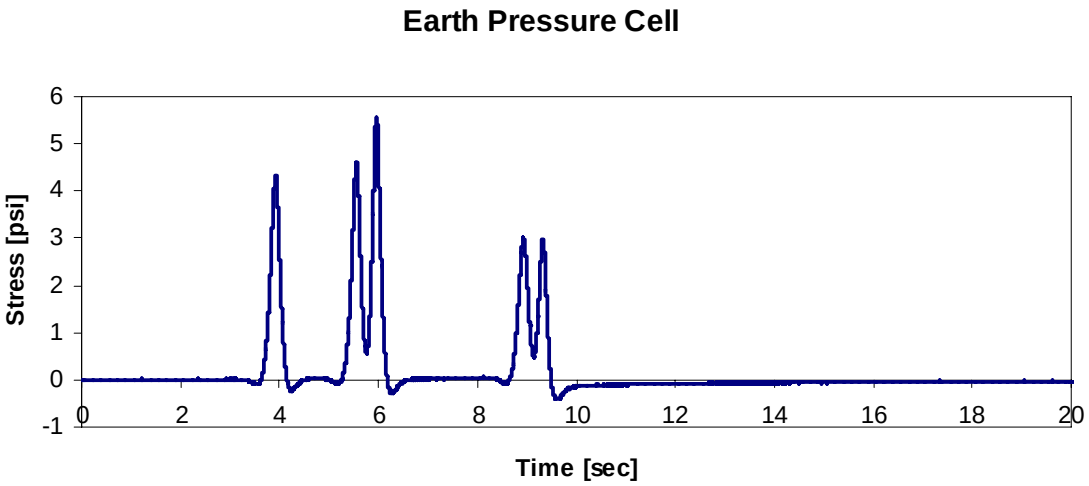

Figure 3.5. Response from a working earth pressure cell

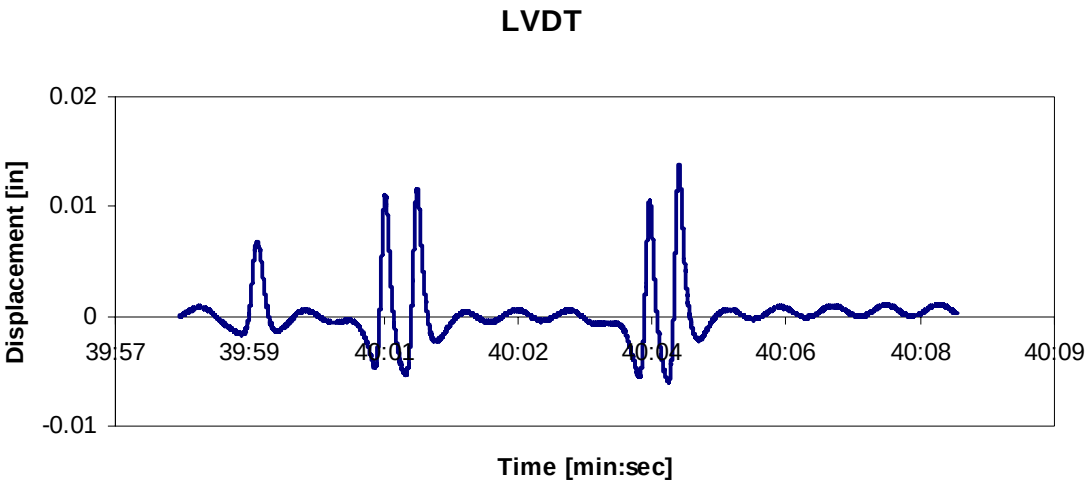

Figure 3.6. Response from a working LVDT

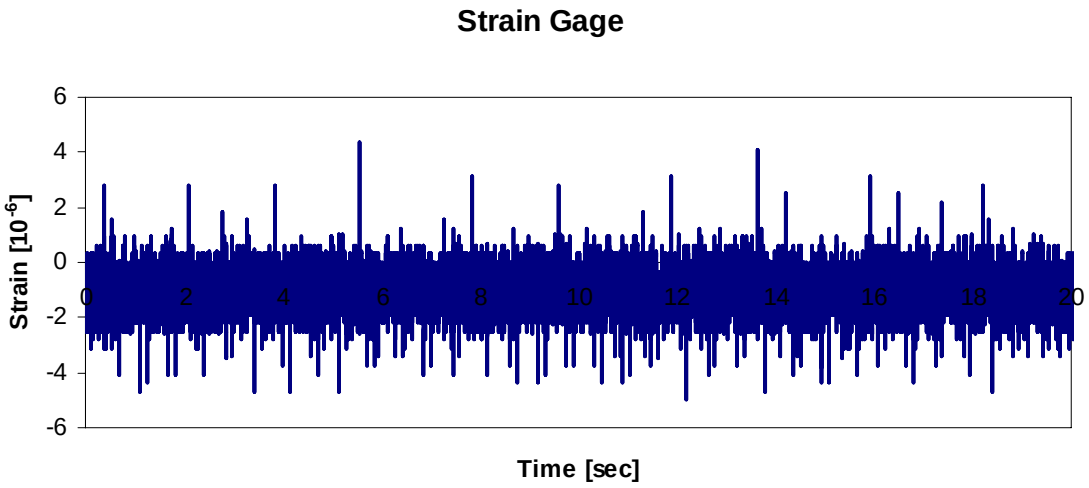

Figure 3.7. Response from a non-working strain gage

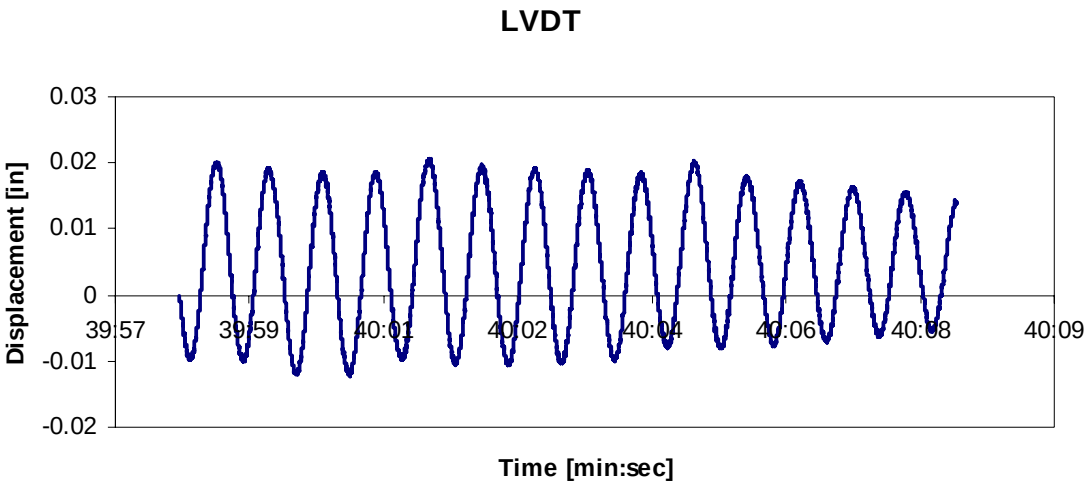

Figure 3.8. Response from a non-working LVDT

3.2.2 Peak-Pick Analysis

Due to the large amount of data points collected from one vehicle pass, a reduction process was necessary to extract characteristic parameters for each response measurement. To achieve this, the Peak-Pick program, developed for MnDOT by the University of Minnesota, Department of Electrical and Computer Engineering, was employed. For the purpose of this analysis, the Peak-Pick program was found to have sufficient efficiency in locating maximum and minimum pavement responses from the time history measurements generated by the vehicle pass. The following figure (Figure 3.9) shows the start-up screen for the Peak-Pick program and Table 3.1 gives a description of each of the options available on the start-up screen. Further elaboration of the information acquired for Table 3.1 and the Peak-Pick program can be found in the Peak-Pick User Guide [10].

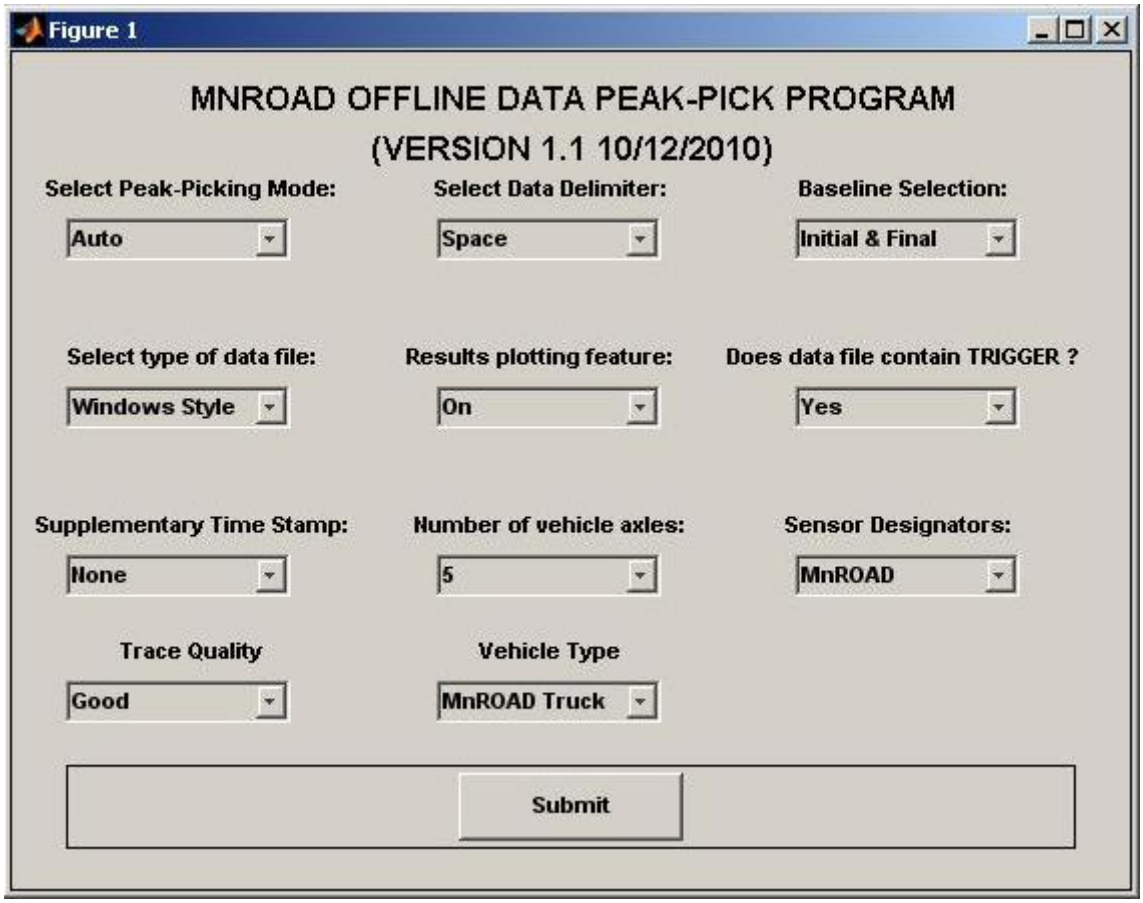

Figure 3.9. Peak-Pick start-up screen

Table 3.1. Peak-Pick program options

Option	Description
Peak-Picking Modes	Seven modes are available for peak picking: Auto, semi-auto, manual, output correction, sensor label correction, output file split, and FWD. In this analysis, only the auto and manual modes were utilized.
Data Delimiter	Data delimiter of the input files can be either space, comma, or tab separated. Data files used in this analysis are comma separated.
Baseline Selection	Baseline selections can be either initial as well as final baseline only or include intermediate baseline values. This option was left at initial and baseline values only.
Data File Type	Four options are available for data type: DOS1, DOS2, WINDOWS, and NI. Two of these selections were used in the analysis: WINDOWS and NI.
Results Plotting Feature	The plotting feature can be either turned on or off for storing the result plots for the response trace analyzed. This option was turned on to enable future checks if necessary.
Trigger Data	Some data files contain a trigger column and should be identified before proceeding with the analysis.
Supplementary Time Stamp	Supplementary time stamps can be present in the form of IRIGB or CIRIG information. In this analysis, no time stamps were present.
Number of Vehicle Axles	This program accommodates 2, 3, 4, 5, and 6 vehicle axles.
Sensor Designators	Sensor designators for the collected data files follow the MnROAD format.
Trace Quality	Trace quality can be either good or bad. This option is especially useful as an additional filtering if the trace is bad.
Vehicle Type	A feature which provides additional picking accuracy for a MnROAD type semi truck. The other option was selected for a non MnROAD semi truck.

Peak-Pick analysis was performed on all collected strain, stress, and deflection data. For this analysis, there were two methods for the data to be analyzed: automatic and manual modes. The automatic mode was the preferred approach. However, in some occasions the peaks and troughs of the waveform were not successfully detected. For those cases manual selection mode was required. In the manual selection, the Peak-Pick user manually picked the peaks of the waveform. A description of the analysis process using Peak-Pick, starting with the automatic selection and followed by manual selection mode is shown below.

Automatic Selection for Strain and Stress Data Files (from Megadec-TCS System)

1. The number of axles on each vehicle tested was identified prior to running the analysis.
2. Data files from the Megadec-TCS acquisition system for strain and stress measurements were previewed to determine if a trigger column was present.
3. On the Peak-Pick start-up window, the following options were selected:
   - Picking Mode: Auto
   - Data Delimiter: Comma
   - Baseline Selection: Initial and Final
   - Data File Type: WINDOWS style
   - Results Plotting Feature: On
   - Trigger Data: Determined by previewing data files
   - Supplementary Time Stamp: None
   - Number of Vehicle Axles: Determined in step 1
   - Sensor Designators: MnROAD
   - Trace Quality: Good, unless a majority of response measurements are bad
   - Vehicle Type: Other, unless the data file belongs to the MnROAD semi trucks (i.e. Mn80 or Mn102)
4. The "Submit" button was clicked and input data files to be analyzed were selected.
5. The directory in which the output file was to be written in was selected. The output file directories were arranged in a systematic file structure discussed later.
6. Finally, sensors that need to be analyzed were selected. Improperly functioning sensors were excluded in the selection. Since sensor names are unique from cell to cell, input data file selection corresponds to the same cell of the pavement section.

Automatic Selection for LVDT Data Files (from NI System)

1. Similar to strain and stress data files, the number of vehicle axles and presence of the trigger column in the data file was determined.
2. All selected options on the Peak-Pick start-up window remained the same as for the strain and stress data files except the following:
   - Data File Type: NI style
3. The remaining steps were identical to the strain and stress data file.

Peak-Pick auto selection mode generates three output items for each input data file after completing the analysis. The items are named in the following format:

- "Results_Auto[input filename].ASC" – contains results of analyzed sensors from the input file.
- "Not_Analyzed_Auto[input filename].ASC" – contains a list of non-analyzed sensors from the input file.
- "pp[input filename]" – a folder containing the result plots for both analyzed and non-analyzed sensors from the input file.

As stated previously, there were some occasions in which the Peak-Pick program, under automatic selection mode was unable to analyze a waveform of the pavement response measurement belonging to a particular sensor. In these cases, the manual selection mode was employed to determine the peaks and troughs of the response measurement for the unanalyzed sensor. Figure 3.10 shows an example of a successful automatic mode analysis and Figure 3.11 shows an example of an unanalyzed sensor waveform which requires manual mode. Unanalyzed sensors corresponding to the input file were listed in files named "Not_Analyzed_Auto[input filename].ASC". It is worth mentioning that some limitations exist for the Peak-Pick automatic selection mode. The detection of the baseline heavily depends on the overall response waveform. If the waveform itself did not contain a consistent baseline, Peak-Pick may select the tail end of the waveform as the baseline. Additionally, if the axle responses peak below the baseline, Peak-Pick will

not be able to select them automatically. In these cases, manual selection of the peaks was required. The following steps describe the Peak-Pick manual selection process.

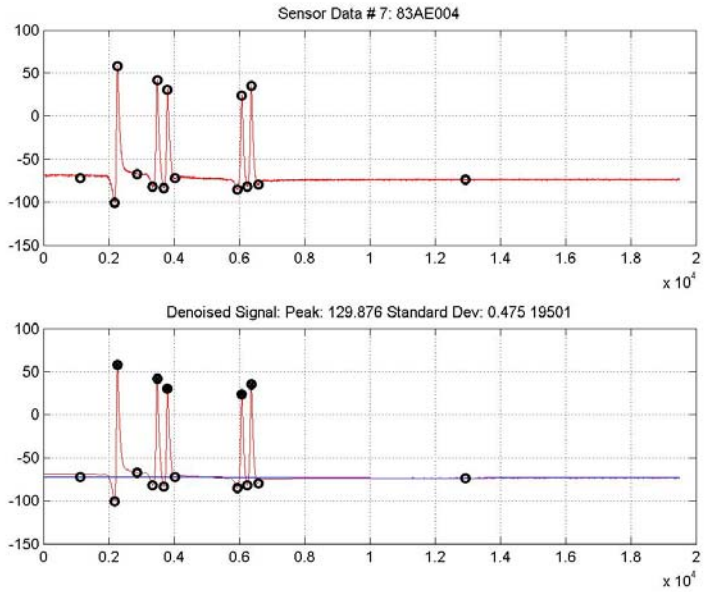

Figure 3.10. Successful automatic selection of Peak-Pick analysis

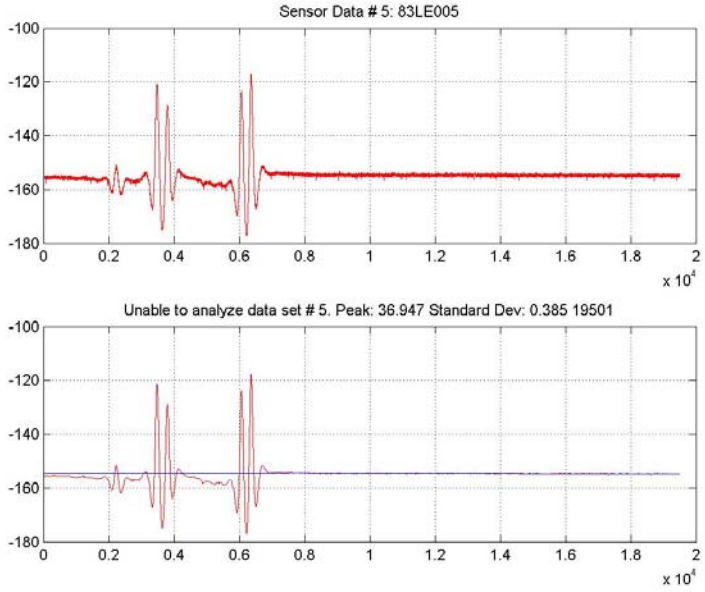

Figure 3.11. Sensor waveform requiring manual selection of Peak-Pick analysis

Manual Selection for Strain and Stress (Megadec-TCS System) and LVDT (NI System)

1. The list of sensors which required manual analysis with Peak-Pick was obtained from the "Not_Analyzed_Auto[input filename].ASC" file for the corresponding input file.
2. Presence of the trigger column and number of vehicle axles were identified for the input data file.
3. All selected options on the Peak-Pick start-up window remained the same as for the strain and stress data files except the following:
   - Picking Mode: Manual
   - Data File Type: WINDOWS style for strain and stress data, NI style for LVDT data
4. The "Submit" button was clicked and the input data file corresponding to the sensor(s) that were not analyzed in automatic mode was selected.
5. Unanalyzed sensors listed within the corresponding "Not_Analyzed_Auto[input filename].ASC" file were selected.
6. When manually selecting peaks, instructions appear in the Peak-Pick window.
7. First, the region of interest was zoomed in to magnify the waveform. Next, the peak axle responses were selected. After this, Peak-Pick will automatically detect the troughs. If peak selections were unsatisfactory, the option to re-pick peaks was selected. Additionally, changes to baseline selections were made if automatic baseline values were inappropriate.
8. This process was repeated for subsequent unanalyzed sensors within the input data file.

Peak-Pick manual selection mode generates two output items for each input data file after completing the analysis. The items are named in the following format:

- "Results_Manual[input filename].ASC" – contains results of analyzed sensors from the input file.
- "pp[input filename]" – a folder containing the result plots for the analyzed sensors from the input file.

3.2.3 Summarizing Peak-Pick Output

Both outputs from the automatic, "Results_Auto[input filename].ASC" and manual, "Results_Manual[input filename].ASC" selection modes generate results in the same format. Table 3.2 gives a description of each column in the output file. The first three columns of the output file represent the sensor identifiers. The following four columns show the time and date when the data was collected. Columns eight to eleven contain the bulk of the information required for this study. The remaining two columns were used for verification and quality control purposes.

Table 3.2. Description of Peak-Pick output result file

Column Number	Column Name	Description
1	Cell Number	Cells 83 and 84 for flexible pavement and Cells 32 and 54 for rigid pavement sections.
2	Sensor	Alphabetical designations given to strain gages, earth pressure cells, and LVDTs.
3	Sensor Number	Numerical designations given strain gages, earth pressure cells, and LVDTs immediately after alphabetical designation.
4	Data Collection Date	Date in which input data file was collected.
5	Hour	Hour in which input data file was collected.
6	Minute	Minute in which input data file was collected.
7	Second	Second in which input data file was collected.
8	Elapsed Time	Elapsed time (in seconds) from the start of the sensor response waveform where the point was extracted.
9	Point Identifier	Identifies the point as baseline (B#), inflection point (IP#), or axle response (AX#).
10	Point Value	Value of response at each point.
11	Peak/Trough/Baseline	Identifies if the point selected is baseline (B), peak (P), or trough (T). This decision is based on the initial baseline.
12	Signal-Noise Ratio	Signal-to-noise ratio (SNR) of the sensor response waveform.
13	Analysis Date	Date in which input file was analyzed using Peak-Pick.

Peak-Pick stores the results in a format which is not customized for this study. To simplify subsequent data analyses, the essential information from the automatic and manual selection output files were combined and arranged into a fashion defined by the columns shown in Table 3.3. Unlike the Peak-Pick output result file, each row in the summary table should correspond to the results for one sensor. In addition, all values corresponding to each sensor were adjusted by subtracting the base value reading.

Table 3.3. Peak-Pick Summary

Column Number	**Column Name**	**Description**
1	Peak-Pick Output Directory	Directory where Peak-Pick output files were stored.
2	Peak-Pick Output Filename	Peak-Pick output filename in .ASC format.
3	Vehicle ID	Unique designations given to tested vehicles.
4	Pass Number	Number which acts as an identifier for a particular combination of controlled test parameters. This number was used when extracting or cross-referencing data for any parameter combinations.
5	Wheel Center Offset	Observed distance from the outer edge of the last axle of the vehicle's tire to the pavement edge.
6	Cell Number	Cells 83 and 84 for flexible pavement and Cells 32 and 54 for rigid pavement section.
7	Sensor ID	Flexible pavement sections consist of nine strain gages (LEs, AEs, TEs), three earth pressure cells (PGs), and three LVDTs each. Rigid pavement sections: Cell 54 contains four strain gages and ten LVDTs, Cell 32 contains six strain gages and two earth pressure cells.
8	Elapsed Time (*n*)	Elapsed time (in seconds) from the start of the sensor response waveform at which point *n* was extracted.
9	Point Identifier (*n*)	Identifies point *n* as baseline (B#), inflection point (IP#), or axle response (AX#).
10	Point Value (*n*)	Extracted value at point *n* of the response trace. Units for strain, stress, and deflection correspond to the raw data file.
11	Peak/Trough/Baseline (*n*)	Identifies if point *n* selected is baseline (B), peak (P), or trough (T). This decision is based on the initial baseline.

An additional table was created on top of the Peak-Pick Summary table. This table contains the maximum and minimum values for each sensor response as per Table 3.4 titled Peak-Pick Max-Min. This table was also supplemented with information such as actual vehicle speed computed from the axle responses, vehicle traffic wander, and vehicle offset relative to the sensor location. A simple Microsoft Excel's Visual Basic for Application macro was written and used extensively in this procedure.

Table 3.4. Peak-Pick Max-Min

Column Number	**Column Name**	**Description**
1	Peak-Pick Output Directory	Directory where Peak-Pick output files were stored.
2	Peak-Pick Output Filename	Peak-Pick output filename in .ASC format.
3	Vehicle ID	Unique designations given to tested vehicles.
4	Pass Number	Number which acts as an identifier for a particular combination of controlled test parameters. This number was used when extracting or cross-referencing data for any parameter combinations.
5	Wheel Center Offset	Observed distance from the outer edge of the last axle of the vehicle's tire to the pavement edge.
6	Sensor ID	Flexible pavement sections consist of nine strain gages (LEs, AEs, TEs), three earth pressure cells (PGs), and three LVDTs each. Rigid pavement sections: Cell 54 contains four strain gages and ten LVDTs, Cell 32 contains six strain gages and two earth pressure cells.
7	Axle	Axle corresponding to maximum value.
8	Max Value	Maximum value of all point values.
9	Axle	Axle corresponding to minimum value.
10	Min Value	Minimum value of all point values.
11	Speed 1	Actual speed computed from time elapsed and distance between first two axles.
12	Speed 2	Actual speed computed from time elapsed and distance between second and third axles.
13	Relative Offset	Wheel center offset relative to sensor location.

3.3 Tekscan Measurements

The objective of conducting the Tekscan test was to obtain tire footprints and contact stress distributions for the vehicles tested in this study. Tekscan measurements were used to obtain the relative vertical stress distributions for each wheel at various load levels. These distributions were then adjusted using the total wheel weight to obtain the actual contact stress distribution. This involved the following steps:

1. Save Tekscan measurements into the ".fsx" format file.
2. Open the ".fsx" file using the I-Scan software.
3. For each wheel, identify the frames with the clearest footprint measurment.
4. Perform linear calibration by selecting the "Tools" pull-down menu and providing length, force, and pressure units.
5. Select the "Frame" button to input the frame number identified earlier for a wheel.
6. Enter the total applied force which corresponds to the wheel load at the tested load level.
7. Save the calibration file (.cal) and movie file (.fsx) separately.

This process was repeated for each wheel in the remaining axles contained in the ".fsx" movie file. A calibration file should exist for each wheel. These calibration files can be loaded separately for further analysis through the calibration menu by selecting the "Load Calibration File" button. Next, the following describes the process to estimate the tire's contact area together with its load distribution from Tekscan measurements.

1. The Tekscan ".fsx" file was opened in I-Scan. The calibration file corresponding to the wheel of interest was loaded and the frame identified in the above process containing the footprint measurement was selected.
2. In the "File" pull-down menu, the "Save ASCII" option was chosen. A "Save ASCII" window appears. Frame data was selected for "Data Type" and "Current

Frame" for Movie Range. Note that frame data should be in terms of contact pressure. The file was then saved as an ASCII, ".asf" file.

3. Load the saved ASCII file in Microsoft Excel. Notice that each cell in the Excel spreadsheet corresponds to one sensel of the Tekscan sensorial mat. Values in the cells represent the pressure exerted onto the sensel. Each sensel has the dimensions 0.6693 in. × 0.6693 in. or area of 0.44796 in^2.
4. Coordinates for each cell in both the horizontal and vertical directions of the entire frame with the origin located at the bottom left corner were introduced.
5. Non-zero entries of the frame were determined to indentify the outline of the gross area of the footprint.
6. Although the contact area and contact stress of the vehicle's footprint was obtained directly from the I-Scan, the values were double checked in this process by multiplying the number of nonzero cells by the sensel area of 0.44796 in^2 to obtain the net contact area, A_{net}. The contact stress was determined by dividing the known wheel load by this net area.
7. The net area was carefully dissected into separate sections shaped as squares (equal number of horizontal and vertical cells of nonzero entries). A maximum number of ten sections were permitted to estimate the net area. This was done by selectively counting the cells in both directions making sure that the dissected squares do not overlap.
8. Each section was represented as a circular area with evenly distributed load in the layered elastic analysis. Therefore, each section must be transformed into a circle with equal area.
9. The centroid of each section weighted by the applied pressure of each sensel was determined. Pressure at sensel i was denoted as P_i located at coordinates (x_i, y_i).
10. The x-coordinate and y-coordinate of the centroid of section n was denoted as $\bar{x}_n$ and $\bar{y}_n$, respectively where

$$\bar{x}_n = \frac{\sum (x_i P_i)_n}{\sum (P_i)_n} \text{ and } \bar{y}_n = \frac{\sum (y_i P_i)_n}{\sum (P_i)_n}$$

11. Coordinates computed here were converted into inches by multiplying with the sensel dimensions of 0.6693 in. in both directions.
12. The area of each section, A_n was computed by multiplying the number of nonzero cells within the section by the sensel area of 0.44796 in^2. Knowing the area of each section, the radius, r_n was subsequently computed.
13. The load applied, F_n onto each section n was determined through

$F_n = \left(\frac{A_n}{A_{net}} \right) (F_{total})$, where F_{total} is the applied wheel load.

The above approach makes use of the applied pressure on each sensel to estimate locations of each section. The location and size of the section's circular area conceptually represents the load distribution of the footprint. Hence it is possible to have these areas overlap. Figure 3.12 illustrates an example of the estimated contact area for a particular footprint.

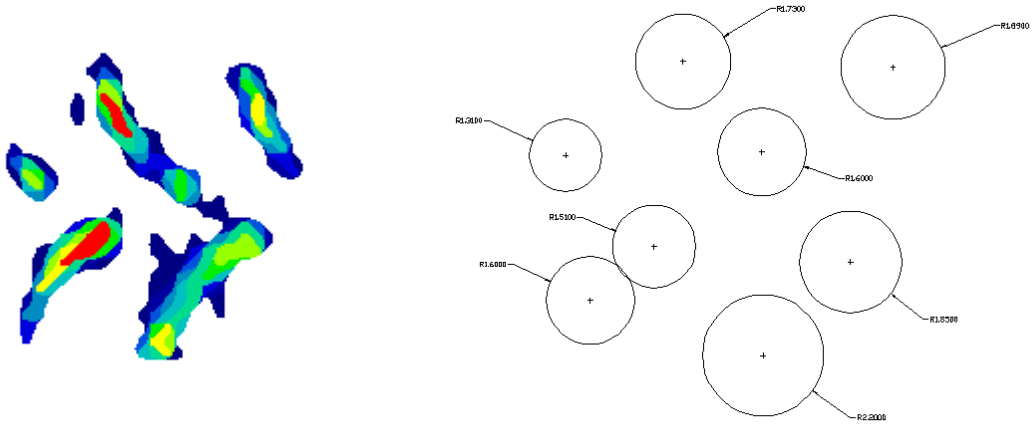

(a) (b)

Figure 3.12. Example of footprint (a) measured using Tekscan (b) multi-circular area representation

3.4 Data Archiving

A consistent structure of folders and sub-folders was created to systematically archive the data collected in each test run. The organization process began with reference to the test program for a given test day and season. Video recordings and Peak-Pick output files were also organized in a similar fashion.

3.4.1 Pavement Response Data

The raw data files were divided and placed into separate folders and subfolders according to the test date, cell number, set number, and data type. The file organization structure with described tiers of folders and subfolders are shown in Table 3.5. The following is an example for a case of strain and stress raw data from 24 August 2009 at 0% load level for Cell 84.

- Field data
  - 08-24-09 0% load
    - Cell 83
    - Cell 84
      - 08-24-09_set1_0%_LVDT-C84
      - 08-24-09_set1_0%_SP-C84
      - 08-24-09_set2_0%_LVDT-C84
      - 08-24-09_set2_0%_SP-C84
        - Raw data files
  - 08-25-09 50% load
  - 08-26-09 50% & 100% load
  - 08-27-09 100% load
  - 08-28-09 50% & 100% load concrete

Table 3.5. Description of folders and subfolders for raw pavement response files

Folder Tier	Designation	Description
1	Field data	The root folder containing all pertinent raw data.
2	[Date]-[Load%]	A subfolder for each day of testing and load levels.
3	[Cell #]	A subfolder for each cell.
4	[Date]-[Set #]-[Load%]-[Data Type]-[Cell #]	A subfolder for each set and data type. There were generally 2 types of data: SP (for strain and pressure) and LVDT. The cell number was included in the designation for clarity.
5	Raw data files	Each data file was named corresponding to the cell number, date of testing, and set number. Each file corresponds to a particular test in accordance with the filled test program.

3.4.2 Video Files

The video files were stored according to test date and cell number. Table 3.6 shows the file organization structure for archiving the video files. The following is an example for video files recorded on 26 August 2008 at 0% load level for Cell 84.

- Videos
  - 08-26-08
    - Cell 83
    - Cell 84
      - Video files
  - 08-27-08
  - 08-28-08
  - 08-29-08

Table 3.6. Description of folders and subfolders for video files

Folder Tier	Designation	Description
1	Videos	The root folder containing all video files.
2	[Date]	A subfolder for each day of testing.
3	[Cell #]	A subfolder for each cell.
4	Video files	Each video file was named according to load level, pass number, target speed, target offset, and vehicle ID.

3.4.3 Peak-Pick Output

The output files generated from the Peak-Pick analysis was organized in a similar fashion to the raw data pavement response file structure. In addition to the file structure for raw data files, two new tiers were added with naming conventions "[Cell #]-[Load Level]-[Vehicle ID]" and "[Peak-Pick Selection Mode] Results". The Peak-Pick output result files should be organized according to the format shown in Table 3.7. An example for the case of 0% load level, Cell 84, Strain and Stress data, Set 2, Vehicle T6 is shown subsequently.

- Peak-Pick Results
  - 0% load
    - Cell 83
    - Cell 84
      - 08-24-09_set1_0%_LVDT-C84
      - 08-24-09_set1_0%_SP-C84
      - 08-24-09_set2_0%_LVDT-C84
      - 08-24-09_set2_0%_SP-C84
        - C84_0%_Mn80
        - C84_0%_Mn102
        - C84_0%_R5
        - C84_0%_T6
          - Auto_Results
            - Peak-Pick auto output files
          - Manual_Results
            - Peak-Pick manual output files
  - 50% load
  - 100% load
  - 50% load concrete
  - 100% load concrete

Table 3.7. Format for folders and subfolders for Peak-Pick output files

Folder Tier	**Designation**	**Description**
1	Peak-Pick Results	The root folder containing all pertinent Peak-Pick data.
2	[Load%]	A subfolder for every load level.
3	[Cell #]	A subfolder for each cell.
4	[Date]-[Set #]-[Load%]-[Data Type]-[Cell #]	A subfolder for each set and data type. There are 2 types of data: SP (for strain and pressure) and LVDT. The cell number was included in the designation for clarity.
5	[Cell #]-[Load%]-[Vehicle]	A subfolder for each tested vehicle.
6	[P-P Selection Mode]-Results	A subfolder separating auto or manual peak selections in Peak-Pick.
7	P-P output files	Generated output files from running Peak-Pick.

Chapter 4 Data Analysis

An evaluation of relative pavement damage induced by various types of agricultural equipments was conducted by comparing measured pavement responses (asphalt strains and subgrade stresses) generated by these vehicles. This chapter presents the analysis based on a comparison of the maximum responses obtained from the vehicle passes. As described in Chapter 3, the Peak-Pick program was used to extract the maximum responses.

Pavement responses are influenced not only by axle loading, but also other factors including environmental effects, pavement structure, and vehicle wheel path (traffic wander). Therefore, these factors should be accounted for in the analysis. The effect of vehicle traffic wander, seasonal changes, time of testing, pavement structure, vehicle weight, tire type, and vehicle speed on measured asphalt strains and subgrade stresses are discussed.

4.1 Effect of Vehicle Traffic Wander

The test program was designed to accommodate the effects of vehicle wheel path. Target offsets were set at various transverse distances from the fog line that the vehicle operator was directed to follow. In addition, the actual traffic wander was measured during the test, as explained in the previous chapters.

The results of the testing confirmed the importance of the traffic wander parameter. It was observed that traffic wander not only affects the maximum response from the same vehicle, but also affects which axle would result in the maximum response. Figure 4.1 and Figure 4.2 show an example of maximum asphalt strains and subgrade stresses, respectively, for five passes generated by vehicle T6 axles at an 80% load level in spring 2009. Note that the horizontal axis in the figures (Rear axle relative offset) denotes the

distance from the center of the most rear wheel axle relative to the location of the sensor; in the case for vehicle T6, the most rear axle is axle 4. It can also be observed that when the rear axle is centered above a sensor, the front axles pass the sensor with an offset. Figure 4.1 demonstrates that the maximum asphalt strain generated by T6 was from the rear axle when the offset was -2 in. For offsets from 11 to 15 in., the maximum asphalt strains were not only reduced by approximately one-third, but the front axles caused higher stains that the rear. It can be observed from Figure 4.2 that the maximum subgrade stress from the T6 vehicle occurred when the offset was 3 in. At this offset and all others, the last axle caused the maximum stress. However, the magnitude of the maximum stress dropped sharply when the offset increased to 11 or more inches.

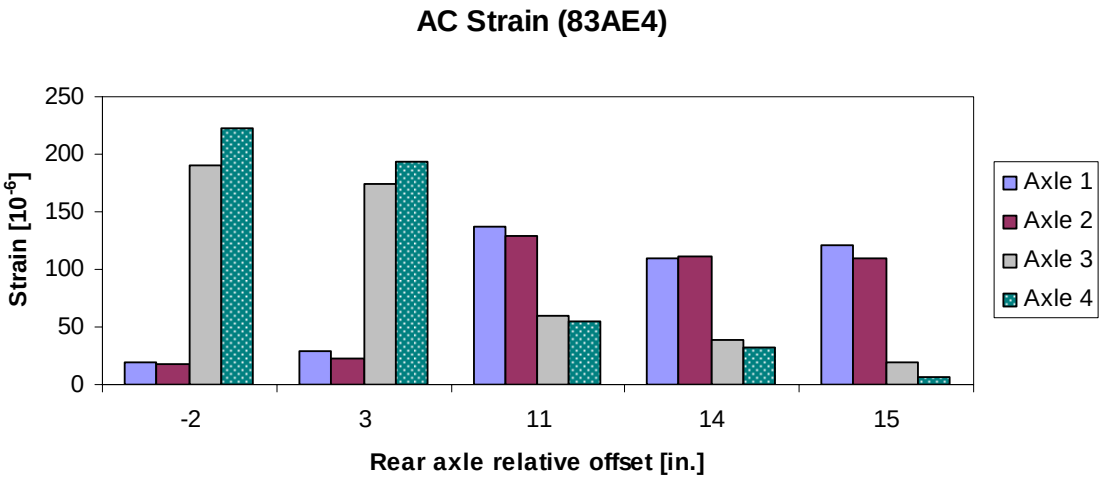

Figure 4.1. Asphalt strain axle responses for vehicle T6 at 80% load level

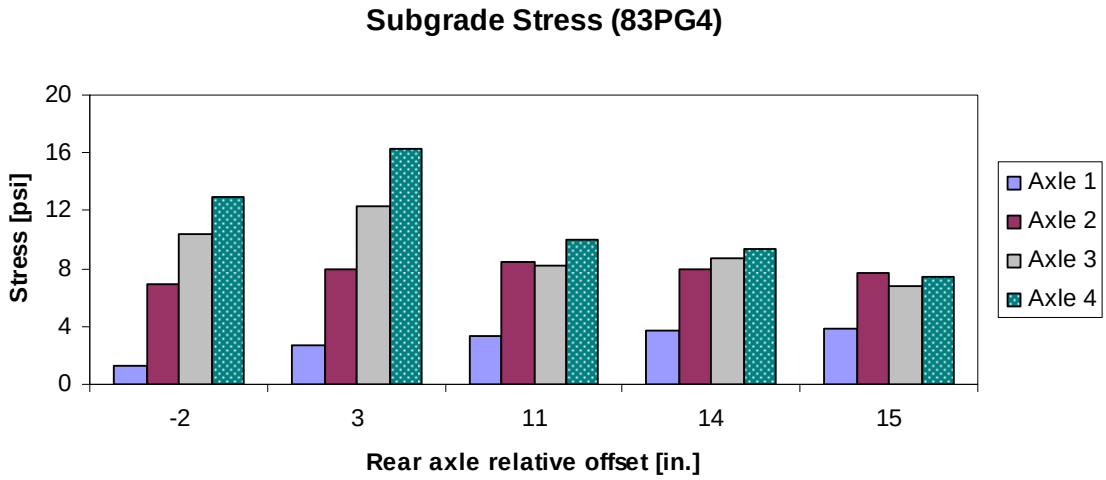

Figure 4.2. Subgrade stress axle responses for vehicle T6 at 80% load level

4.2 Effect of Seasonal Changes

The properties of a pavement structure are dependent on environmental conditions such as moisture content and temperature. In winter, the saturated base and subgrade layers would freeze, causing a significant increase in stiffness. As the temperature increases, the frozen base layer begins to thaw, resulting in an undrained condition as the water becomes trapped between the impermeable asphalt layer and the frozen subgrade within the pavement structure. During this period, the cohesionless and saturated base and subgrade layers will experience a decrease in stiffness and strength as thawing continues. The overall structural capacity of the pavement will be reduced significantly. This is the main reason for spring load restrictions in regions experiencing freeze-thaw environments. Furthermore, the elastic and viscoelastic properties of the asphalt layer are both susceptible to temperature changes. At low temperatures, asphalt becomes stiff and behaves as a brittle material. At higher temperatures, the asphalt stiffness is reduced and the material is more ductile.

With these effects in mind, field testing was conducted twice a year in the spring and fall seasons. Test vehicles were selected based on availability, application frequency, and recommendations by the industry. Ideally, each vehicle should have been tested at least once in the spring and once in the fall season. However, due to availability constraints, this could not be fulfilled. It should be noted that in some instances, a slightly different type of tractor model was tested in place of the original tractor with the tanker remaining the same. To maintain consistency, the capacity and axle configuration of these replacement tractors were aimed to be as similar to the original as possible.

MnROAD standard 80-kip truck Mn80 was used as the control vehicle throughout this study. Therefore, its pavement responses were used as the reference measurements to evaluate the effects of seasonal changes on pavement response. It is important to note that the number of passes made by Mn80 varied for different testing days. Fewer passes of Mn80 could result in less coverage of different wheel path offsets. This has potential to ultimately affect the maximum response measurements, since the offset causing the highest response may not have been covered. The number of passes made by Mn80 on a particular test day at the flexible pavement section is summarized in Table 4.1. Figure 4.3 through Figure 4.7 show the maximum asphalt strain and subgrade stress values for each test day from Cells 83 and 84 from Mn80. It can be observed that there are significant seasonal variations in the measured stresses and strains. In addition, there are some significant daily fluctuations in the measured responses due to temperature variation.

Table 4.1. Number of passes made by Mn80 at the flexible pavement section

Day	Number of Passes
S08-day1	2
S08-day2	4
F08-day1	15
F08-day2	20
F08-day3	5
S09-day1	15
S09-day2	13
S09-day3	12
S09-day4	20
F09-day1	29
F09-day2	28
F09-day3	41
F09-day4	44
S10-day1	68
S10-day2	71
S10-day3	72
F10-day1	68
F10-day2	74
TOTAL	601

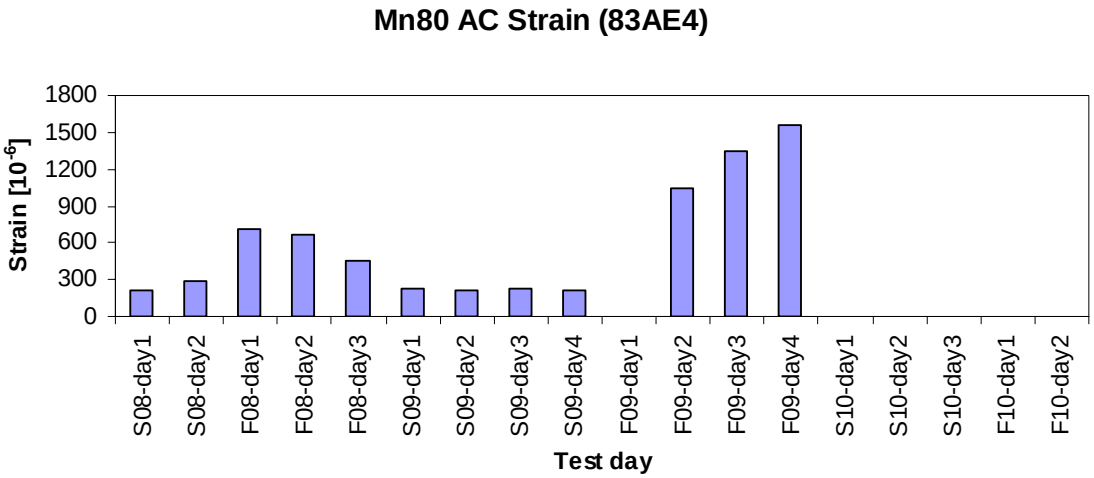

Figure 4.3. Cell 83 angled asphalt strain generated by vehicle Mn80

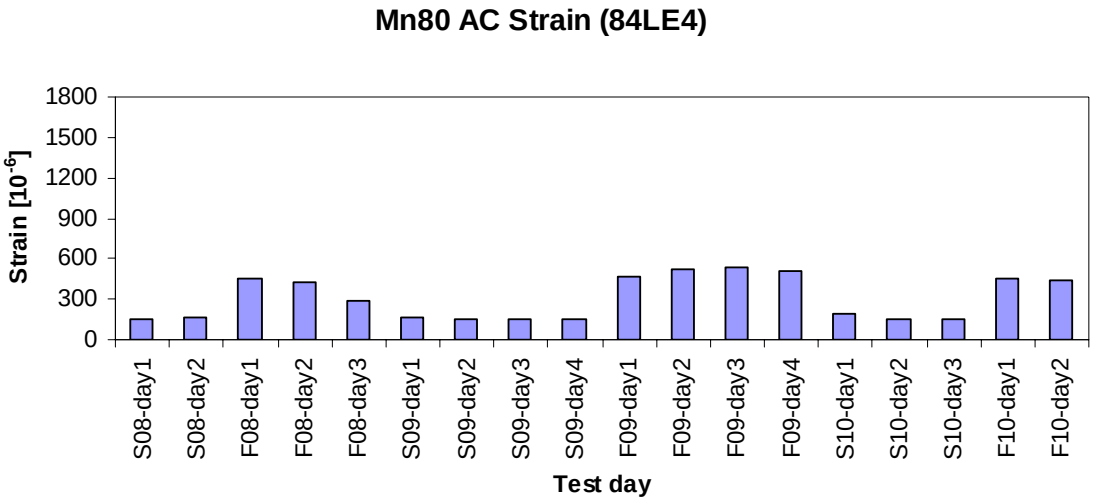

Figure 4.4. Cell 84 longitudinal asphalt strain generated by vehicle Mn80

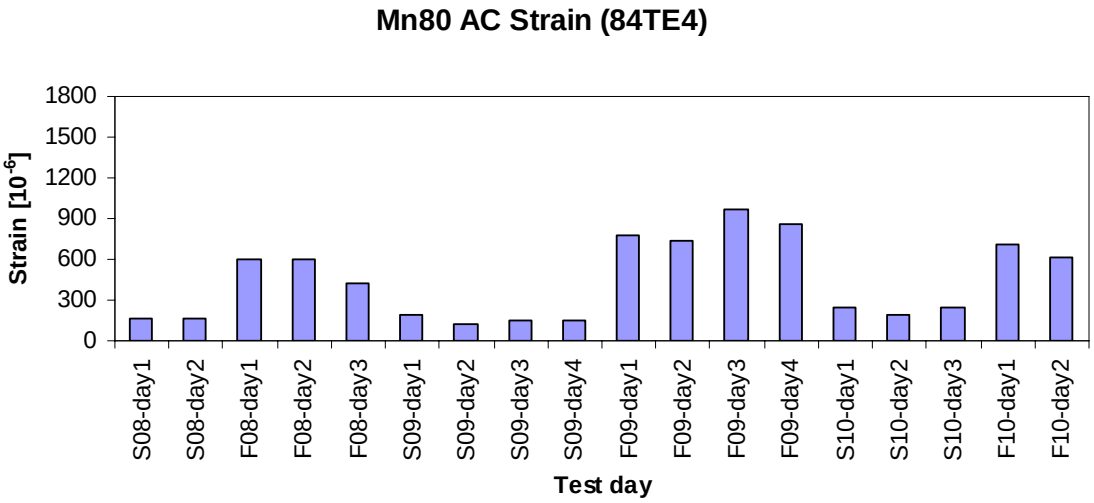

Figure 4.5. Cell 84 transverse asphalt strain generated by vehicle Mn80

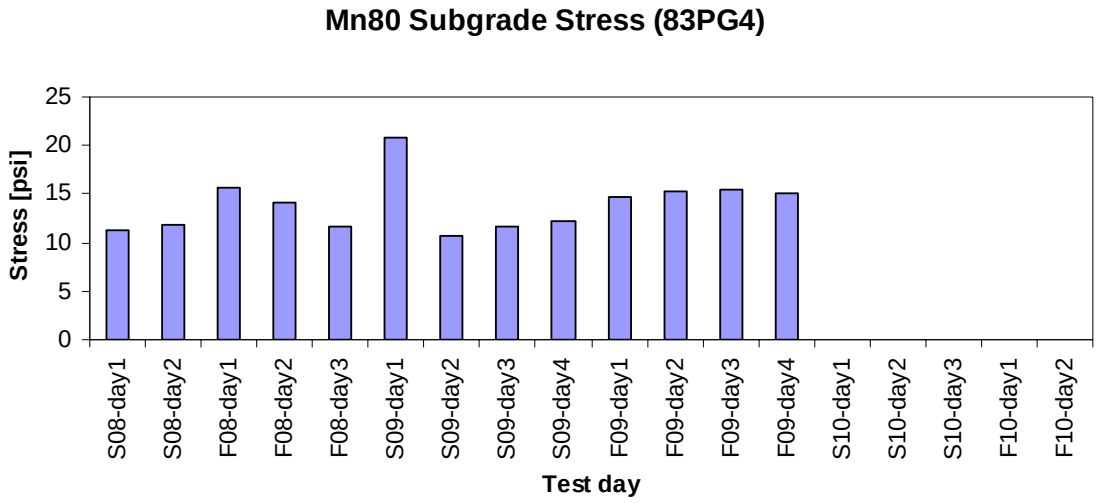

Figure 4.6. Cell 83 vertical subgrade stress generated by vehicle Mn80

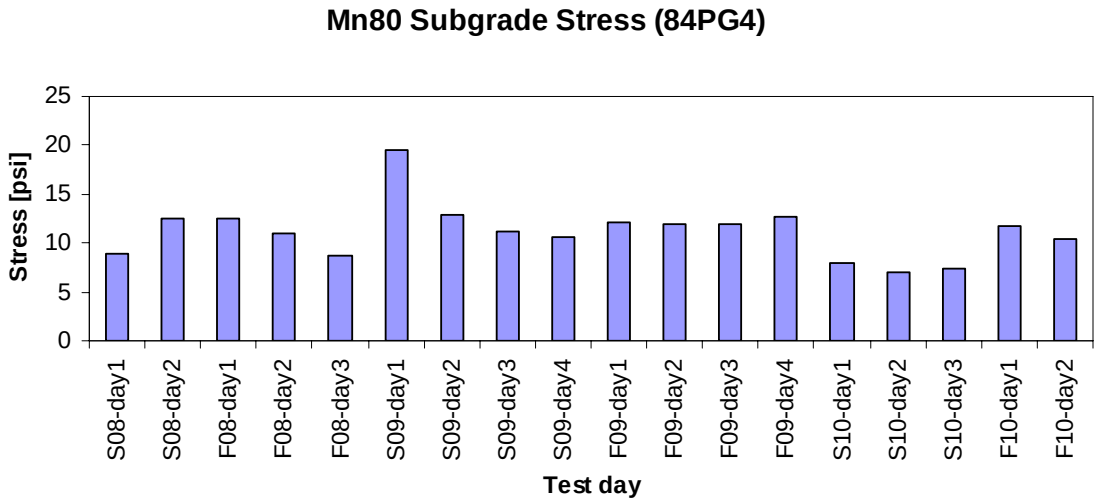

Figure 4.7. Cell 84 vertical subgrade stress generated by vehicle Mn80

Figure 4.3 through Figure 4.5 show that measured asphalt strains were lower in the spring seasons compared to the fall seasons for both Cells 83 and 84. In the spring, the average angled strain (strain gage 83AE4) in Cell 83 was only 23% of the average angled strain in fall. Average longitudinal strain (strain gage 84LE4) in Cell 84 during spring was 34% of the average longitudinal strain during fall. Average transverse strain (strain gage

84TE4) in Cell 84 during spring was 25% of the average transverse strain in fall. This trend was anticipated, since with warmer pavement temperatures, asphalt stiffness is reduced, which leads to higher strains. A 2-sample *t*-test was performed to compare maximum asphalt strains generated between spring and fall seasons. At a 0.05 significance level, the *t*-test suggested that the strain responses in the spring were lower than in the fall. It was also observed that transverse strains were generally larger than longitudinal strains under vehicle Mn80. The higher strain measurements in fall suggest that the asphalt layer is more susceptible to fatigue like damage during that season.

The unusually large angled strains in Cell 83 during fall 2009 testing was assumed to be caused by additional external factors influencing the strain gage. The pavement section at Cell 83 failed during spring 2009 due to a longitudinal crack, followed by immense rutting at approximately fifteen feet from the sensor array. The failed section was repaired in preparation for fall 2009, but once again failed during testing. In this case, the failure was located approximately four feet from the sensor array. This failure most likely caused changes within the pavement structure and in turn, affected the material properties of the structure within close proximity of the strain gage. Conversely, the pavement section at Cell 84 exhibited no visible damage.

The average maximum subgrade stress in the spring was 90% and 95% of the maximum stresses in the fall for Cell 83 (earth pressure cell 83PG4) and Cell 84 (earth pressure cell 84PG4), respectively. Although this implies that subgrade stresses were only slightly higher in fall compared to spring, there were no strong correlations for measured vertical subgrade stresses with test seasons. Notice that a spike in subgrade stress occurred on day 1 of spring 2009. A possible explanation for this occurrence is the frequent freeze-thaw cycle in spring. During spring (or late spring), the frozen base and subgrade layers should begin to thaw, greatly reducing the stiffness and strength of those layers. The reason that the spike on day 1 of spring 2009 shows otherwise could be due to the subgrade layer, which was still frozen. Excluding the spike on day 1 of spring 2009, the *t*-test suggested that there was a difference between maximum measured subgrade

stresses in the fall and spring seasons at Cell 83, but not at Cell 84. A more thorough examination should be performed to investigate subgrade stresses as a function of moisture content within the base and subgrade layers.

The comparisons of the responses from the 80-kip MnROAD truck (Mn80) could not be reproduced for other agricultural vehicles directly because the vehicle weights were varied for each day. In order to demonstrate the seasonal effects on pavement responses for other vehicles, a correction factor was introduced (see section titled "Effect of Vehicle and Axle Weight"). Apart from the apparent effects of seasonal changes on pavement responses, the results also suggest that daily fluctuations in asphalt strains and subgrade stresses exist. The subsequent section examines how temperature changes during the day affect pavement responses.

4.3 Effect of Time of Testing

The test program was designed to account for changing pavement temperatures as well. For example, during the time of testing in one day the pavement temperature varied from 80ºF to 87ºF in the fall of 2009 and from 40ºF to 50ºF in the spring of 2009. Since the asphalt layer properties are highly sensitive to temperature changes, it is crucial to capture pavement responses generated by these heavy vehicles at various pavement temperatures. To do so, testing for one day at the same load level was conducted at two times: in the morning and in the afternoon. By doing so, the larger difference between pavement temperatures was successfully distinguished, where morning (AM) tests represented colder temperatures and afternoon (PM) tests represented warmer temperatures.

For the sake of this comparison, the maximum axle response measurements from each of the vehicle passes were extracted and plotted against the last axles' position relative to the sensor location. Figure 4.8 through Figure 4.11 show the maximum response distribution across the pavement width relative to the sensor location at Cell 84 for

vehicle Mn80 for spring and fall seasons. Figure 4.12 through Figure 4.15 show the extracted maximum strain and stress responses between morning and afternoon tests for Cell 84 during spring and fall seasons for tested vehicles.

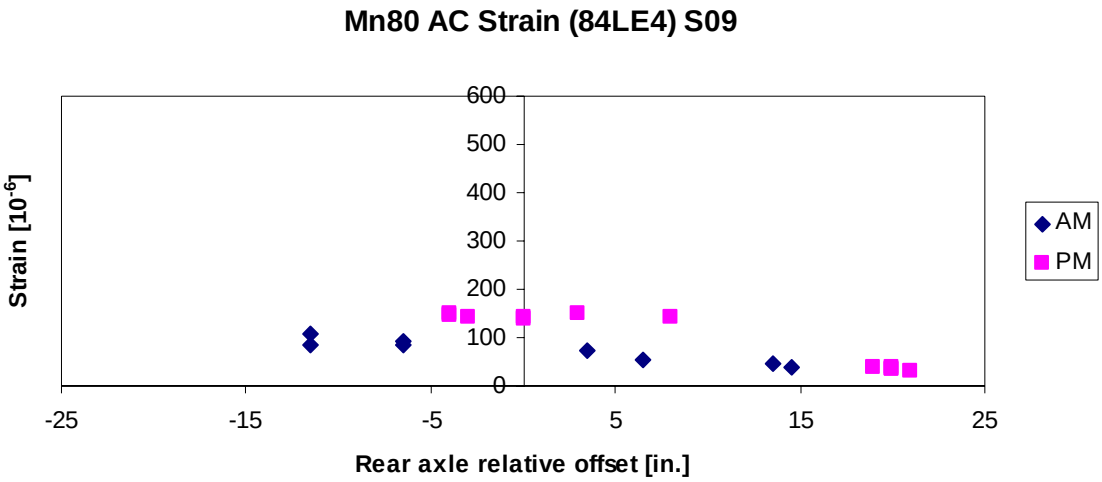

Figure 4.8. Cell 84 longitudinal asphalt strain generated by Mn80 in spring 2009

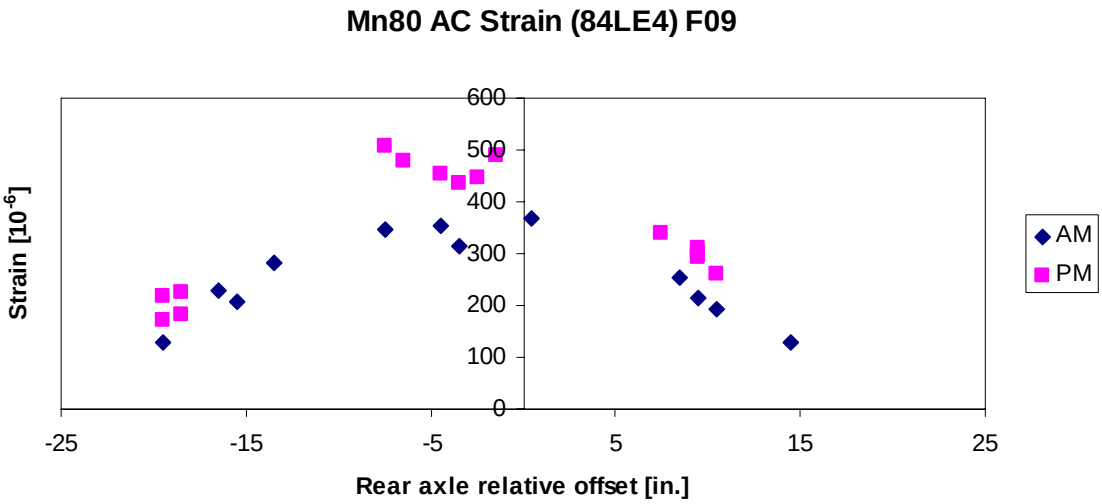

Figure 4.9. Cell 84 longitudinal asphalt strain generated by Mn80 in fall 2009

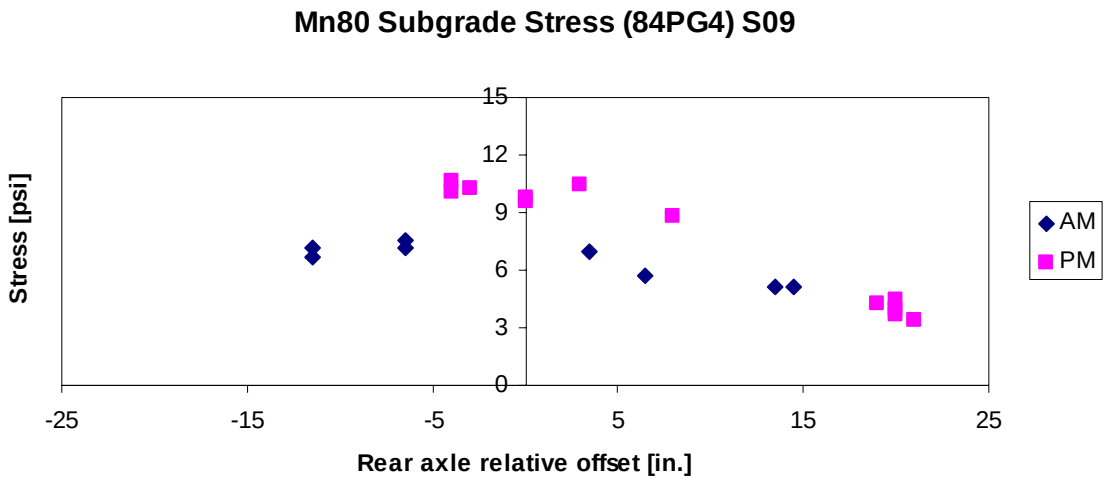

Figure 4.10. Cell 84 vertical subgrade stress generated by Mn80 in spring 2009

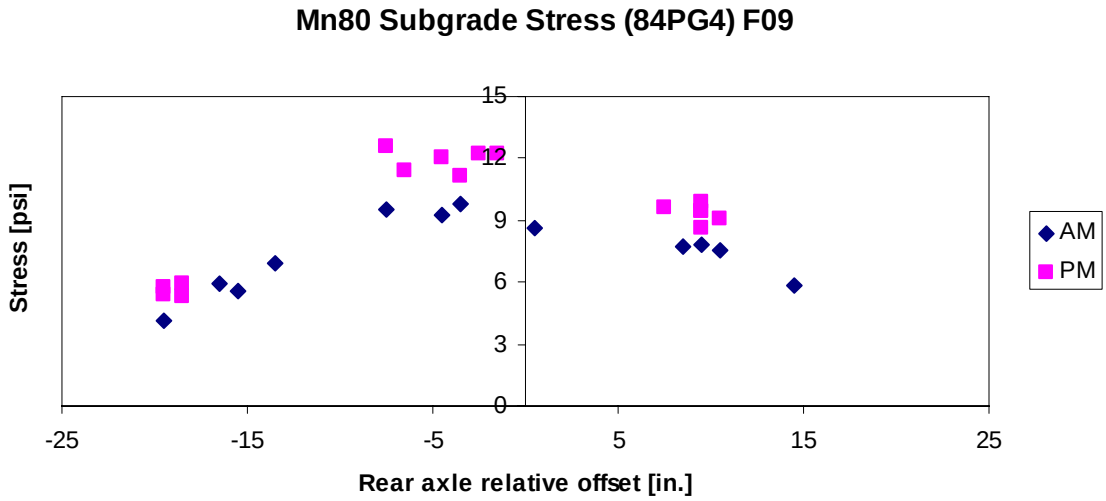

Figure 4.11. Cell 84 vertical subgrade stress generated by Mn80 in fall 2009

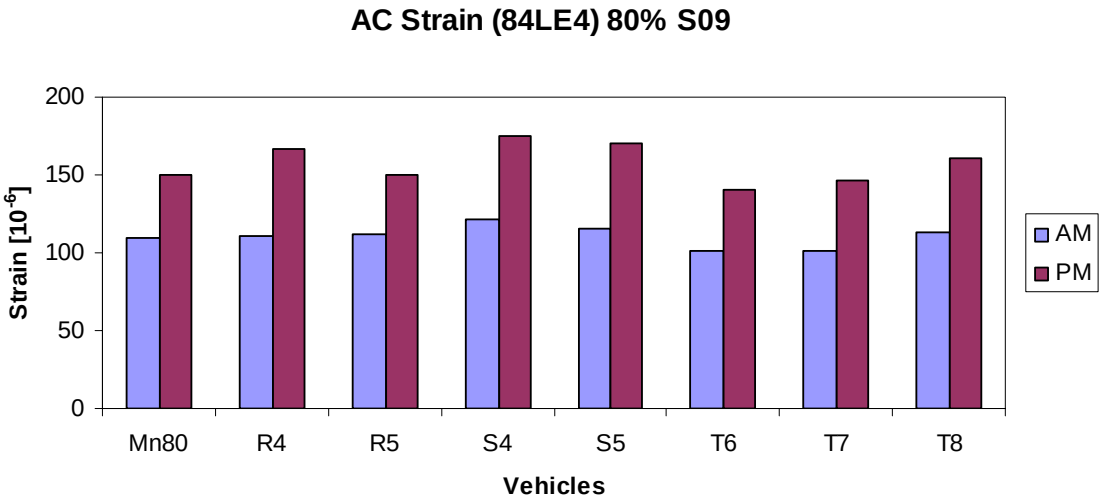

Figure 4.12. Morning and afternoon maximum longitudinal asphalt strains at Cell 84 for vehicles loaded at 80% load level in spring 2009

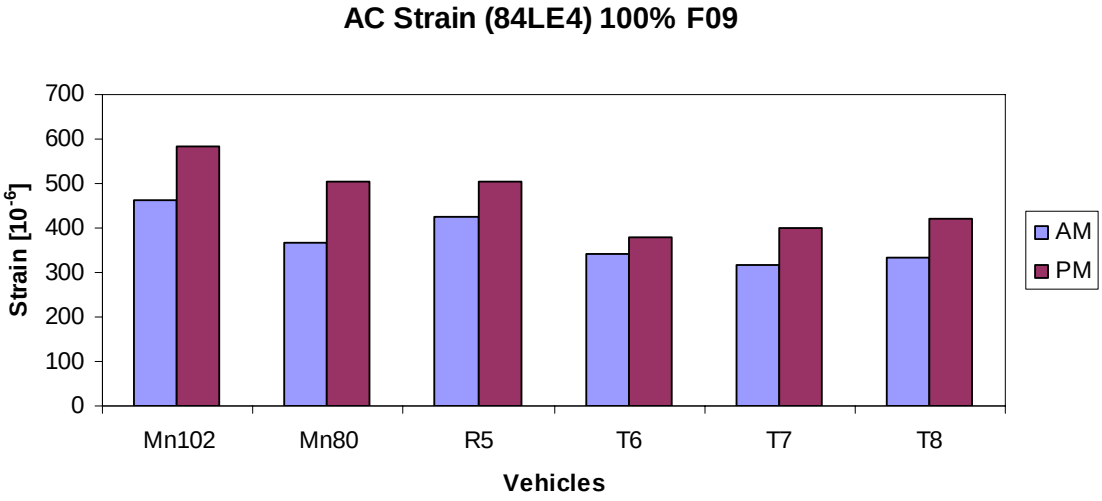

Figure 4.13. Morning and afternoon maximum longitudinal asphalt strains at Cell 84 for vehicles loaded at 100% load level in fall 2009

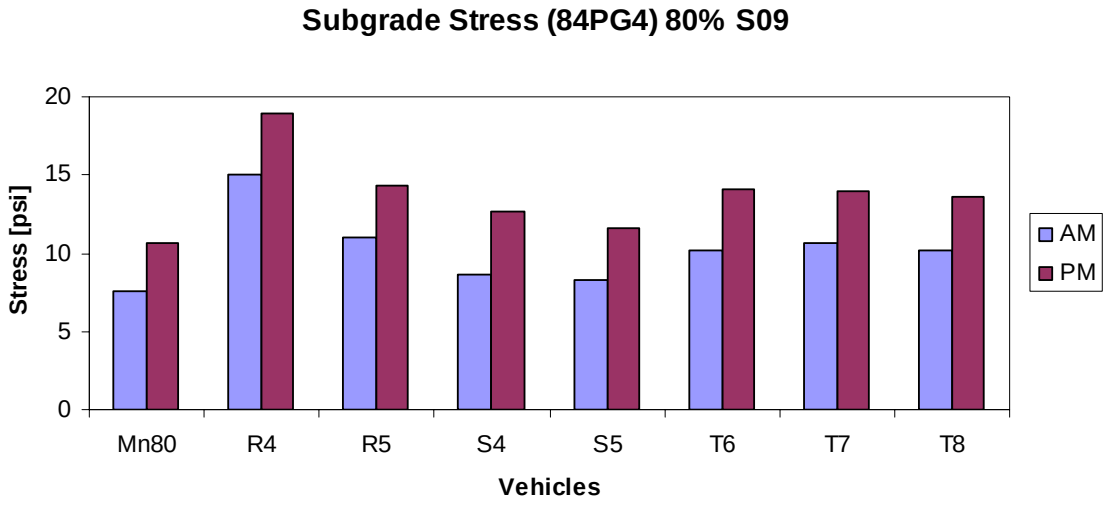

Figure 4.14. Morning and afternoon maximum vertical subgrade stresses at Cell 84 for vehicles loaded at 80% load level in spring 2009

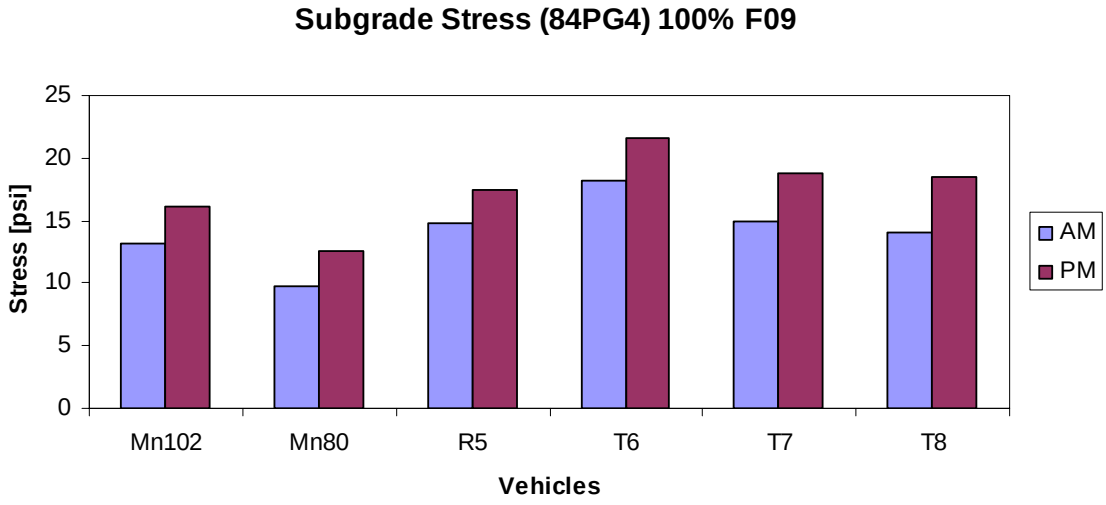

Figure 4.15. Morning and afternoon maximum vertical subgrade stresses at Cell 84 for vehicles loaded at 100% load level in fall 2009

Figure 4.8 through Figure 4.11 indicate that Mn80 passes in the afternoon (PM) generate larger asphalt strains and subgrade stresses compared to tests performed in the morning (AM). For the same relative offset, longitudinal asphalt strains measured in spring 2009 exhibit a difference of approximately 50% between AM and PM testing. However, the difference for similar offsets was roughly 30% in fall 2009. On the other hand, recorded subgrade stresses yielded a 30% difference in spring and 20% difference in fall between AM and PM testing. It is evident that temperature changes effects both strain and stress responses. This observation for vehicle Mn80 is a recurring trend for all other tested vehicles. Figure 4.12 through Figure 4.15 represent the extracted maximum strain and stress responses generated by the respective vehicles across the pavement width between morning and afternoon tests. The paired *t*-test was performed to test the significance between morning and afternoon responses for agricultural vehicles loaded at 80% and 100 % load levels in spring 2009 and fall 2009 tests, respectively. At a 0.05 significance level, the *t*-test suggested that both asphalt strains and subgrade stresses measured in the spring and fall seasons were indeed larger in the afternoon than in the morning.

Preliminary observations suggest that asphalt strains and subgrade stresses were significantly lower in the morning than in the afternoon. To be more precise in evaluating this issue, pavement response measurements should be corrected for asphalt temperature. Additionally, pavement distress development was not observed during testing in the morning sessions and significant displacements of the pavement surface were clearly visible in the afternoon sessions as the loaded agricultural vehicles made their passes. The pavement cross-section characteristics also influenced pavement responses as discussed in the next section.

4.4 Effect of Pavement Structure

Two flexible pavement sections were constructed specifically for this study at the MnROAD facility. Table 2.1 describes the structural geometry of the flexible pavement sections. The objective was to evaluate the effect of asphalt and base layer thicknesses, as well as shoulder type, on pavement responses. To achieve this objective, the maximum strain and stress responses across the pavement width were extracted for each vehicle and compared between Cell 83 (thin section) and Cell 84 (thick section). Due to failure of longitudinal and transverse strain gages in Cell 83 and angled strain gage in Cell 84, a comparison between strains with the same orientation was not possible. Instead, the largest values among the longitudinal and transverse strains from Cell 84 were compared against angled strains from Cell 83. Bar charts in Figure 4.16 through Figure 4.23 show the measured responses.

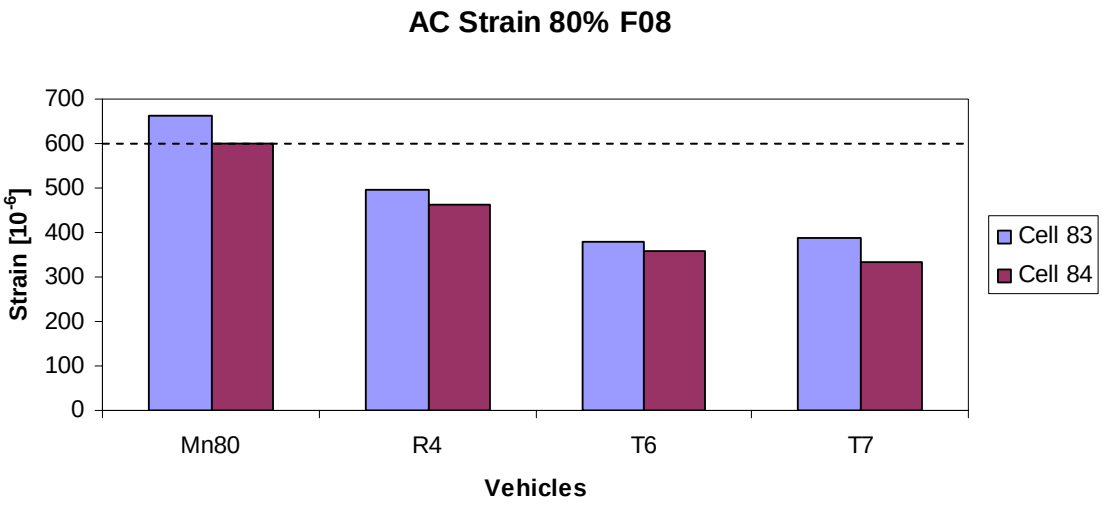

Figure 4.16. Maximum asphalt strains between Cell 83 and 84 for fall 2008 at 80% load level

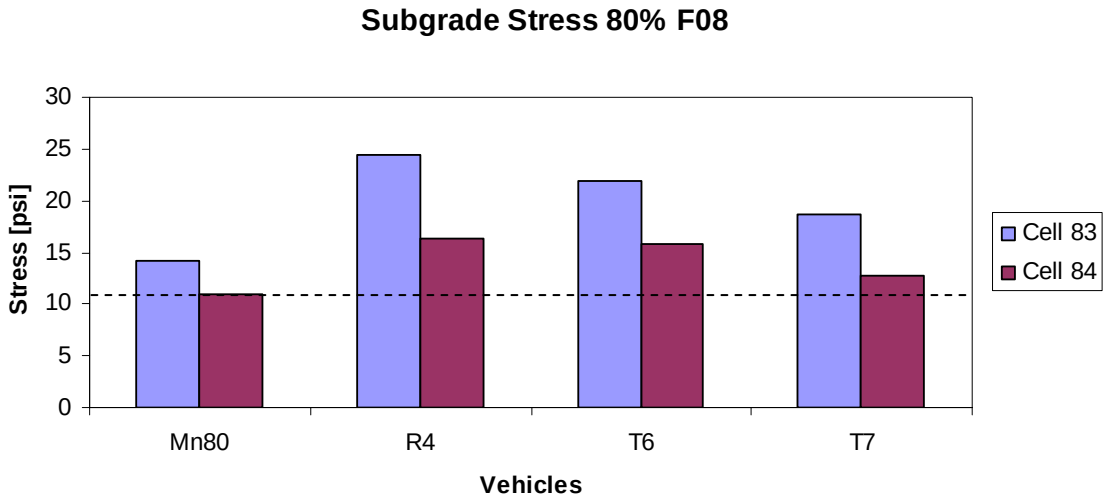

Figure 4.17. Maximum subgrade stresses between Cell 83 and 84 for fall 2008 at 80% load level

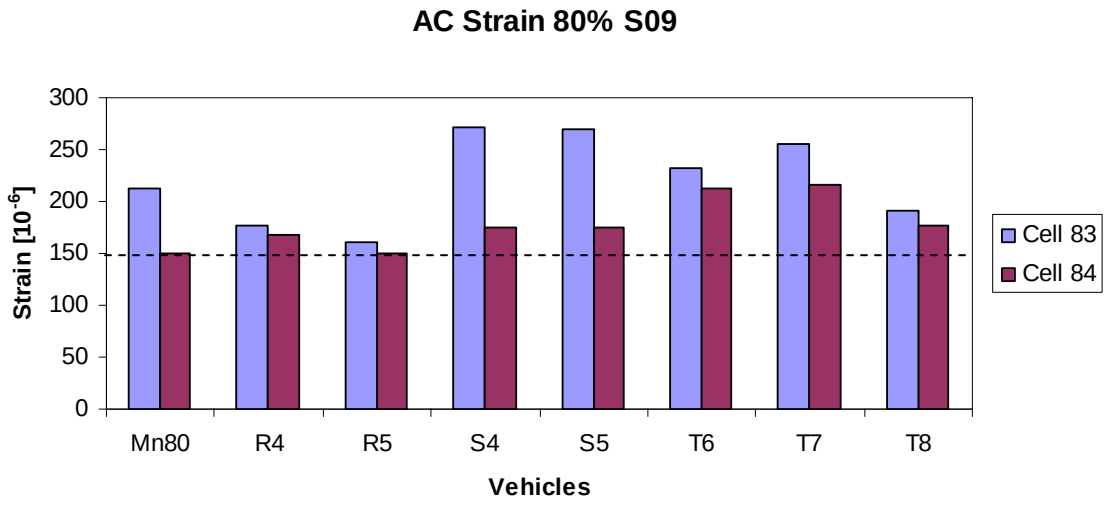

Figure 4.18. Maximum asphalt strains between Cell 83 and 84 for spring 2009 at 80% load level

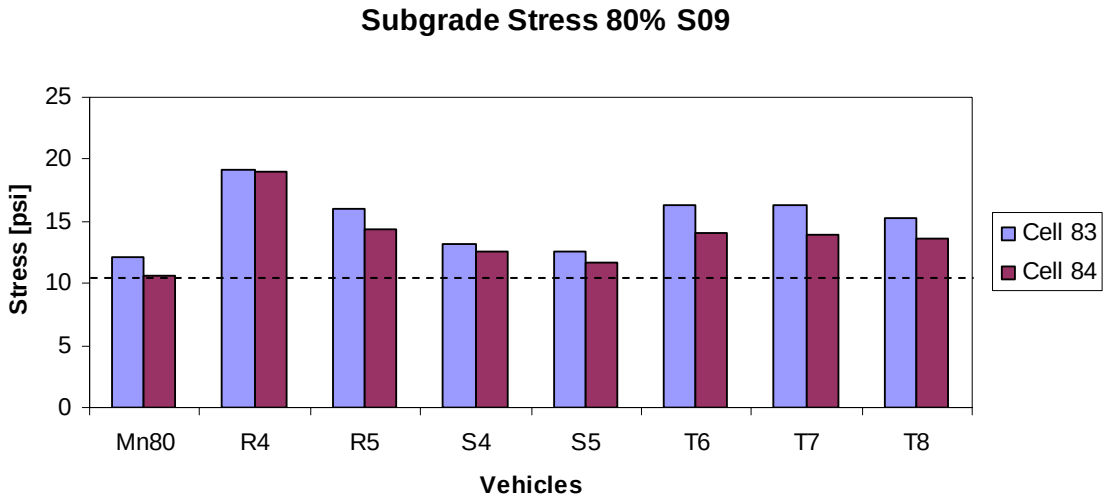

Figure 4.19. Maximum subgrade stresses between Cell 83 and 84 for spring 2009 at 80% load level

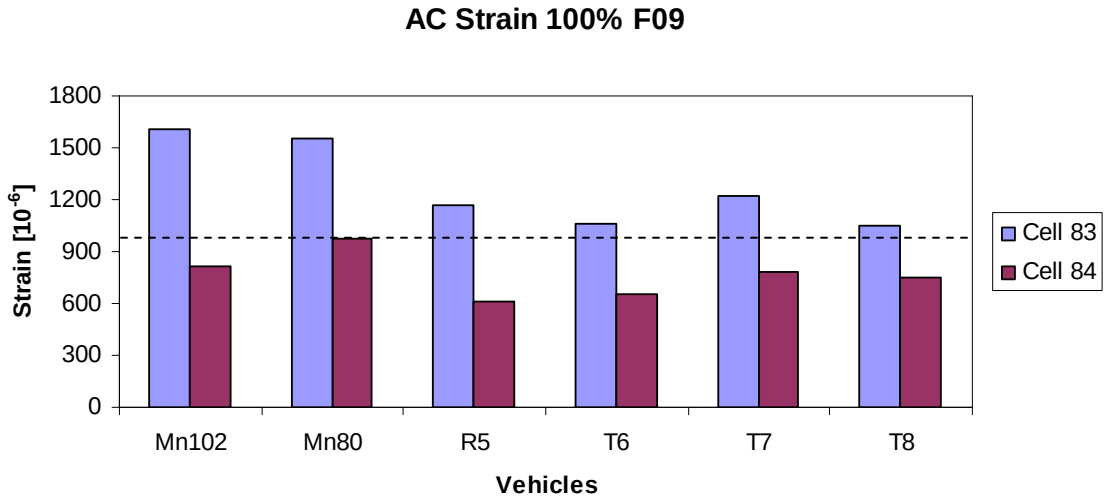

Figure 4.20. Maximum asphalt strains between Cell 83 and 84 for fall 2009 at 100% load level

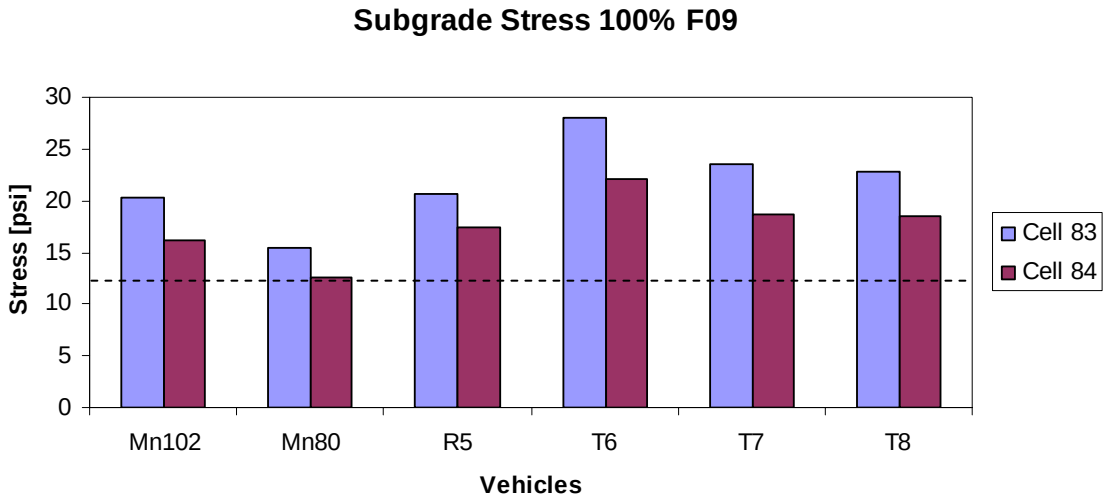

Figure 4.21. Maximum subgrade stresses between Cell 83 and 84 for fall 2009 at 100% load level

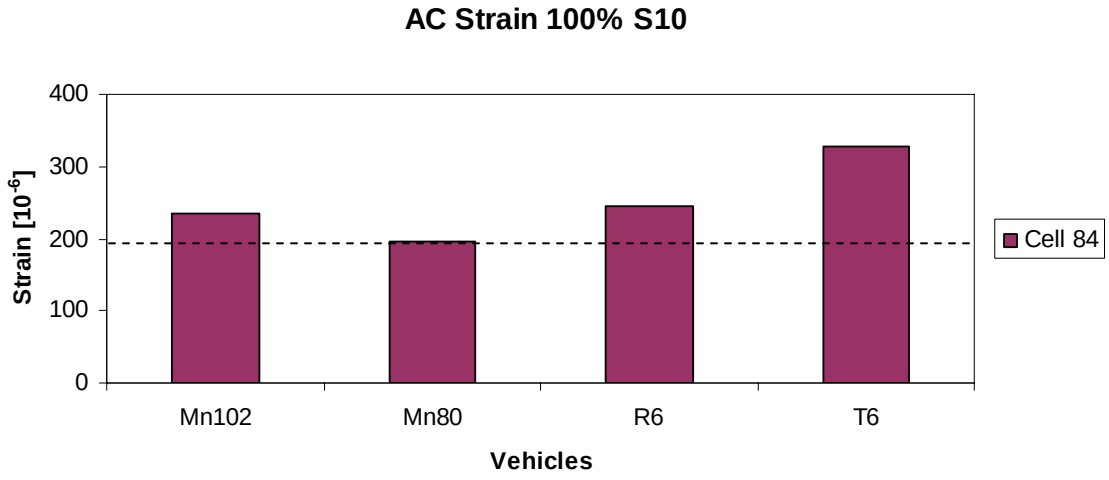

Figure 4.22. Maximum asphalt strains of Cell 84 for spring 2010 at 100% load level

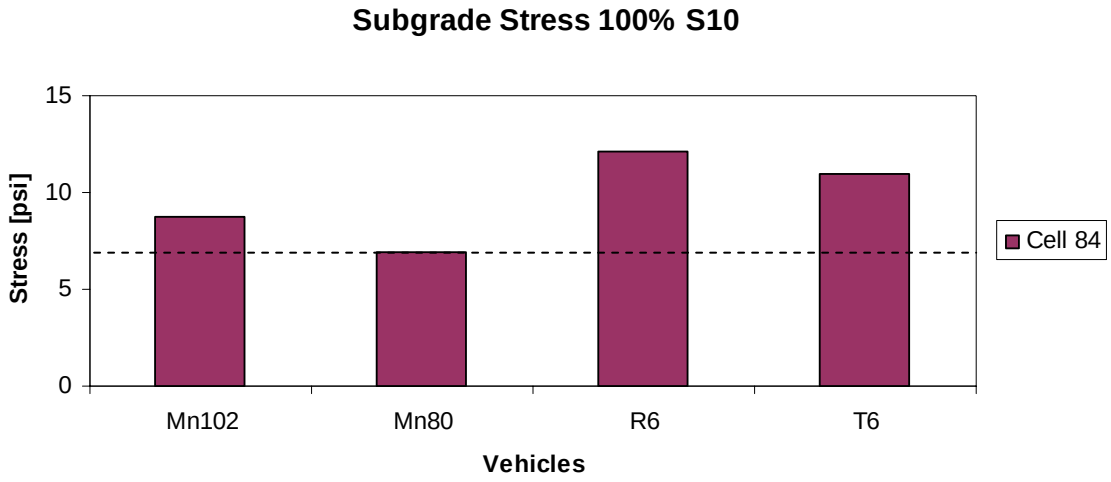

Figure 4.23. Maximum subgrade stresses of Cell 84 for spring 2010 at 100% load level

As expected, the thicker asphalt and base layers of Cell 84 resulted in lower asphalt strains and subgrade stresses. This overall trend was true for all vehicles at every test season. The horizontal dashed line in the bar charts indicate the maximum response generated by the Mn80 vehicle at Cell 84. Cell 84 was designed as a 10-ton road on which an 80-kip semi (Mn80) can legally travel on in any season. Cell 83 was designed with a significantly lower capacity, as a 7-ton road. Asphalt strains generated by the agricultural vehicles R4, T6, and T7 loaded at 80% in fall 2008 were lower than Mn80, but the opposite occurred for subgrade stresses. In spring 2009 however, agricultural vehicles S4, S5, R4, R5, T6, T7, and T8 loaded at 80% recorded higher strain and stress responses compared to Mn80. In fall 2009, agricultural vehicles R5, T6, T7, and T8 loaded at 100% recorded lower strains than Mn80, but higher subgrade stresses.

As expected, subgrade stresses produced by Mn80 were consistently lower than tested agricultural vehicles in all seasons. Axle weights for the agricultural vehicles at 80% and 100% load levels were significantly higher as compared to Mn80, which led to higher stresses. However, Mn80 produced larger asphalt strains than tested agricultural vehicles in fall 2008 (80% load level) and fall 2009 (100% load level), while the opposite was

observed in spring 2009 (80% load level) and spring 2010 (100% load level). An attempt to explain this phenomenon through the layered elastic theory was unsuccessful.

Plotting the maximum subgrade stress responses from a particular vehicle pass against its corresponding offset relative to the sensor location reveals an additional effect of the pavement cross-section. Responses generated by vehicle R5 during spring 2009 at 80% load level and vehicle T6 during fall 2009 at 100% load level are presented for Cells 83 and 84 in Figure 4.24 through Figure 4.27.

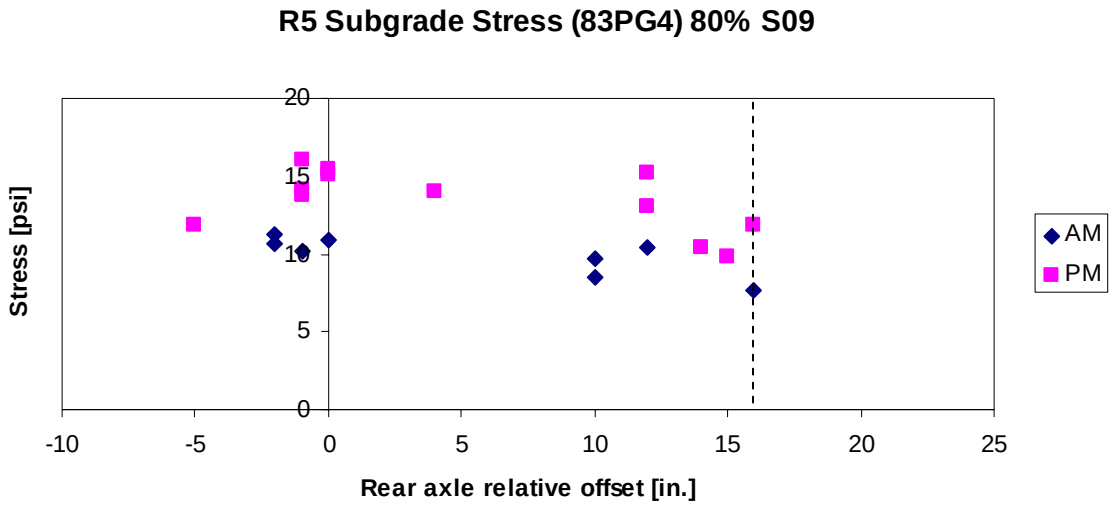

Figure 4.24. Cell 83 vertical subgrade stress generated by R5 in spring 2009 at 80% load level

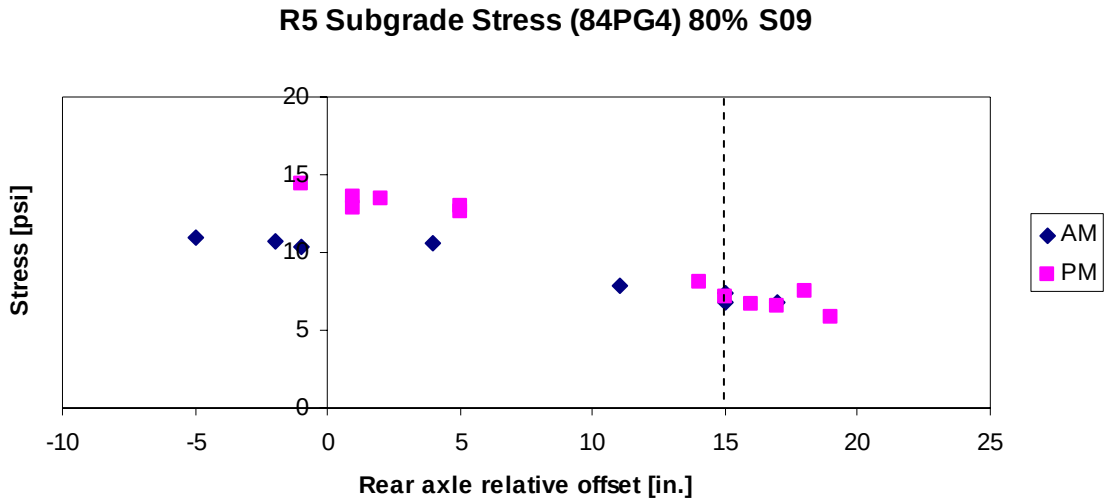

Figure 4.25. Cell 84 vertical subgrade stress generated by R5 in spring 2009 at 80% load level

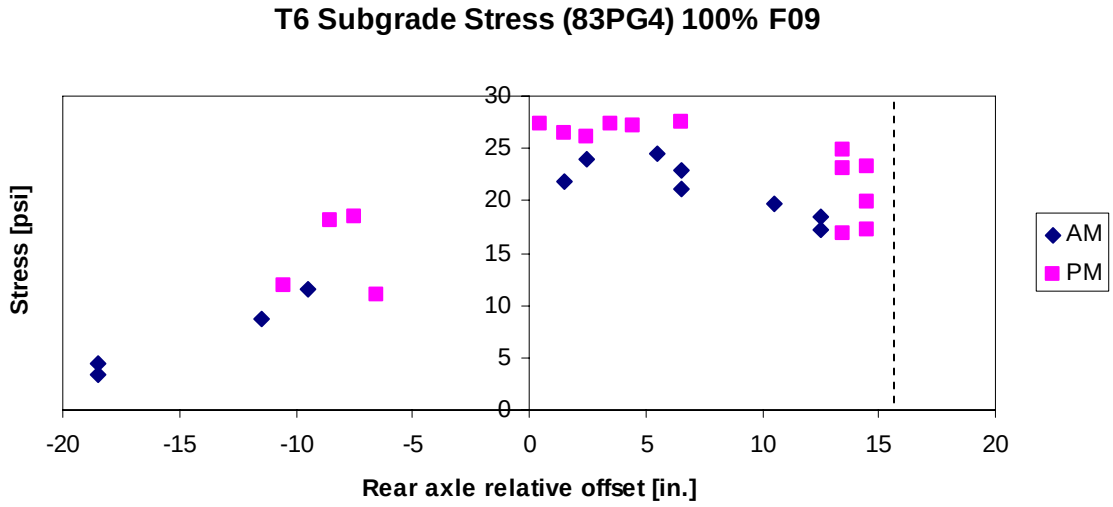

Figure 4.26. Cell 83 vertical subgrade stress generated by T6 in fall 2009 at 100% load level

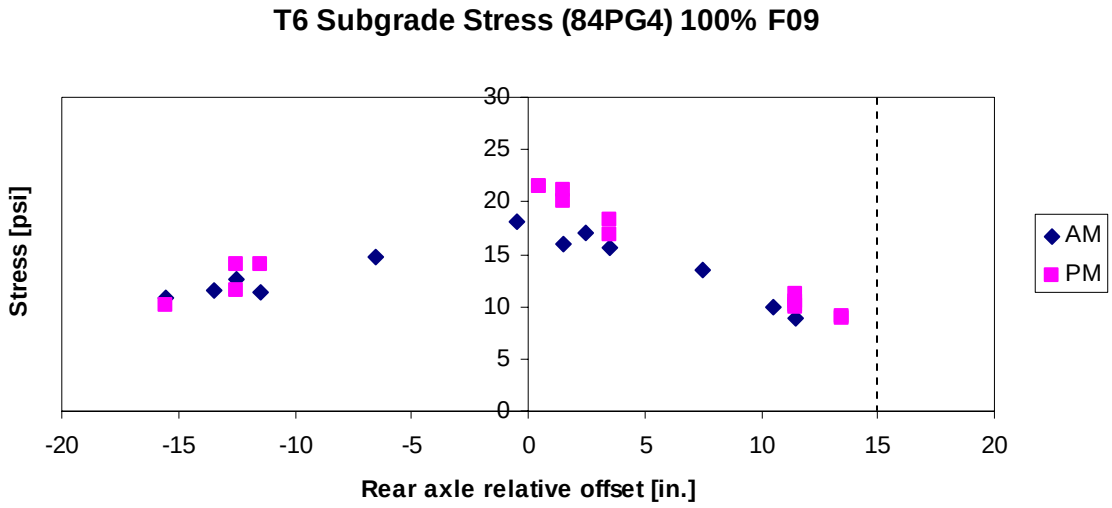

Figure 4.27. Cell 84 vertical subgrade stress generated by T6 in fall 2009 at 100% load level

It was observed that for Cell 84, measured subgrade stresses were reduced when the offset was significantly different from zero (directly over the sensor, approximately 15 in. from the pavement lane edge). This decrease can be observed for both positive (toward the shoulder) and negative (towards the centerline) offsets. The recorded subgrade stresses for wheel path locations above the sensor were twice as high as those recorded for the wheel paths closer to the pavement edge for both vehicles R5 and T6. It should be noted that the reduction in the maximum measured stress does not mean there is a reduction in the maximum subgrade stresses. The maximum subgrade stress should occur directly under the load, so it cannot be measured for the offset wheel paths due to lack of sensors under those locations.

Unlike Cell 84, Cell 83 did not exhibit significant reduction in the measured subgrade stress for positive wheel path offsets. This means that deviation in the wheel path toward the pavement edge did not reduce subgrade stresses at the pressure cell location, which is 16 in. away from the pavement edge. It is reasonable to assume that the maximum subgrade stress directly below the axle loads at positive offsets is much higher than those measured by the earth pressure cell. This suggests that absence of a paved shoulder

significantly increases the maximum subgrade stresses when the wheel path is near the pavement edge, as illustrated in Figure 4.28.

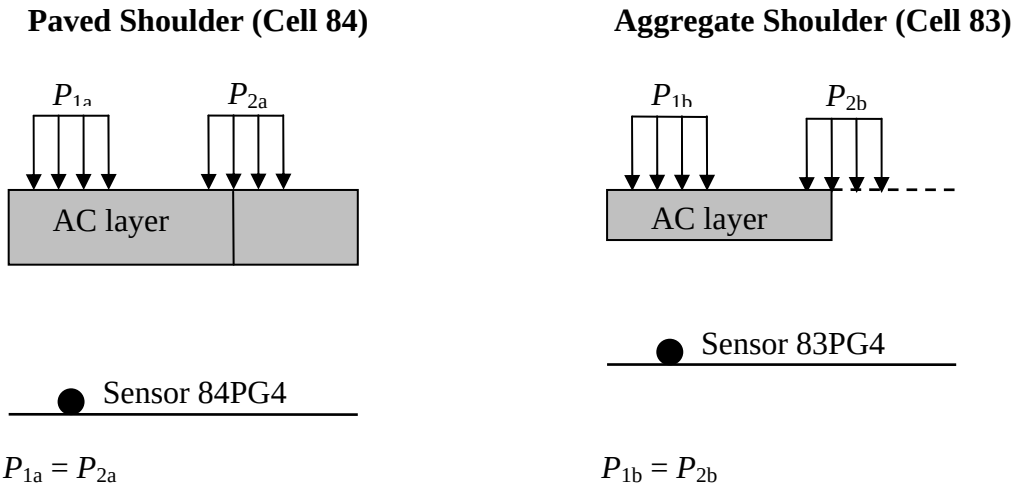

Figure 4.28. Cross-section view of pave and unpaved sections

A similar effect was observed for asphalt strains. Figure 4.29 through Figure 4.34 show that when the wheel path was translated toward the shoulder and away from the sensor, the measured asphalt strains in Cell 84 were significantly reduced. However, measured strains for Cell 83 were not reduced for similar loading conditions. For vehicle R5, strain responses were decreased by approximately 7% as the wheel path approached the pavement edge for Cell 83. For Cell 84 longitudinal strain, the decrease was roughly 50% and 70% for transverse strain. For vehicle T6, the decrease in angle strain for Cell 83 was only 2% and the decrease for Cell 84 longitudinal strain was approximately 25%. For the transverse strain in Cell 84, there was an increase of 4% as the vehicle's wheel path approached the pavement edge. The difference in responses of Cells 83 and 84 for different wheel path locations are due to the effect of different pavement shoulders. Cell 83 has an aggregate shoulder and Cell 84 has an asphalt shoulder. Cell 83, which has an aggregate shoulder, experienced higher coverage of the critical responses at the sensor location than Cell 84. This clearly demonstrates the importance of the structural benefits of the asphalt shoulder.

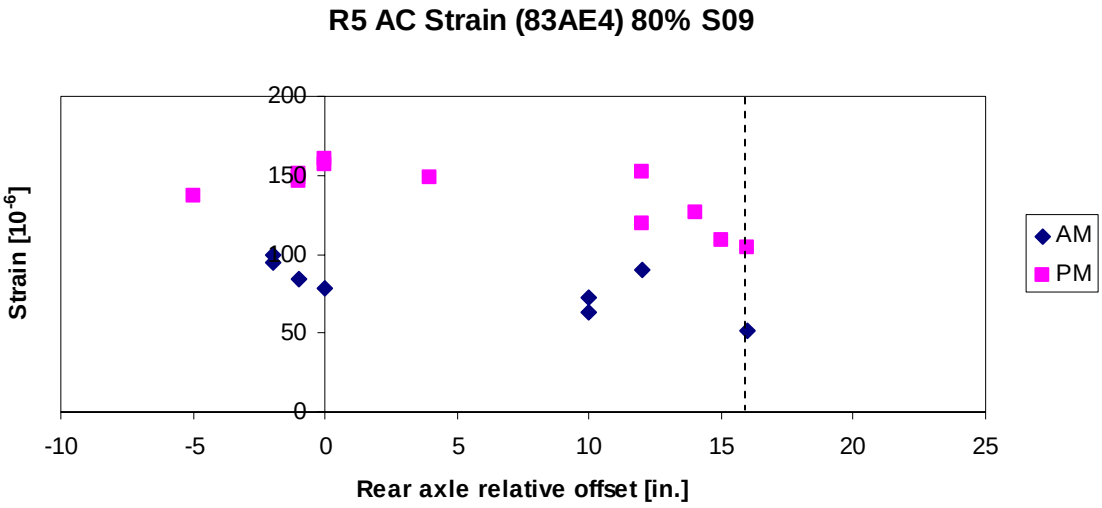

Figure 4.29. Cell 83 angled asphalt strain generated by R5 in spring 2009 at 80% load level

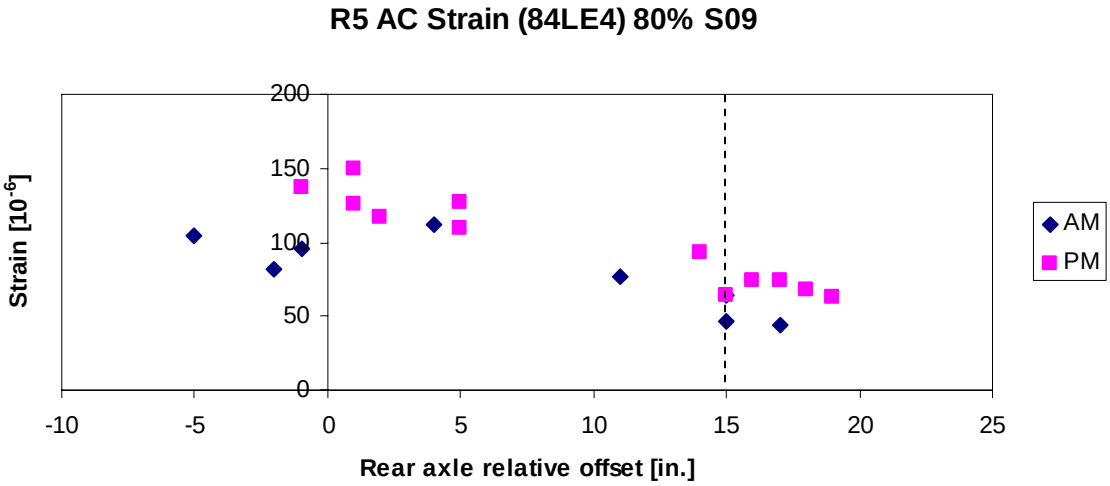

Figure 4.30. Cell 84 longitudinal asphalt strain generated by R5 in spring 2009 at 80% load level

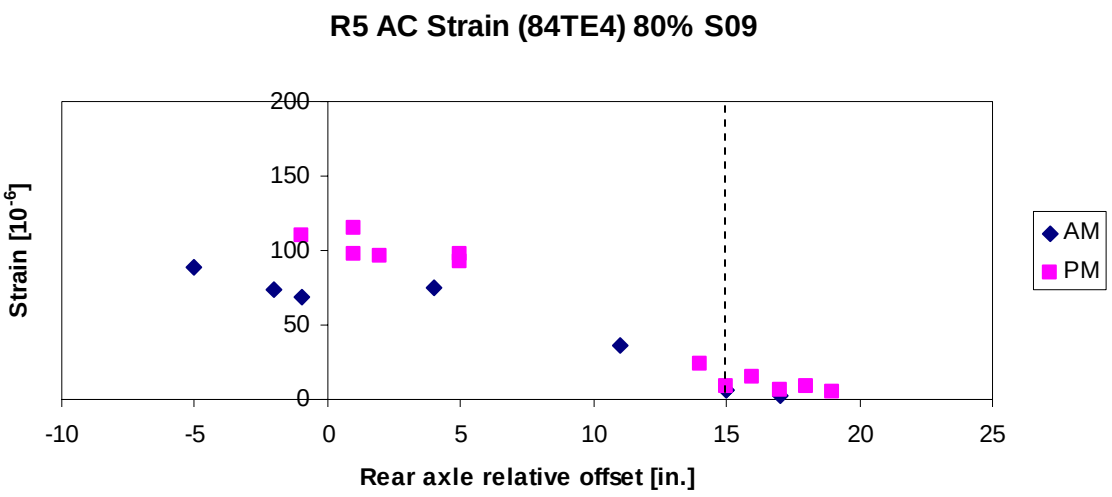

Figure 4.31. Cell 84 transverse asphalt strain generated by R5 in spring 2009 at 80% load level

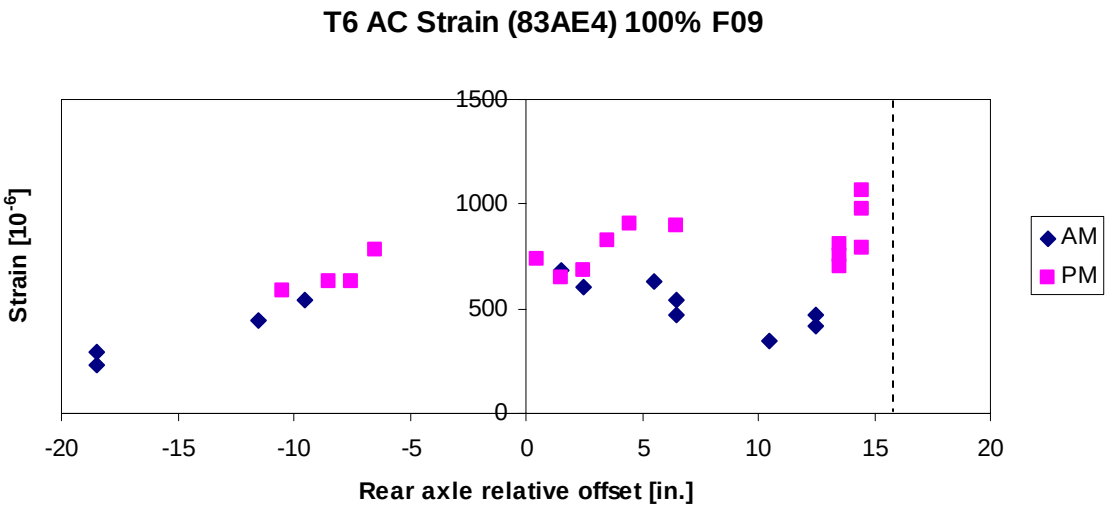

Figure 4.32. Cell 83 angled asphalt strain generated by T6 in fall 2009 at 100% load level

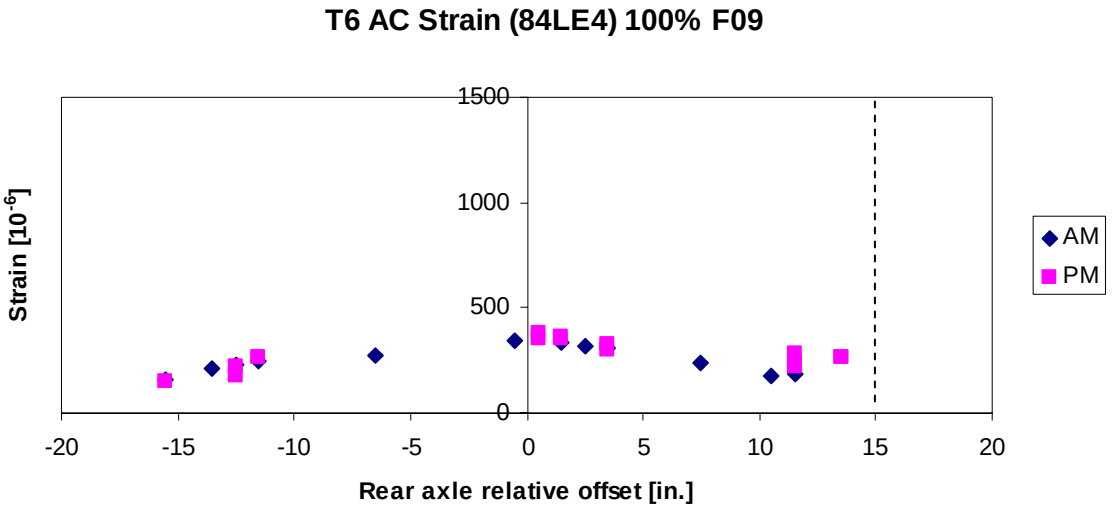

Figure 4.33. Cell 84 longitudinal asphalt strain generated by T6 in fall 2009 at 100% load level

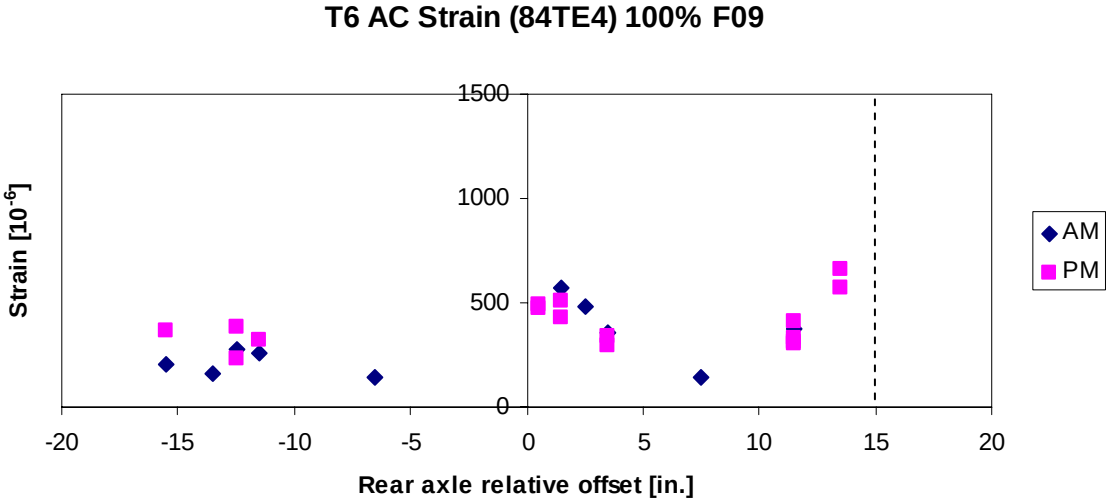

Figure 4.34. Cell 84 transverse asphalt strain generated by T6 in fall 2009 at 100% load level

4.5 Effect of Vehicle and Axle Weight

4.5.1 Effect of Vehicle Weight

The pavement responses in Cell 84 from vehicles S5 for spring 2009 and T6 for fall 2009 are presented in Figure 4.35 through Figure 4.40. The maximum strain and stress responses from a particular vehicle pass were plotted against its corresponding offset relative to the sensor location. Figure 4.35 through Figure 4.37 show the response measurements for vehicle S5, and Figure 4.38 through Figure 4.40 for vehicle T6. Gross vehicle weights are shown in the legends.

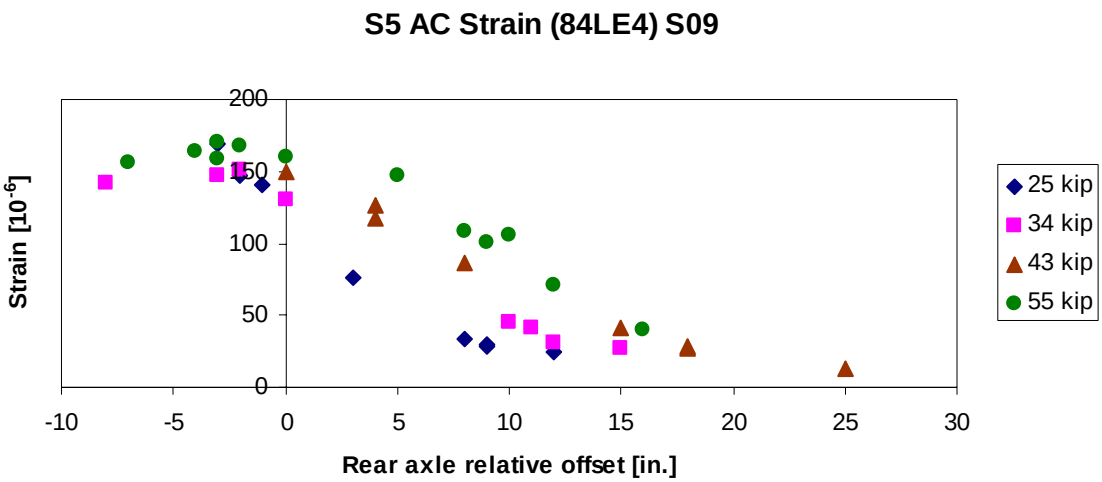

Figure 4.35. Cell 84 longitudinal asphalt strain generated by S5 in spring 2009 at various gross weights

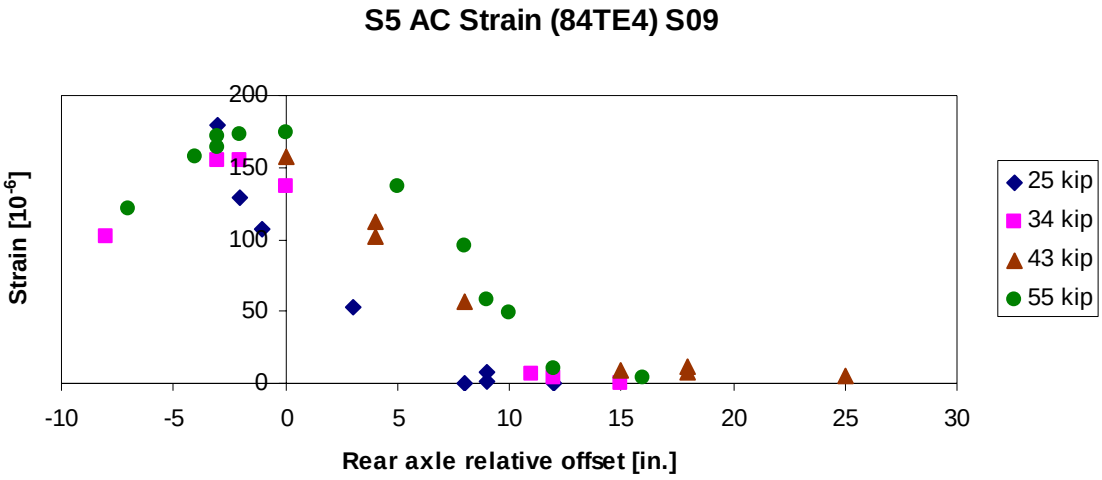

Figure 4.36. Cell 84 transverse asphalt strain generated by S5 in spring 2009 at various gross weights

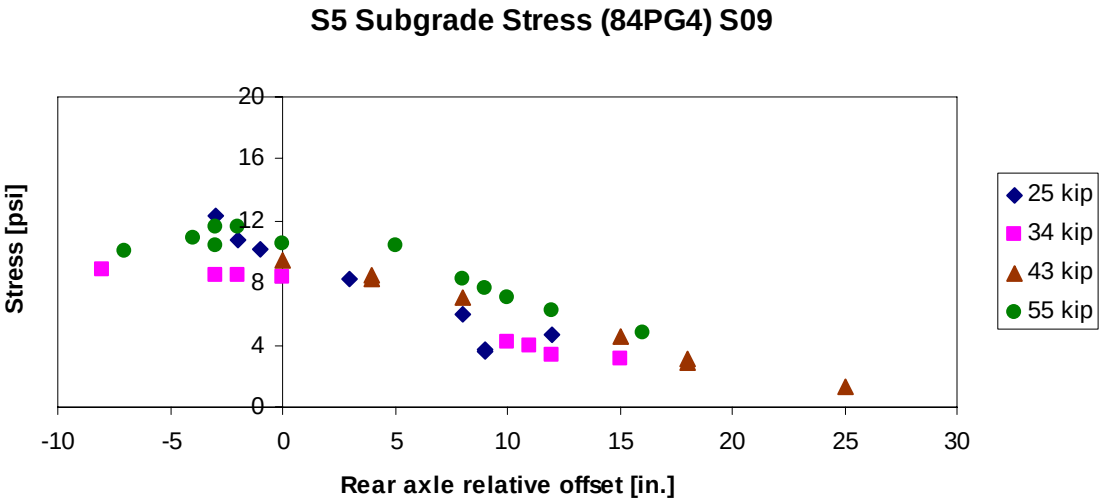

Figure 4.37. Cell 84 vertical subgrade stress generated by S5 in spring 2009 at various gross weights

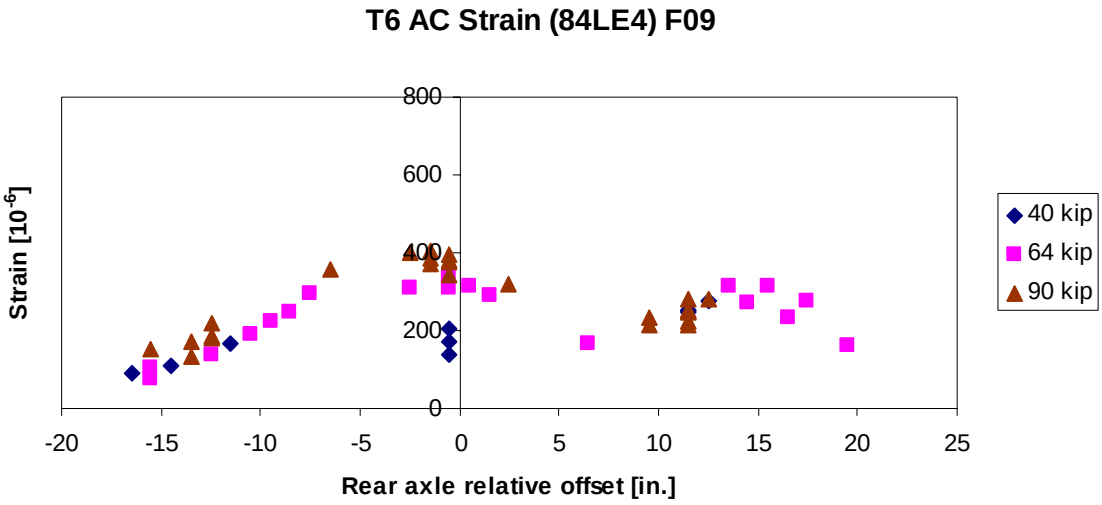

Figure 4.38. Cell 84 longitudinal asphalt strain generated by T6 in fall 2009 at various gross weights

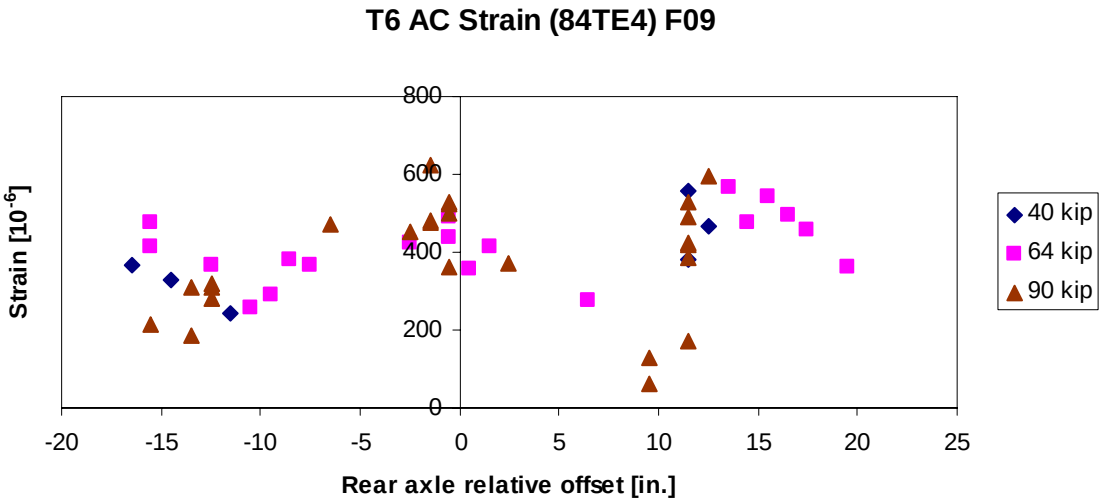

Figure 4.39. Cell 84 transverse asphalt strain generated by T6 in fall 2009 at various gross weights

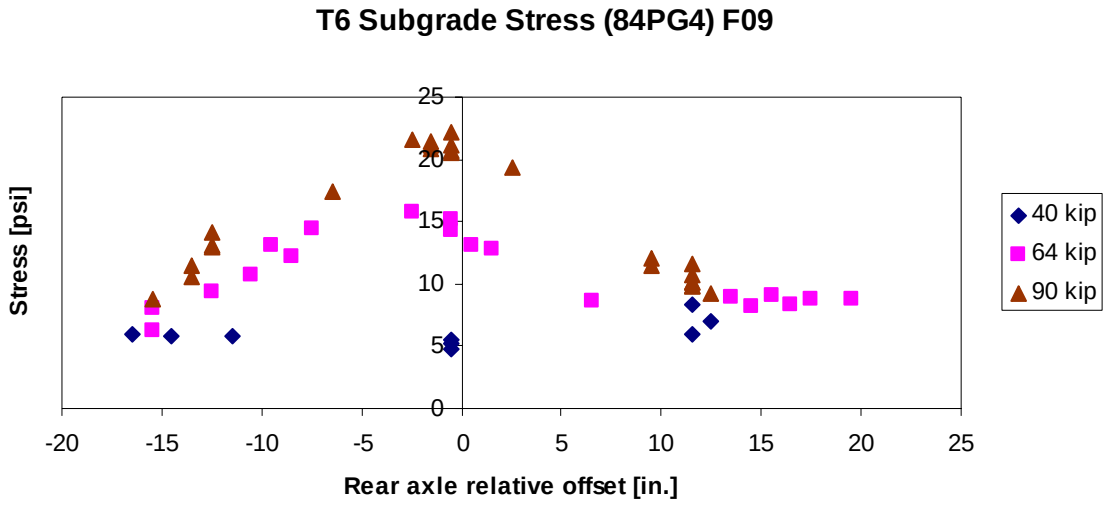

Figure 4.40. Cell 84 vertical subgrade stress generated by T6 in fall 2009 at various gross weights

It can be observed that longitudinal and transverse strain responses generated by vehicle S5 (Figure 4.35 and Figure 4.36) steadily increase as vehicle weight increases. However, subgrade stresses for vehicle S5 for a gross weight of 25,000 lb (25 kip) were larger than at 55,000 lb (55 kip). This can be explained by referring to Figure 4.7 from the "Effect of Seasonal Changes" section, which clearly shows a spike on the first day of spring 2009 testing for the Mn80 truck. This test day corresponds to the same day in which vehicle S5 was tested at 25 kip. Measurements collected on that day also resulted in the same trend for the other vehicles. An increase in longitudinal strains and subgrade stresses as vehicle weight increased was also observed for vehicle T6 in fall 2009, as shown in Figure 4.38 and Figure 4.40, respectively. Responses for transverse strains however were not as clear and no strong correlation was observed between transverse strains with gross vehicle weight for T6. Overall, there was an increase in stresses and strains as vehicle weight increased. However, it should be noted that tests for different vehicle weights (load levels) were conducted on different days, hence daily fluctuations and seasonal effects should be considered. Strain responses in spring were typically much "cleaner" compared to fall, and this may be due to several factors, including change in characteristics of the asphalt layer, frequency of vehicle passes, and time interval between

vehicle passes. It should be noted that the figures represent the maximum responses from the vehicles, and not from individual axles. An increase in gross vehicle weight did not lead to a proportional increase in axle weight, as will be discussed in subsequent sections.

4.5.2 Effect of Vehicle Type

Testing was conducted with the agricultural vehicles loaded at different load levels: 0%, 25%, 50%, 80%, and 100% of full tank capacity, while control vehicles Mn80 and Mn102 remained at the same weight. Weights of all vehicles were measured for every load level and this information is summarized in Appendix B. Table 4.2 and Table 4.3 summarize the gross weight of the vehicles for spring 2009 and fall 2009, respectively. This section focuses on changes in pavement responses as vehicle weight changes. An increase in vehicle weight should be reflected by an increase in pavement responses. As stated previously, pavement responses for vehicle Mn80 at Cell 84 were used as a benchmark to compare responses for other vehicles. Figure 4.41 through Figure 4.46 show the maximum strain and stress responses for agricultural vehicles for spring 2009 and fall 2009 at Cell 84.

Table 4.2. Gross weight for vehicles tested during spring 2009

Vehicle	**Gross Vehicle Weight [lb]**			
	0%	**25%**	**50%**	**80%**
S4	27,860	36,260	46,980	57,580
S5	25,180	34,040	42,940	54,840
R4	36,520	41,180	48,060	53,240
R5	31,480	35,520	39,600	43,740
T6	38,780	50,620	63,240	70,220
T7	58,540	72,840	88,050	103,600
T8	58,900	80,340	102,080	123,840
Mn80	79,560			

Table 4.3. Gross weight for vehicles tested during fall 2009

Vehicle	Gross Vehicle Weight [lb]		
	0%	50%	80%
R5	31,730	39,950	47,100
T6	39,710	64,400	89,500
T7	45,100	75,600	105,200
T8	58,200	97,600	134,200
Mn80	81,090		

Analysis of Figure 4.41 through Figure 4.46 shows that, as a general trend, an increase in vehicle weight leads to an increase in pavement responses. However, this increase is not proportional to the increase in vehicle weight, and for some vehicles, the responses decreased when the vehicle weight increased. Several factors may have contributed to this trend:

- Since different vehicle weights were conducted on different days, the climatic factors such as temperature could have affected the results. Vehicle Mn80 will be used later to adjust the results for this effect.
- The increase in gross vehicle weight does not lead to a proportional increase in vehicle axle weights. As can be observed from Table 4.4, an increase in gross weight for vehicle T6 significantly affects axle weights for the 3rd and 4th axles, while the 1st and 2nd axles are mostly unaffected. Moreover, the second axle has the highest axle weight for 0%, 25%, and 50%, while the 4th axle has the highest weight for 80% load level. The maximum responses shown in Figure 4.41 through Figure 4.46 can be produced by various axles for different load levels.

Table 4.4. Vehicle T6 axle weights at various load levels

Axle	0%	25%	50%	80%
	[lb]	[lb]	[lb]	[lb]
Axle 1	13,220	12,660	11,940	11,600
Axle 2	17,600	17,700	20,860	22,420
Axle 3	7,140	12,420	16,620	22,440
Axle 4	7,900	13,760	19,760	26,640
Total	**45,860**	**56,540**	**69,180**	**83,100**

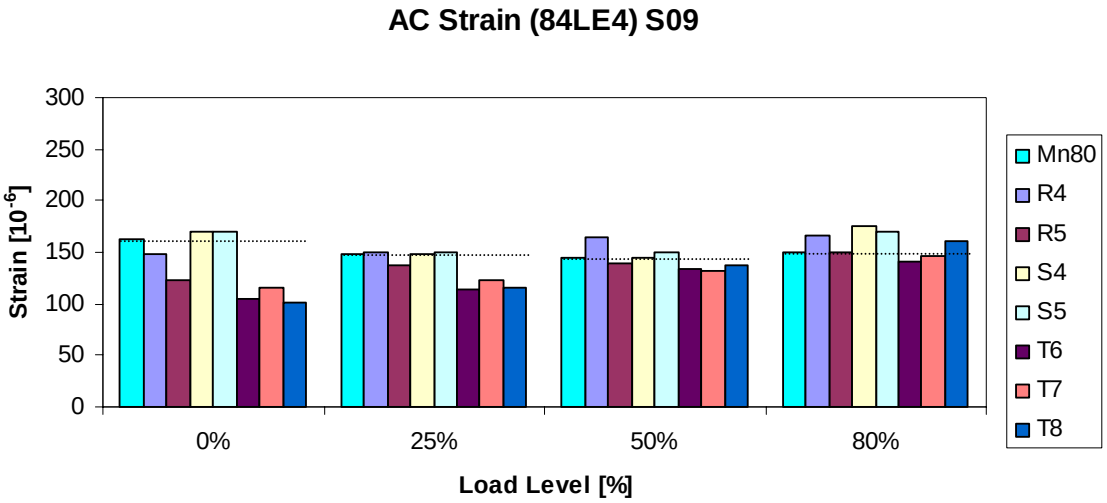

Figure 4.41. Longitudinal asphalt strain at Cell 84 generated by vehicles tested at 0%, 25%, 50%, and 80% in spring 2009

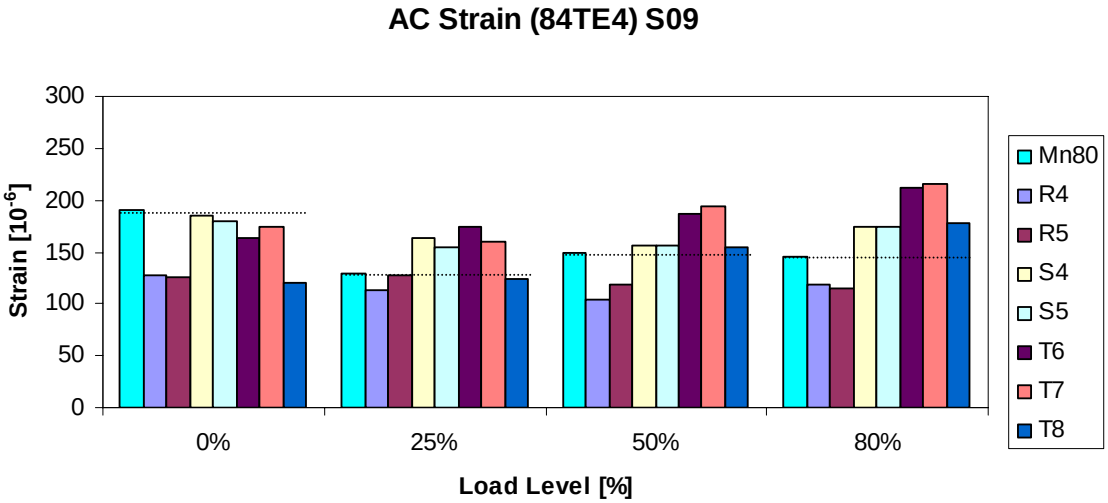

Figure 4.42. Transverse asphalt strain at Cell 84 generated by vehicles tested at 0%, 25%, 50%, and 80% in spring 2009

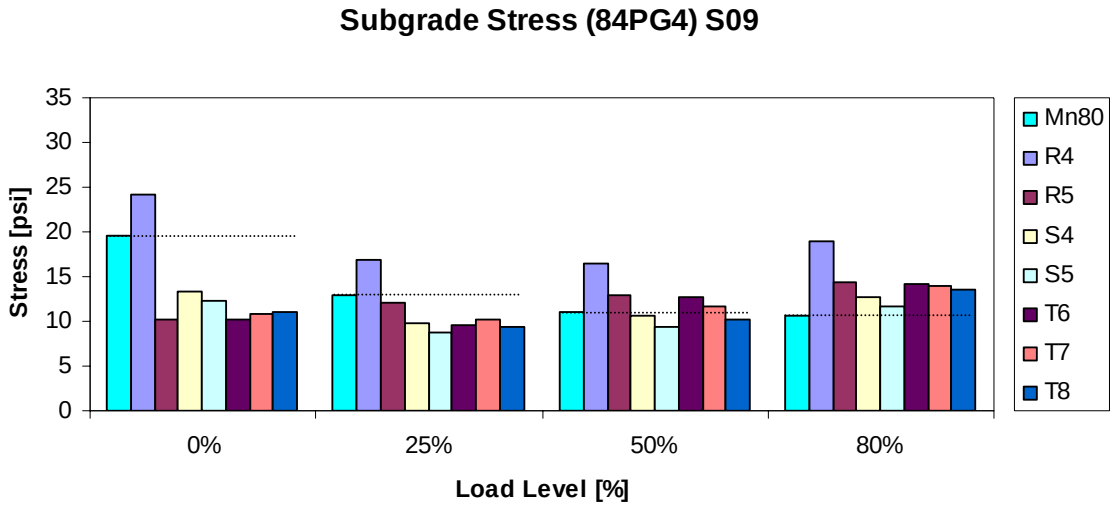

Figure 4.43. Vertical subgrade stress at Cell 84 generated by vehicles tested at 0%, 25%, 50%, and 80% in spring 2009

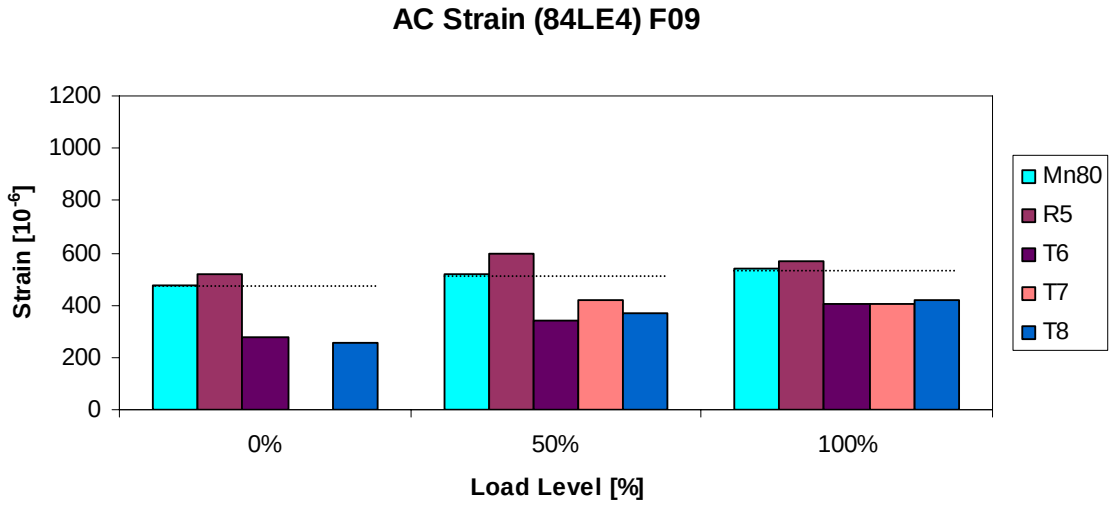

Figure 4.44. Longitudinal asphalt strain at Cell 84 generated by vehicles tested at 0%, 50%, and 100% in fall 2009

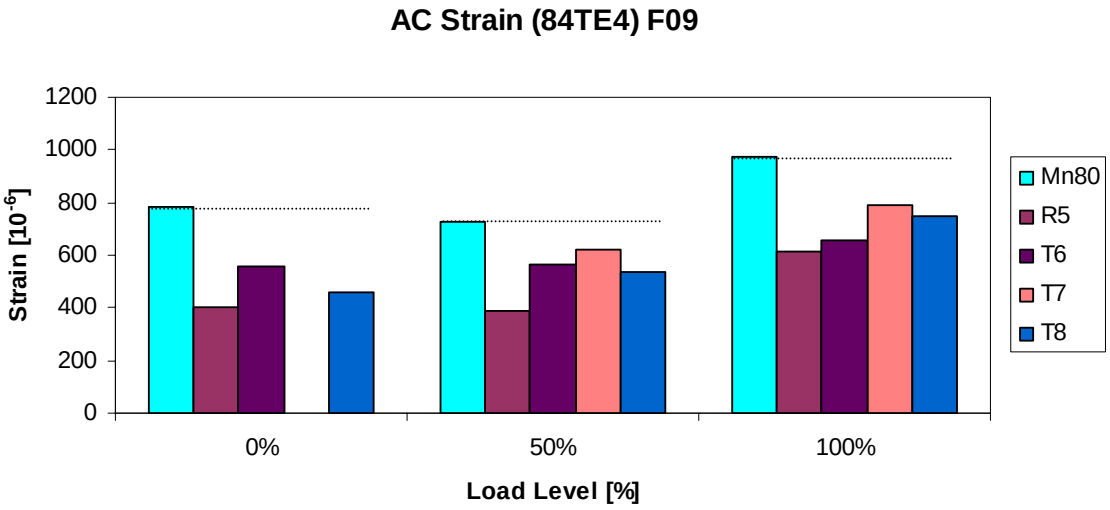

Figure 4.45. Transverse asphalt strain at Cell 84 generated by vehicles tested at 0%, 50%, and 100% in fall 2009

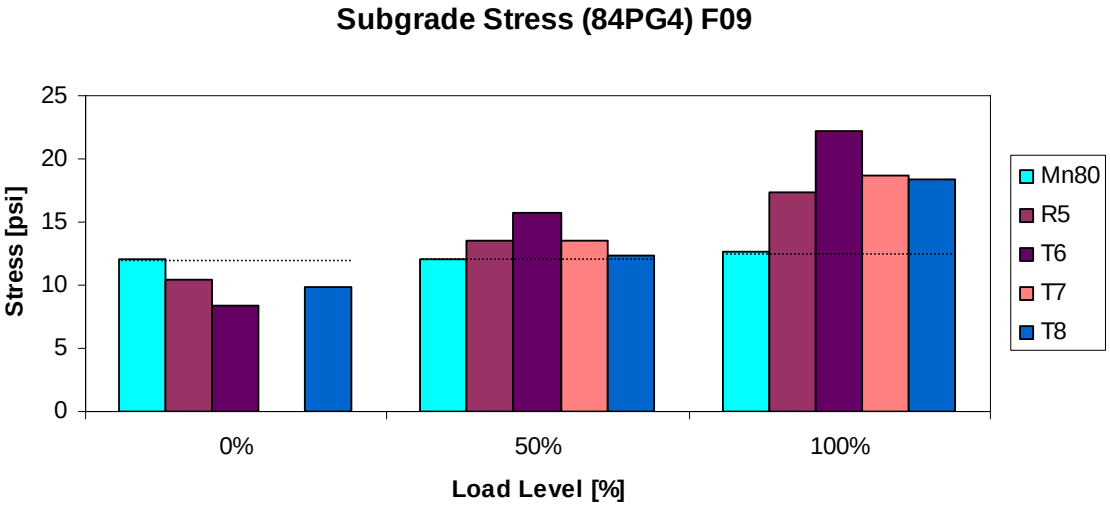

Figure 4.46. Vertical subgrade stress at Cell 84 generated by vehicles tested at 0%, 50%, and 100% in fall 2009

One of the objectives of this study was to compare pavement responses from various agricultural vehicles to a standard 5-axle 80-kip semi truck, which was represented by the Mn80 vehicle. Figure 4.41 through Figure 4.46 show that agricultural vehicles tested in

this study at 80% and 100% of full capacity produce higher subgrade stresses (84PG4) compared to the standard 5-axle 80-kip semi truck (Mn80) in both spring and fall seasons. An increase in subgrade stresses compared to Mn80 ranged from 4% to 80% in spring 2009 and 35% to 80% in fall 2009 for agricultural vehicles loaded over 80% load level. On the other hand, asphalt strain levels generated by the agricultural vehicles were dependent on test season. In spring, both longitudinal (84LE4) and transverse (84TE4) strains generated by Mn80 were typically smaller than the agricultural vehicles except for vehicle T6 for 84LE4 and vehicles R4 and R5 for 84TE4, even at 100% load capacity. In the fall, this trend was reversed with Mn80 producing larger strains than the other agricultural vehicles. In the spring of 2009, the S4 and T7 vehicles resulted in asphalt strains 20% and 48% higher than the Mn80 truck strains, respectively. In fall 2009, the difference in asphalt strain between vehicle T7 and Mn80 truck was -20%. An attempt to explain this trend using layered elastic analysis was not successful. Comparisons between the pavement responses across the pavement width generated by the agricultural vehicles and Mn80 are presented in Appendix D.

4.5.3 Effect of the Number of Axles

In the past decade, vehicle manufacturers of the agricultural industry began to design and produce larger equipment with larger capacities. However, in order to be operating legally on public roads, weight restrictions must be met. To achieve this goal, vehicles are equipped with additional axles. In this study, the responses from vehicles T6, T7, and T8 shown in Figure 4.47, were compared. These vehicles are equipped with four, five, and six total axles, respectively, and have tank capacities of 6,000 gallons, 7,300 gallons, and 9,500 gallons, respectively. Table 4.5 shows the axle weights of these vehicles loaded up to 100% when tested in fall 2009. Figure 4.48 shows the vertical subgrade stress responses at Cell 84 generated by those three vehicles.

T6 – 4 axles (John Deere 8230, 6,000 gal)

T7 - 5 axles (Case IH 335, 7,300 gal)

T8 – 6 axles (Case IH 335, 9,500 gal)

Figure 4.47. Vehicles with increasing tank capacity and axle number

Table 4.5. Axle weights of vehicles T6, T7, and T8 at 100% in fall 2009

Equipment	**Axle**	**T6 (6,000 gal)**	**T7 (7,300 gal)**	**T8 (9,500 gal)**
		[lb]	**[lb]**	**[lb]**
Tractor	Axle 1	8,100	6,900	14,800
	Axle 2	21,400	19,800	25,200
Tanker	Axle 3	26,500	26,300	23,300
	Axle 4	33,500	26,200	23,700
	Axle 5		26,000	23,500
	Axle 6			23,700
Gross vehicle weight		**89,500**	**105,200**	**134,200**

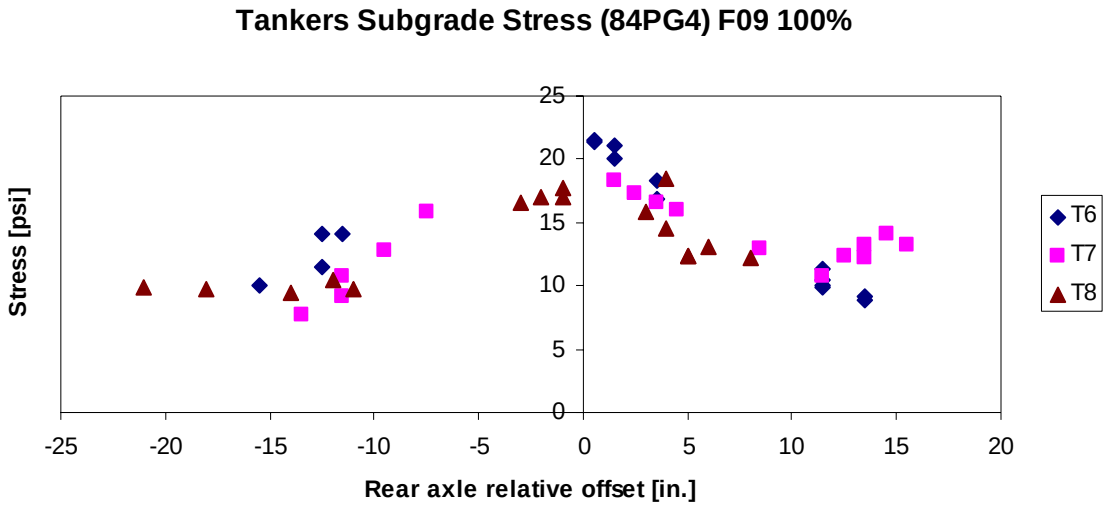

Figure 4.48. Cell 84 vertical subgrade stress generated by vehicles T6, T7, and T8 at 100% load level in fall 2009

Analysis of Table 4.5 shows that although the gross weight of T6 is the lowest amongst these vehicles, its last axles exhibited the highest load (33,500 lb). Vehicle T8 had the highest gross weight. However, since the tanker had four axles, each of them resulted in a relatively low axle weight of 23,700 lb. It is interesting to note that the most loaded axle was not an axle on the tanker, but rather a rear tractor axle (axle two), which had a weight of 25,200 lb. As should be expected, vehicle T6 resulted in the highest subgrade stress while vehicle T8 resulted in the lowest subgrade stress.

Referring to Table 4.5, note that the first two axles for all three vehicles belong to the tractor. The axle weights of interest here are those belonging to the tankers, which are axles three to six. Increasing the tank capacity evidently increases the overall vehicle weight. By adding axles to the tankers, the weight per axle was successfully decreased with vehicle T6 having the heaviest tanker axle at 33,500 lb, T7 at 26,300 lb, and T8 at 23,700 lb. Figure 4.43 and Figure 4.46 show that vertical subgrade stresses for T6 was largest, followed by T7 and finally T8 for both spring 2009 and fall 2009 test. Figure 4.48 clearly shows that vehicle T6 generates larger subgrade stresses than the other two vehicles. Hence, for a larger tank capacity, equipping the tanker with additional axles

can potentially reduce the subgrade stresses. Unfortunately, a similar trend was not observed for asphalt strains. It is worth mentioning that this comparison may not accurately describe the benefits of having additional axles, since the tankers of vehicles T6, T7, and T8 were of non-similar sizes.

4.5.4 Effect of Axle Weight

As was discussed, the effect of gross vehicle weight on pavement responses did not show consistent results. This was attributed to several factors: 1) an increase in gross vehicle weight is not proportionally distributed to the axle weights; 2) the maximum response may be generated by different axles; and 3) different vehicle weights were tested on different days under different temperature conditions. To account for the effect of axle weight, the response from the rear axle of vehicle T6 was analyzed. A simple correction factor, d_i, was introduced to account for climatic effects. This correction factor is based on responses obtained from the control vehicle Mn80.

$$\hat{\sigma}_{T6i} = \sigma_{T6i}\left(\frac{\sigma_{Mn80o}}{\sigma_{Mn80i}}\right) = \frac{\sigma_{T6i}}{d_i} \qquad \text{Eqn 4.1}$$

where $\hat{\sigma}_{T6i}$ is the adjusted subgrade stress from the rear axle of vehicle T6 for *i*th day

σ_{T6i} is the measured subgrade stress from the rear axle of vehicle T6 on *i*th day

σ_{Mn80o} is the reference subgrade stress for vehicle Mn80

σ_{Mn80i} is the measured subgrade stress for vehicle Mn80 on *i*th day

d_i is the ratio between measured subgrade stress on *i*th day and reference stress for vehicle Mn80

A similar equation was used to determine adjusted strain values by substituting strain measurements for stress measurements in Eqn 4.1. To maintain consistency, the correction factor is always based on the responses generated by the heaviest axle of

Mn80. The adjustment process was the performed on the maximum response generated by the heaviest axle of the vehicle of interest across the entire pavement width. This step is important to identify the relationship between axle responses and axle weight instead of using the maximum response across the vehicle axles and total vehicle weight, which may be misleading. Strain and stress responses for vehicle T6 from Cells 83 and 84 were adjusted for everyday of testing for fall 2008, spring 2009, fall 2009, and spring 2010.

Response measurements on the fourth day of testing during fall 2008 were selected as the reference Mn80 response. The relationship between adjusted strain and stress responses and axle weight for vehicle T6 is shown in Figure 4.49 to Figure 4.53. Figure 4.54 and Figure 4.55 show a comparison between both Cells 83 and 84. This evaluation was made by selecting the maximum between adjusted longitudinal (84LE4) and transverse (84TE4) strains from Cell 84 and comparing it to angled strain (83AE4) of Cell 83.

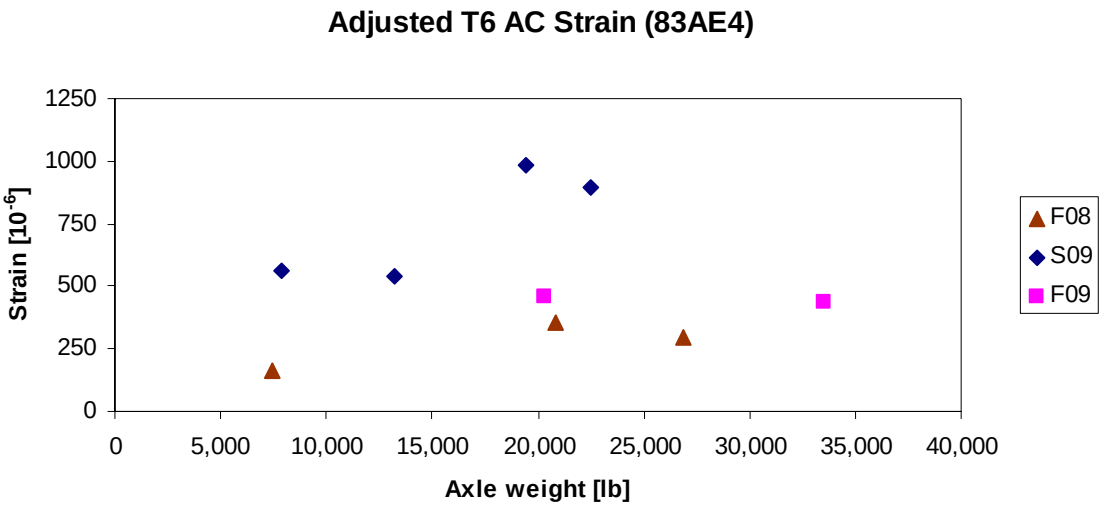

Figure 4.49. Adjusted angled asphalt strain response from Cell 83 for vehicle T6

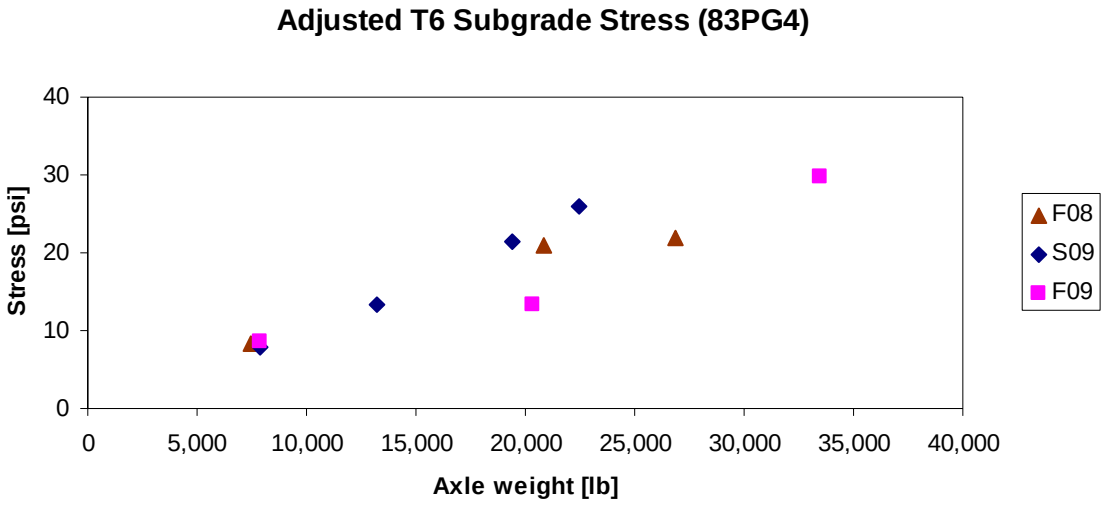

Figure 4.50. Adjusted vertical subgrade stress response from Cell 83 for vehicle T6

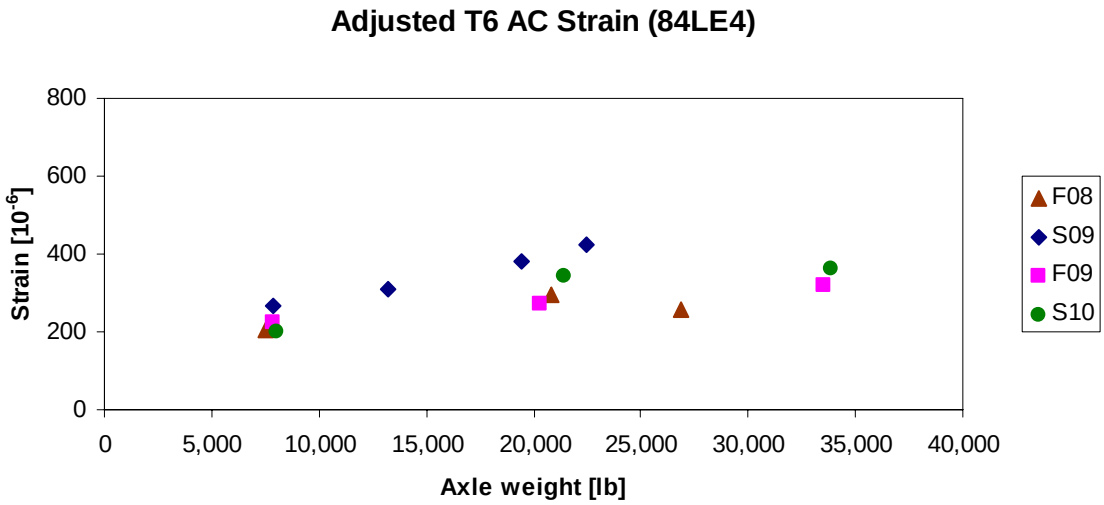

Figure 4.51. Adjusted longitudinal asphalt strain response from Cell 84 for vehicle T6

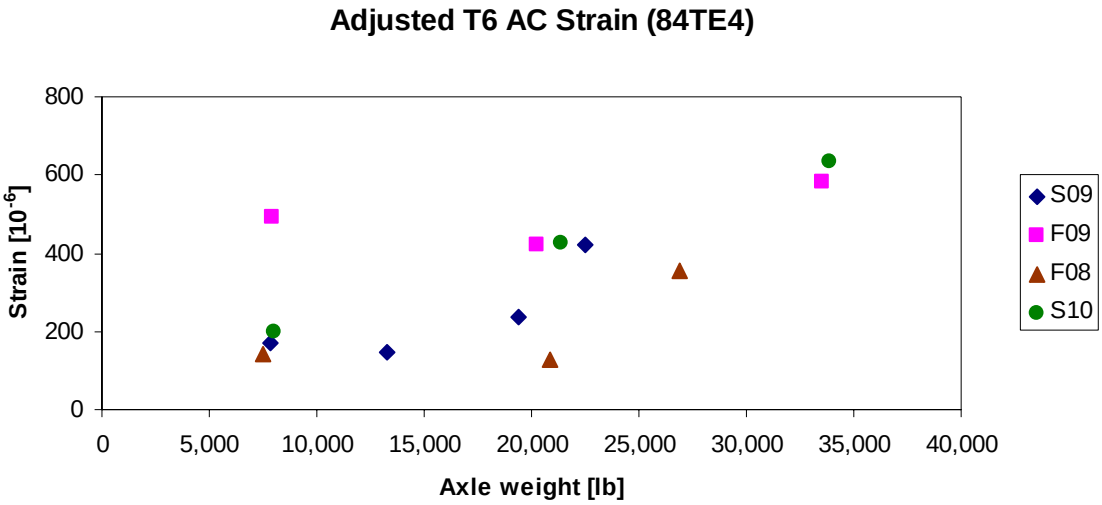

Figure 4.52. Adjusted transverse asphalt strain response from Cell 84 for vehicle T6

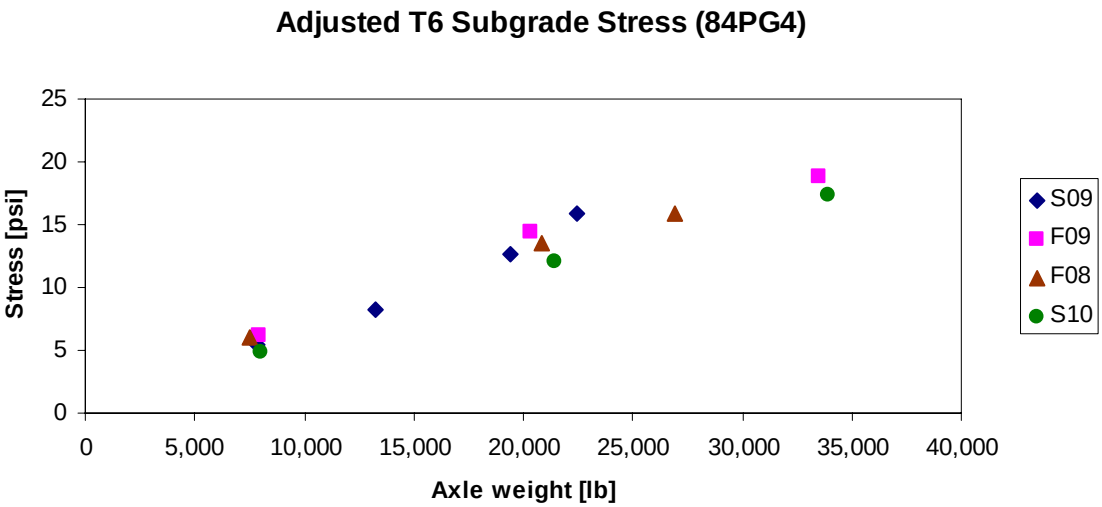

Figure 4.53. Adjusted vertical subgrade stress response from Cell 84 for vehicle T6

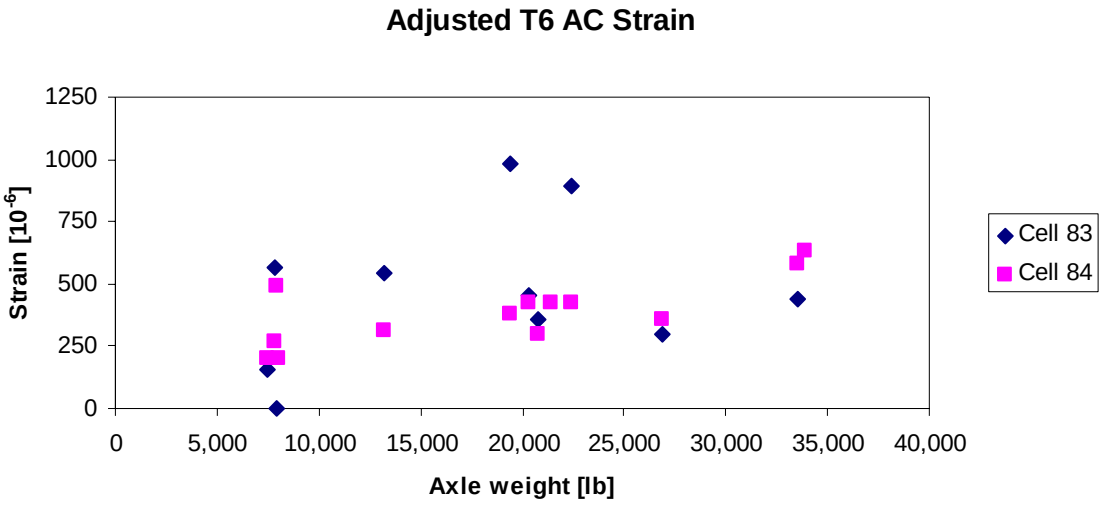

Figure 4.54. Adjusted asphalt strain responses for vehicle T6 between Cells 83 and 84

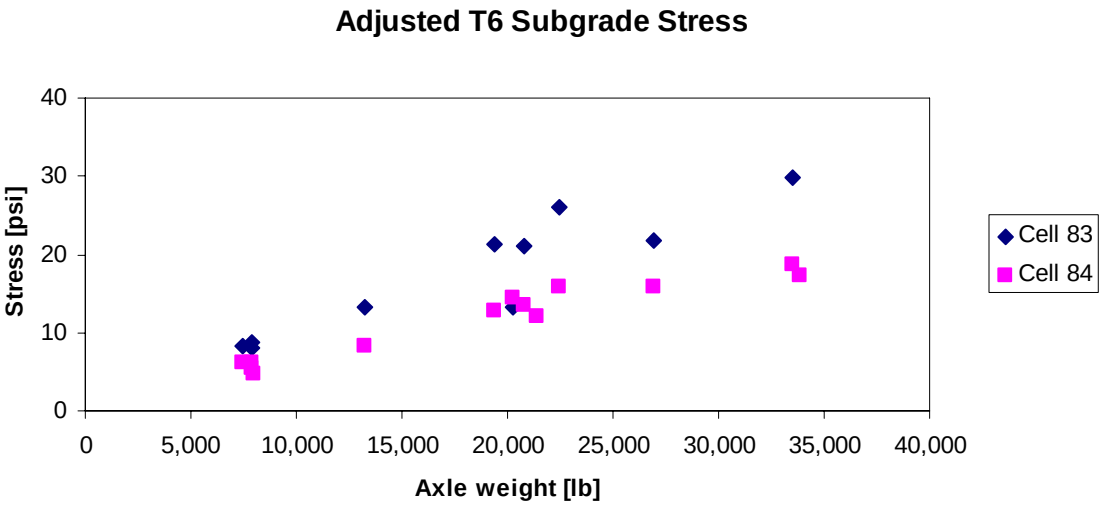

Figure 4.55. Adjusted subgrade stress responses for vehicle T6 between Cells 83 and 84

The purpose of this exercise was to negate daily fluctuations in measured responses. It was observed that adjusted subgrade stress responses for vehicle T6 from both Cells 83 and 84 have a linear relationship with axle weight, where a stronger linear correlation exists for Cell 84. Adjusted asphalt strains from Cells 83 and 84 increase with increasing axle weight. However, there is a significant scatter and the relationship is nonlinear. A

possible explanation is the effect of traffic wander and higher sensitivity to temperature effect that cannot be accounted for with a simple adjustment such as the one described above. This effect requires further investigation.

4.6 Effect of Tire Type

In the agricultural industry, flotation tires are becoming increasingly popular due to their wider footprint and lower inflation pressure, which allows the vehicle to travel over soil and unbound aggregate material with minimal compaction and rutting. With a wider footprint coupled with low inflation pressure, the wheel load is distributed over a larger area, thus reducing the stress applied to the soil. This has proved to be beneficial in the industry where less soil compaction and rutting decreases soil damage. An issue arises as to whether this characteristic can be translated directly to pavement performance.

In this section, two similar straight trucks with the same tank capacity of 4,400 gallons were fitted with two different tire types on the tanks, one with regular radial ply dual tire configuration (Vehicle S4), and the other with a flotation single tire configuration (Vehicle S5) as shown in Figure 4.56. Comparisons were made using contact area and contact stress measurements from Tekscan. Additionally, asphalt strains and subgrade stresses produced by these two vehicles were evaluated.

(a) (b)

Figure 4.56. Straight trucks denoted as (a) vehicle S4 fitted with radial tires (b) vehicle S5 fitted with flotation tires

Tekscan measurements for both vehicles S4 and S5 were taken at load levels of 0%, 50%, and 80%. Because of the size constraint of the Tekscan equipment, only one side of each vehicle axle was recorded. The measurements were then calibrated with the actual wheel load corresponding to the load level. Table 4.6 summarizes the Tekscan results for both S4 and S5. In order to visualize the growth in contact area and change in contact stress as wheel load increases, plots were prepared as shown in Figure 4.57 and Figure 4.58. Additionally, an illustration of how the contact areas of the third axle for both vehicles change with increasing axle weight is shown in Figure 4.59.

Table 4.6. Tekscan summary for vehicle S4 and S5

Vehicle	Load Level [%]	Axle	Filename	Wheel Load [lb]	Frame	Contact Area [in.^{2}]	Average Stress [psi]
S4	0	1	S2_A1LA	5,580	7	56.89	98.1
	0	2	S2_A**2**-3LB	3,680	26	52.41	70.2
	0	3	S2_A2-**3**LB	3,400	45	44.35	76.7
	50	1	S2_A1RC50	6,040	211	68.54	88.1
	50	2	S2_A**2**-3RD50	7,800	18	96.31	81
	50	3	S2_A2-**3**RC50	8,040	30	104.38	77
	80	1	S2_A1RB80	6,460	30	79.74	81
	80	2	S2_A**2**-3RA80	9,680	85	103.03	94
	80	3	S2_A2-**3**RB80	10,300	98	126.77	81.2
S5	0	1	S1_A1LA	6,400	16	72.57	88.2
	0	2	S1_A**2**-3LA	4,300	10	51.52	83.5
	0	3	S1_A2-**3**LA	3,460	21	50.62	68.4
	50	1	S1_A1RA50	7,900	51	81.53	96.9
	50	2	S1_A**2**-3RA50	7,500	50	83.77	89.5
	50	3	S1_A2-**3**RB50	8,390	76	103.48	81.1
	80	1	S1_A1RA80	8,780	54	89.14	98.5
	80	2	S1_A**2**-3RA80	9,980	22	105.72	94.4
	80	3	S1_A2-**3**RA80	10,000	33	136.63	73.2

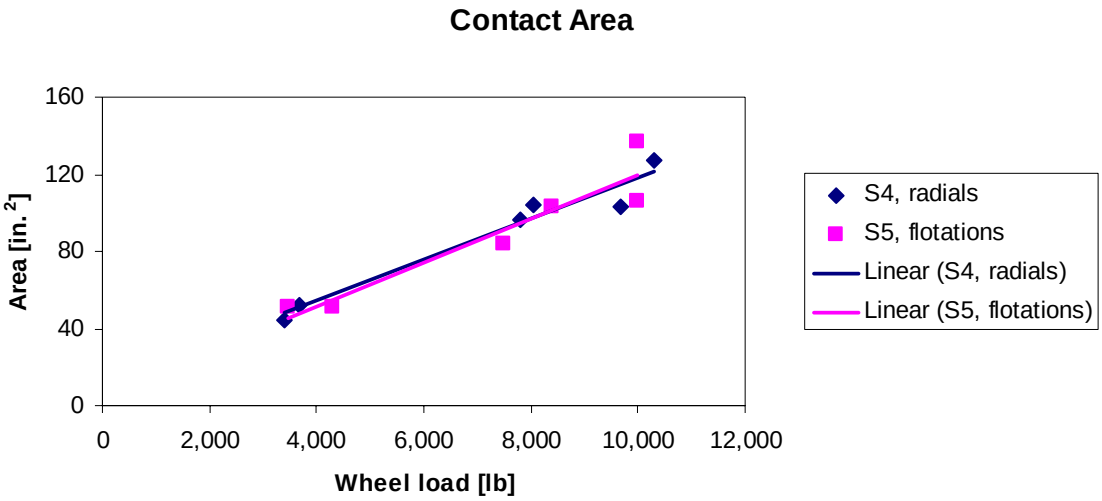

Figure 4.57. Contact area measurements for vehicles S4 and S5

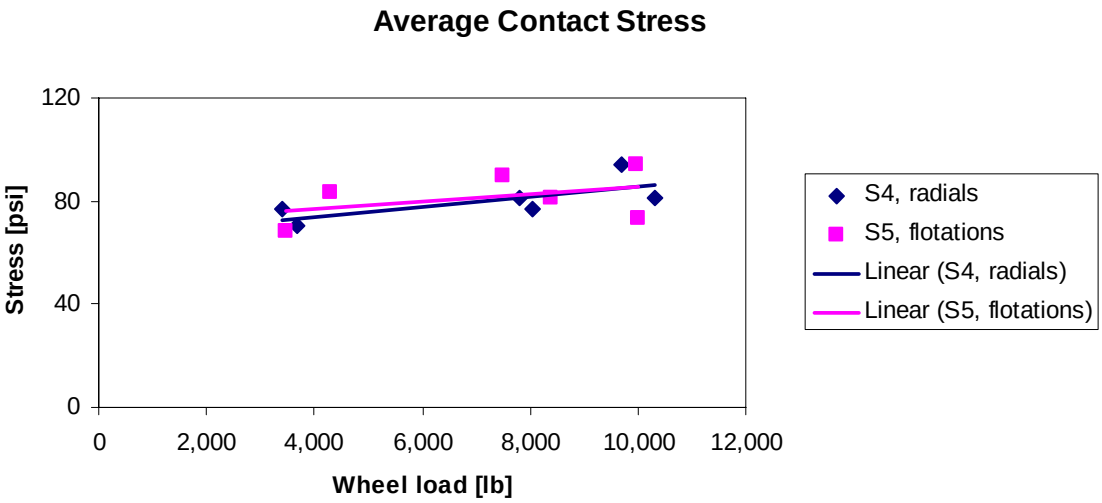

Figure 4.58. Average contact stress measurements for vehicles S4 and S5

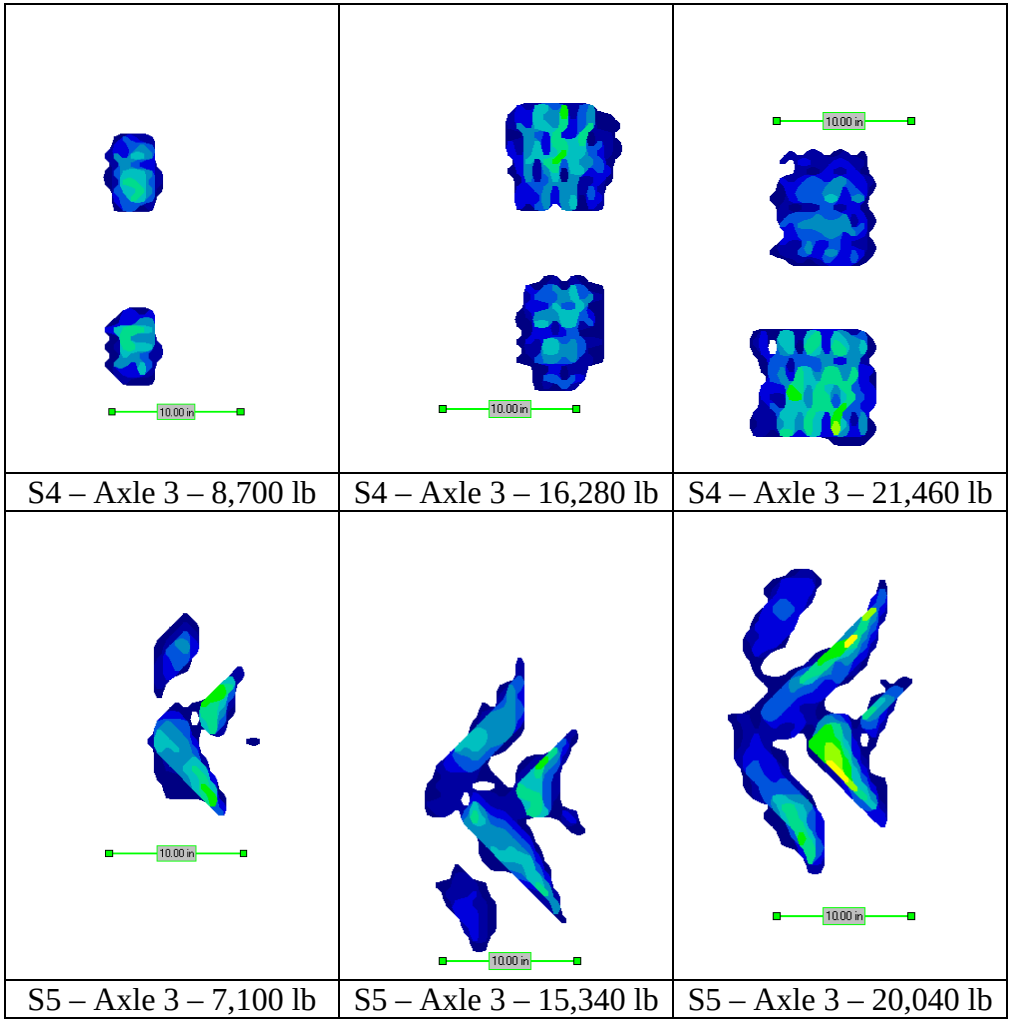

S4 – Axle 3 – 8,700 lb	S4 – Axle 3 – 16,280 lb	S4 – Axle 3 – 21,460 lb
S5 – Axle 3 – 7,100 lb	S5 – Axle 3 – 15,340 lb	S5 – Axle 3 – 20,040 lb

Figure 4.59. Measured footprints for the third axle of vehicle S4 and S5 with corresponding axle weight

Vehicles S4 and S5 are equipped with tires that can deform under load and still maintain their structural capacity. Regular radial ply dual tires fitted onto vehicle S4 and flotation tires fitted onto vehicle S5 demonstrate an increase in contact area as the wheel load increases. A trendline fitted across the data points in Figure 4.57 shows that both tire types were similar in terms of contact area growth. The average contact stress for both vehicles also increased with wheel load levels, but the increase was not as significant because of the larger contact area. There was no significant difference between the two tire types, as shown in Figure 4.58.

Recognizing that the contact area and average contact stress for both vehicles were very similar, the pavement response measurements were also evaluated to distinguish any benefits of flotation tires on pavement performance. To accomplish this comparison, the analysis was performed by excluding responses generated by the steering axles of both these vehicles. This ensures that the comparison was made exclusively between radial and flotation tires on the vehicles' tanks. Table 4.7 shows the total tank weights for both vehicles S4 and S5. Figure 4.60 through Figure 4.67 show Cells 83 and 84 pavement responses generated at load levels of 0% and 80% during spring 2009.

Table 4.7. Tank weights for vehicles S4 and S5

Load Level	S4's Tank	S5's Tank
0%	15,180 lb	14,040 lb
80%	40,980 lb	39,440 lb

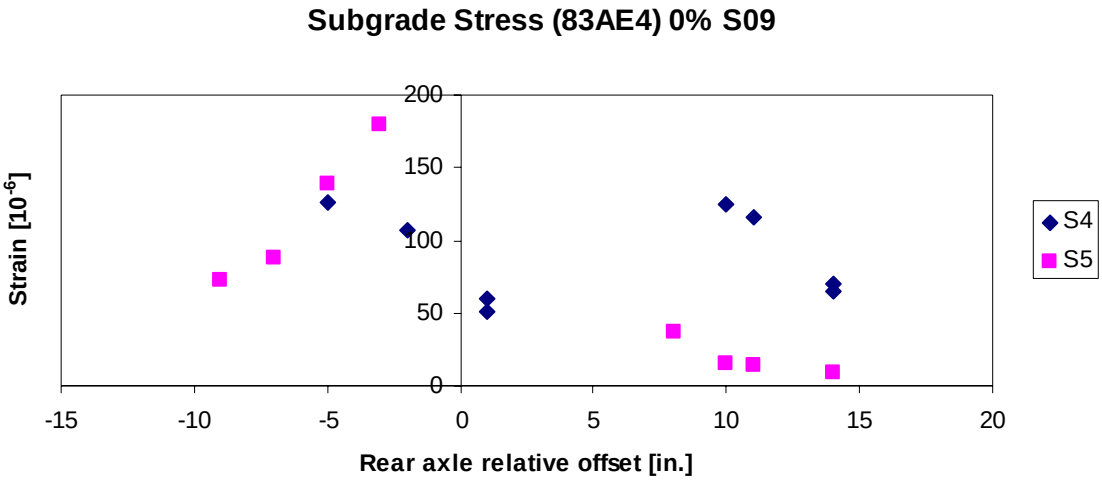

Figure 4.60. Cell 83 angled asphalt strain generated at 0% load level for vehicles S4 and S5

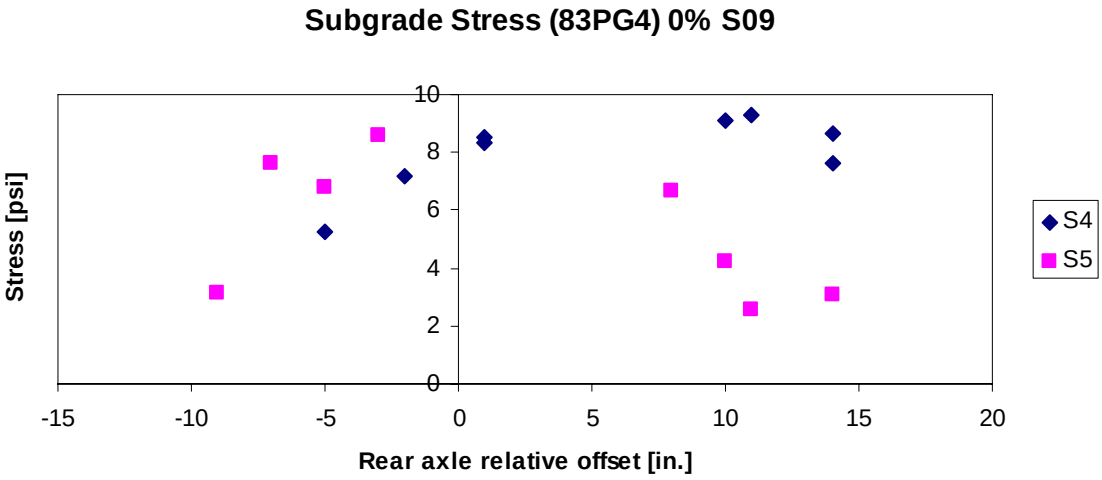

Figure 4.61. Cell 83 vertical subgrade stress generated at 0% load level for vehicles S4 and S5

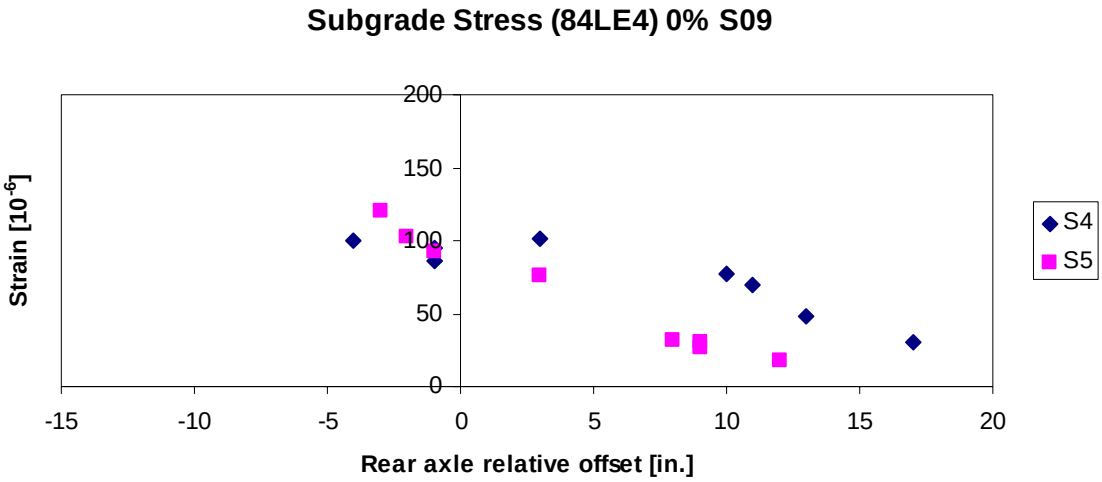

Figure 4.62. Cell 84 longitudinal asphalt strain generated at 0% load level for vehicles S4 and S5

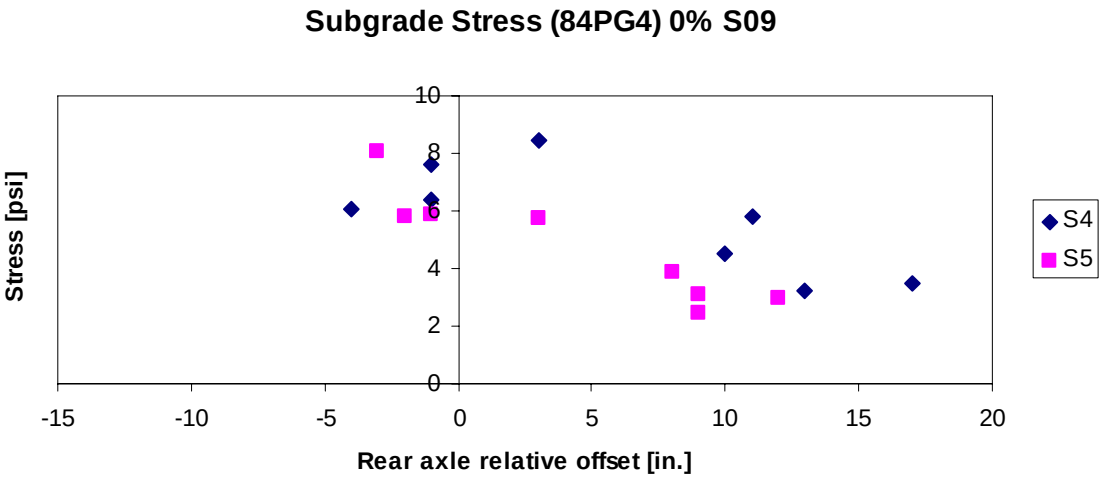

Figure 4.63. Cell 84 vertical subgrade stress generated at 0% load level for vehicles S4 and S5

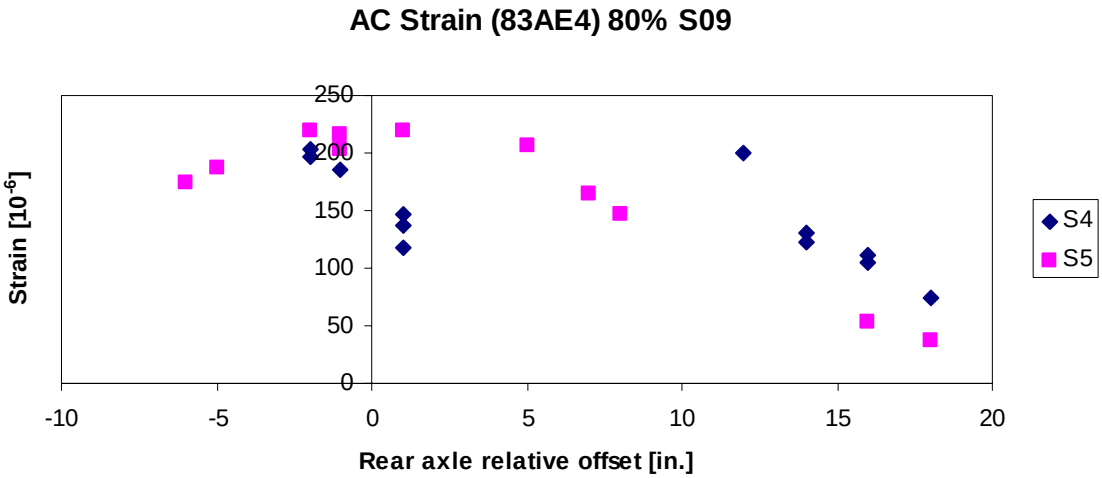

Figure 4.64. Cell 83 angled asphalt strain generated at 80% load level for vehicles S4 and S5

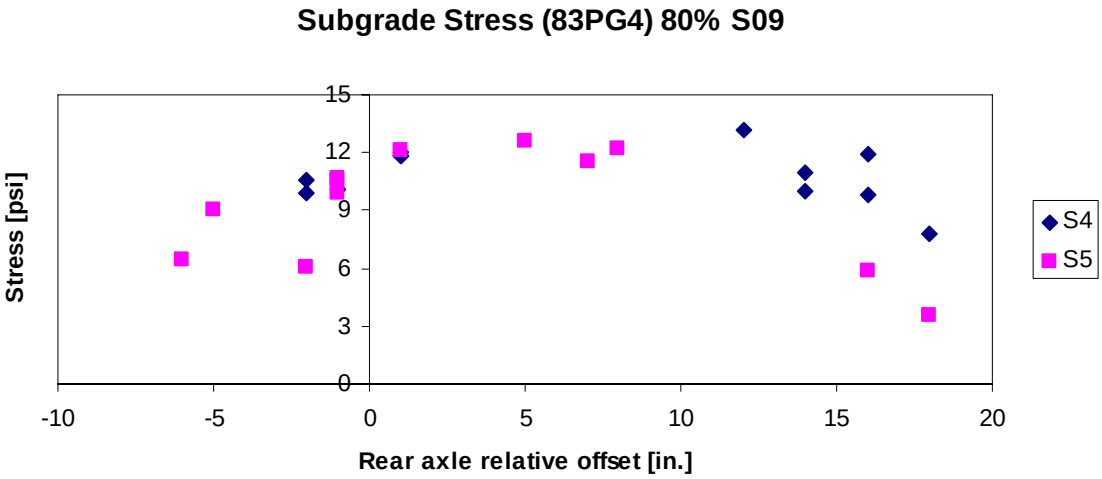

Figure 4.65. Cell 83 vertical subgrade stress generated at 80% load level for vehicles S4 and S5

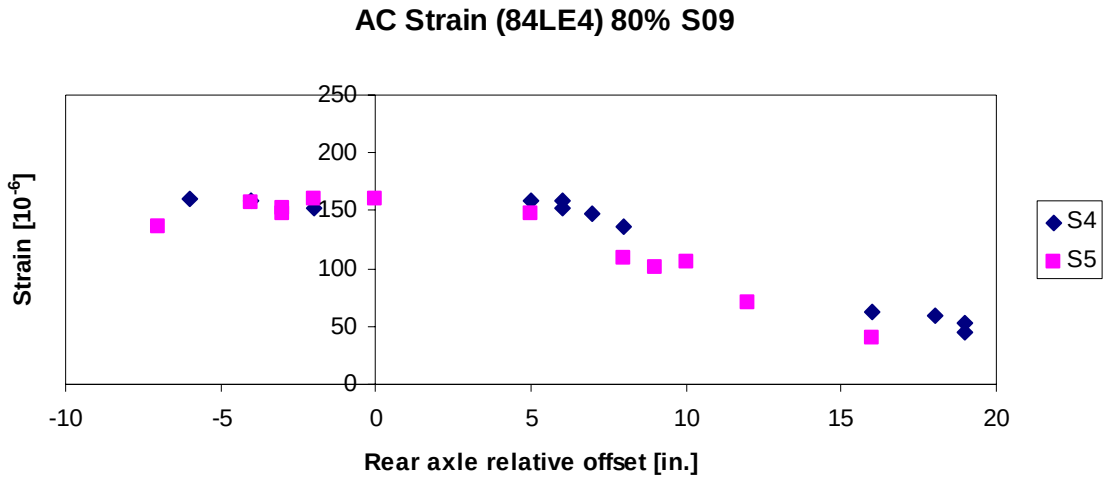

Figure 4.66. Cell 84 longitudinal asphalt strain generated at 80% load level for vehicles S4 and S5

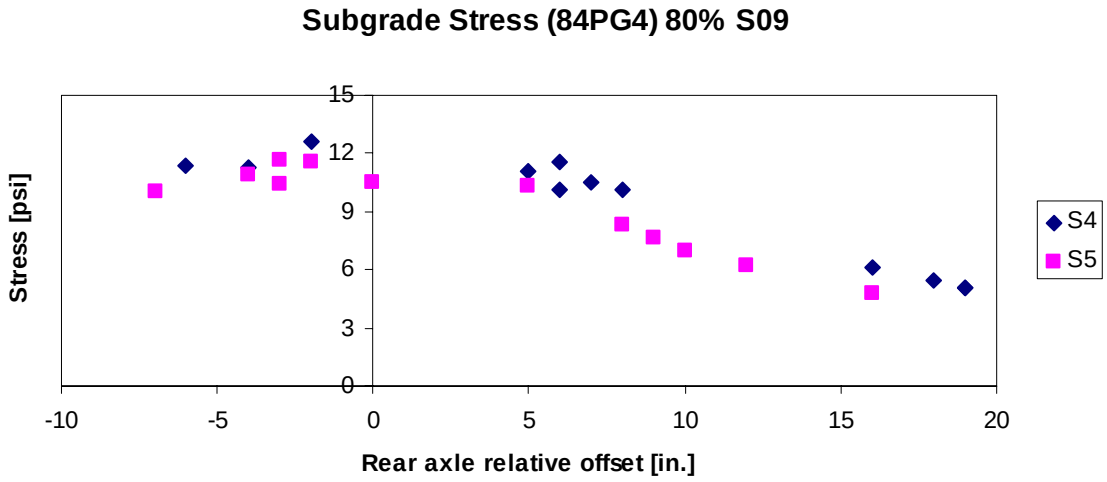

Figure 4.67. Cell 84 vertical subgrade stress generated at 80% load level for vehicles S4 and S5

Results show that vehicle S4 produces larger asphalt strains and subgrade stresses at 0% load levels on both Cells 83 and 84. When loaded to 80%, maximum asphalt strains of both vehicles at Cell 83 remain similar, but the distribution across the pavement width was not. Maximum responses for vehicle S5 were recorded when the vehicles' wheel

path was close to the sensor. For vehicle S4, the maximum occurs when the wheel path was toward the pavement shoulder (positive direction). At Cell 84, the response distributions across the pavement width show a decreasing trend, as both vehicles travel away from the sensor toward the shoulder. This not only shows the benefits of a paved shoulder, but also allows for a more objective representation between responses of both vehicles S4 and S5. Although maximum values were approximately similar, vehicle S4 was observed to consistently produce slightly larger strains and stresses across the pavement width.

The observed pavement response distributions in Cell 83 can be attributed to the difference in axle configuration between the two vehicles. Vehicle S4 was equipped with dual radial tires whereas S5 was equipped with a single flotation tire on one side of an axle. Because of the dual tire configuration (the half axle load is applied onto two separate wheels) the observed response distribution for vehicle S4 occurred when one side of the dual tires is completely on the aggregate shoulder and the other on the asphalt pavement. On the other hand, the center of the applied load of vehicle S5 was confined within the footprint of a single flotation tire, which allows for a more uniform distribution of the vehicle weight.

4.7 Effect of Vehicle Speed

Asphalt layers have viscoelastic properties and thus the stress-strain relationship is dependent on the loading rate. In general, the longer the duration of the load, the higher the asphalt strains. In this study, vehicles were tested at creep speed, 5 mph, 10 mph, and high speed (approximately 15 to 25 mph) to investigate the dependence of both asphalt strains and subgrade stresses on loading rate. Unfortunately, vehicles could not be tested at operating speeds (approximately 35 mph) due to the layout of the farm loop testing site. Nevertheless, vehicle T6 was presented here for tests performed in fall 2009 at 100% load level. Figure 4.68 through Figure 4.72 show the pavement responses across the pavement width relative to the sensor location. The following figures show the measured strain and stress measurements corresponding to target vehicle speeds. To ensure that the target speeds accurately describe the actual speed of the vehicle, the elapsed time of the axle responses obtained through the results of the Peak-Pick analysis was used to calculate the actual speed. Knowing the spacing between the vehicles' axles and the time between axle responses, the actual speed of the vehicle was determined. For this computation, it was sufficient to utilize the time elapsed of the first and second axle. The time elapsed recorded under the earth pressure cells (PG sensors) were used because they provide the cleanest and most consistent response waveforms. The actual speed of vehicle T6 presented in this section is summarized in Table 4.8.

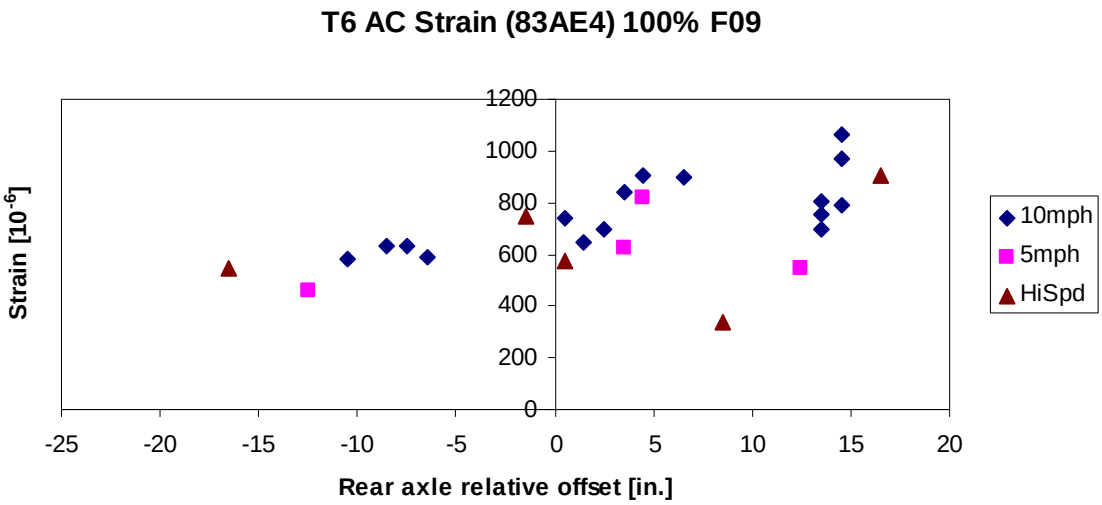

Figure 4.68. Cell 83 angled asphalt strain generated by vehicle T6 at various speeds in fall 2009

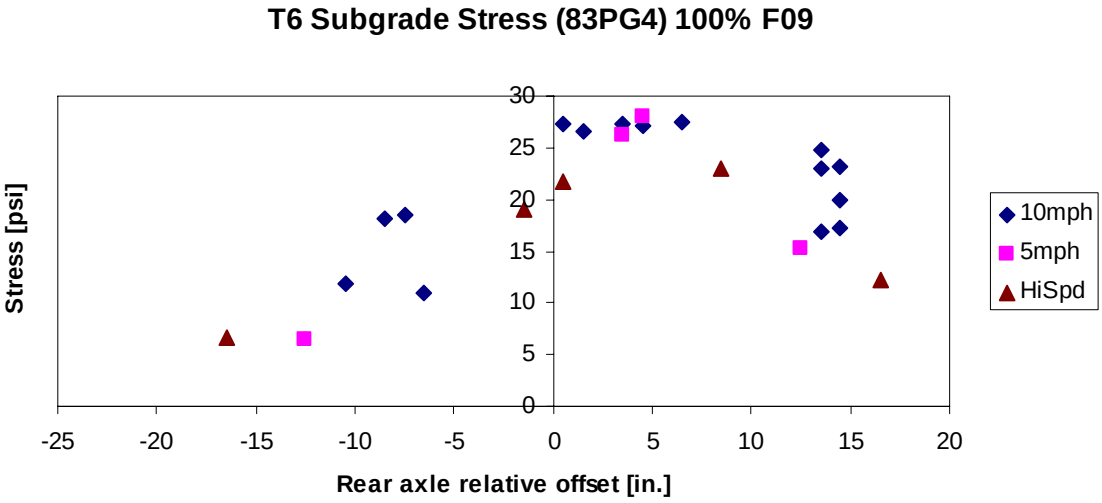

Figure 4.69. Cell 83 vertical subgrade stress generated by vehicle T6 at various speeds in fall 2009

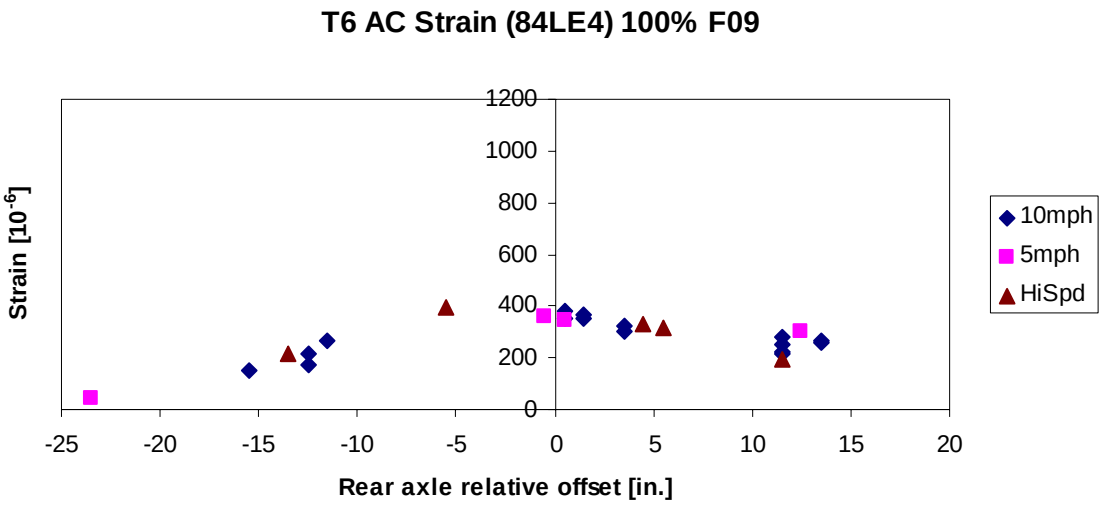

Figure 4.70. Cell 84 longitudinal asphalt strain generated by vehicle T6 at various speeds in fall 2009

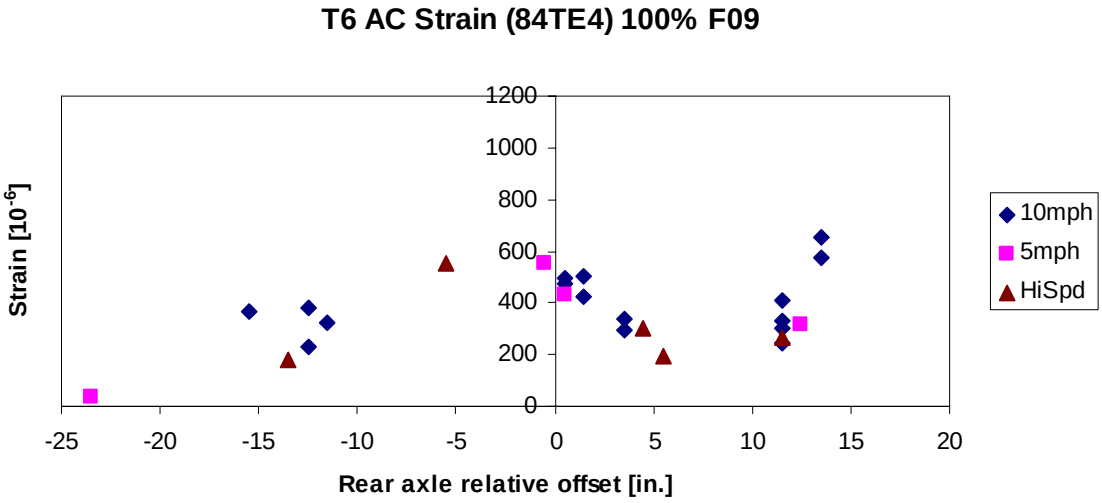

Figure 4.71. Cell 84 transverse asphalt strain generated by vehicle T6 at various speeds in fall 2009

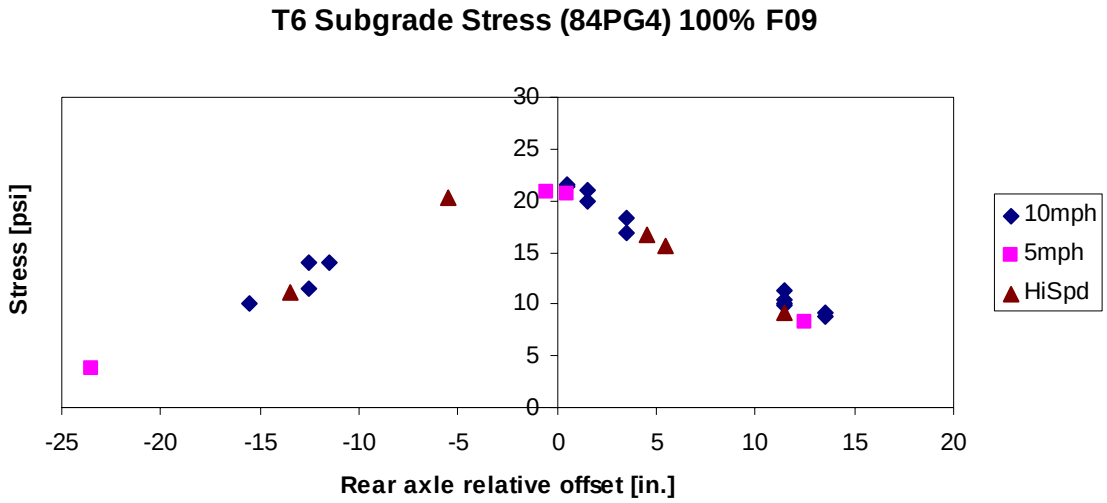

Figure 4.72. Cell 84 vertical subgrade stress generated by vehicle T6 at various speeds in fall 2009

Table 4.8. Computed actual speeds for vehicle T6

Target Speed	Actual Average Speed		Standard Deviation	
	Cell 83	Cell 84	Cell 83	Cell 84
5 mph	5.32 mph	5.30 mph	0.08 mph	0.08 mph
10 mph	10.36 mph	10.26 mph	0.46 mph	0.27 mph
High Speed	15.23 mph	15.56 mph	0.78 mph	0.29 mph

Analysis of Table 4.8 shows that the actual vehicle speeds were consistent with the target speeds. The standard deviations were no more than 1 mph from the average actual speed. Also, at high speeds, T6 was travelling at approximately 15 mph. The pavement responses show no strong correlation with vehicle speed. It was expected that asphalt strains should be highest for passes at 5 mph, and decrease as the vehicle speed increased. This trend was not obvious for vehicle T6 as well as other vehicles. Therefore, it can be concluded that strains were not significantly affected for the range of speeds and conditions of this study.

4.8 Tekscan Measurements

Heavy agricultural vehicles are equipped with tires that impart complex stress distributions. As explained in the previous section, tire footprints are different for various tire types and load levels. The purpose of conducting the Tekscan testing was to measure the tire footprint of the agricultural vehicles and obtain the tire loading pattern as vehicle weight increases. Vehicle T1 was used as an example in this section.

Vehicle T1 consisted of a John Deere 8430 tractor pulling a 6,000 gallon Houle tank. The first two axles belonged to the tractor and the last two belonged to the tank. When the tank was loaded, the majority of the total vehicle weight was shifted to the last two axles (i.e. axles three and four). An example of the tire footprints belonging to the third and fourth axles of vehicle T1 as axle weight increases are shown in Figure 4.73. The subsequent figure, Figure 4.74 shows the change in contact area for each axle as the axle weight increases. The left side vertical axis represents the contact area for the bar plots and the right side vertical axis represents the axle load for the line plots. The same type of figure was presented for average contact stress shown in Figure 4.75 with the left side vertical axis representing the contact stress. Appendix E contains the change in contact area and contact stress with axle weight for other vehicles tested with Tekscan.

Additionally, an overall comparison was made across all vehicles tested with Tekscan. The comparison was performed by selecting values for the axle with the highest axle weight when loaded to 80% load level. The values for that same axle were extracted at 0% load level to determine changes in contact area and contact stress. Table 4.9 summarizes the heaviest axle for all vehicles. Figure 4.76 illustrates the changes in contact area between 0% and 80% load levels whereas Figure 4.77 shows the changes in contact stress.

	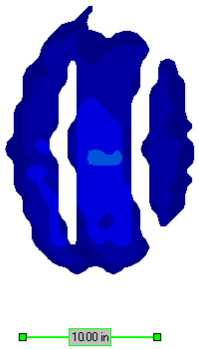	
T1 – Axle 3 – 6,280 lb	T1 – Axle 3 – 16,760 lb	T1 – Axle 3 – 21,000 lb
	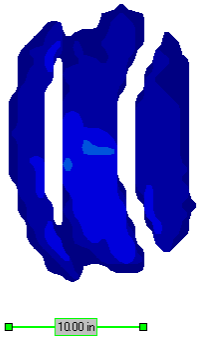	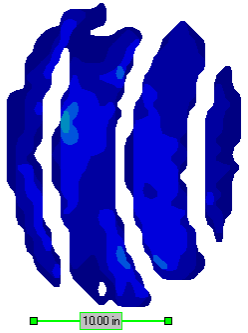
T1 – Axle 4 – 7,980 lb	T1 – Axle 4 – 19,550 lb	T1 – Axle 4 – 24,680 lb

Figure 4.73. Measured footprints for the third and fourth axles of vehicle T1 with corresponding axle weight

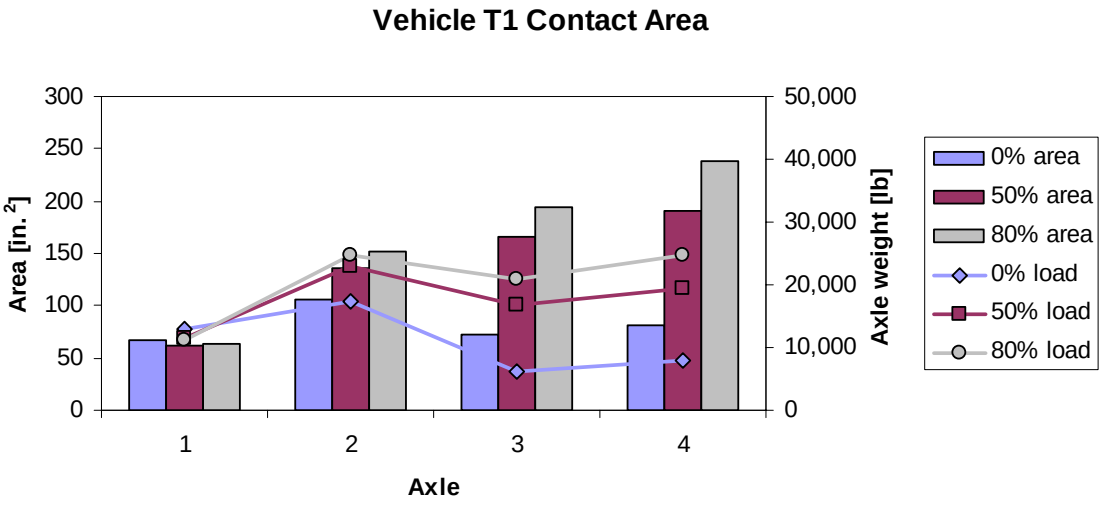

Figure 4.74. Change in contact area as axle load increases for vehicle T1's axles

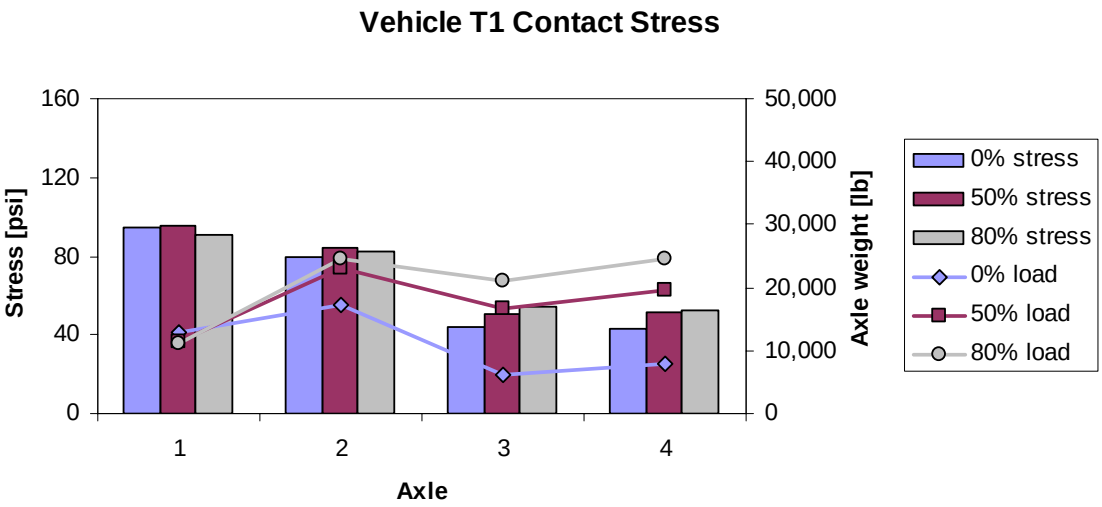

Figure 4.75. Change in average contact stress as axle load increases for vehicle T1's axles

Table 4.9. Heaviest axle at 80% load level

Vehicle	Axle	Axle Weight [lb]
S4	3	20,240
S5	3	19,900
R4	2	38,420
S3	2	30,600
T1	4	24,680
T2	3	16,920
T6	4	26,640
T7	2	22,680
T8	4	20,360
Mn80 (80 kip)	5	18,000

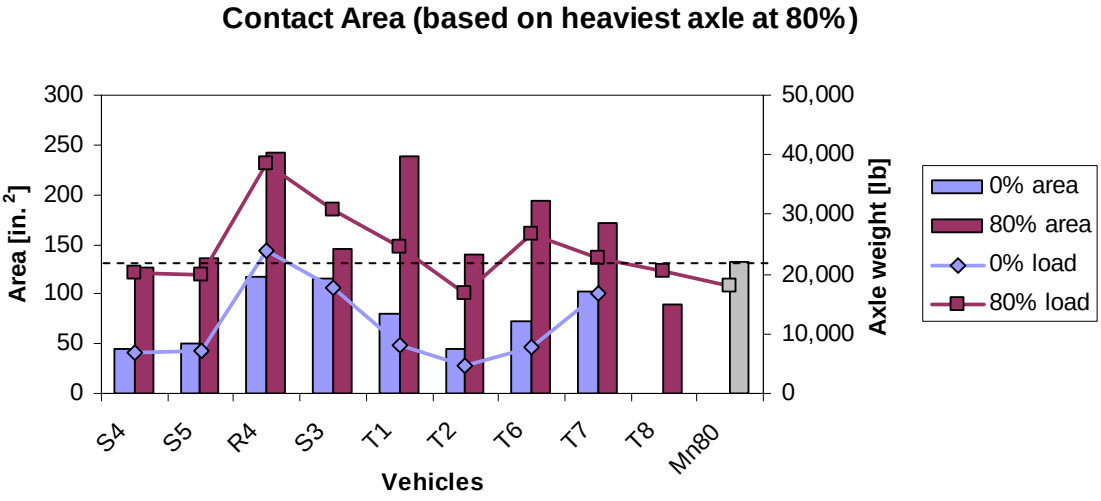

Figure 4.76. Contact area comparison between 0% and 80% load levels

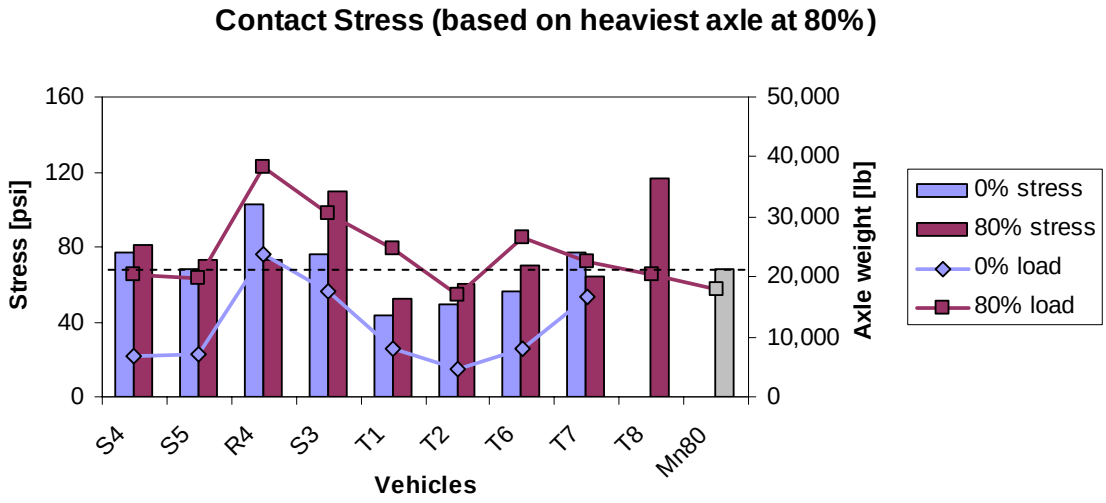

Figure 4.77. Average contact stress comparison between 0% and 80% load levels

Figure 4.74 shows that as the axle load increases the contact area increases as well. The increase in axle load has a minimal effect on average contact stress as shown in Figure 4.75. The increase in average contact stress is not significant due to the increase in contact area (Figure 4.76). For the majority of vehicles, an increase in axle load also leads to an increase in contact stress, although not proportionally. In some cases, the contact stress decreased with increasing load, as shown in Figure 4.77 for vehicles R4 and T7. Contact stress for vehicle S3 however, increased more than the other vehicles. This can be explained by how little the contact area expanded under the 80% load level. It should be noted that for all vehicles tested with Tekscan except T2, their measured axle weights loaded at 80% were higher than the maximum axle weight measured for Mn80. It is also worth noting that there are potential errors when performing the Tekscan test and processing the Tekscan data. For instance, Tekscan measurements could be affected by the acceleration of the vehicle as it rolls across the sensorial mat. This acceleration can cause the material inside the vehicle tank to shift which affects the exerted load between axles. Additionally, the Tekscan tests were performed with a moving load, but the post calibration was performed statically.

Apart from obtaining the contact area and average contact stress of these vehicles, manipulating the Tekscan measurements provided additional information regarding the loading pattern and load distribution of these tires. Knowing the load distributions of these complex tires greatly increases the accuracy in computer modeling. The conventional method of applying load to mimic a vehicle footprint in layered elastic theory is by approximating it with a uniformly distributed circular area. However, the complexity of agricultural vehicles' tires is not precisely modeled as such. Instead of using one loaded circular area, the entire actual footprint was estimated with several smaller circles called the multi-circular area representation. Figure 4.78 shows multi-circular area estimation for the second axle of vehicle T7. The effect of modeling the footprint using the gross area versus the multi-circular area estimation was quite considerable. This information was extensively used in the layered elastic modeling section discussed in the next chapter.

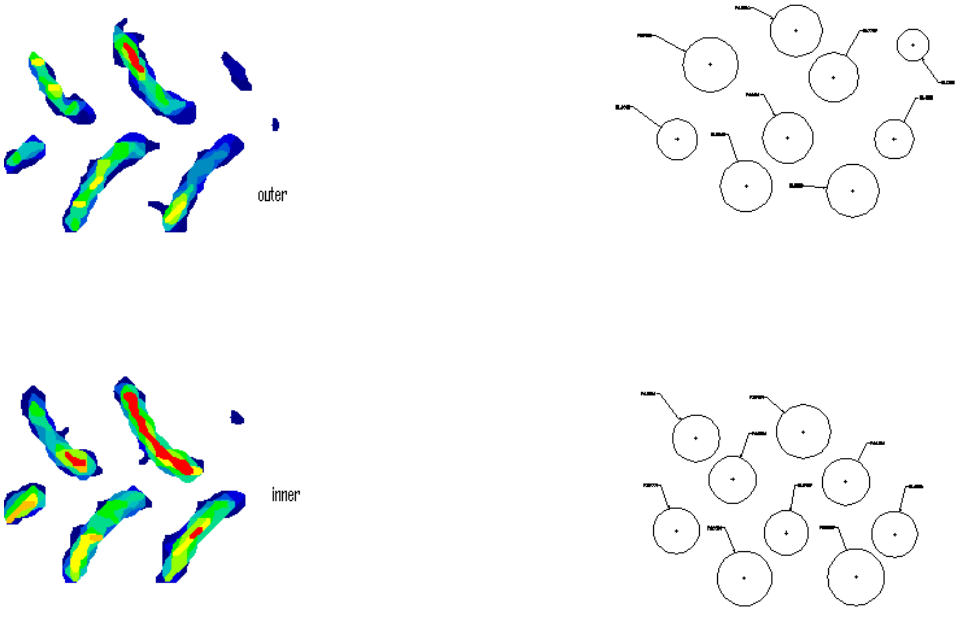

(a) (b)

Figure 4.78. Second axle footprint of vehicle T7 (a) measured using Tekscan (b) multi-circular area representation

4.9 Summary

As stated previously, pavement responses are influenced by axle loads, environmental effects, pavement structure, and vehicle wheel path. Analysis showed that the transverse location of the vehicles' wheel path affects which axle was responsible for the maximum pavement responses.

Asphalt strain responses were consistently lower in the spring compared to the fall season. However, observations showed no strong correlation between subgrade stresses and seasonal changes. Testing performed in the morning resulted in lower asphalt strains and subgrade stresses compared to testing performed in the afternoon. Agricultural vehicles loaded at 80% and 100% load levels recorded larger subgrade stresses compared to the control vehicle (Mn80) during testing in both spring and fall seasons. Asphalt strains generated by the agricultural vehicles in the spring tests recorded higher asphalt strains than vehicle Mn80. However, testing conducted in the fall seasons resulted in vehicle Mn80 generating larger asphalt strains compared to the tested agricultural vehicles.

A thicker asphalt and base layers resulted in lower asphalt strain and subgrade stress responses. Additionally, the absence of a paved shoulder greatly increases both asphalt strain and subgrade stress measurements as the vehicles' wheel path approaches the pavement edge. Analysis showed that an increase in gross vehicle weight resulted in an increase in asphalt strain and subgrade stress. No significant benefits were observed between flotation tires and radial tires in pavement responses. Preliminary analysis showed no significant effect of the range of tested vehicle speed. Tekscan measurements showed that the agricultural vehicles' contact area increased as axle weight increased. The increase in average contact stress was not significant as axle weight increase due to the growth in contact area.

Chapter 5 Semi-Analytical Modeling

5.1 Background

Although the full scale testing provided a wealth of information on pavement responses from agricultural equipment, it could not cover all combinations of vehicle types and site conditions of interest. To address this limitation, a semi-analytical model capable of extrapolating the results of the field testing should be developed. Although development of such a model is beyond the scope of this thesis, some preliminary modeling efforts related to verification of trends observed in the study and material parameter identification have been conducted. This chapter summarizes some of these activities.

In the past, various mechanical models have been utilized to predict pavement responses from heavy vehicle loading. Loulizi et al. (2006) conducted 3D finite element modeling using the general purpose finite element package, ABAQUS, to validate pavement responses collected at the Virginia Smart Road [11]. Novak et al. (2003) performed 3D finite element analysis using the general purpose software, ADINA, along with a sophisticated method of determining contact stresses of radial tires. They included contact stresses in the vertical, longitudinal, and transverse directions [12]. Park et al. (2005) conducted 3D finite element analysis using ABAQUS and used measured tire contact stresses from the vehicle-road-surface-pressure-transducer-array (VRSPTA). The ABAQUS results were then compared to layered elastic analysis using BISAR and were found to be comparable [13]. Siddharthan et al. (2005) investigated pavement responses of off-road vehicles with complex tire patterns through a 3D moving load finite layer analysis. The applied tire contact stresses were also obtained through VRSPTA. It was found that predicted responses differed from field measured values by up to approximately 30% [14].

Layered elastic theory was used as the main modeling tool at this stage of the project. This is largely due to its common use in pavement design methodologies and also for its simplicity and low computational time. A detailed description of the layered elastic theory is discussed by Huang (2004) [15]. The major assumptions within the layered elastic theory include:

1. Layers are homogenous, isotropic, and linear elastic.
2. No body forces or temperature strains are considered.
3. Each layer has finite thickness except the last layer which has infinite depth.
4. Layers are infinite in the lateral direction.
5. There are no discontinuities within each layer.
6. Load is applied statically and uniformly over a circular area giving an axisymmetric solution.

Two layered elastic programs, MnLayer and BISAR, were used to investigate the importance of detailed modeling of tire contact area and contact stress of agricultural vehicles. Additionally, a backcalculation framework using an optimization tool known as DAKOTA was included. This backcalculation method made use of measured stresses and strains under vehicle loading and falling weight deflectometer (FWD) deflections to determine the pavement layers' Young's moduli.

5.2 Vehicle Contact Area Analysis

Several studies have been conducted on the effects of tire-pavement interaction on pavement responses. These studies suggested that obtaining realistic representations of the tire footprint and contact stresses are crucial in achieving a more accurate prediction of pavement responses in the modeling process [12, 14, 16]. In this study, Tekscan measurements of the footprint of agricultural vehicles' tires were utilized to model pavement-tire interaction using the layered elastic software, BISAR. This allowed for a

comparison with simplified tire-contact modeling using the equivalent net area and the equivalent gross area. These comparisons are described below.

Figure 5.1 and Figure 5.2 illustrate the contact areas used in this analysis for T7s first and third axles, respectively. Figure 5.1(a) shows the actual footprint measured using Tekscan, which represents the net contact area. This net area was converted into an equivalent circular area. Figure 5.1(b) shows the footprint within a boxed area, which represents the gross contact area and also an equivalent circular area. Figure 5.1(c) shows the multi-circular area derived from the actual footprint and weighted by the calibrated stress distribution. The same sequence is shown in Figure 5.2 for the third axle. The first axle's equivalent net area was determined to be 75.26 $in.^2$ with a radius of 4.89 in. The gross area was 236.97 $in.^2$ with a radius of 8.69 in. The third axle's equivalent net and gross areas were 189.49 $in.^2$ and 380.77 $in.^2$, respectively. The corresponding radii were 7.77 in. and 11.01 in., respectively. Load information for the equivalent net and gross contact areas for both axles are shown in Table 5.1. Table 5.2 summarizes the values of the multi-circular contact areas, including the load coordinates with the origin located at the centroid of the footprint.

Pavement geometric structure mimics those of Cell 84, with asphalt and base layer thicknesses of 5.5 in. and 9.0 in., respectively. Pavement material properties used for this analysis represent typical Young's moduli values for the pavement layers [6, 17]. Young's moduli for the asphalt, base and subgrade were assigned to be 500 ksi, 25 ksi, and 10 ksi, respectively. Poisson's ratios were assumed to be 0.35, 0.40, and 0.45 for the asphalt, base and subgrade layers, respectively.

A layered elastic analysis program, BISAR, was used to simulate the pavement responses that were measured in the field, such as longitudinal (*xx*) and transverse (*yy*) strains at the bottom of the asphalt layer and vertical (*zz*) stresses at the top of the subgrade. Analysis points for equivalent contact area cases (net and gross) were located under the center of the load. For multi-circular tire footprint representation, analysis points were spaced 2.5

in. apart in both the *x* and *y* directions. A grid over the evaluation points from -7.5 in. to 7.5 in. in both the *x* and *y* directions was used in the analysis of the first axle. A grid over the evaluation points from -7.5 in. to 7.5 in. in the *x* direction and -7.5 in. to 10 in. in the *y* direction was used in the analysis of the third axle. Additional analysis points were placed directly under each circle of the multi-circular loads for both axle cases.

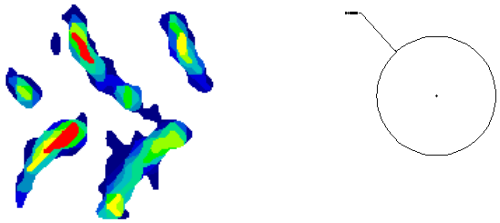

(a)

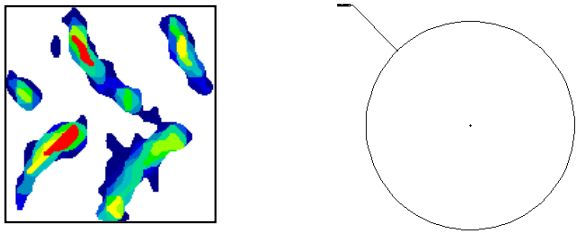

(b)

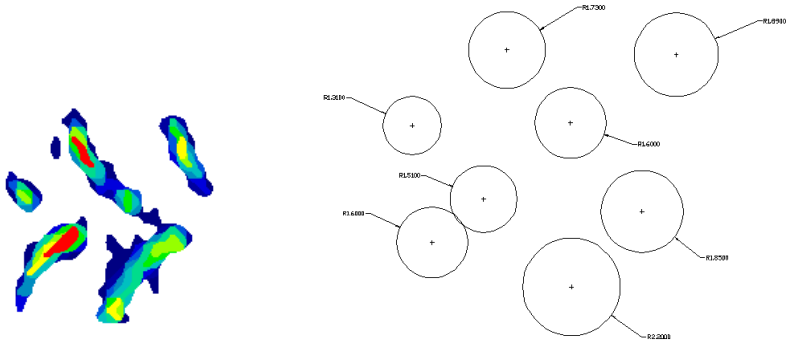

(c)

Figure 5.1. Vehicle T7's first axle footprint modeling using (a) equivalent net contact area (b) equivalent gross contact area (c) multi-circular area representation

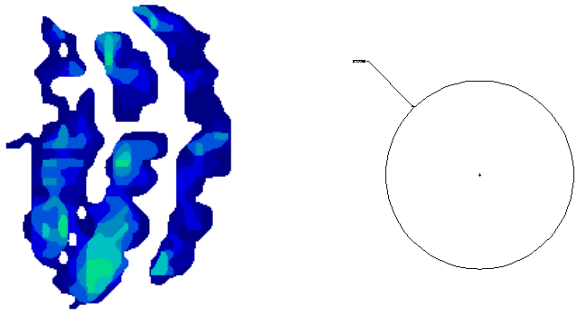

(a)

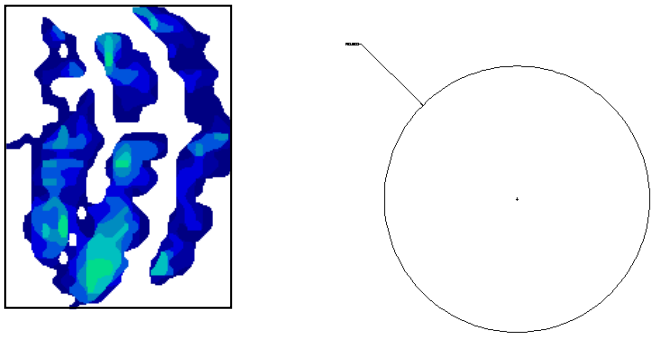

(b)

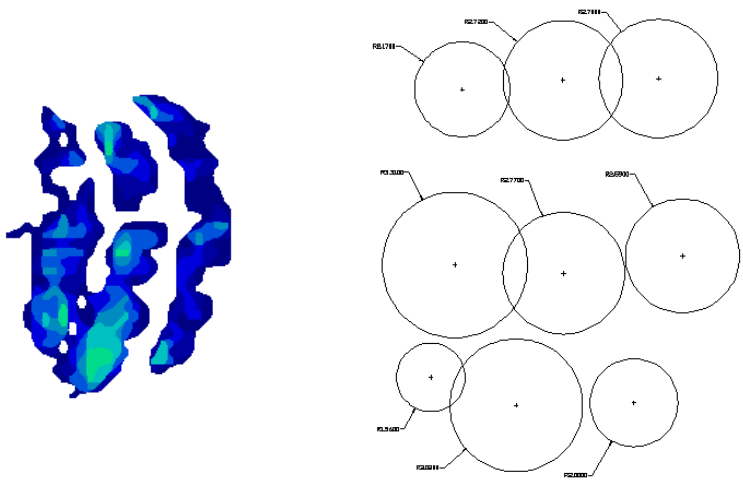

(c)

Figure 5.2. Vehicle T7's third axle footprint modeling using (a) equivalent net contact area (b) equivalent gross contact area (c) multi-circular area representation

Table 5.1. Equivalent net and gross contact areas for vehicle T7

Axle	Area	Area [in.^{2}]	Radius [in.]	Load [lb]	Stress [psi]
Axle 1	Net	75.26	4.89	4860	64.58
Axle 1	Gross	236.97	8.69	4860	20.51
Axle 3	Net	189.49	7.77	8780	46.34
Axle 3	Gross	380.77	11.01	8780	23.06

Table 5.2. Multi-circular area representation values for vehicle T7's first and third axle

Axle	Section	*x*-coord [in.]	*y*-coord [in.]	Area [in.^{2}]	Radius [in.]	Load [lb]	Stress [psi]
Axle 1	1	-6.10	1.99	5.38	1.31	347.13	64.58
	2	-5.21	-3.28	8.06	1.60	520.70	64.58
	3	-1.83	5.40	9.41	1.73	607.48	64.58
	4	-2.88	-1.33	7.17	1.51	462.84	64.58
	5	1.03	2.11	8.06	1.60	520.70	64.58
	6	1.07	-5.28	15.23	2.20	983.54	64.58
	7	5.80	5.19	11.20	1.89	723.19	64.58
	8	4.26	-1.89	10.75	1.85	694.27	64.58
Axle 3	1	-3.64	8.11	14.78	2.17	684.96	46.34
	2	-3.97	0.12	34.49	3.31	1598.25	46.34
	3	-5.06	-5.00	7.62	1.56	352.86	46.34
	4	0.94	8.53	23.29	2.72	1079.34	46.34
	5	0.98	-0.26	24.19	2.77	1120.85	46.34
	6	-1.19	-6.27	28.67	3.02	1328.42	46.34
	7	5.29	8.61	22.85	2.70	1058.58	46.34
	8	6.38	0.54	21.05	2.59	975.56	46.34
	9	4.17	-6.16	12.54	2.00	581.18	46.34

Table 5.3. Maximum computed responses for vehicle T7's first and third axle

Axle	Area	Longitudinal AC Strain (*xx*) [$\times 10^{-6}$]	Transverse AC Strain (*yy*) [$\times 10^{-6}$]	Vertical Subgrade Stress (*zz*) [psi]
Axle 1	Net	154	154	3.27
	Gross	90	90	2.95
	Multi-circular	100	97	3.01
Axle 3	Net	184	184	5.49
	Gross	122	122	4.91
	Multi-circular	163	139	5.10

Results of the layered elastic analysis are shown in Table 5.3. As expected, strain and stress responses computed using equivalent net contact area were larger than those calculated using the equivalent gross contact area. These discrepancies were more profound for asphalt strains than subgrade stresses. This can be explained by the complexity of the tire footprint and how it affects near surface responses. As the analysis point moves away from the applied load, the effects of the load distribution geometry (footprint) are less significant. One of the benefits of modeling using both net and gross contact areas is the ability to establish a lower and upper limit in computed responses. However, multi-circular representation of the tire contact generally provides a more accurate and realistic representation of the vehicle load distribution and improved the accuracy in response prediction. This proves to be an important aspect to be considered, especially when it comes to simulating responses as a function of traffic wander.

5.3 Traffic Wander Simulation

To further evaluate the importance of vehicle traffic wander, a layered elastic simulation using BISAR was performed for a footprint belonging to the third axle of vehicle T7 using the multi-circular footprint estimation as previously mentioned. This analysis was performed to show that changes in the lateral direction of the wheel load would affect the resulting strain at the bottom of the asphalt layer and stress on top of the subgrade. The simulated pavement structure mimics the pavement section of Cell 84, with details shown in Table 5.4. Figure 5.2(c) shows the footprint obtained using Tekscan and corresponding multi-circular footprint estimation used for the layered elastic analysis. Evaluation points were situated along the lateral direction from the center of the load to simulate various vehicle offsets.

To validate the field observation that traffic wander influences pavement responses, simulated asphalt strains and subgrade stresses were compared to the measurements obtained from the field. Pavement responses generated by vehicle T7's third axle were examined. To eliminate the effects of layer material properties and focus on the effects

of traffic wander on pavement responses, the simulated longitudinal and transverse asphalt strains were normalized using their respective maximum simulated strain values. This normalization was also performed for simulated subgrade stresses. In addition, field measurements were also normalized to their respective maximum values. Figure 5.3 shows the resulting normalized measured and simulated transverse and longitudinal asphalt strains, and Figure 5.4 shows the resulting normalized measured and simulated vertical subgrade stresses.

Table 5.4. BISAR pavement structure input parameters

Layer	Young's Modulus	Poisson's Ratio	Thickness
1. Asphalt	500,000 psi	0.35	5.50 in.
2. Base	15,000 psi	0.40	9.00 in.
3. Subgrade	7,000 psi	0.45	

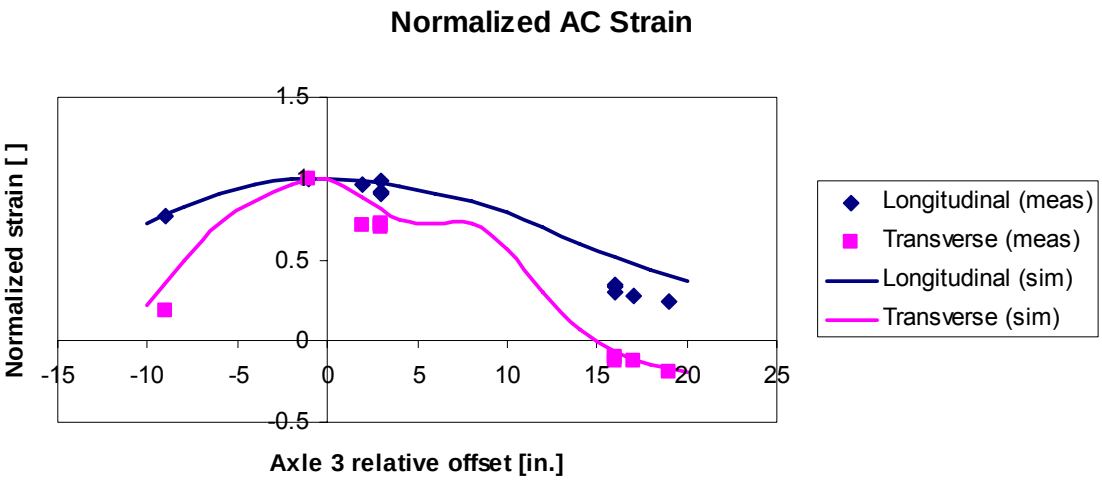

Figure 5.3. Normalized measured and simulated longitudinal and transverse asphalt strains

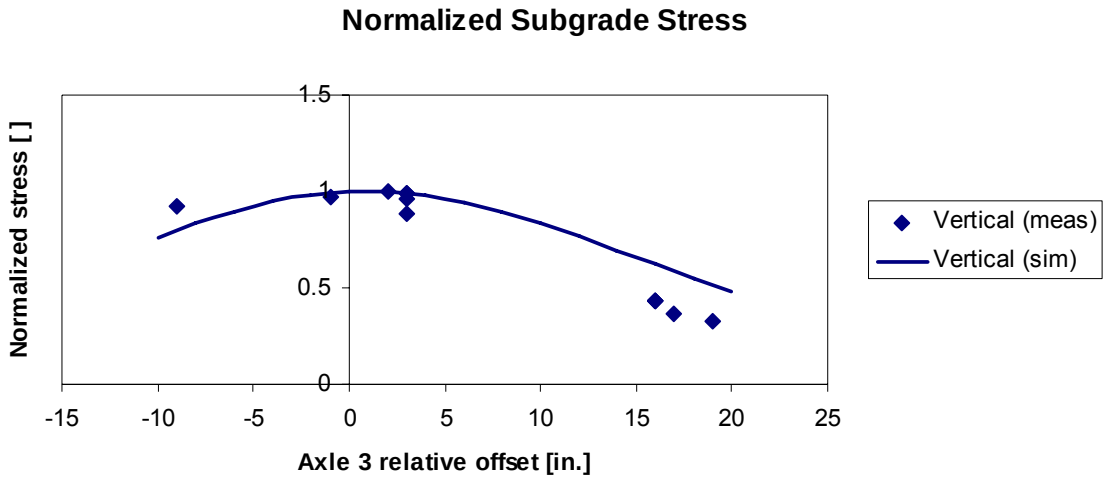

Figure 5.4. Normalized measured and simulated vertical subgrade stress

Figure 5.3 and Figure 5.4 show an excellent agreement between measured and simulated trends. Figure 5.3 shows that both measured and calculated strains significantly decrease as the load moves away from the sensor. This trend is more pronounced for the transverse strains as compared to longitudinal strains, although it is still significant for the longitudinal strains. For example, deviation of the footprint more than 15 in. from the sensor caused a reduction in longitudinal strains by more than half. For the same deviation from the sensor, the transverse strain changes from tension to compression. Similar trends can be observed in Figure 5.4 for subgrade stresses. For example, deviation of the footprint more than 15 in. from the sensor caused a reduction in subgrade stresses by half. This analysis shows that field measurements and theoretical predictions agree that the applied load position has a profound effect on pavement responses.

5.4 Backcalculation Analysis

Elastic properties in the pavement layer are important parameters for layered elastic analysis. These parameters are usually determined either from laboratory studies or FWD testing. Although these methods are widely accepted in pavement modeling, it is desirable to check if the parameters can be obtained from measured stresses and strains. In this study, a numerical optimization framework was developed to perform a backcalculation analysis to obtain the layers' Young's moduli by matching the measured pavement responses. This process utilizes two programs: the layered elastic software called MnLayer and the optimization software called DAKOTA.

DAKOTA, developed by Sandia National Laboratories, is an abbreviation for Design Analysis Kit for Optimization and Terascale Applications which main purpose is to function as a toolkit for optimization methods, parameter estimation, and uncertainty quantification, among others. The application of DAKOTA requires a user defined simulation code, evaluation of the performance objectives, and parameter/variable adjustment commands. Coupling together these items creates an iterative optimization environment that outputs an optimal solution as defined in the performance objectives [18]. In the case of the backcalculation optimization process employed here, the simulation code is the layered elastic software MnLayer, the performance objective or cost function is the error between computed and measured data, and the parameters are the Young's moduli values of the pavement layers. Figure 5.5 shows a flow chart illustrating the overall schematic of the optimization process.

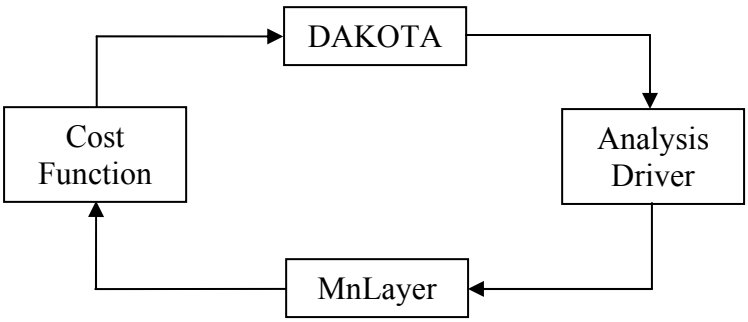

Figure 5.5. Flow chart of the optimization process

The general objective of this optimization process is to determine the Young's moduli for the asphalt, base, and subgrade layers denoted as $E1$, $E2$, and $E3$, respectively. This is done by minimizing discrepancies between measurements obtained in the field generated by a particular vehicle pass and corresponding responses predicted by MnLayer. The process begins with assignment of an initial value for each layer moduli defined in the DAKOTA input file. Next, the analysis driver transfers the moduli values into the MnLayer input file via user defined scripts. The layered elastic analysis is then performed to calculate stress on the top of the subgrade and strain at the bottom of the asphalt layer. The maximum calculated stress and strain values are then extracted and compared to the field measured stress and strain to obtain the cost function, e, expressed in Eqn 5.1 also through a user defined script.

$$e = \left(1 - \frac{\varepsilon_{calc}}{\varepsilon_{meas}}\right)^2 + \left(1 - \frac{\sigma_{calc}}{\sigma_{meas}}\right)^2 \qquad \text{Eqn 5.1}$$

where e is the cost function

ε_{calc} is the calculated strain

ε_{meas} is the measured strain

σ_{calc} is the calculated stress

σ_{meas} is the measured stress

After the cost function, *e*, is computed, it is returned to DAKOTA, which determines a new set of values for *E*1, *E*2, and *E*3. The iteration continues until an acceptable cost function is reached or until the maximum number of iterations is met. The optimization method DAKOTA employs is in the COLINY (Common Optimization Library Interface) library, which contains nongradient-based optimization algorithms suited for this exercise [18]. In the COLINY library, a local optimization method is used, known as the pattern search. The COLINY optimization method also supports upper and lower limits, as well as nonlinear constraints imposed on the parameters. An example of the iteration process was performed for the rear tandem axles (axles 4 and 5) of vehicle Mn80 at -2.5 in. offset. This example used the measured asphalt strain and subgrade stress values of 426 $\times 10^{-6}$ and 12.21 psi, respectively. Figure 5.6 through Figure 5.8 show an example of the iteration process for *E*1, *E*2, and *E*3, while Figure 5.9 shows the convergence of the cost function, *e*. The figures show the convergence pattern for each of the moduli values and the cost function using the pattern search optimization method. According to Figure 5.9, the minimum cost function, *e* was obtained at iteration number 163 with a value of 1.24 $\times 10^{-9}$. Analysis of Figure 5.6 through Figure 5.8 showed that the Young's moduli for the asphalt (*E*1), base (*E*2), and subgrade (*E*3) layers converged to 565,844 psi, 8,054 psi, and 6,274 psi, respectively at iteration number 163.

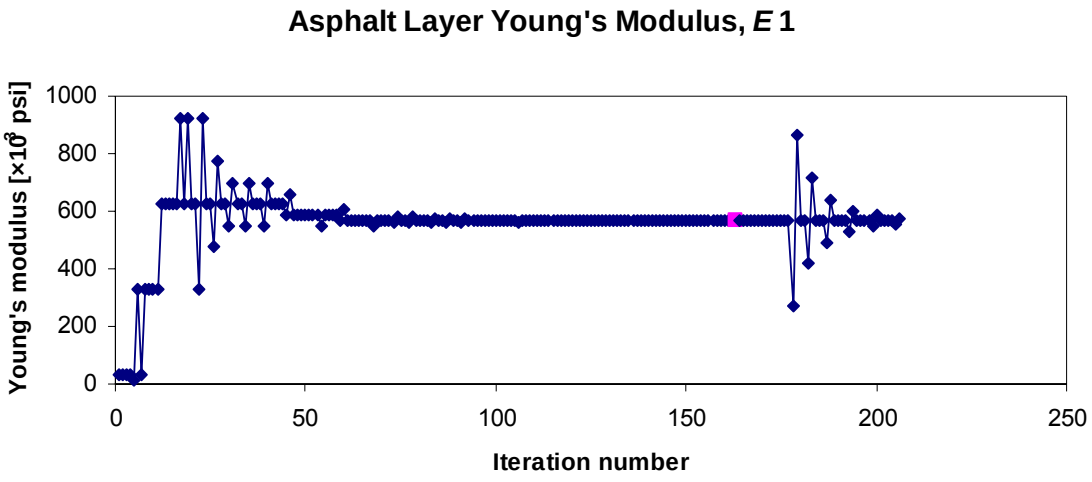

Figure 5.6. Convergence pattern for asphalt layer Young's modulus, *E*1

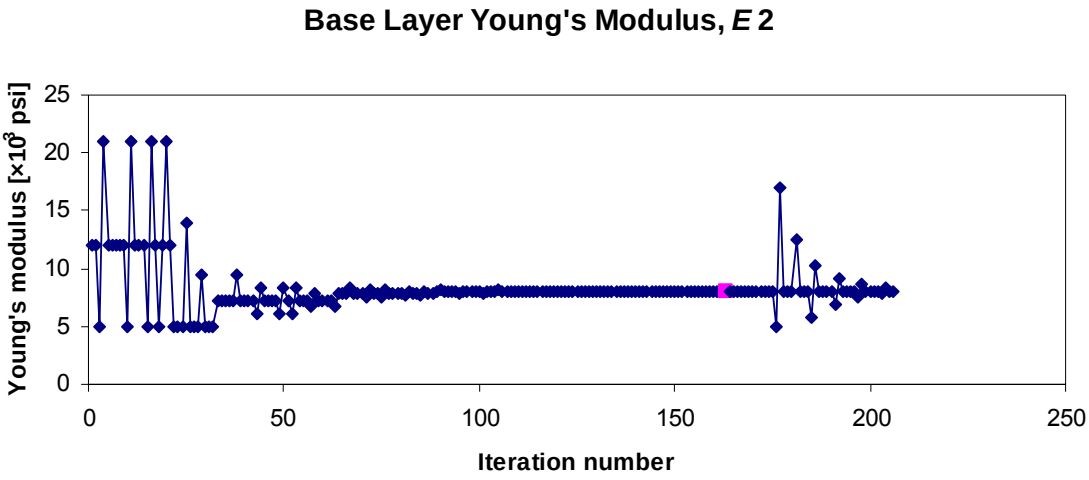

Figure 5.7. Convergence pattern for base layer Young's modulus, *E*2

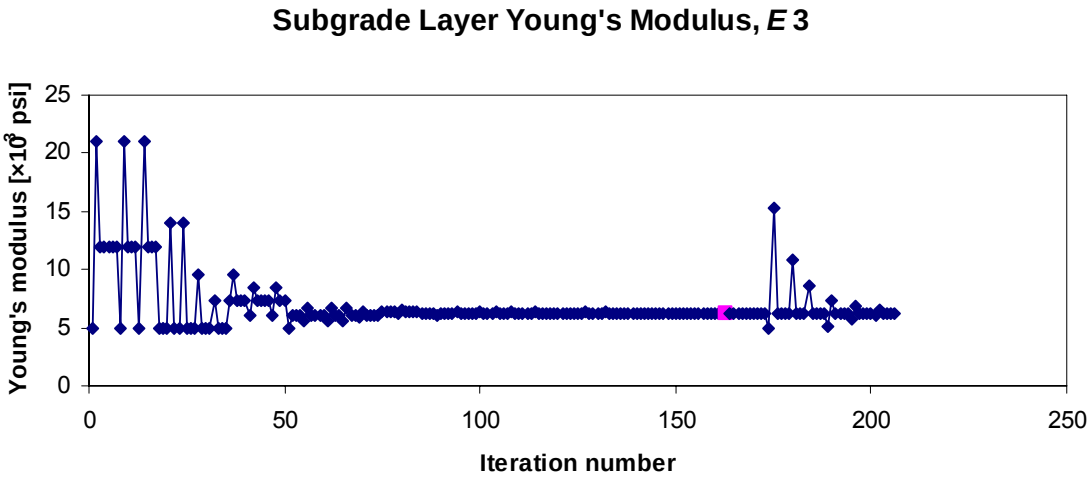

Figure 5.8. Convergence pattern for subgrade layer Young's modulus, *E*3

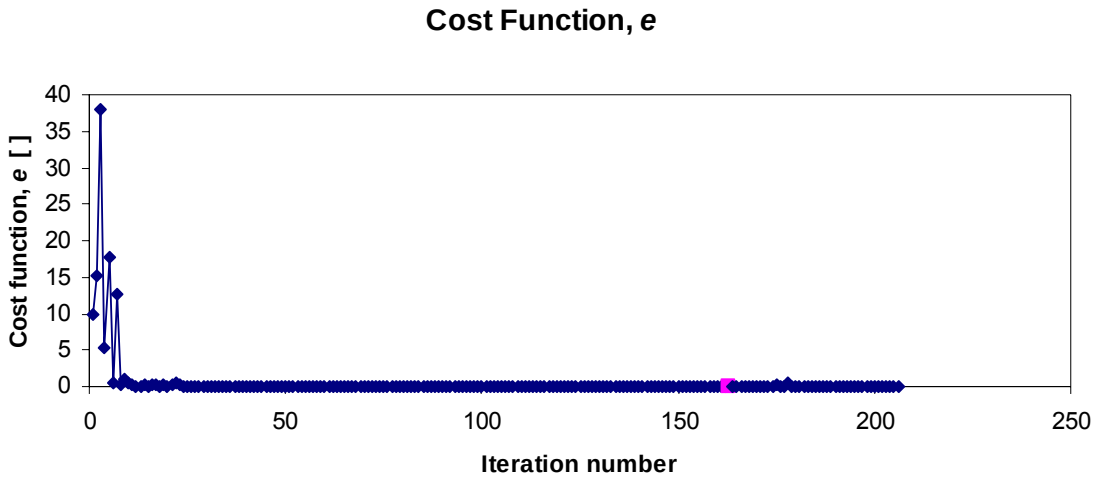

Figure 5.9. Convergence pattern for cost function, *e*

5.4.1 Backcalculation through Vehicle Loading

An example of the DAKOTA-MnLayer backcalculation optimization process is presented here to introduce the initial capabilities of this framework. A preliminary backcalculation was performed based on seasonal changes to observe how moduli values were affected. Responses collected for the trailers' tandem axle of vehicle Mn80 (axles 4 and 5) were extracted and the maximum axle responses between axles 4 and 5 were used as the variables to evaluate *e*. These axles were chosen because they represent the heaviest axles of the vehicle. The upper and lower bounds of the optimized parameters (i.e. *E*1, *E*2, and *E*3) were adjusted based on typical moduli ranges found in the literature for different seasons. The Young's modulus for the asphalt layer, *E*1, was assumed to be generally lower in the fall compared to the spring season. The modulus for the subgrade, *E*3, was assumed to be very stiff in spring due to its frozen state. Poisson's ratio, *v*, for the asphalt, base, and subgrade layers were set at 0.35, 0.40, and 0.45, respectively. Pavement geometric structure of Cell 84 was analyzed. Additionally, a constraint was imposed such that parameter *E*2 could not be less than *E*3 for simulations performed for the fall season. However, in the spring season the constraint was removed. Table 5.5

summarizes the initial values, upper bounds, and lower bounds used for this process. Evaluation of measured vertical subgrade stress and longitudinal asphalt strain responses generated by vehicle Mn80s' axles 4 and 5 at Cell 84 for spring and fall seasons are shown in Table 5.6.

Young's moduli for the pavement layers are affected by the surrounding climatic environment. The backcalculation analysis was performed under the presumption that effect of temperature and moisture on pavement responses can be reflected by the stiffness (moduli) of the pavement layers. According to Table 5.7, backcalculated moduli within the specified bounds were deemed to be valid, since they produced cost functions that were very close to zero. This further solidifies the assumptions previously made, where the asphalt moduli are lower in fall than in spring and that the subgrade layer was very stiff in spring. A forward analysis was later performed using the backcalculated moduli values to check the accuracy of the optimization. This was achieved by regenerating asphalt strains and subgrade stresses for vehicle Mn80s' rear tandem axles under the same conditions as the backcalculation. Table 5.8 shows the measured and simulated asphalt strains and subgrade stresses for both the fall and spring seasons. The forward analysis results proved to be satisfactory.

Table 5.5. Parameter initial values, upper, and lower bounds

Fall Season*	***E*1 [ksi]**	***E*2 [ksi]**	***E*3 [ksi]**
Initial Value	30	12	12
Lower Bound	15	5	5
Upper Bound	500	50	50
Spring Season**	***E*1 [ksi]**	***E*2 [ksi]**	***E*3 [ksi]**
Initial Value	500	12	250
Lower Bound	250	1	150
Upper Bound	2,000	50	300

*Contraint $E2 \geq E3$
** No constraint

Table 5.6. Response measurement variables for spring and fall seasons at Cell 84

Season	Axle	Relative Offset [in.]	Longitudinal AC Strain (*xx*) [$\times 10^{-6}$]	Vertical Subgrade Stress (*zz*) [psi]
Fall	Axle 4	-3.5	434	11.13
	Axle 5	-3.5	377	9.15
Spring	Axle 4	-3.0	133	9.75
	Axle 5	-3.0	136	9.81

Table 5.7. Backcalculated Young's modulus values

Season	*E*1 [ksi]	*E*2 [ksi]	*E*3 [ksi]	*e* [ ]
Fall	66.4	25.4	24.6	9.5×10^{-10}
Spring	715.2	17.5	273.6	3.9×10^{-7}

Table 5.8. Forward analysis using backcalculated moduli

Season	Relative Offset [in.]	Longitudinal AC Strain (*xx*) [$\times 10^{-6}$]		Vertical Subgrade Stress (*zz*) [psi]	
		Measured	Simulated	Measured	Simulated
Fall	-3.5	434	434	11.13	11.13
Spring	-3.0	136	136	9.81	9.81

5.4.2 Backcalculation through FWD Loading

Another example used to demonstrate the DAKOTA-MnLayer framework is shown in this section with a comparison of backcalculated moduli using combinations of pavement surface deflections, horizontal strain at the bottom of the asphalt layer, and vertical subgrade stress measurements. Asphalt strain and subgrade stress responses generated by dropping the falling weight deflectometer (FWD) load directly on top of the marked sensor location were measured. In addition, the pavement deflection basin was measured by the FWD device itself at 0, 8, 12, 18, 24, and 36 in. from the center of the load. Loads applied by the FWD were 13 kip over an area with a radius 5.9 in. The FWD testing was performed in July and September of 2010. Therefore, the parameter upper and lower bounds were changed accordingly to address the constraint where *E*2 could not be less

than *E*3. The backcalculation of the layer moduli were conducted to match the following measured responses:

- surface deflections only (case δ_i)
- subgrade stress and surface deflections (case σ - δ_i)
- asphalt strain and surface deflections (case ε - δ_i)
- subgrade stress and asphalt strain (case σ - ε)
- surface deflections and asphalt strain and subgrade stress (case δ_i - ε - σ)

In order to accommodate the additional variables to be evaluated in the optimization process, computation of the cost function, *e*, was modified as shown by Eqn 5.2. This modified *e* allows for the inclusion or exclusion of certain variables by changing the weight factor, *w*. If a variable was considered in analysis than the corresponding weight factor was set to be 1 whereas excluded variables had a weight factor of 0.

$$e = \left(1 - \frac{\varepsilon_{calc}}{\varepsilon_{meas}}\right)^2 (w_1) + \left(1 - \frac{\sigma_{calc}}{\sigma_{meas}}\right)^2 (w_2) + \sum_{i=1}^{6} \left(1 - \frac{\delta_{calc\,i}}{\delta_{meas\,i}}\right)^2 (w_{i+2}) \qquad \text{Eqn 5.2}$$

where e is the cost function

ε_{calc} is the calculated strain

ε_{meas} is the measured strain

σ_{calc} is the calculated stress

σ_{meas} is the measured stress

$\delta_{calc\,i}$ is the *i*th calculated deflection

$\delta_{meas\,i}$ is the *i*th measured deflection

w is the weight factor (either 0 or 1)

i is the number of deflection points (from 1 to 6 in this case)

Table 5.9 shows the measured data collected from the FWD test in July and Table 5.10 shows the backcalculated results using the case of ε-δ_i and case δ_i only. The forward analysis results using the backcalculated moduli values are shown in Table 5.11. It can be observed that there is a significant discrepancy (more than an order of magnitude) between the measured and calculated subgrade stresses. This prompted an additional investigation which resulted in a hypothesis that the marked location of the earth pressure cell was incorrect. To examine this hypothesis, subgrade stresses were simulated at various distances from the marked pressure cell location. Two sets of the layer material properties from Table 5.10 were used in these simulations. The results of this analysis are presented in Figure 5.10. An analysis of Figure 5.10 shows that the approximate location of the earth pressure cell with a field measurement of 0.39 psi are 36 in. and 42 in. depending on the set of Young's moduli used in the analysis. Additional testing performed using magnetic tomography device, MIT Scan T2 confirmed that the location of the pressure cell sensor was marked incorrectly and the correct location is approximately 42 in. apart in the longitudinal direction.

Table 5.9. Measurement details for July 2010 FWD test

Response	Value
ε [$\times 10^{-6}$]	290
σ [psi]	0.39
δ - 0 in. [in.]	0.034
δ - 8 in. [in.]	0.026
δ - 12 in. [in.]	0.021
δ - 18 in. [in.]	0.015
δ - 24 in. [in.]	0.011
δ - 36 in. [in.]	0.006

Table 5.10. Backcalculated Young's moduli values for July 2010 FWD test

Case	*E*1 [ksi]	*E*2 [ksi]	*E*3 [ksi]	*e* [ ]
δ_i only	229.4	14.5	14.5	9.0×10^{-3}
ε - δ_i	632.0	14.1	14.1	1.5×10^{-1}

Table 5.11. Forward analysis results for two cases: δ_i only and ε - δ_i

Response	Case δ_i only	Case ε - δ_i
	Value	Value
ε [$\times 10^{-6}$]	636	333
σ [psi]	13.68	9.37
δ - 0 in. [in.]	0.035	0.026
δ - 8 in. [in.]	0.026	0.022
δ - 12 in. [in.]	0.021	0.019
δ - 18 in. [in.]	0.015	0.015
δ - 24 in. [in.]	0.011	0.011
δ - 36 in. [in.]	0.007	0.007

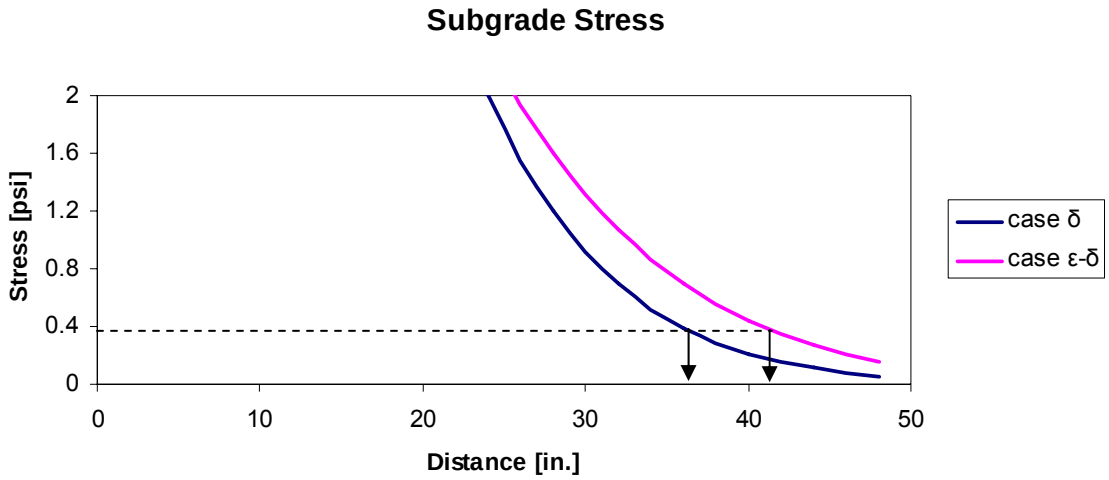

Figure 5.10. Simulated subgrade stresses at varying locations for cases ε - δ_i and δ_i

Additional FWD testing was conducted in September 2010 using the confirmed sensor location. The measured data as well as the results of the backcalculation analysis are summarized in Table 5.12 and Table 5.13, respectively. To evaluate the accuracy of these moduli, a forward analysis using the backalculated moduli was conducted for the

same FWD load to regenerate the asphalt strain and subgrade stress. The results of the forward analysis are shown in Table 5.14. Due to the axisymmetric nature of the layered elastic theory, asphalt strains directly beneath the center of the load are the same in both longitudinal and transverse directions. These newly computed strains and stresses were compared to the actual field responses and the error was computed using Eqn 5.1.

Table 5.12. Measurement details for September 2010 FWD test

Response	Value
ε [$\times 10^{-6}$]	219
σ [psi]	7.06
δ - 0 in. [in.]	0.027
δ - 8 in. [in.]	0.023
δ - 12 in. [in.]	0.019
δ - 18 in. [in.]	0.015
δ - 24 in. [in.]	0.011
δ - 36 in. [in.]	0.006

Table 5.13. Backcalculated Young's moduli values for September 2010 FWD test

Case	*E*1 [ksi]	*E*2 [ksi]	*E*3 [ksi]	*e* [ ]
δ_i only	401.8	15.2	15.2	1.2×10^{-2}
σ - δ_i	858.1	14.2	14.2	1.2×10^{-1}
ε - δ_i	961.4	14.2	14.2	1.3×10^{-1}
σ - ε	1001.9	27.5	11.8	2.8×10^{-9}
δ_i - ε - σ	1019.0	14.2	14.2	1.4×10^{-1}

Table 5.14. Forward analysis using backcalculated moduli

Case	Asphalt Strain [$\times 10^{-6}$]	Subgrade Stress [psi]	Error [ ]
δ_i only	445	11.58	1.5
σ - δ_i	269	8.36	8.6×10^{-2}
ε - δ_i	248	7.97	3.4×10^{-2}
σ - ε	219	7.06	8.0×10^{-7}
δ_i - ε - σ	238	7.76	1.7×10^{-2}

As expected, the case where σ-ε are used in the DAKOTA-MnLayer optimization process yielded the best results with the lowest error amongst all cases since it was optimized to match the same values. Case δ_i-ε-σ produced the second lowest error followed by case ε-δ_i, case σ-δ_i, and finally case δ_i only. When using deflection data only, both asphalt strain and subgrade stress are overestimated. It is interesting to note that the use of the deflection data in determination of Young's moduli parameters leads to an overestimation of the asphalt strains in the subsequent forward analysis. This suggests that there is a possibility of incorrect sensor depth location. The analysis suggests that the sensor is located at the bottom of the asphalt layer that may cause over-predictions of the asphalt strains. This hypothesis should be further investigated in future field testing and verified with coring. Another observation is that combining the deflection data with strain and/or stress responses proved to be helpful in the backcalculation process.

The measurements obtained from the FWD testing conducted in September 2010 were also used to verify the gage factor settings of the strain gages installed at the flexible pavement test sections. As mentioned in Chapter 2, throughout this study, the strain gage factor of two (GF2) was used as per manufacturer's recommendation. Since strain is a direct derivative of displacement, backcalculated Young's moduli for the asphalt layer, $E1$, using cases ε-δ_i and δ_i only should result in comparable values. However, this was not observed in Table 5.13 with $E1$ for case δ_i only being 41% of $E1$ for case ε-δ_i. This led to a presumption that the strain gages might be incorrectly calibrated. MnROAD personnel currently suggest the use of gage factor one (GF1), which multiplies the current strain values by two. Backcalculation was performed to compare the Young's moduli of the pavement layers obtained using measured strains adjusted for GF1. Measurements from Table 5.12 were used for this analysis where the strain value using GF1 was 438 $\times 10^{-6}$. A change in the strain value affected cases σ-ε, ε-δ_i, and δ_i-ε-σ, therefore, only these cases were evaluated. Table 5.15 summarizes the backcalculated Young's moduli for this comparison. The backcalculated moduli values were then used to perform a forward analysis to simulate subgrade stresses and asphalt strains for each of the cases

as shown in Table 5.16. Eqn 5.1 was used to compute the error between the simulated and measured responses corresponding to the respective measured strain values for GF1 and GF2.

Table 5.15. Comparison of backcalculated Young's moduli between GF1 and GF2

Gage Factor	Case	*E*1 [ksi]	*E*2 [ksi]	*E*3 [ksi]	*e* [ ]
NA	δ_i only	401.8	15.2	15.2	1.2×10^{-2}
	σ - δ_i	858.1	14.2	14.2	1.2×10^{-1}
GF2	ε - δ_i	961.4	14.2	14.2	1.3×10^{-1}
	σ - ε	1001.9	27.5	11.8	2.8×10^{-9}
	δ_i - ε - σ	1019.0	14.2	14.2	1.4×10^{-1}
GF1	ε - δ_i	407.5	15.4	15.4	1.9×10^{-2}
	σ - ε	565.8	8.1	6.3	1.2×10^{-9}
	δ_i - ε - σ	645.2	14.2	14.2	2.3×10^{-1}

Table 5.16. Forward analysis using backcalculated moduli for GF1 and GF2

Gage Factor	Case	Asphalt Strain [$\times 10^{-6}$]	Subgrade Stress [psi]	GF2 Error [ ]	GF1 Error [ ]
NA	δ_i only	445	11.58	1.5	4.1×10^{-1}
	σ - δ_i	269	8.36	8.6×10^{-2}	1.8×10^{-1}
GF2	ε - δ_i	248	7.97	3.4×10^{-2}	NA
	σ - ε	219	7.06	8.0×10^{-7}	
	δ_i - ε - σ	238	7.76	1.7×10^{-2}	
GF1	ε - δ_i	439	11.56	NA	4.1×10^{-1}
	σ - ε	438	7.06		3.6×10^{-9}
	δ_i - ε - σ	330	9.41		1.7×10^{-1}

The value for *E*1 backcalculated from case δ_i only was 401.8 ksi. This value was used as a benchmark to evaluate the difference between cases of GF2 and GF1. Referring to case ε - δ_i for GF1 and GF2, it was found that GF1 resulted in a more comparable *E*1 value at 407.5 ksi while *E*1 for GF2 was 961.4 ksi. Recall that the measured subgrade stress was 7.06 psi and the measured strain for GF2 was 219 $\times 10^{-6}$. The adjusted

measured strain for GF1 was 438 $\times 10^{-6}$. Table 5.16 shows that the simulated strains for case ε-δ_i of GF1 and GF2 match reasonably well with their corresponding measured strains. However, simulated strain for case ε-δ_i of GF1 was closer to the strain simulated through case δ_i only. On the other hand, simulated stresses for case ε-δ_i of GF1 and GF2 were larger than the measured stress at approximately 60% and 13%, respectively. Asphalt strain which was corrected using GF1 yielded results that were more comparable to the deflection data (case δ_i only) measured from the FWD testing. However, a forward analysis using backcalculated Young's moduli for GF1 greatly overestimates subgrade stresses whereas backcalculated moduli for GF2 resulted in more favorable simulated stresses. This analysis is currently inconclusive and an in-depth investigation should be performed by calibrating the strain gages with a known displacement.

5.5 Summary

The purpose of this section was to introduce a preliminary mechanistic model aiming to verify the trends observed in field testing as well as identify the material parameters that can be used for future structural modeling of pavement responses from agricultural vehicles. The layered elastic analysis programs, MnLayer and BISAR were used in the analysis. The importance of detailed modeling of the tire footprint was demonstrated. The layered elastic analysis also confirmed the field-observed effect of traffic wander. The optimization program DAKOTA was combined with MnLayer for material characterization. It was shown that the combination of MnLayer and DAKOTA provide a capability to determine the material parameters that lead to a close match between the predicted and measured pavement responses. This framework was also useful for verification of the location of the sensors and strain gage factor settings.

Chapter 6 Conclusions

Agricultural equipment manufacturers have been producing equipment with larger capacity to meet the demands of the agricultural industry. Agricultural vehicles today are equipped with innovations such as improved tire designs, flotation tires, and steerable axles. However, equipments with larger capacities result in heavier vehicle axle weights. This causes concerns to pavement owners because the potential for pavement damage in public highways and local roads increase due to heavy vehicle loading. This study was initiated to investigate the validity of these concerns. Full scale accelerated pavement testing was conducted at the MnROAD test facility to determine pavement responses generated by heavy agricultural equipment loading. These responses were compared to a typical 5-axle 80-kip semi truck.

Both flexible and rigid pavements were tested in this study. This thesis presented analysis for the flexible pavement sections. Cell 83 represented a thinner pavement rated as a 7-ton road while Cell 84 represented a thicker pavement rated as a 10-ton road. Both sections were instrumented with strain gages, LVDTs, earth pressure cells, and thermocouples. Testing was conducted twice a year: once in the month of March and once in the month of August. A total of twelve agricultural vehicles were tested together with two 5-axle semi trucks designated as control vehicles.

Preliminary data analysis of the collected data was performed and numerous effects on pavement responses were identified. These effects ranged from traffic wander to time of testing. The following summarizes the findings of this study:

- The lateral position of the vehicle's wheel path or traffic wander relative to the sensor location had a profound effect on the measured responses. Actual measurements of the vehicle traffic wander provided pavement response distribution across the pavement width relative to the sensor location. Maximum

responses may be generated by different vehicle axles depending on response type, load level, and axle configuration.

- Effects of seasonal changes were observed through analysis performed on pavement responses from the standard Mn80 truck. Measured asphalt strains in fall seasons were larger than those measured in the spring due to the less stiff asphalt layer. This trend was not observed for subgrade stresses.

- Analysis of response variation within each day showed that both asphalt strains and subgrade stresses measured in the morning were lower than those measured in the afternoon for all vehicles during spring and fall seasons. Additionally, there were no signs of distress propagation in the morning sessions while visible damage was observed in some of the afternoon sessions.

- A thicker pavement structure resulted in lower asphalt strains and subgrade stresses. As the vehicle moved toward the pavement edge, measured pavement responses decreased significantly with the presence of a paved shoulder. An unpaved (aggregate) shoulder provided little support at the pavement edge resulting in the lack of any decrease in pavement responses as the vehicle moved toward the shoulder.

- An increase in gross vehicle weight did not lead to a proportional increase in individual axle weights. It was observed that an increase in gross vehicle weight resulted in an increase in both asphalt strain and subgrade stress responses, although not proportionally to the gross weight increase. Adding more axles to the equipments' tanker successfully reduced axle weights. It was also observed that subgrade stresses increase linearly with individual axle weight but this trend was not observed for asphalt strains.

- All agricultural vehicles loaded above 80% load level generated higher subgrade stresses compared to the standard Mn80 truck regardless of test season.

- Asphalt strains were lower for the Mn80 truck compared to the agricultural vehicles loaded above 80% load level in the spring seasons. However, in the fall seasons, asphalt strains were consistently higher for Mn80 compared to the other vehicles. It should also be noted that at 80% load level, the weight of the heaviest axle of all the agricultural vehicles was larger than the heaviest axle of Mn80 except for vehicle T2.

- Benefits of flotation tires (on vehicle S5) over radial ply tires (on vehicle S4) were not significant. Changes in contact area and average contact stress were similar as axle weight increases for both tire types. The pavement responses across the pavement width were slightly higher for vehicle S4 with radial tires.

- The effect of vehicle speed on pavement responses was not significant in this study. This may be due to the narrow range of tested vehicle speeds (up to 25 mph).

- Layered elastic programs BISAR and MnLayer were used in the modeling analysis. Pavement responses simulated using the equivalent net contact area were larger than responses simulated for the gross contact area. Tekscan measurements were used to obtain a multi-circular area estimation of the vehicles' footprint. This detailed modeling of the tire footprint yielded a more realistic representation of the actual vehicle footprint.

- Using the multi-circular area estimation and BISAR, the effect of traffic wander on pavement responses was reconfirmed.

- The DAKOTA-MnLayer optimization framework was introduced here to aid in the backcalculation analysis to determine the Young's moduli of the pavement layers. This optimization framework was capable of determining pavement material properties which resulted in a close match between predicted responses and field measurements.

Bibliography

[1] Minnesota Department of Agriculture. (2010). *Agriculture - The Foundation of Minnesota's Economy*. Retrieved from http://www.mda.state.mn.us/news/publications/kids/maitc/agprofile.pdf.

[2] United States Department of Agriculture. (2009). *2007 Census of Agriculture*. Retrieved from http://www.agcensus.usda.gov/Publications/2007/Full_Report/index.asp.

[3] Phares, B. M, Wipf, T., Ceylan, H. (2005). *Impacts of Overweight Implements of Husbandry on Minnesota Roads and Bridges*. Minnesota Department of Transportation, Synthesis Report MN/RC-2005-05, Minnesota.

[4] Oman, M., Deusen, D. V., Olson, R. (2001). *Scoping Study*: *Impact of Agricultural Equipment on Minnesota's Low Volume Roads*. Minnesota Department of Transportation, Final Report, Minnesota.

[5] Fanous, F., Coree, B., Wood, D. (1999). *Response of Iowa Pavements to Heavy Agricultural Loads*. Center for Transportation Research and Education at Iowa State University, Interim Report, Iowa.

[6] Fanous, F., Coree, B., Wood, D. (2000). *Response of Iowa Pavements to a Tracked Agricultural Vehicle*. Center for Transportation Research and Education at Iowa State University, Final Report, Iowa.

[7] Sebaaly, P. E., Siddharthan, R. V., El-Desouky, M., Pirathapan, Y., Hitti, E., Vivekanathan, Y. (2002). *Effects of Off-Road Tires on Flexible and Granular Pavements*. South Dakota Department of Transportation, Final Report SD1999-15-F, South Dakota

[8] Tekscan, Inc. (2007). *I-Scan® User Manual v.5.9x*. Massachusetts.

[9] Clyne, T. (2009). *Cell 83 Forensic*. Minnesota Department of Transportation, Report, Minnesota.

[10] Srirangarajan, S., Tewfik, S. H. (2007*). MnROAD Offline Data Peak-Picking Program User Guide*. Department of Electrical and Computer Engineering, University of Minnesota, Minnesota.

[11] Loulizi, A., Al-Qadi, I. L., Elseifi, M. (2006). Difference between In Situ Flexible Pavement Measured and Calculated Stresses and Strains. *Journal of Transportation Engineering, 132(7)*, 574-579.

[12] Novak, M., Birgisson, B., Roque, R. (2003). Tire Contact Stresses and Their Effects on Instability Rutting of Asphalt Mixture Pavements. *Transportation Research Record, 1853*, 150-156

[13] Park, D., Fernando, E., Leidy, J. (2005). Evaluation of Predicted Pavement Response with Measured Tire Contact Stresses. *Transportation Research Record, 1919*, 160-170.

[14] Siddharthan, R. V., Sebaaly, P. E., El-Desouky, M., Strand, D., Huft, D. (2005). Heavy Off-Road Vehicle Tire-Pavement Interactions and Response. *Journal of Transportation Engineering, 131(3)*, 239-247.

[15] Huang, Y. H. (2004). *Pavement Analysis and Design* (*Second Edition*). New Jersey, Pearson Prentice Hall.
[16] Al-Qadi, I. L., Yoo, P. J., Elseifi, M. A., Janajreh, I. (2005). Effects of Tire Configurations on Pavement Damage. *Journal of the Association of Asphalt Paving Technologists, 74*, 921-962.
[17] Sebaaly, P. E., Siddharthan, R. V., El-Desouky, M., Strand, D., Huft, D. (2003). Effect of Off-Road Equipment on Flexible Pavements. *Transportation Research Record, 1821*, 29-38.
[18] Sandia National Laboratories. (2010). *DAKOTA, A Multilevel Parallel Object-Oriented Framework for Design Optimization, Parameter Estimation, Uncertainty Quantification, and Sensitivity Analysis Version 5.0 User's Manual*. California
[19] Willis, J. R., Timm, D. (2009). Repeatability of Asphalt Strain Measurements Under Falling Weight Deflectometer Loading. *Transportation Research Record, 2094*, 3-11.
[20] de Jong, D.L., Peutz, M.G. F., Korswagen, A.R. (1979) *Computer Program BISAR, Layered Systems under Normal and Tangential Surface Loads*. Koninklijke/Shell Laboratorium, Amsterdam.
[21] Khazanovich, L., Wang, Q. (2007). MnLayer High-Performance Layered Elastic Analysis Program. *Transportation Research Record, 2037*, 63-75.
[22] Willis, J. R. (2008). A Synthesis of Practical and Appropriate Instrumentation Use for Accelerated Pavement Testing in the United States. *Proceedings, International Conference on Accelerated Pavement Testing 2008*, Madrid, Spain.
[23] Theyse, H. L. (2002). *Stiffness, Strength, and Performance of Unbound Aggregate Material: Application of South African HVS and Laboratory Results to California Flexible Pavements*. University of California Pavement Research Center, Report, California.
[24] Von Quintus, H. L., Simpson, A. L. (2002). *Back-Calculation of Layer Parameters for LTPP Test Sections, Volume II: Layered Elastic Analysis for Flexible and Rigid Pavements*. Federal Highway Administration, Final Report FHWA-RD-01-113, Virginia.
[25] de Beer, M., Fisher, C., Jooste, F. (1997). Determination of Pneumatic Tyre/Pavement Interface Contact Stresses under Moving Loads and Some Effects on Pavements with Thin Asphalt Surfacing Layers. *Proceedings, Eighth International Conference of Asphalt Pavements, Vol. 1*, 179-226.
[26] Chadbourn, B. A., Newcomb, D. E., Timm, D. H. (1997). Measured and Theoretical Comparisons of Traffic Loads and Pavement Response Distributions. *Proceedings, Eighth International Conference of Asphalt Pavements, Vol. 1*, 229-238.
[27] Dai, S. T., Van Deusen, D., de Beer, M., Rettner, D., Cochran, G. (1997). Investigation of Flexible Pavement Response to Truck Speed and FWD Load Through Instrumented Pavements. *Proceedings, Eighth International Conference of Asphalt Pavements, Vol. 1*, 141-160.
[28] Weissman, S. L. (1999). Influence of Tire-Pavement Contact Stress Distribution on Development of Distress Mechanisms in Pavements. *Transportation Research Record, 1655*, 161-167.

[29] Gillespie, T. D., Karamihas, S. M., Cebon, D., Sayers, M. W., Nasim, M. A., Hansen, W., Ehsan, N. (1992). *Effects of Heavy Vehicle Characteristics on Pavement Responses and Performance*, National Cooperative Highway Research Program (NCHRP), Final Report UMTRI 92-2, Washington D.C.

[30] Gaurav, S., Wojtkiewicz, S., Khazanovich, L. (in-press). Optimal Design of Flexible Pavements using a Framework of DAKOTA and MEPDG. *International Journal of Pavement Engineering*.

[31] Moore, D. S., McCabe, G. P., Craig, B. A. (2009). *Introduction to the Practice of Statistics* (*Sixth Edition*). New York, W. H. Freeman and Company.

[32] Das, B. M. (2005). *Fundamentals of Geotechnical Engineering* (*Second Edition*). Ontario, Canada, Thomson Canada Limited.

[33] Chou, P. C., Pagano, N. J. (1992). *Elasticity*: *Tensor, Dyadic, and Engineering Approaches*. New York, Dover.

Appendix A Test Program Example

The following shows a portion of the test program used for Cell 83 on the 16 March 2009 test. Table A.1 shows the test program before the start of testing with the actual time, strain gage filename and LVDT filename columns empty. The empty columns were filled during the test as shown in Table A.2. It should be mentioned that the Megadec-TCS filenames correspond to the data file collected for strain and stress measurements and the NI filenames correspond to the displacement measurements.

Table A.1. Example of empty test program

Test #	Actual Time	Pass	Vehicle	Load Level [%]	Speed [mph]	Offset [in.]	Cell 83	
							Megadec-TCS Filename	NI Filename
1		1	S4	0	5	12		
2		1	S5	0	5	12		
3		1	T6	0	5	12		
4		1	T7	0	5	12		
5		1	T8	0	5	12		
6		1	Mn80	0	5	12		
7		1	MN102	0	5	12		
8		2	S4	0	5	0		
9		2	S5	0	5	0		
10		2	T6	0	5	0		
11		2	T7	0	5	0		
12		2	T8	0	5	0		
13		2	Mn80	0	5	0		
14		2	MN102	0	5	0		
15		3	S4	0	10	0		
16		3	S5	0	10	0		
17		3	T6	0	10	0		
18		3	T7	0	10	0		
19		3	T8	0	10	0		
20		3	Mn80	0	10	0		
21		3	MN102	0	10	0		

Table A.2. Example of filled test program

Test #	Actual Time	Pass	Vehicle	Load Level [%]	Speed [mph]	Offset [in.]	Cell 83	
							Megadec-TCS Filename	NI Filename
1	10:56 AM	1	S4	0	5	12	Cell 83 03-16-09 Set1_1_2	Cell 83 LVDT 3-16-09_0001
2	11:00 AM	1	S5	0	5	12	Cell 83 03-16-09 Set1_1_3	Cell 83 LVDT 3-16-09_0002
3	11:01 AM	1	T6	0	5	12	Cell 83 03-16-09 Set1_1_4	Cell 83 LVDT 3-16-09_0003
4	11:03 AM	1	T7	0	5	12	Cell 83 03-16-09 Set1_1_5	Cell 83 LVDT 3-16-09_0004
5	11:06 AM	1	T8	0	5	12	Cell 83 03-16-09 Set1_1_6	Cell 83 LVDT 3-16-09_0005
6	11:08 AM	1	Mn80	0	5	12	Cell 83 03-16-09 Set1_1_7	Cell 83 LVDT 3-16-09_0006
7	11:09 AM	1	MN102	0	5	12	Cell 83 03-16-09 Set1_1_8	Cell 83 LVDT 3-16-09_0007
8	11:11 AM	2	S4	0	5	0	Cell 83 03-16-09 Set1_1_9	Cell 83 LVDT 3-16-09_0008
9	11:13 AM	2	S5	0	5	0	Cell 83 03-16-09 Set1_1_10	Cell 83 LVDT 3-16-09_0009
10	11:14 AM	2	T6	0	5	0	Cell 83 03-16-09 Set1_1_11	Cell 83 LVDT 3-16-09_0010
11	11:16 AM	2	T7	0	5	0	Cell 83 03-16-09 Set1_1_12	Cell 83 LVDT 3-16-09_0011
12	11:17 AM	2	T8	0	5	0	Cell 83 03-16-09 Set1_1_13	Cell 83 LVDT 3-16-09_0012
13	11:18 AM	2	Mn80	0	5	0	Cell 83 03-16-09 Set1_1_14	Cell 83 LVDT 3-16-09_0013
14	11:19 AM	2	MN102	0	5	0	Cell 83 03-16-09 Set1_1_15	Cell 83 LVDT 3-16-09_0014
15	11:20 AM	3	S4	0	10	0	Cell 83 03-16-09 Set1_1_16	Cell 83 LVDT 3-16-09_0015
16	11:21 AM	3	S5	0	10	0	Cell 83 03-16-09 Set1_1_17	Cell 83 LVDT 3-16-09_0016
17	11:22 AM	3	T6	0	10	0	Cell 83 03-16-09 Set1_1_18	Cell 83 LVDT 3-16-09_0017
18	11:23 AM	3	T7	0	10	0	Cell 83 03-16-09 Set1_1_19	Cell 83 LVDT 3-16-09_0018
19	11:24 AM	3	T8	0	10	0	Cell 83 03-16-09 Set1_1_20	Cell 83 LVDT 3-16-09_0019
20	11:25 AM	3	Mn80	0	10	0	Cell 83 03-16-09 Set1_1_21	Cell 83 LVDT 3-16-09_0020
21	11:25 AM	3	MN102	0	10	0	Cell 83 03-16-09 Set1_1_22	Cell 83 LVDT 3-16-09_0021

Appendix B Vehicle Axle Weight and Dimension

Vehicle axle weights are tabulated in this section for all tested load levels and test season. All weights are measured and presented in pounds as shown in Table B.1 through Table B.6. Consequently, the axle configurations and dimensions of tested vehicles are presented as shown in Figure B.1 through Figure B.4. All dimensions were measured and presented in inches.

Table B.1. Vehicle axle weights for spring 2008 test

Vehicle	**S4, Homemade, 4,400 gal**				**S5, Homemade, 4,400 gal**				**T1, John Deere 8430, 6,000 gal**			
Load Level	**0%**	**25%**	**50%**	**80%**	**0%**	**25%**	**50%**	**80%**	**0%**	**25%**	**50%**	**80%**
Axle 1	10,440	11,600	12,560	13,540	12,700	14,180	15,700	17,520	12,940	12,360	11,440	11,080
Axle 2	7,700	11,000	15,060	19,320	8,320	12,120	15,740	19,760	17,300	19,220	23,000	24,560
Axle 3	6,820	11,200	15,540	20,240	7,080	10,860	15,150	19,900	6,280	11,540	16,760	21,000
Axle 4									7,980	13,440	19,550	24,680
Axle 5												
Axle 6												
Total	24,960	33,800	43,160	53,100	28,100	37,160	46,590	57,180	44,500	56,560	70,750	81,320
Vehicle	**S3, Terragator 8204**				**T2, M.Ferguson 8470, 4,000 gal**				**T6, John Deere 8430, 6,000 gal**			
Load Level	**0%**	**25%**	**50%**	**80%**	**0%**	**25%**	**50%**	**80%**	**0%**	**25%**	**50%**	**80%**
Axle 1	13,920	14,000	14,120	14,980	9,080	9,060	8,580	8,400	13,220	12,660	11,940	11,600
Axle 2	17,680	20,880	24,820	30,600	12,700	13,460	15,220	16,180	17,600	17,700	20,860	22,420
Axle 3					4,520	8,260	12,100	16,920	7,140	12,420	16,620	22,440
Axle 4					4,480	7,660	11,440	15,620	7,900	13,760	19,760	26,640
Axle 5												
Axle 6												
Total	31,600	34,880	38,940	45,580	30,780	38,440	47,340	57,120	45,860	56,540	69,180	83,100

Table B.2. Vehicle axle weights for fall 2008 test

Vehicle	R4, Terragator 9203				T6, John Deere 8430, 6,000 gal				T7, Case IH 245, 7,300 gal			
Load Level	**0%**	**25%**	**50%**	**80%**	**0%**	**25%**	**50%**	**80%**	**0%**	**25%**	**50%**	**80%**
Axle 1	13,700	13,760	14,440	14,940	13,390	12,600	11,900	11,660	11,620	11,040	11,100	9,580
Axle 2	23,840	28,640	32,820	38,420	16,980	19,200	20,660	22,640	16,820	18,880	19,500	22,680
Axle 3					7,560	12,740	17,920	24,880	6,380	10,680	14,420	19,380
Axle 4					7,480	14,360	20,820	26,900	6,600	10,980	15,940	21,040
Axle 5									6,520	10,540	15,900	21,120
Axle 6												
Total	37,540	42,400	47,260	53,360	45,410	58,900	71,300	86,080	47,940	62,120	76,860	93,800

Vehicle	T8, Case IH 485, 9,500 gal				Mn80
Load Level	**0%**	**25%**	**50%**	**80%**	**80-kip**
Axle 1	26,480	25,620		25,200	12,000
Axle 2	26,950	30,220		34,540	17,000
Axle 3	6,120	9,670		18,240	17,000
Axle 4	6,140	10,660		20,360	16,000
Axle 5	6,080	10,380		20,220	18,000
Axle 6	6,520	10,400		20,220	
Total	78,290	96,950		138,780	80,000

Table B.3. Vehicle axle weights for spring 2009 test

Vehicle	S4, Homemade, 4,400 gal				S5, Homemade, 4,400 gal				R4, Terragator 9203			
Load Level	**0%**	**25%**	**50%**	**80%**	**0%**	**25%**	**50%**	**80%**	**0%**	**25%**	**50%**	**80%**
Axle 1	12,680	13,940	15,100	16,600	11,140	12,080	13,280	15,400	12,800	13,020	13,620	13,900
Axle 2	6,480	9,900	15,600	19,520	6,940	11,120	14,320	19,400	23,720	28,160	34,440	39,340
Axle 3	8,700	12,420	16,280	21,460	7,100	10,840	15,340	20,040				
Axle 4												
Axle 5												
Axle 6												
Total	27,860	36,260	46,980	57,580	25,180	34,040	42,940	54,840	36,520	41,180	48,060	53,240
Vehicle	**R5, Terragator 8144**				**T6, John Deere 8230, 6,000 gal**				**T7, Case IH 335, 7,300 gal**			
Load Level	**0%**	**25%**	**50%**	**80%**	**0%**	**25%**	**50%**	**80%**	**0%**	**25%**	**50%**	**80%**
Axle 1	15,240	15,580	16,260	16,780	7,900	7,500	7,240	6,320	13,880	13,760	11,820	17,240
Axle 2	16,240	19,940	23,340	26,960	15,860	17,720	19,140	20,960	19,020	20,440	23,080	18,360
Axle 3					7,140	12,160	17,460	20,480	8,520	12,680	17,680	22,840
Axle 4					7,880	13,240	19,400	22,460	8,440	12,780	17,540	22,720
Axle 5									8,680	13,180	17,930	22,440
Axle 6												
Total	31,480	35,520	39,600	43,740	38,780	50,620	63,240	70,220	58,540	72,840	88,050	103,600

Vehicle	T8, Case IH 335, 9,500 gal				Mn80	Mn102
Load Level	**0%**	**25%**	**50%**	**80%**	**80-kip**	**102-kip**
Axle 1	17,400	17,800	17,240	15,540	11,640	12,880
Axle 2	18,060	21,480	22,260	26,040	17,080	22,180
Axle 3	5,660	9,700	14,540	18,760	16,760	21,540
Axle 4	6,100	10,500	16,200	21,280	18,460	22,680
Axle 5	5,720	10,240	16,060	20,840	15,620	22,960
Axle 6	5,960	10,620	15,780	21,380		
Total	58,900	80,340	102,080	123,840	79,560	10,2240

Table B.4. Vehicle axle weights for fall 2009 test

Vehicle	R5, Terragator 8144			T6, John Deere 8230, 6,000 gal			T7, Case IH 275, 7,300 gal		
Load Level	**0%**	**50%**	**100%**	**0%**	**50%**	**100%**	**0%**	**50%**	**100%**
Axle 1	15,290	16,450	17,150	9,110	8,900	8,100	8,800	8,100	6,900
Axle 2	16,440	23,500	29,950	15,710	18,600	21,400	13,500	16,400	19,800
Axle 3				6,990	16,600	26,500	7,700	17,100	26,300
Axle 4				7,900	20,300	33,500	7,500	16,900	26,200
Axle 5							7,600	17,100	26,000
Axle 6									
Total	31,730	39,950	47,100	39,710	64,400	89,500	45,100	75,600	105,200

Vehicle	T8, Case IH 335, 9,500 gal			Mn80	Mn102
Load Level	**0%**	**50%**	**100%**	**80-kip**	**102-kip**
Axle 1	16,800	16,100	14,800	12,100	12,780
Axle 2	18,000	21,000	25,200	17,440	24,440
Axle 3	5,900	14,900	23,300	16,050	20,780
Axle 4	5,900	15,100	23,700	18,830	24,330
Axle 5	5,700	15,100	23,500	16,670	22,910
Axle 6	5,900	15,400	23,700		
Total	58,200	97,600	134,200	81,090	105,240

Table B.5. Vehicle axle weights for spring 2010 test

Vehicle	R6, Terragator 3104			T6, John Deere 8230, 6,000 gal			Mn80	Mn102
Load Level	0%	50%	100%	0%	50%	100%	80-kip	102-kip
Axle 1	24,150	28,300	32,800	8,200	7,500	6,200	12,550	12,200
Axle 2	17,900	28,700	41,900	17,600	21,000	23,500	16,000	22,950
Axle 3				7,200	16,900	26,000	17,800	22,250
Axle 4				8,000	21,400	33,900	16,000	20,700
Axle 5							17,800	25,000
Axle 6								
Total	42,050	57,000	74,700	41,000	66,800	89,600	80,150	103,100

Table B.6. Vehicle axle weights for fall 2010 test

Vehicle	G1, Case IH 9330, 1,000 bushels		T6, New Holland TG245, 6,000 gal		Mn80	Mn102
Load Level	0%	100%	0%	100%	80-kip	102-kip
Axle 1	12,600	11,500	11,400	11,200	11,450	12,400
Axle 2	14,800	18,700	17,500	23,000	17,200	22,950
Axle 3	10,500	57,200	7,000	24,700	17,200	22,250
Axle 4			7,900	31,400	14,300	19,900
Axle 5					19,300	25,600
Axle 6						
Total	37,900	87,400	43,800	90,300	79,450	103,100

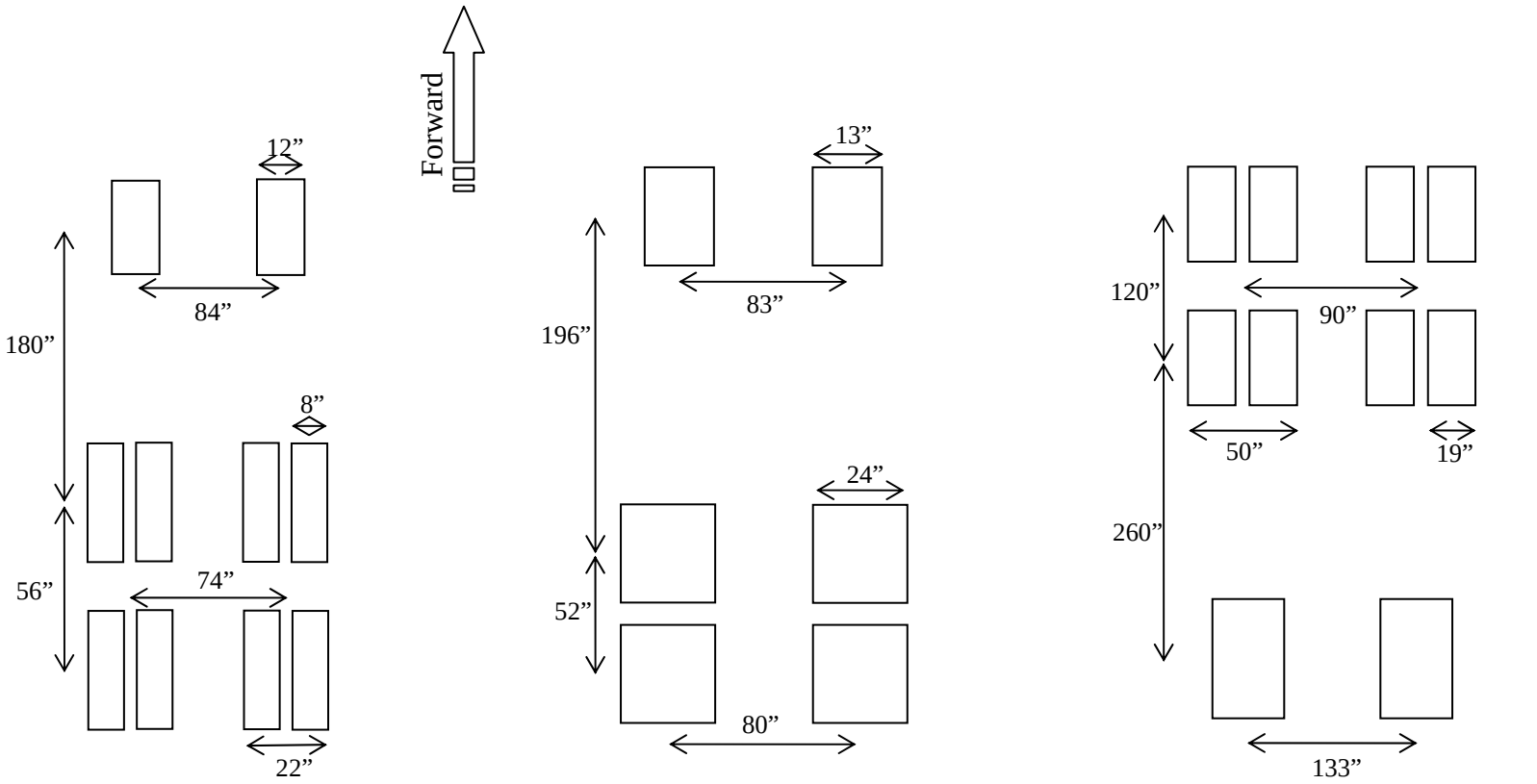

S4 (Homemade 4,400 gal – radial tires) S5 (Homemade 4,400 gal – flotation tires) G1 (Case IH 9330, 1,000 bushels)

Figure B.1. Dimensions for vehicles S4, S5, and G1

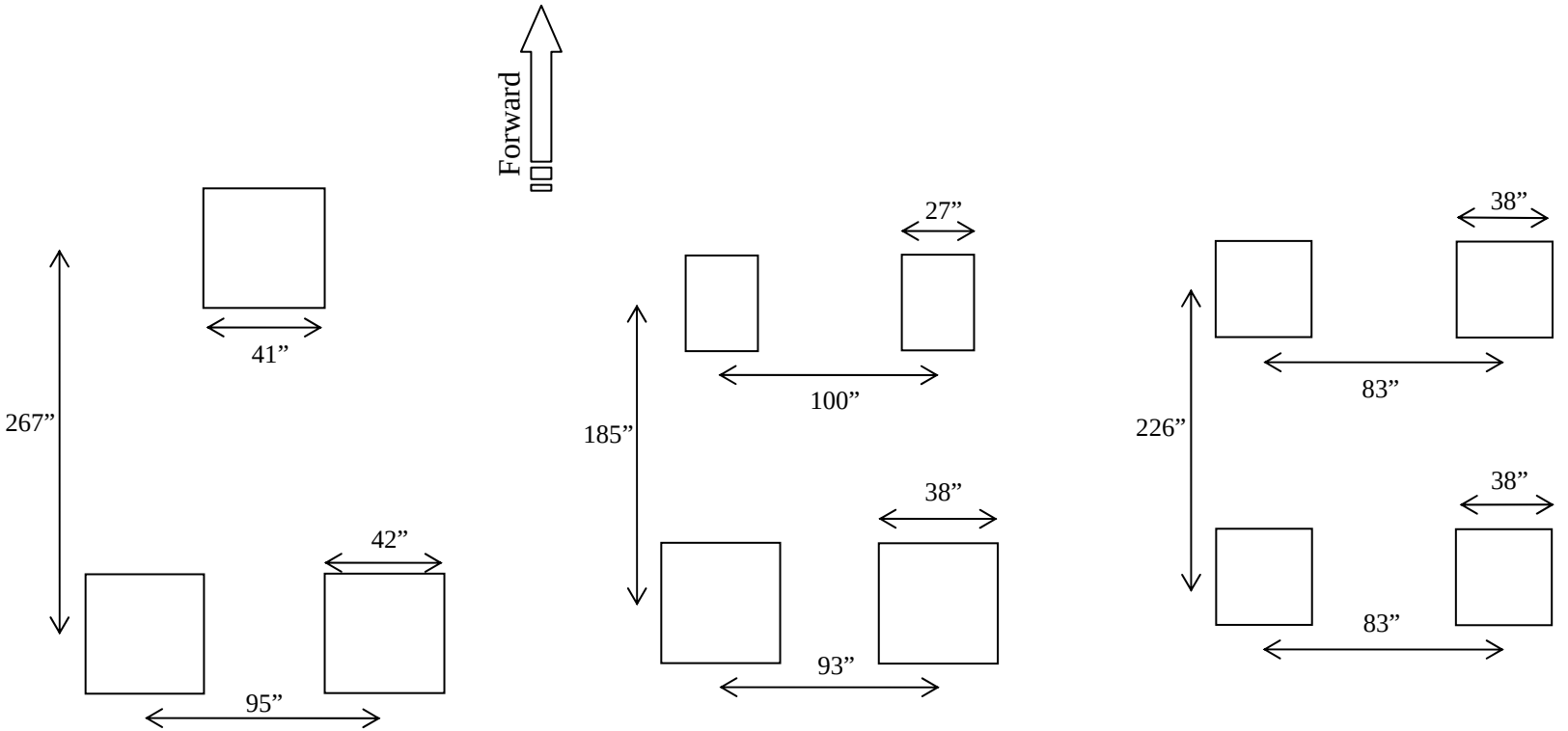

R4 (AGCO Terragator 9203) R5 (AGCO Terragator 8144) R6 (ACGO Terragator 3104)

Figure B.2. Dimensions for vehicles R4, R5, and R6

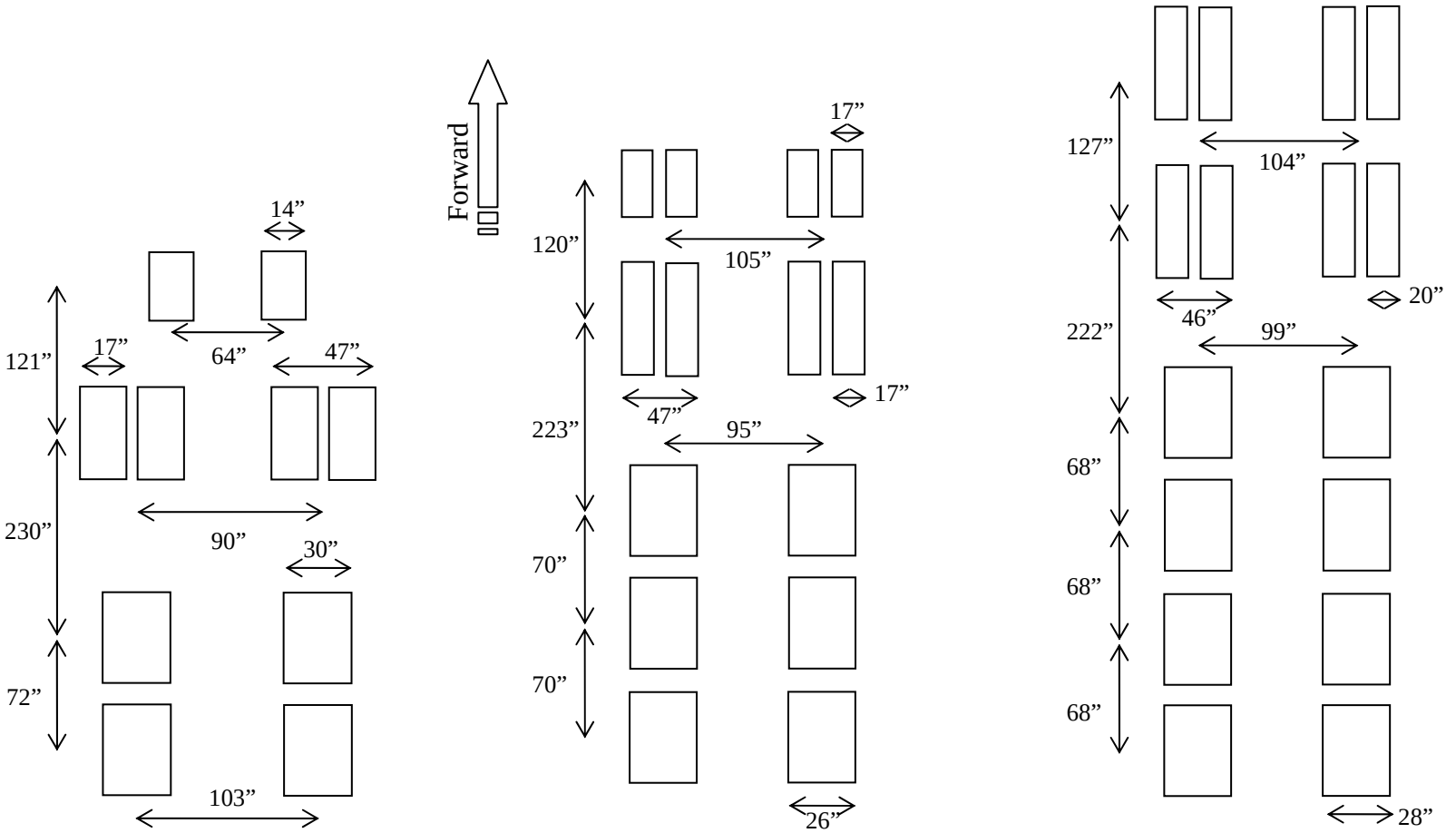

T6 (John Deere 8203, 6,000 gal) T7 (Case IH 335, 7,300 gal) T8 (Case IH 335, 9,500 gal)

Figure B.3. Dimensions for vehicles T6, T7, and T8

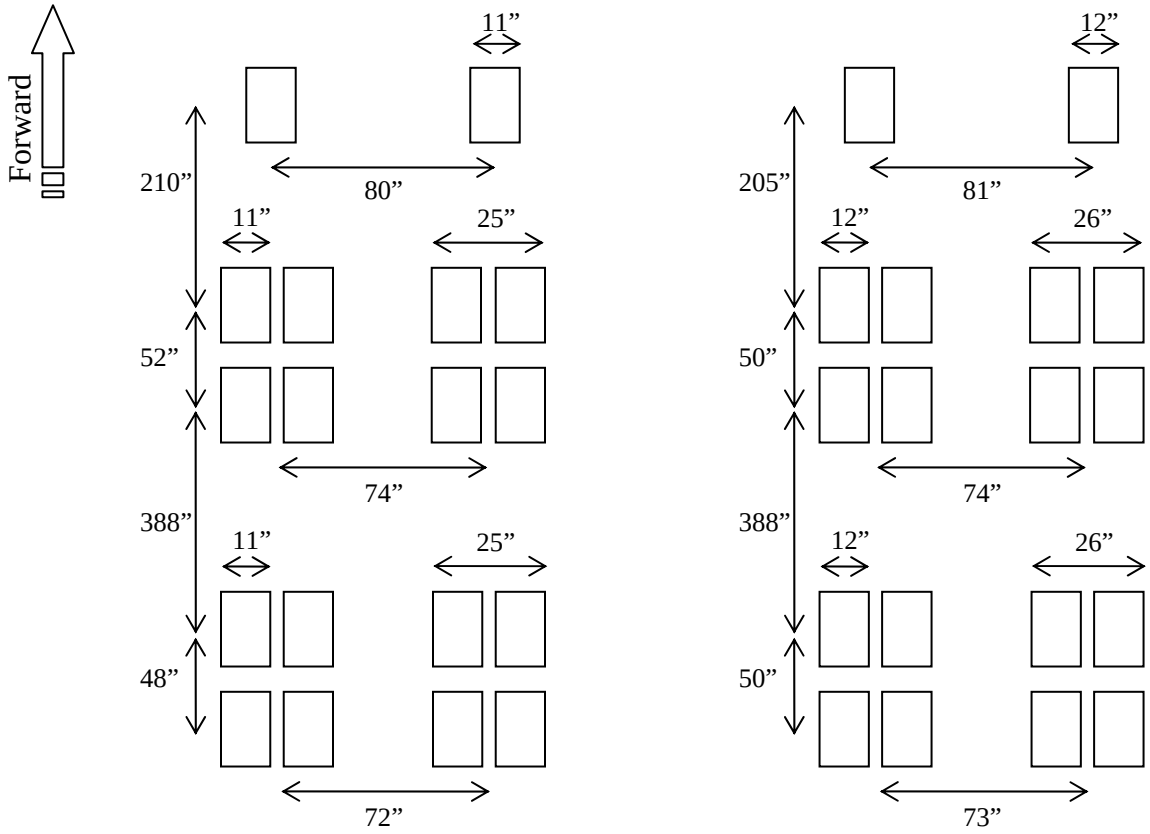

Mn80 (Navistar 80-kip) Mn102 (Mack 102-kip)

Figure B.4. Dimensions for vehicles Mn80 and Mn102

Appendix C Sensor Status

This section contains the status of sensors located at the flexible pavement sections. This includes sensors from the Megadec-TCS and NI data acquisition systems. Sensor status for all tested seasons for both Cells 83 and 84 are presented in Table C.1 and Table C.2, respectively.

Table C.1. Sensor status for Cell 83

System	Sensor	Spring 2008	Fall 2008	Spring 2009	Fall 2009	Spring 2010	Fall 2010
Megadec-TCS	83TE4	working	working	not working	not working	not working	not working
	83TE5	working	working	working	working	not working	not working
	83TE6	working	not working	not working	not working	not working	not working
	83LE4	not working	not working	not working	not working	not working	not working
	83LE5	working	working	working	working	working	not working
	83LE6	not working	not working	working	working	working	not working
	83AE4	working	working	working	working	not working	not working
	83AE5	not working	not working	not working	not working	not working	not working
	83AE6	working	working	working	working	working	not working
	83PG4	working	working	working	working	not working	not working
	83PG5	working	working	working	working	not working	not working
	83PG6	working	working	working	working	not working	not working
NI	83AL1	not working	working	working	not working	not working	not working
	83AH2	not working	working	working	not working	not working	not working
	83AV3	not working	working	working	not working	not working	not working

Table C.2. Sensor status for Cell 84

System	Sensor	Spring 2008	Fall 2008	Spring 2009	Fall 2009	Spring 2010	Fall 2010
Megadec-TCS	84TE4	working	working	working	working	working	working
	84TE5	working	working	working	working	working	working
	84TE6	not working	not working	not working	not working	not working	not working
	84LE4	working	working	working	working	working	working
	84LE5	working	working	working	working	working	working
	84LE6	not working	not working	not working	not working	not working	not working
	84AE4	not working	not working	not working	not working	not working	not working
	84AE5	working	working	working	working	working	working
	84AE6	working	working	working	working	working	working
	84PG4	working	working	working	working	working	working
	84PG5	working	working	working	working	working	working
	84PG6	working	working	working	working	working	working
NI	84AL1	not working	working	not working	not working	not working	working
	84AH2	not working	not working	working	working	working	not working
	84AV3	not working	not working	working	not working	not working	not working

Appendix D Pavement Response Data

This section provides charts of pavement responses generated by all tested agricultural vehicles compared against the responses generated by the control vehicle Mn80. Only pavement responses at the highest load levels tested for each test season were presented here. For Cell 83, sensors 83AE4 and 83PG4 are presented. For Cell 84, sensors 84LE4, 84TE4, and 84PG4 are presented. Additionally, the pavement responses were plotted against the vehicles' wheel path relative to the sensor location. Figure D.1 through Figure D.5 show responses for test during the fall 2008 season. Figure D.6 through Figure D.15 show responses for tests conducted in the spring 2009 season. Figure D.16 through Figure D.25 show responses for tests conducted in fall 2009. Figure D.26 through Figure D.28 show responses for tests conducted in spring 2010 and Figure D.29 through Figure D.34 show responses for tests conducted in fall 2010.

D.1 Fall 2008

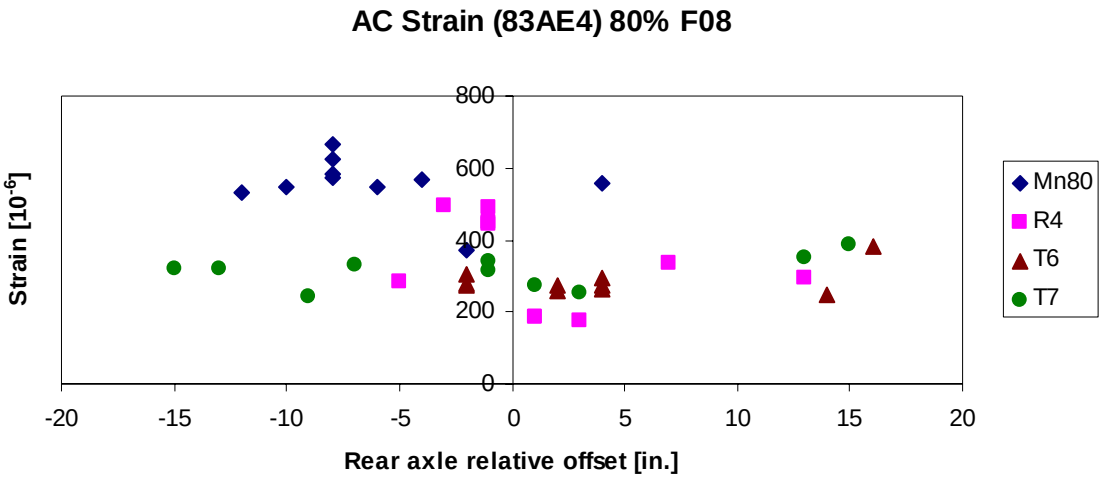

Figure D.1. Cell 83 angled asphalt strain at 80% load level in fall 2008 for vehicles Mn80, R4, T6, and T7

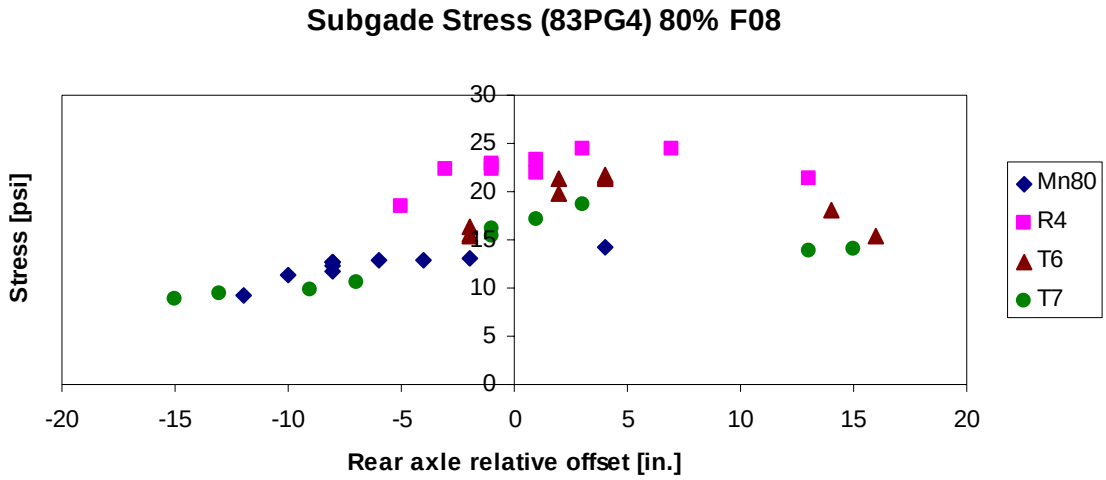

Figure D.2. Cell 83 subgrade stress at 80% load level in fall 2008 for vehicles Mn80, R4, T6, and T7

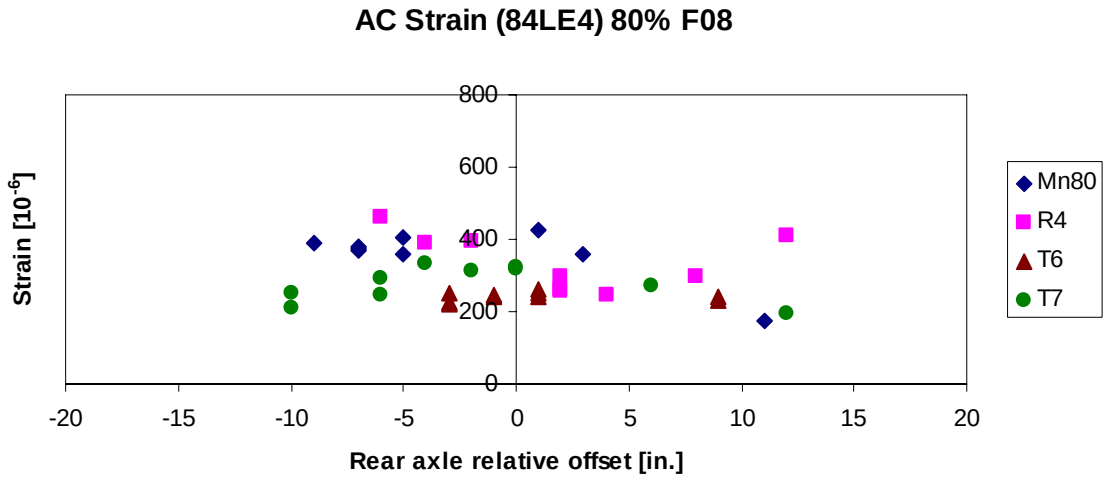

Figure D.3. Cell 84 longitudinal asphalt strain at 80% load level in fall 2008 for vehicles Mn80, R4, T6, and T7

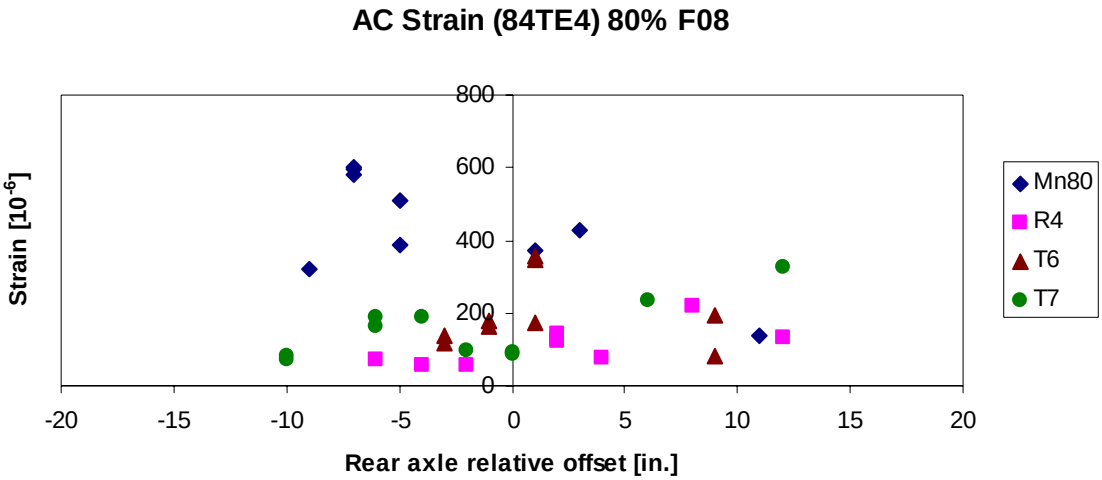

Figure D.4. Cell 84 transverse asphalt strain at 80% load level in fall 2008 for vehicles Mn80, R4, T6, and T7

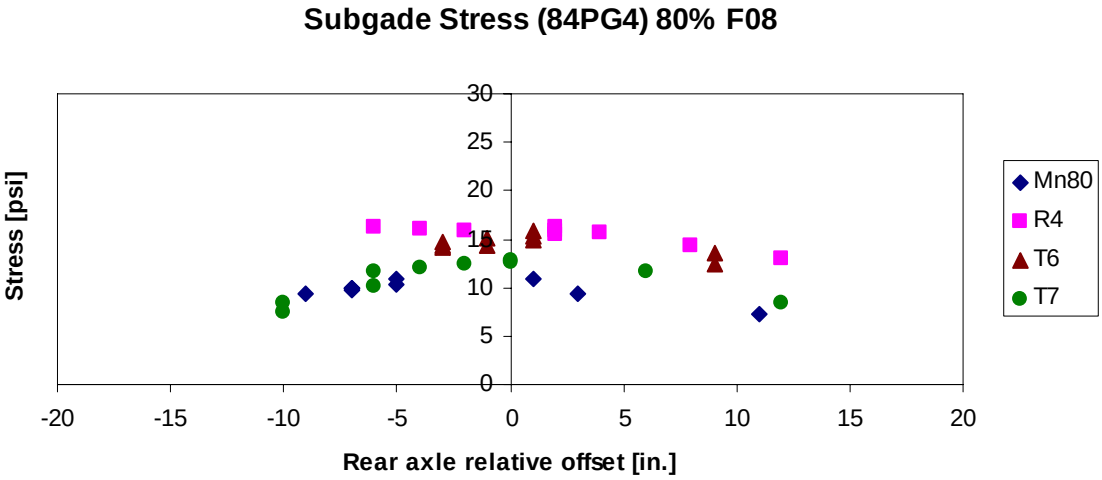

Figure D.5. Cell 84 subgrade stress at 80% load level in fall 2008 for vehicles Mn80, R4, T6, and T7

D.2 Spring 2009

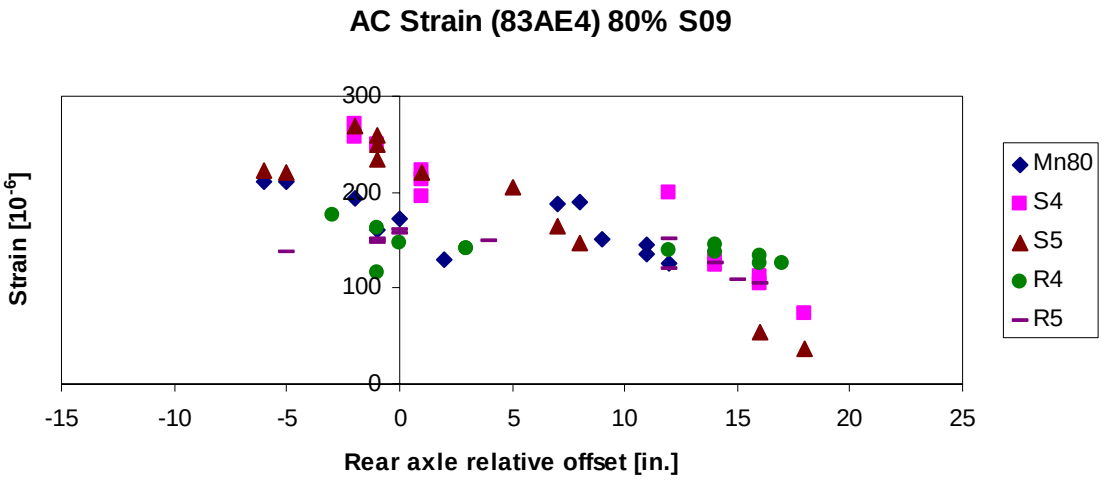

Figure D.6. Cell 83 angled asphalt strain at 80% load level in spring 2009 for vehicles Mn80, S4, S5, R4, and R5

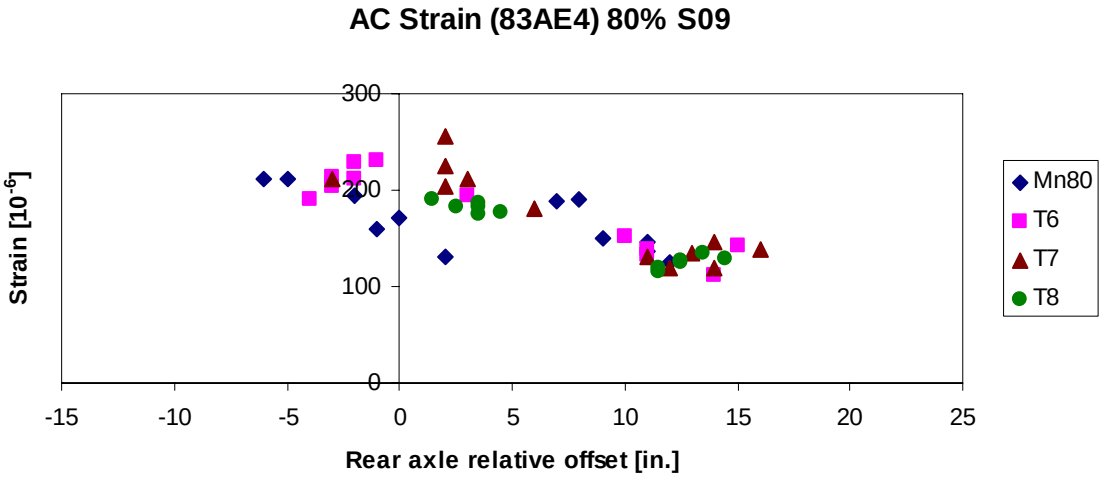

Figure D.7. Cell 83 angled asphalt strain at 80% load level in spring 2009 for vehicles Mn80, T6, T7, and T8

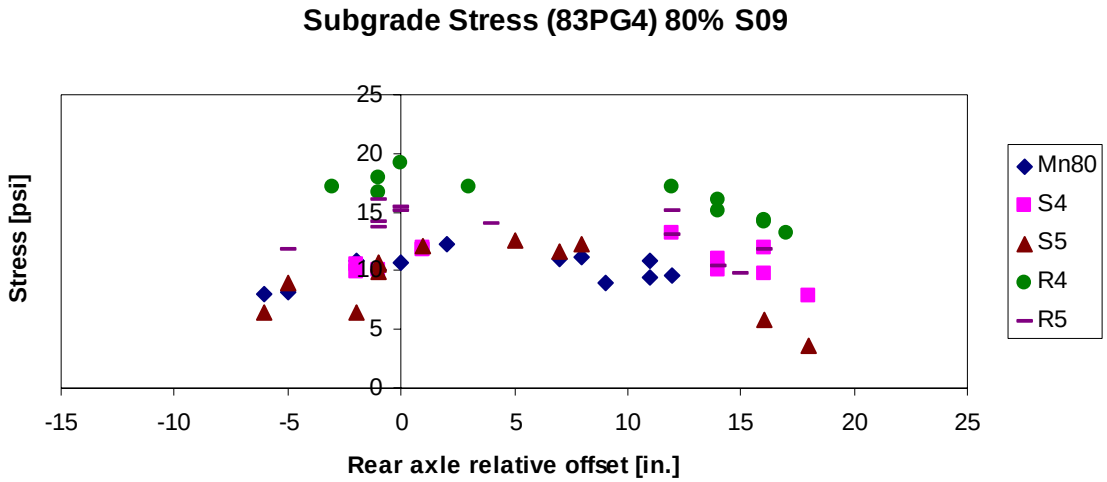

Figure D.8. Cell 83 subgrade stress at 80% load level in spring 2009 for vehicles Mn80, S4, S5, R4, and R5

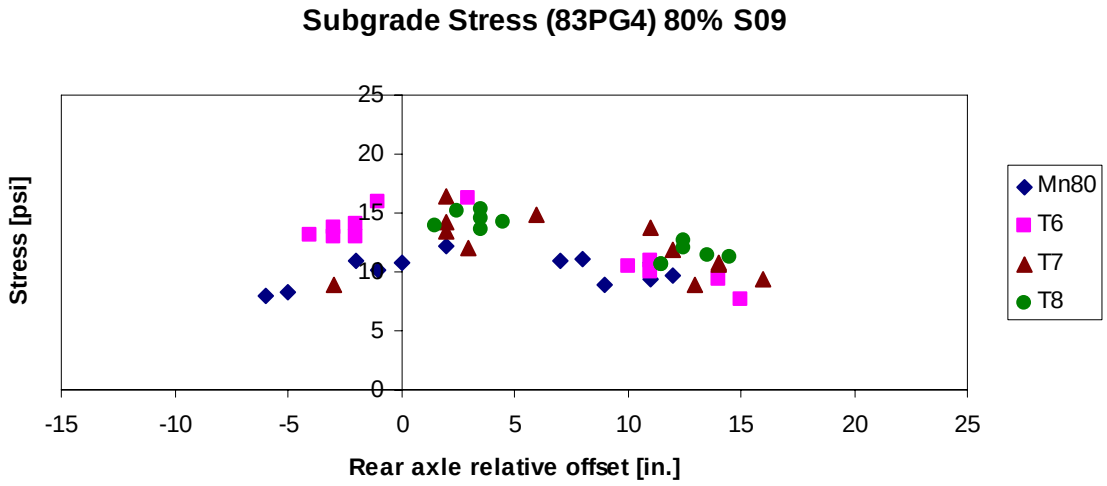

Figure D.9. Cell 83 subgrade stress at 80% load level in spring 2009 for vehicles Mn80, T6, T7, and T8

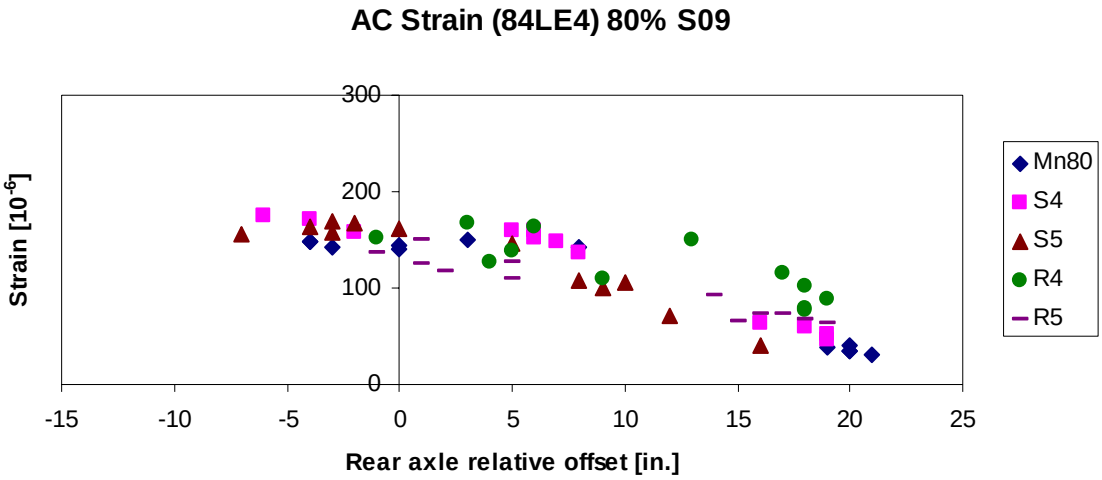

Figure D.10. Cell 84 longitudinal asphalt strain at 80% load level in spring 2009 for vehicles Mn80, S4, S5, R4, and R5

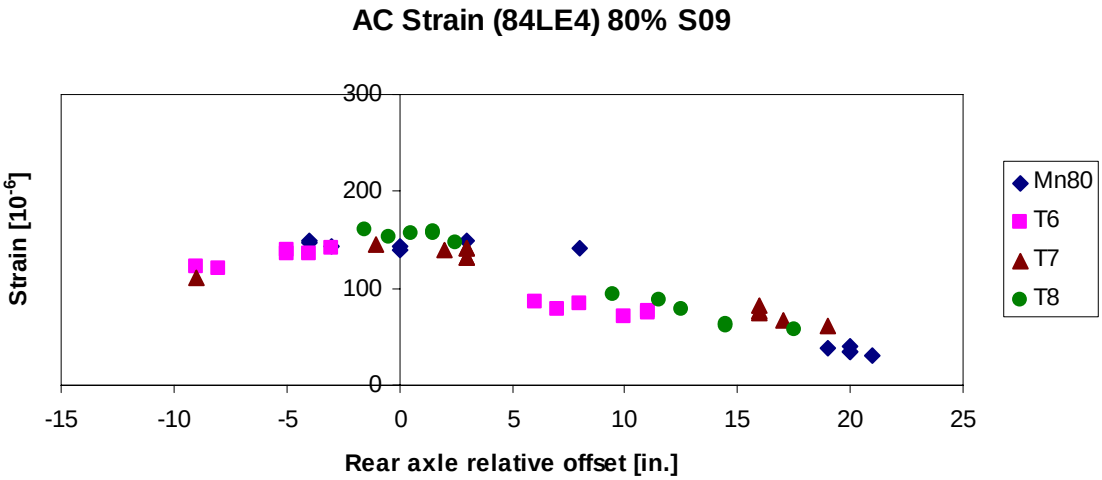

Figure D.11. Cell 84 longitudinal asphalt strain at 80% load level in spring 2009 for vehicles Mn80, T6, T7, and T8

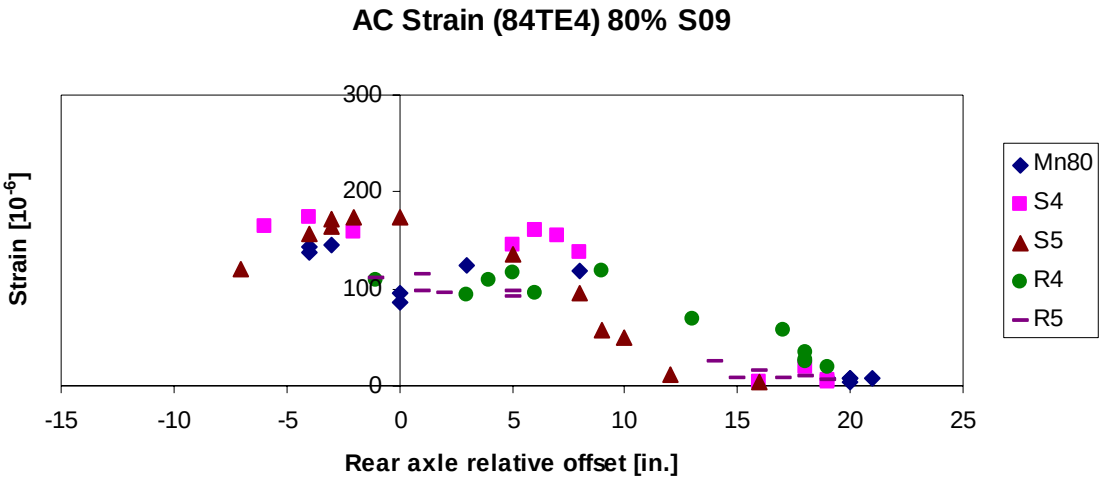

Figure D.12. Cell 84 transverse asphalt strain at 80% load level in spring 2009 for vehicles Mn80, S4, S5, R4, and R5

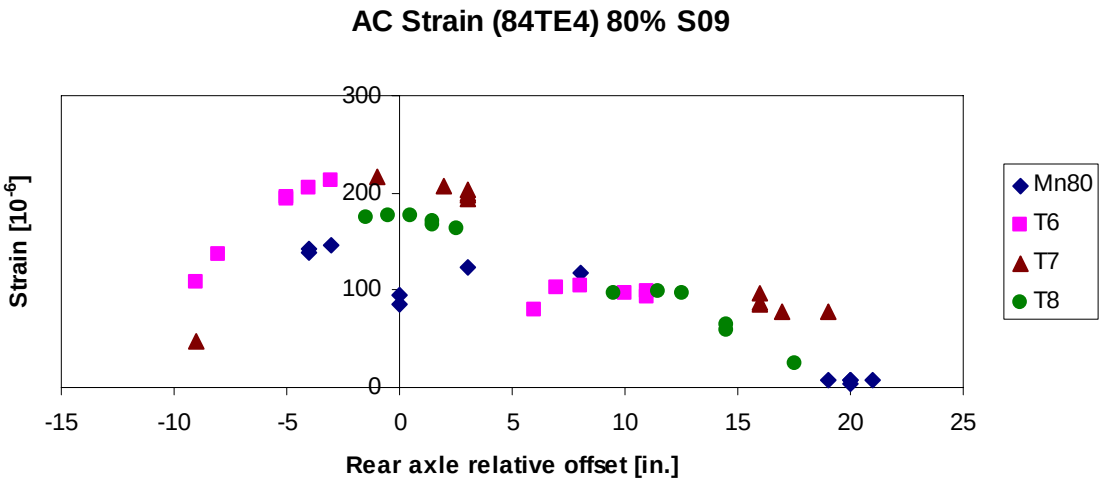

Figure D.13. Cell 84 transverse asphalt strain at 80% load level in spring 2009 for vehicles Mn80, T6, T7, and T8

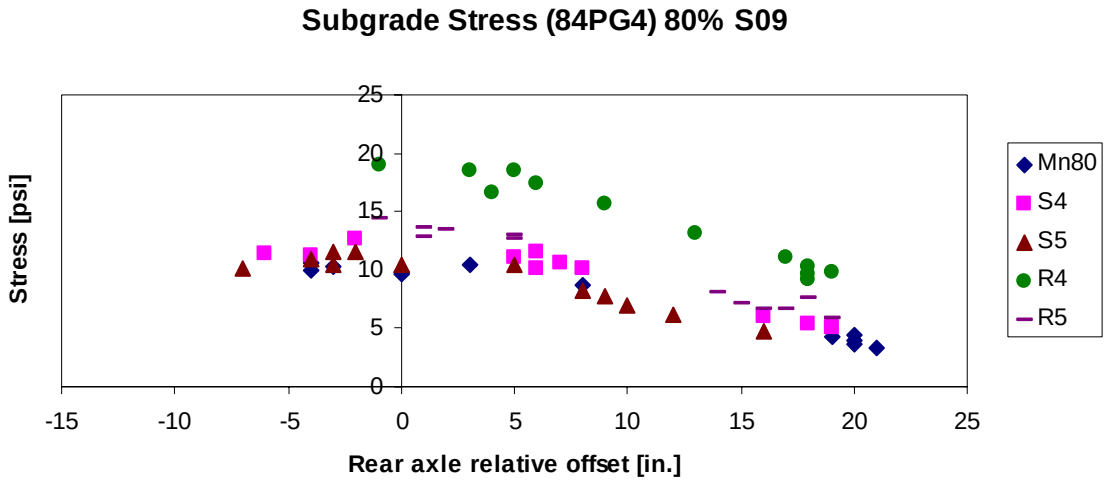

Figure D.14. Cell 84 subgrade stress at 80% load level in spring 2009 for vehicles Mn80, S4, S5, R4, and R5

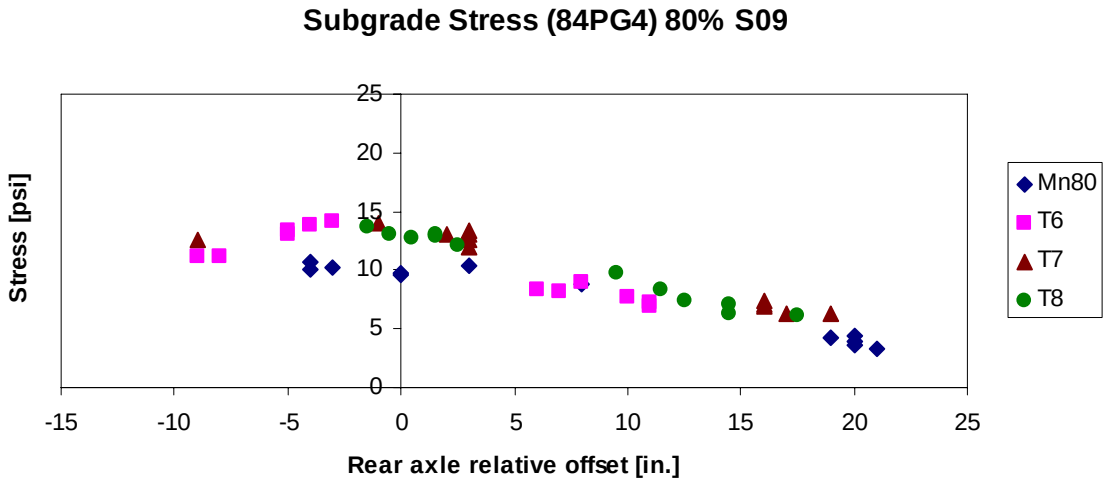

Figure D.15. Cell 84 subgrade stress at 80% load level in spring 2009 for vehicles Mn80, T6, T7, and T8

D.3 Fall 2009

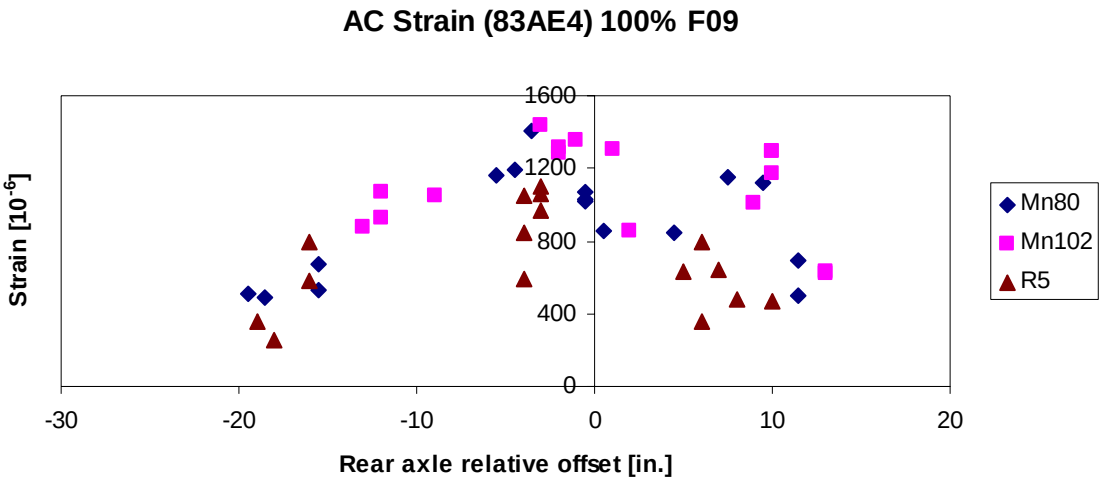

Figure D.16. Cell 83 angled asphalt strain at 100% load level in fall 2009 for vehicles Mn80, Mn102, and R5

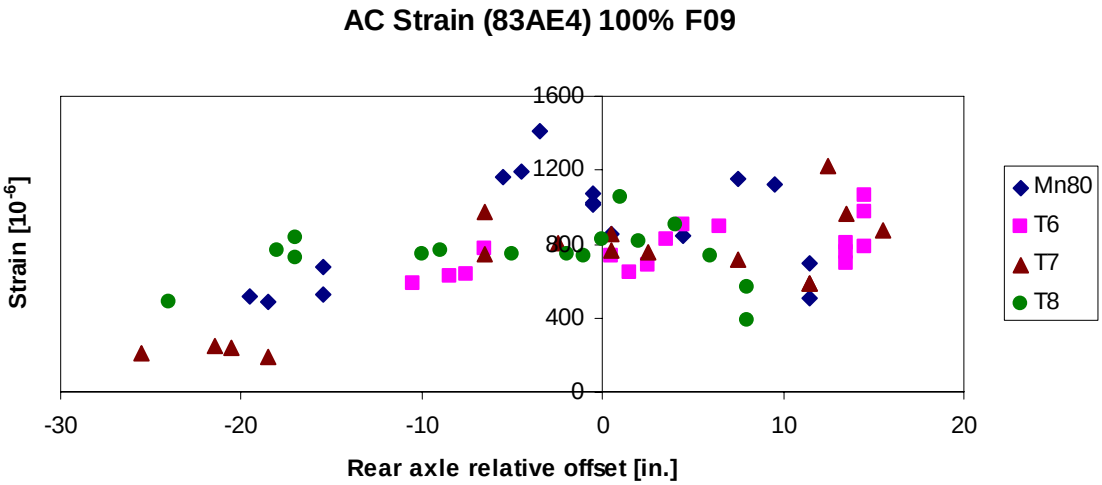

Figure D.17. Cell 83 angled asphalt strain at 100% load level in fall 2009 for vehicles Mn80, T6, T7, and T8

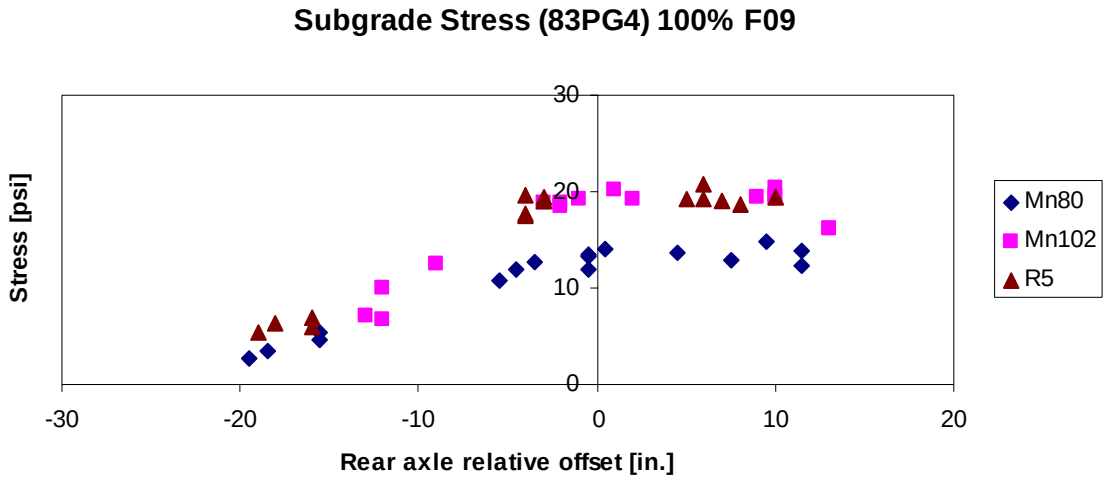

Figure D.18. Cell 83 subgrade stress at 100% load level in fall 2009 for vehicles Mn80, Mn102, and R5

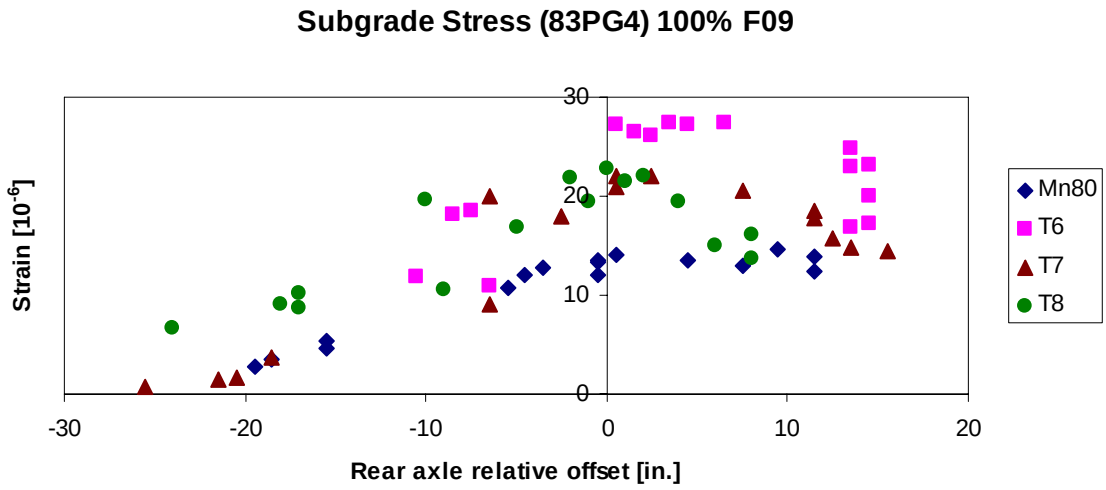

Figure D.19. Cell 83 subgrade stress at 100% load level in fall 2009 for vehicles Mn80, T6, T7, and T8

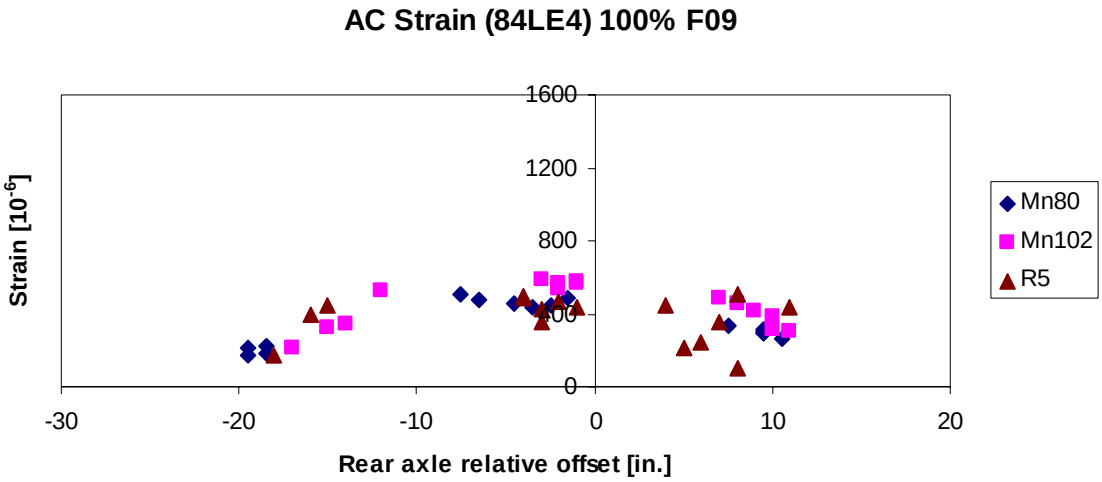

Figure D.20. Cell 84 longitudinal asphalt strain at 100% load level in fall 2009 for vehicles Mn80, Mn102, and R5

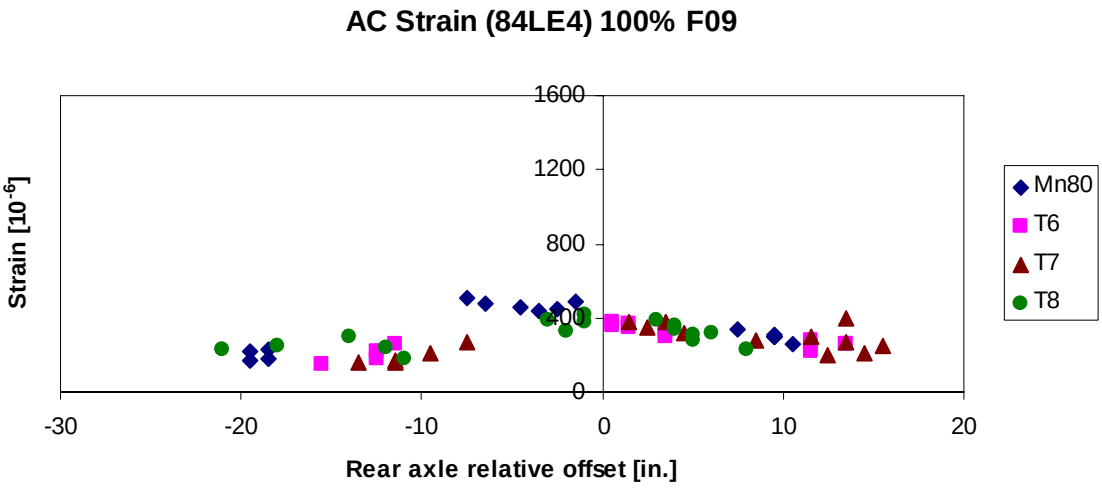

Figure D.21. Cell 84 longitudinal asphalt strain at 100% load level in fall 2009 for vehicles Mn80, T6, T7, and T8

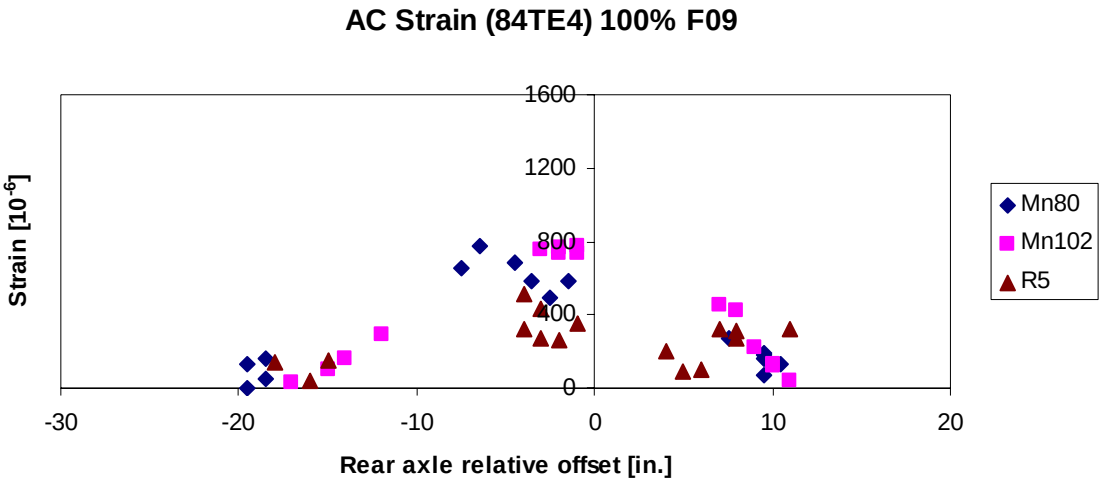

Figure D.22. Cell 84 transverse asphalt strain at 100% load level in fall 2009 for vehicles Mn80, Mn102, and R5

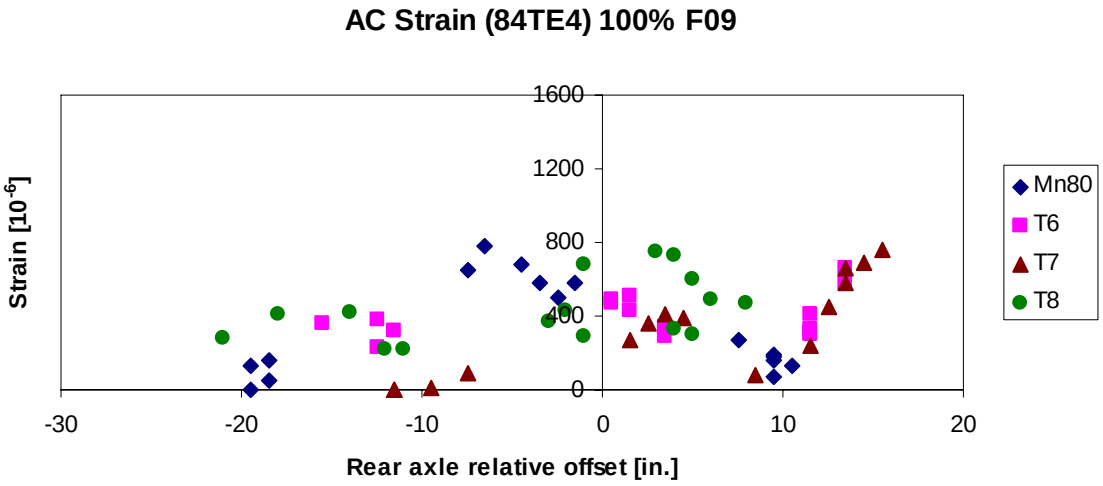

Figure D.23. Cell 84 transverse asphalt strain at 100% load level in fall 2009 for vehicles Mn80, T6, T7, and T8

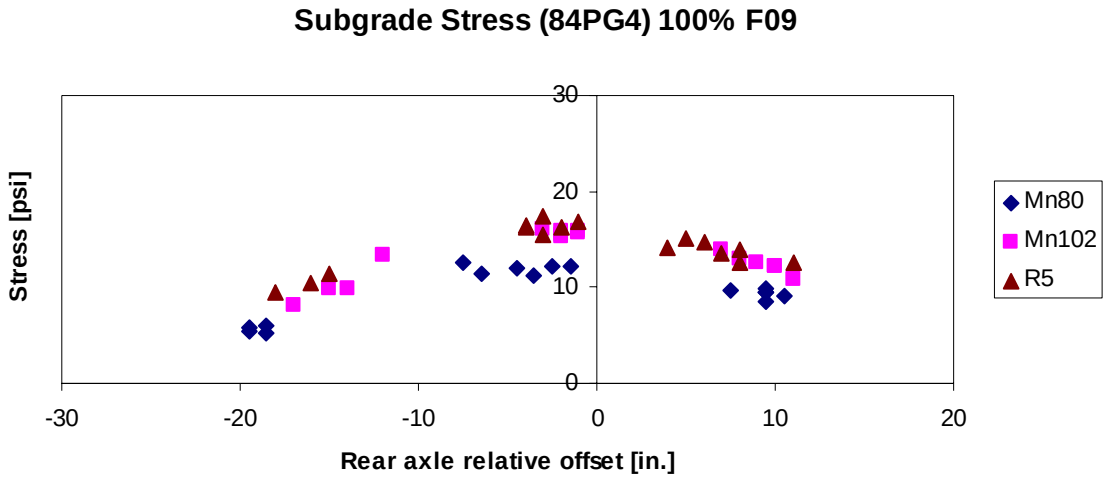

Figure D.24. Cell 84 subgrade stress at 100% load level in fall 2009 for vehicles Mn80, Mn102, and R5

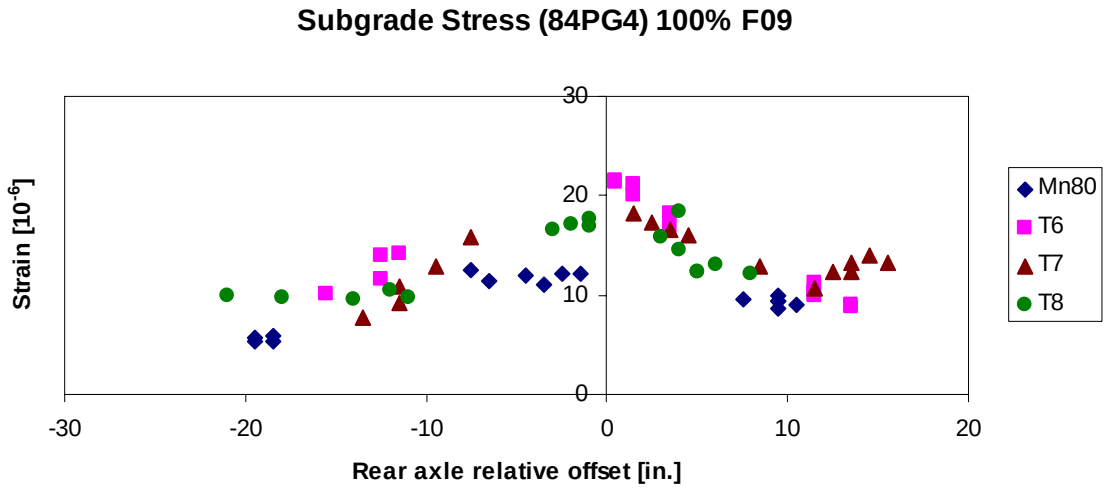

Figure D.25. Cell 84 subgrade stress at 100% load level in fall 2009 for vehicles Mn80, T6, T7, and T8

D.4 Spring 2010

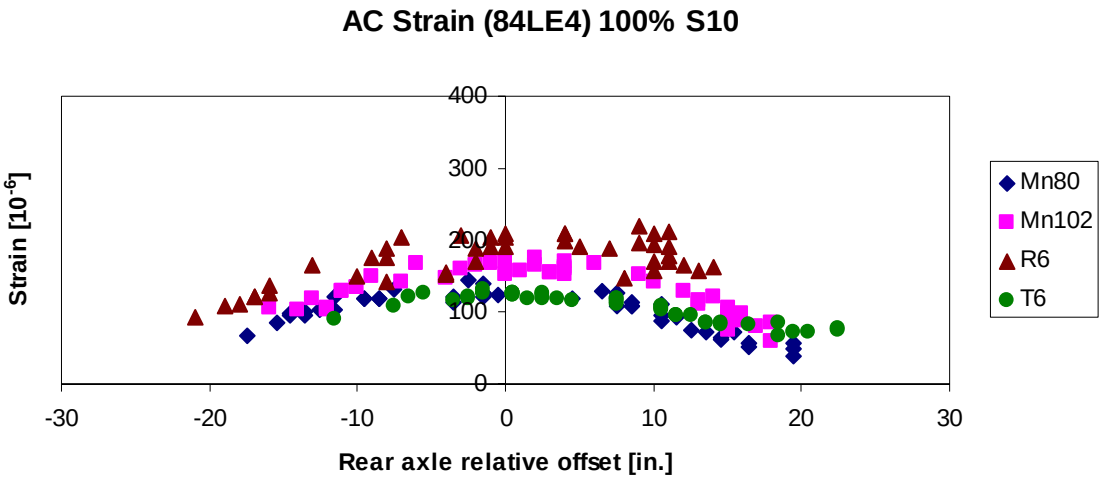

Figure D.26. Cell 84 longitudinal asphalt strain at 100% load level in spring 2010 for vehicles Mn80, Mn102, R6, and T6

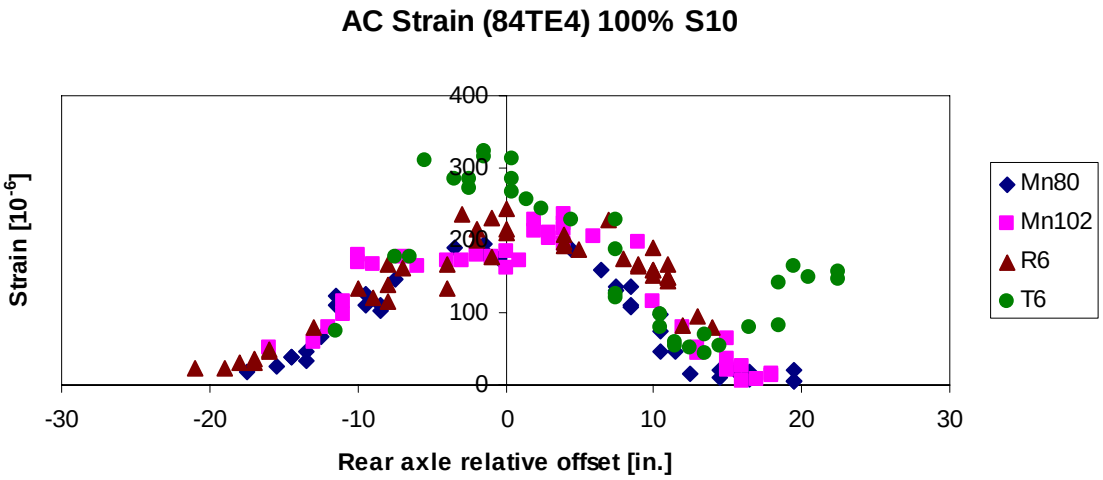

Figure D.27. Cell 84 transverse asphalt strain at 100% load level in spring 2010 for vehicles Mn80, Mn102, R6, and T6

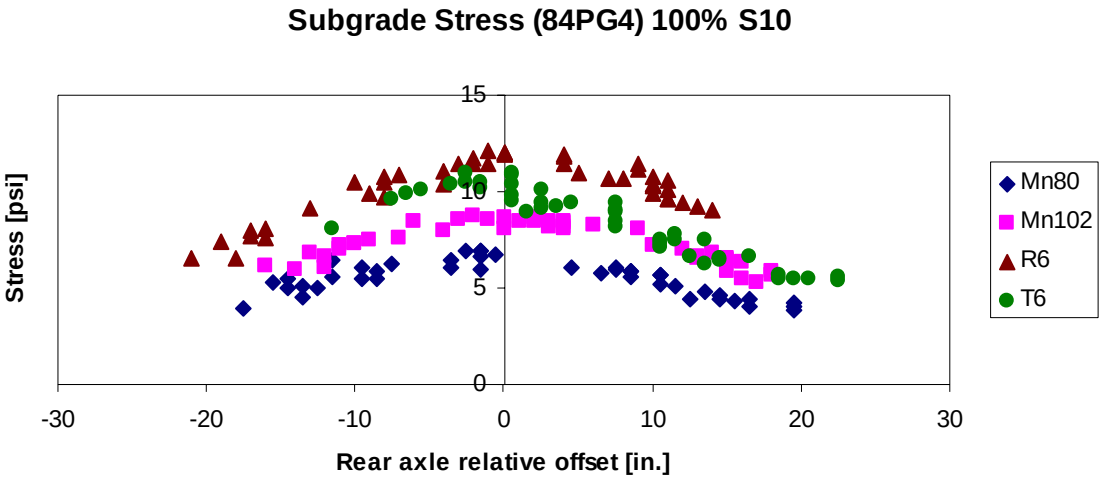

Figure D.28. Cell 84 subgrade stress at 100% load level in spring 2010 for vehicles Mn80, Mn102, R6, and T6

D.5 Fall 2010

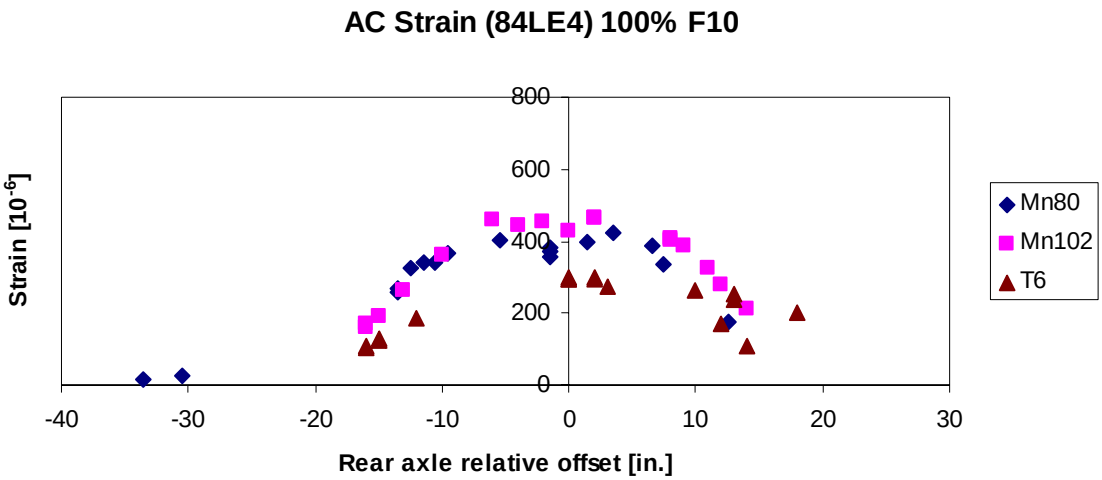

Figure D.29. Cell 84 longitudinal asphalt strain at 100% load level in fall 2010 for vehicles Mn80, Mn102, and T6

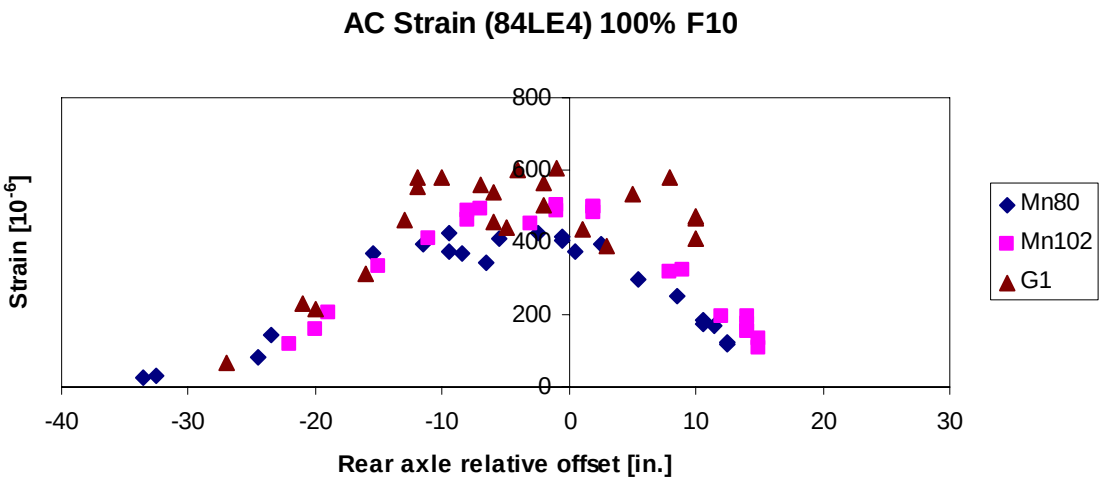

Figure D.30. Cell 84 longitudinal asphalt strain at 100% load level in fall 2010 for vehicles Mn80, Mn102, and G1

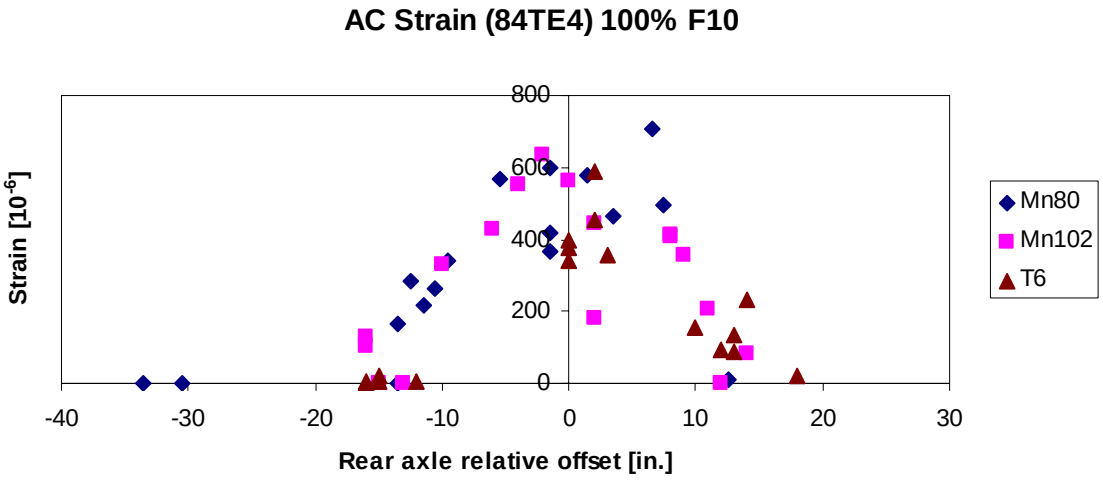

Figure D.31. Cell 84 transverse asphalt strain at 100% load level in fall 2010 for vehicles Mn80, Mn102, and T6

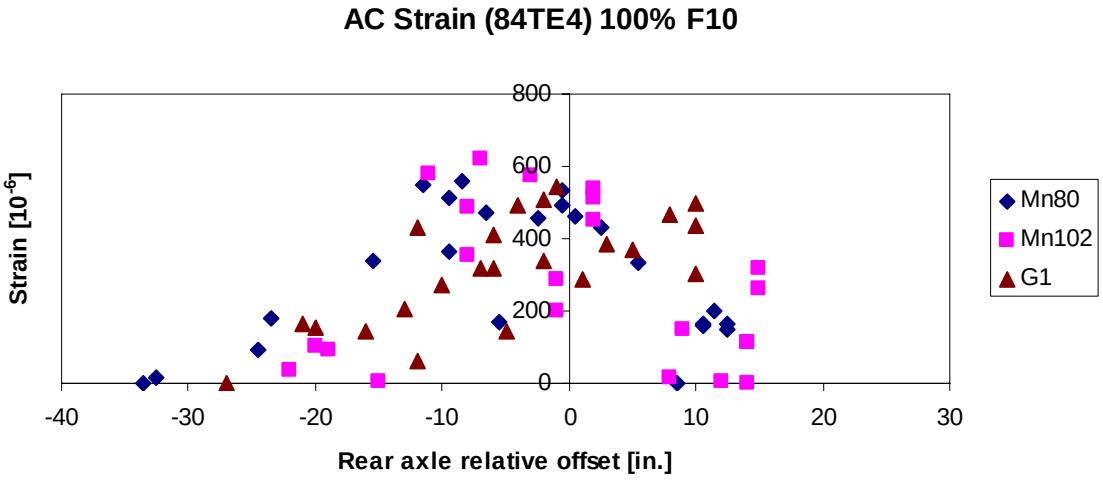

Figure D.32. Cell 84 transverse asphalt strain at 100% load level in fall 2010 for vehicles Mn80, Mn102, and G1

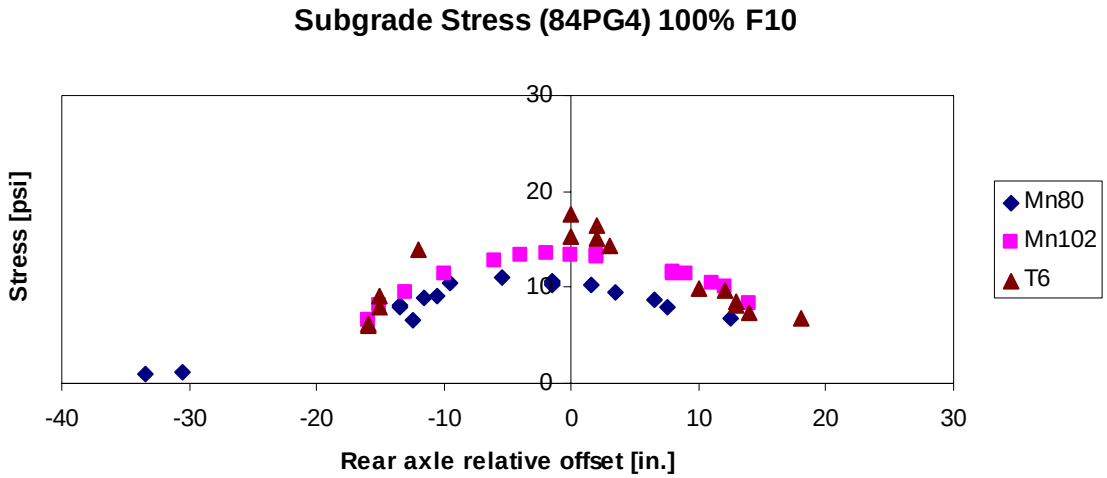

Figure D.33. Cell 84 subgrade stress at 100% load level in fall 2010 for vehicles Mn80, Mn102, and T6

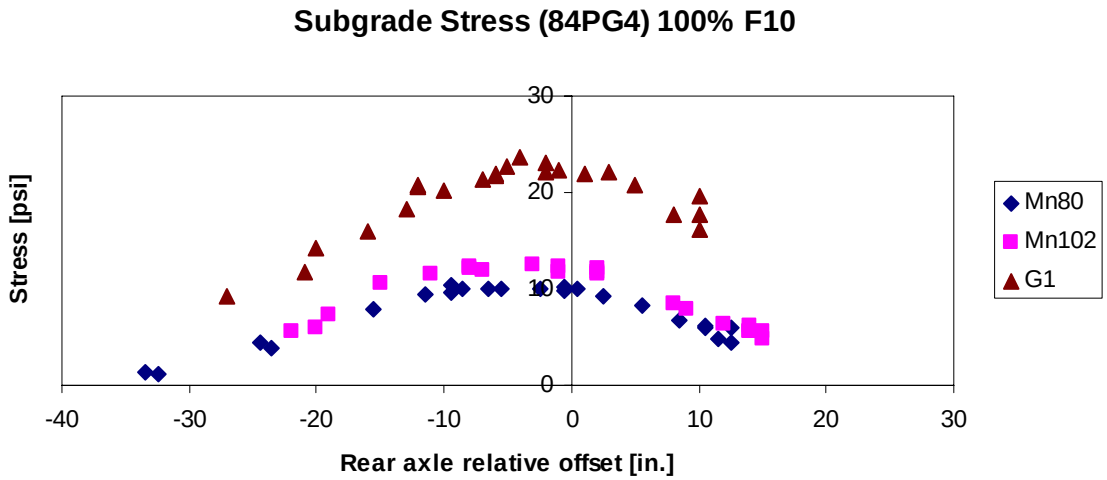

Figure D.34. Cell 84 subgrade stress at 100% load level in fall 2010 for vehicles Mn80, Mn102, and G1

Appendix E Tekscan Measurements

This section includes the measured contact area and average contact stress for vehicles tested using Tekscan. Contact area and average contact stress were plotted for each of the vehicle's axles. The left vertical axes of the following plots correspond to the measured contact area or average contact stress. The right vertical axes correspond to the axle weight. Tekscan measurements are shown in Figure E.1 through Figure E.20.

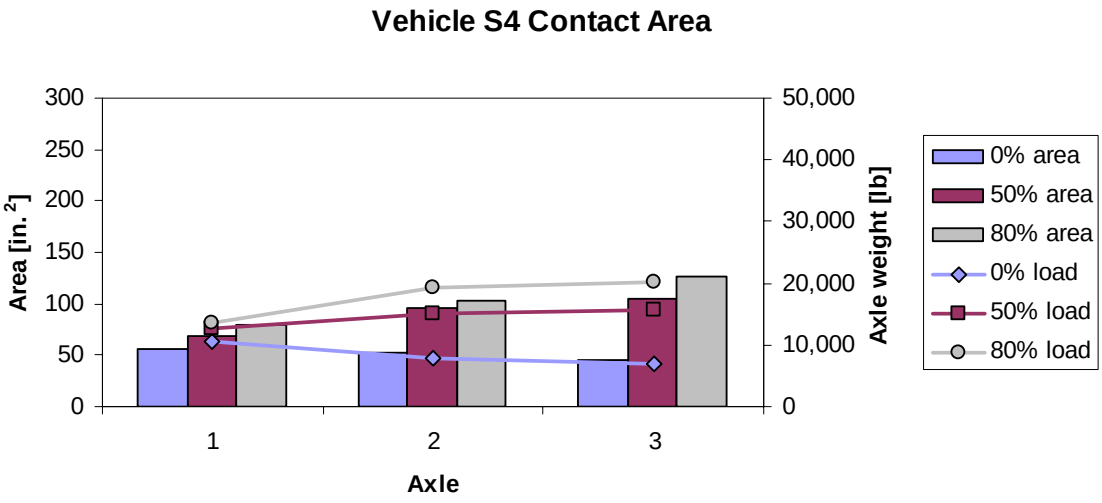

Figure E.1. Contact area for vehicle S4 at 0%, 50%, and 80% load levels

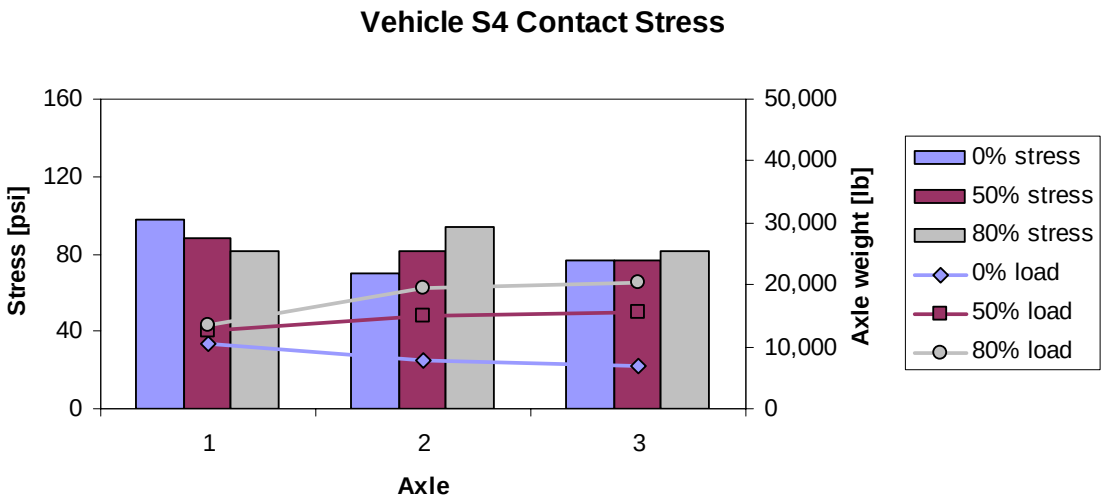

Figure E.2. Average contact stress for vehicle S4 at 0%, 50%, and 80% load levels

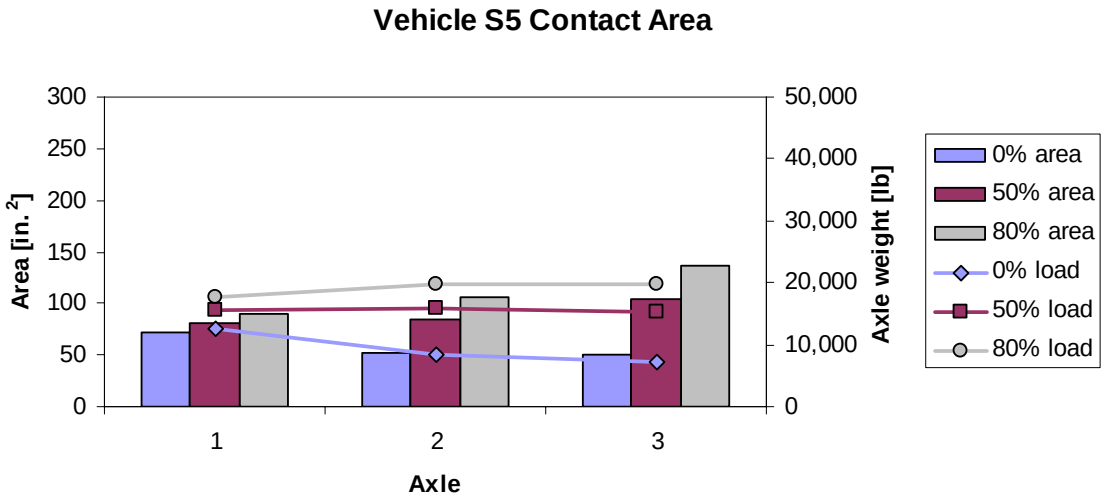

Figure E.3. Contact area for vehicle S5 at 0%, 50%, and 80% load levels

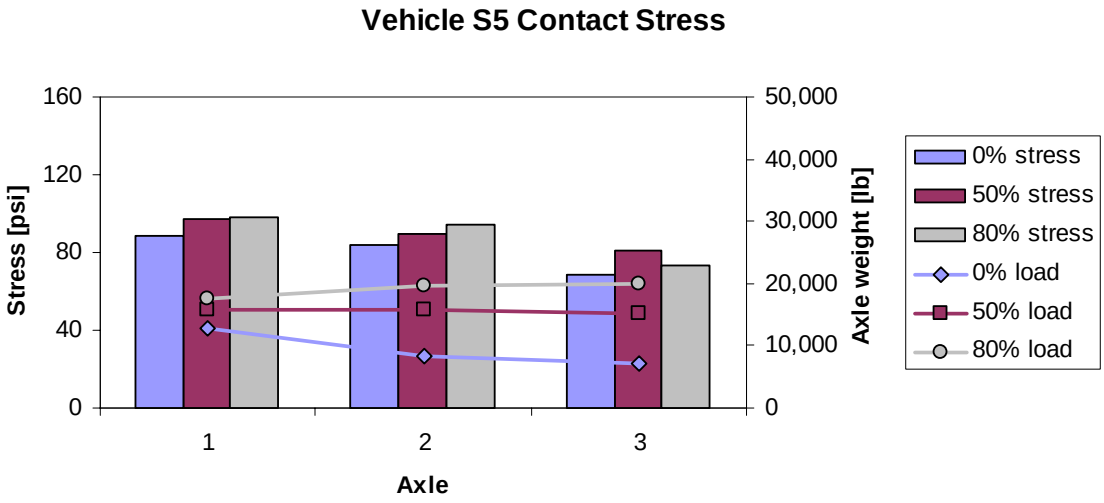

Figure E.4. Average contact stress for vehicle S5 at 0%, 50%, and 80% load levels

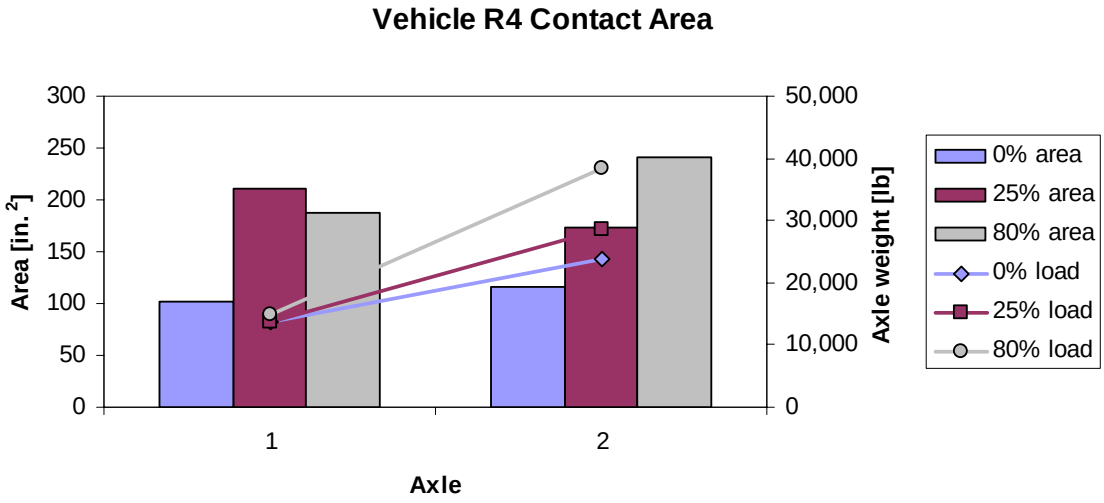

Figure E.5. Contact area for vehicle R4 at 0%, 25%, and 80% load levels

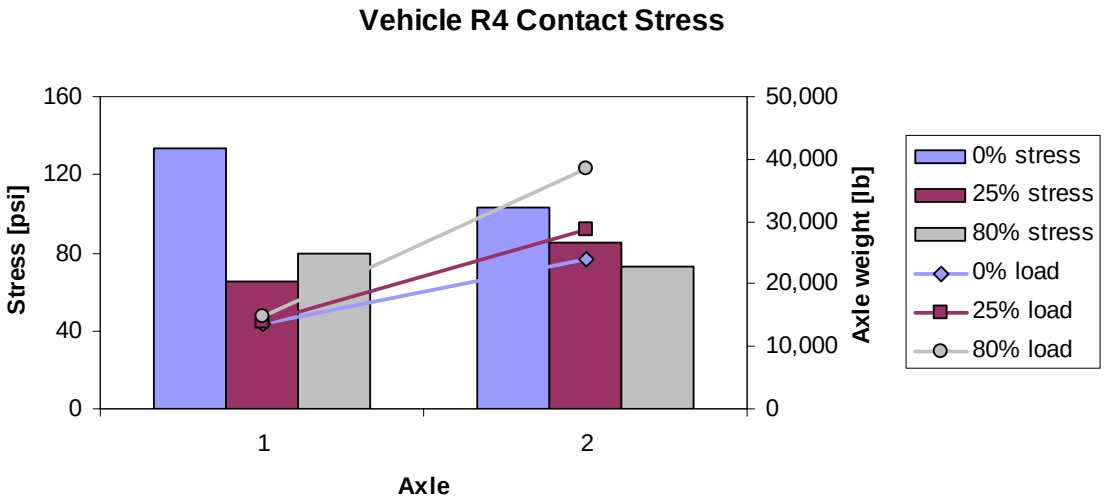

Figure E.6. Average contact stress for vehicle R4 at 0%, 25%, and 80% load levels

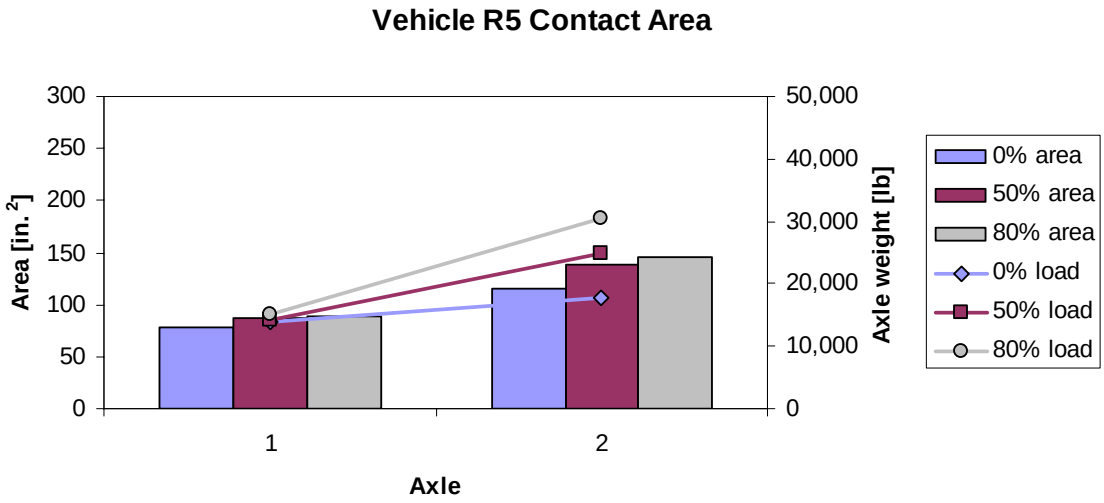

Figure E.7. Contact area for vehicle R5 at 0%, 50%, and 80% load levels

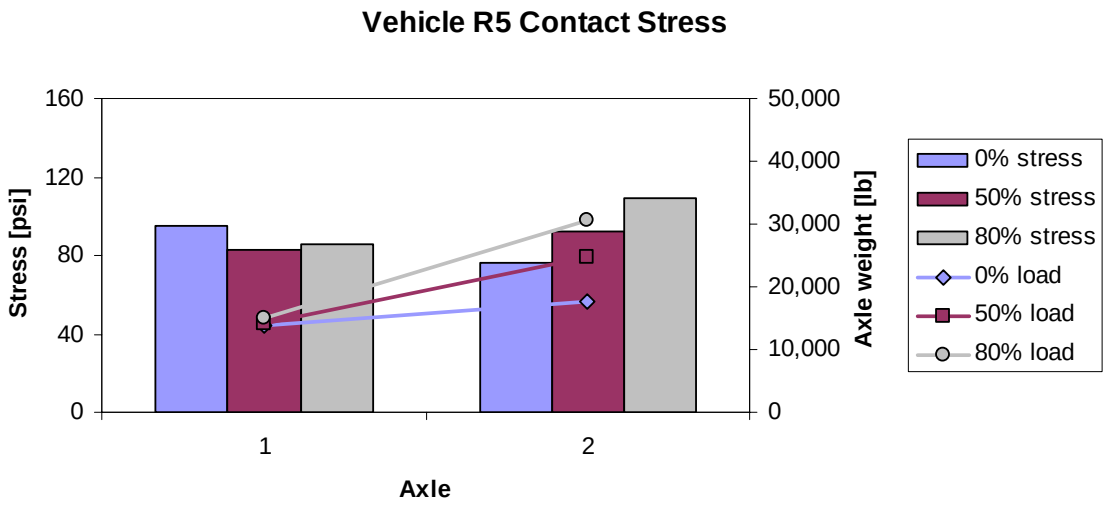

Figure E.8. Average contact stress for vehicle R5 at 0%, 50%, and 80% load levels

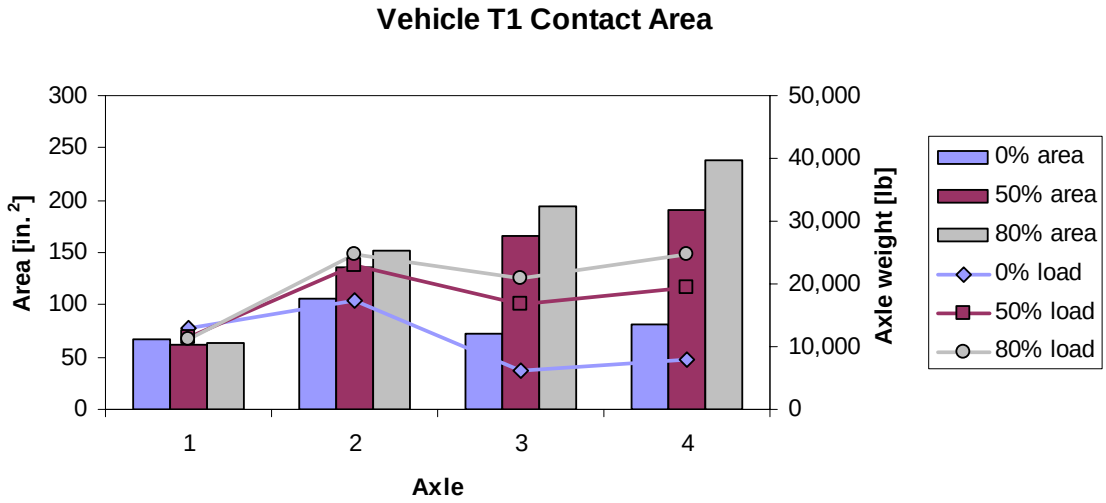

Figure E.9. Contact area for vehicle T1 at 0%, 50%, and 80% load levels

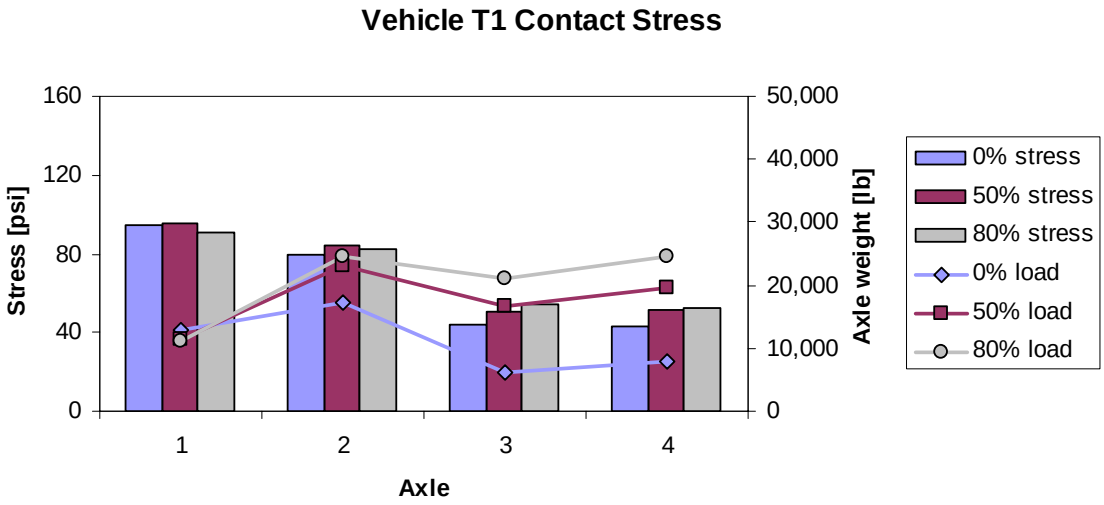

Figure E.10. Average contact stress for vehicle T1 at 0%, 50%, and 80% load levels

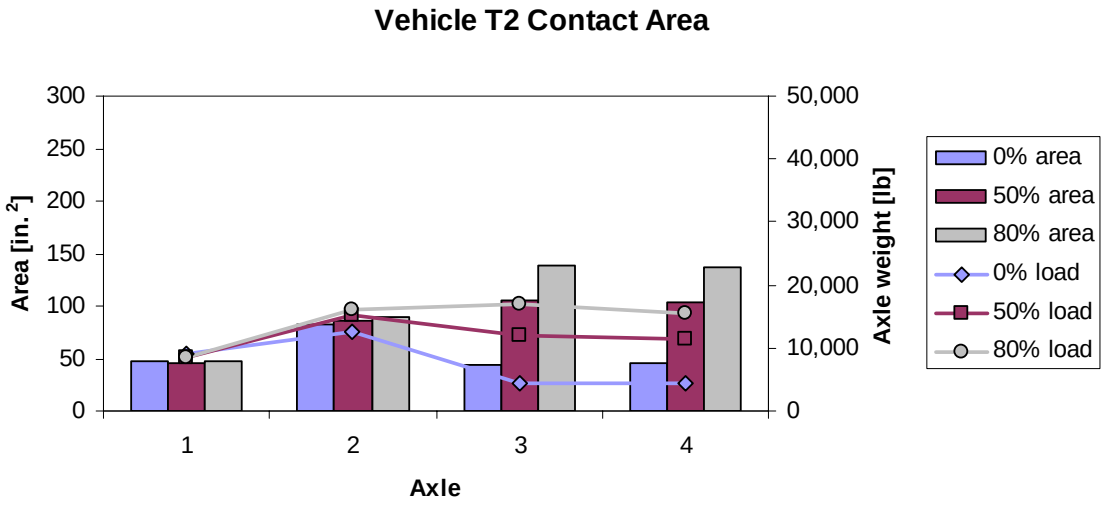

Figure E.11. Contact area for vehicle T2 at 0%, 50%, and 80% load levels

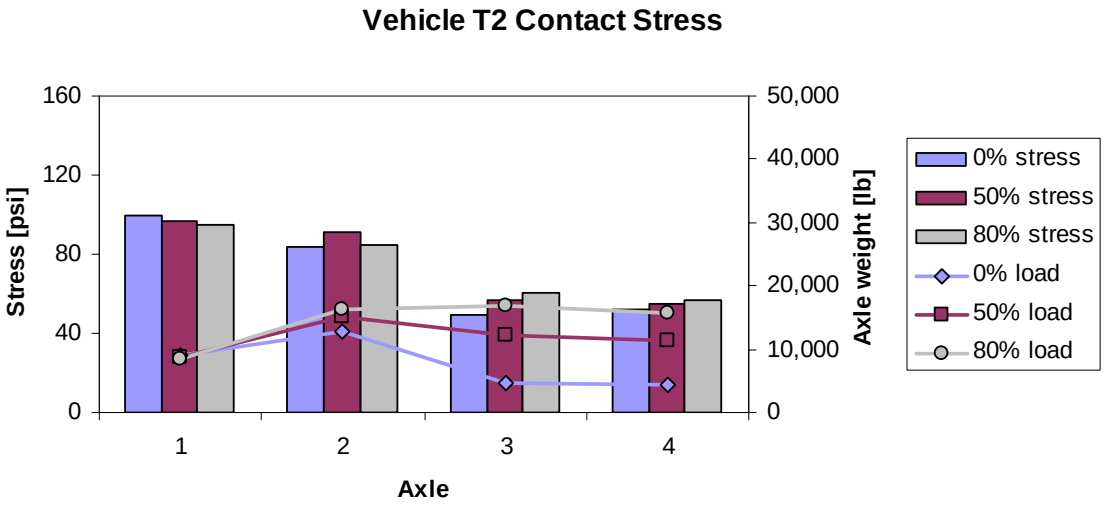

Figure E.12. Average contact stress for vehicle T2 at 0%, 50%, and 80% load levels

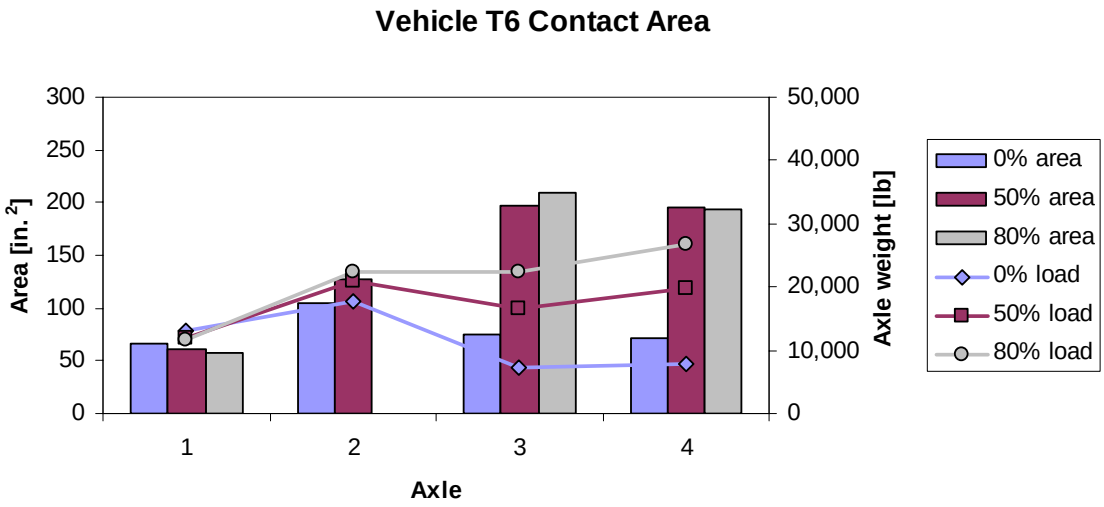

Figure E.13. Contact area for vehicle T6 at 0%, 50%, and 80% load levels

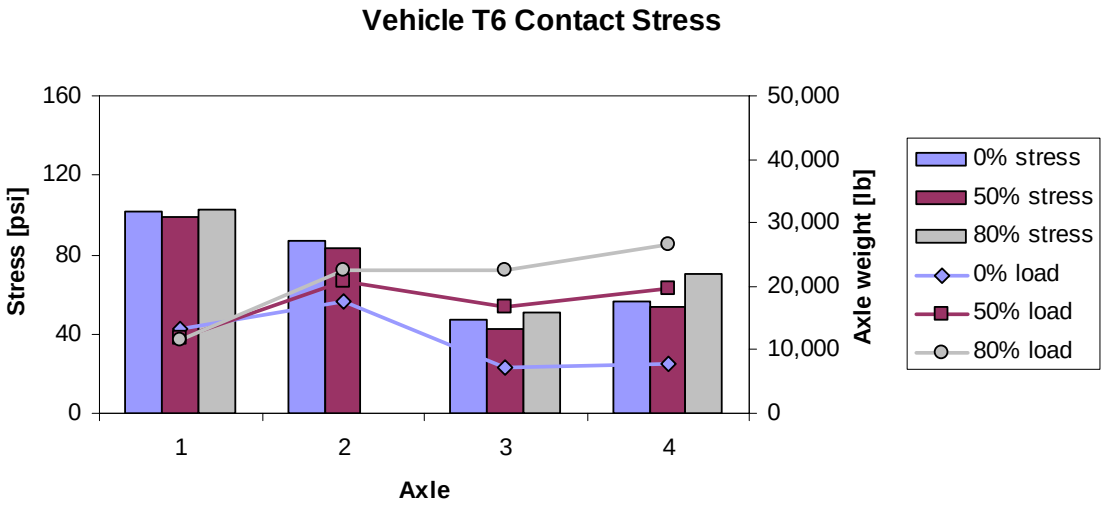

Figure E.14. Average contact stress for vehicle T6 at 0%, 50%, and 80% load levels

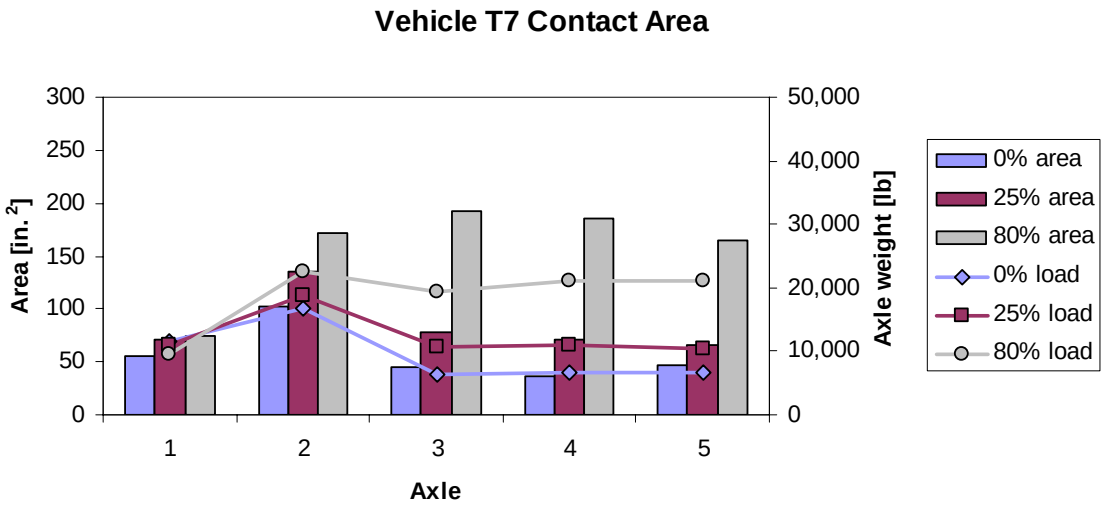

Figure E.15. Contact area for vehicle T7 at 0%, 25%, and 80% load levels

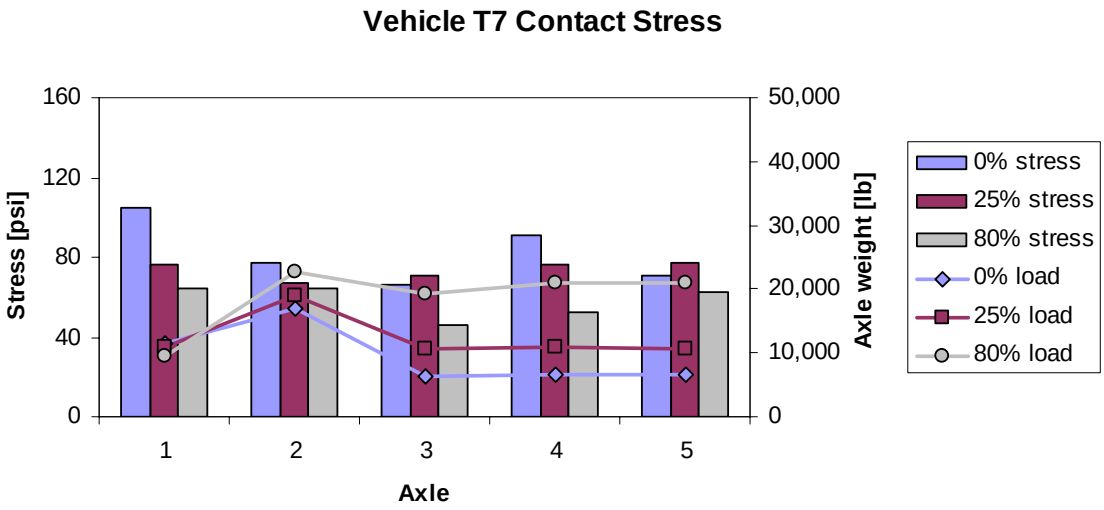

Figure E.16. Average contact stress for vehicle T7 at 0%, 25%, and 80% load levels

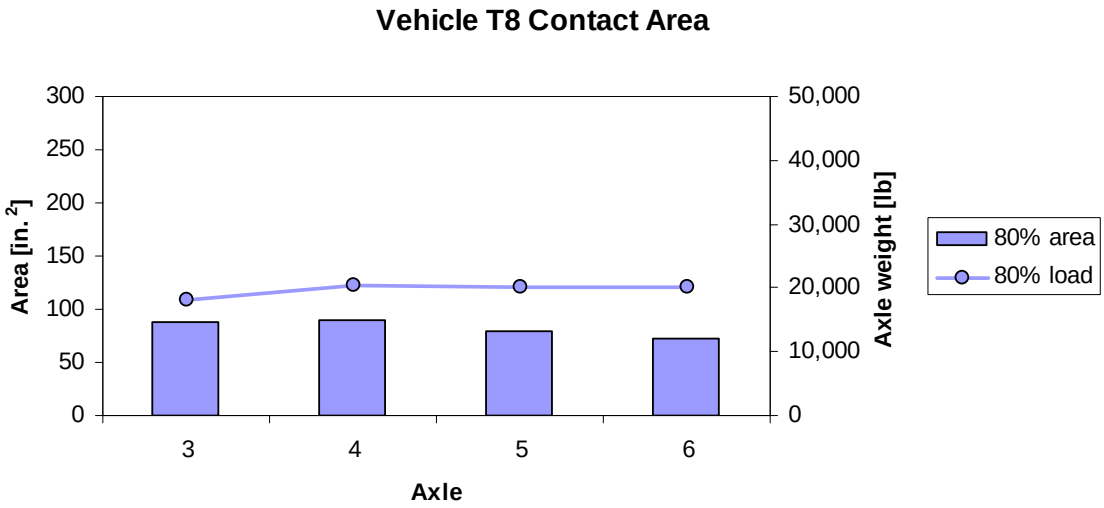

Figure E.17. Contact area for vehicle T8 at 80% load level

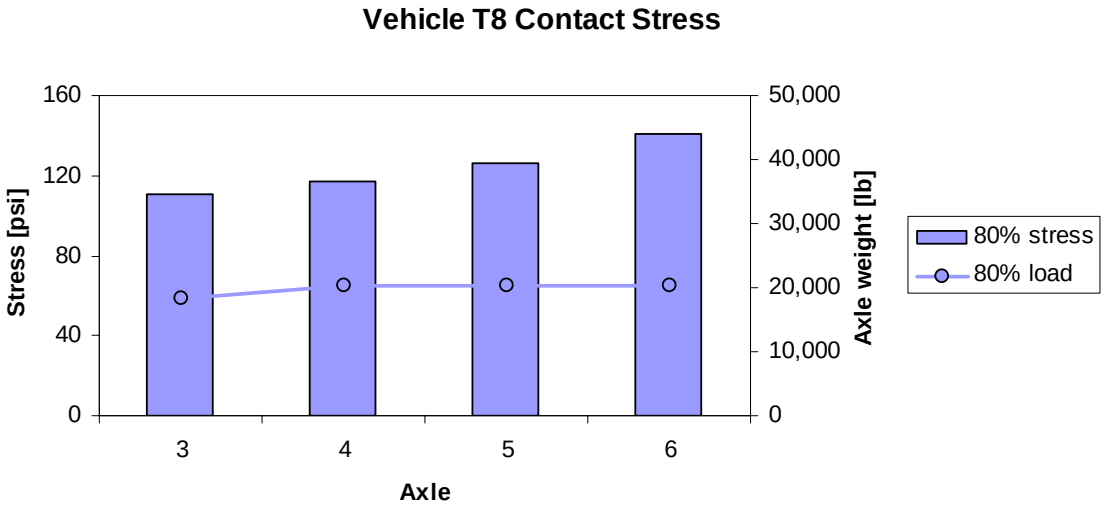

Figure E.18. Average contact stress for vehicle T8 at 80% load level

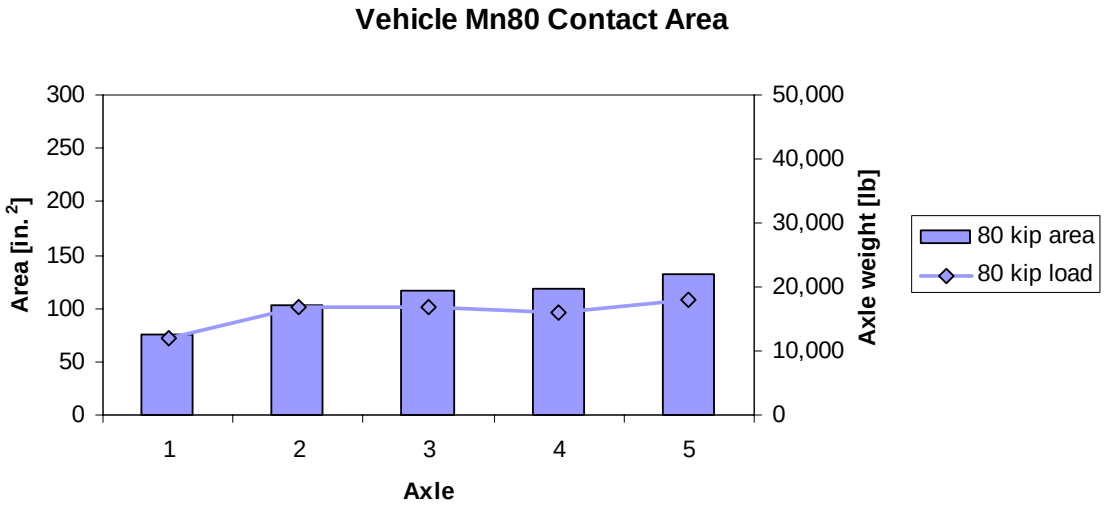

Figure E.19. Contact area for vehicle Mn80 at 80 kip

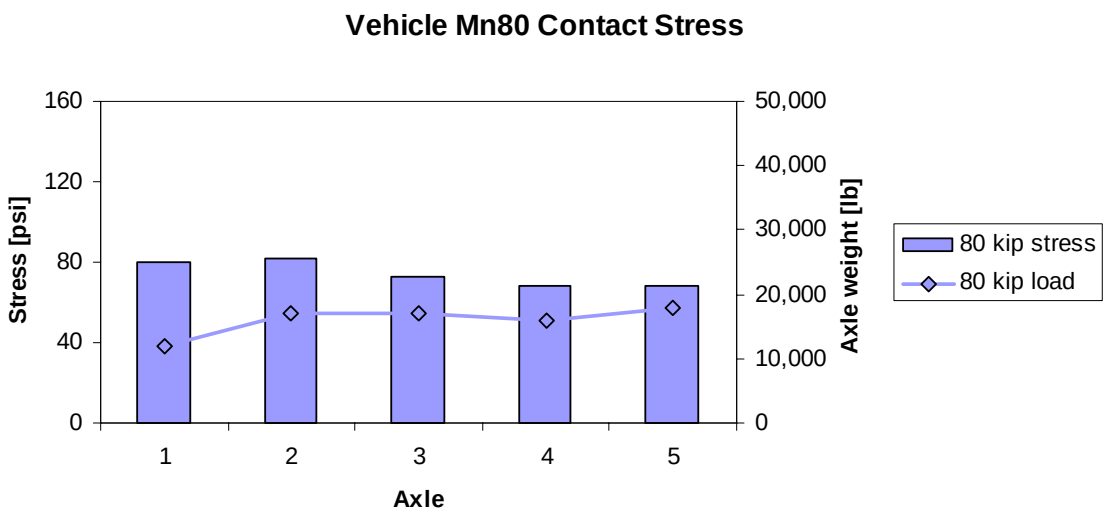

Figure E.20. Average contact stress for vehicle Mn80 at 80 kip